

RESCUE VESSEL OPERATION FOR FLOOD EVACUATION PROTOCOL

ARTICLES FOR FACULTY MEMBERS

Title/Author	A survey of crowd evacuation on passenger ships: Recent advances and future challenges / Liu, K., Ma, Y., Chen, M., Wang, K., & Zheng, K.
Source	<p><i>Ocean Engineering</i> Volume 263 (2022) Pages 1-16 https://doi.org/10.1016/j.oceaneng.2022.112403 (Database: ScienceDirect)</p>
Title/Author	An autonomous coverage path planning algorithm for maritime search and rescue of persons-in-water based on deep reinforcement learning / Wu, J., Cheng, L., Chu, S., & Song, Y.
Source	<p><i>Ocean Engineering</i> Volume 291 (2024) 116403 Pages 1-21 https://doi.org/10.1016/J.OCEANENG.2023.116403 (Database: ScienceDirect)</p>
Title/Author	Analysis of flood evacuation process in vulnerable community with mutual aid mechanism: An agent-based simulation framework / Wang, Z., Huang, J., Wang, H., Kang, J., & Cao, W.
Source	<p><i>International Journal of Environmental Research and Public Health</i> Volume 17 Issue 2 (2020) Pages 1-21 https://doi.org/10.3390/ijerph17020560 (Database: MDPI)</p>

RESCUE VESSEL OPERATION FOR FLOOD EVACUATION PROTOCOL

ARTICLES FOR FACULTY MEMBERS

<p>Title/Author</p>	<p>Autonomous surface vessel for search and rescue operation / Mansor, H., Norhisam, M. H., Abidin, Z. Z., & Gunawan, T. S.</p>
<p>Source</p>	<p><i>Bulletin of Electrical Engineering and Informatics</i> Volume 10 Issue 3 (2021) Pages 1701–1708 https://doi.org/10.11591/EEI.V10I3.2599 (Database: IAES)</p>
<p>Title/Author</p>	<p>Estimation of the Evacuation Time According to Different Flood Depths / Suwanno, P., Yaibok, C., Tsumita, N., Fukuda, A., Theerathitichaipa, K., Seefong, M., Jomnonkwao, S., & Kasemsri, R.</p>
<p>Source</p>	<p><i>Sustainability (Switzerland)</i> Volume 15 Issue 7 (2023) Pages 1-23 https://doi.org/10.3390/su15076305 (Database: MDPI)</p>
<p>Title/Author</p>	<p>Flood evacuation mapping using a time-distance cartogram / Park, S., Lee, G., & Kim, J. O.</p>
<p>Source</p>	<p><i>ISPRS International Journal of Geo-Information</i> Volume 9 Issue 4 (2020) Pages 1-15 https://doi.org/10.3390/ijgi9040207 (Database: MDPI)</p>

RESCUE VESSEL OPERATION FOR FLOOD EVACUATION PROTOCOL

ARTICLES FOR FACULTY MEMBERS

<p>Title/Author</p>	<p>Flood evacuation routes based on spatiotemporal inundation risk assessment / Lee, Y. H., Kim, H. Il, Han, K. Y., & Hong, W. H.</p>
<p>Source</p>	<p><i>Water (Switzerland)</i> Volume 12 Issue 8 (2020) Pages 1-18 https://doi.org/10.3390/w12082271 (Database: MDPI)</p>
<p>Title/Author</p>	<p>Research on Optimal Model of Maritime Search and Rescue Route for Rescue of Multiple Distress Targets / Ho, W. C., Shen, J. H., Liu, C. P., & Chen, Y. W.</p>
<p>Source</p>	<p><i>Journal of Marine Science and Engineering</i> Volume 10 Issue 4 (2022) Pages 1-16 https://doi.org/10.3390/jmse10040460 (Database: MDPI)</p>
<p>Title/Author</p>	<p>Time to rescue for different paths to survival following a marine incident / Solberg, K. E., Jensen, J. E., Barane, E., Hagen, S., Kjøl, A., Johansen, G., & Gudmestad, O. T.</p>
<p>Title/Author</p>	<p><i>Journal of Marine Science and Engineering</i> Volume 8 Issue 12 (2020) Pages 1-16 https://doi.org/10.3390/jmse8120997 (Database: MDPI)</p>

ARTICLES FOR FACULTY MEMBERS

RESCUE VESSEL OPERATION FOR FLOOD EVACUATION PROTOCOL

Title/Author	A survey of crowd evacuation on passenger ships: Recent advances and future challenges / Liu, K., Ma, Y., Chen, M., Wang, K., & Zheng, K.
Source	<i>Ocean Engineering</i> Volume 263 (2022) Pages 1-16 https://doi.org/10.1016/j.oceaneng.2022.112403 (Database: ScienceDirect)



Review

A survey of crowd evacuation on passenger ships: Recent advances and future challenges

Kezhong Liu^a, Yuting Ma^a, Mozi Chen^{a,*}, Kehao Wang^b, Kai Zheng^a

^a School of Navigation, Wuhan University of Technology, Wuhan, China

^b School of Electronics and Information Engineering, Wuhan University of Technology, Wuhan, China

ARTICLE INFO

Keywords:

Building evacuation
Ship passenger evacuation
Passenger evacuation behavior
Passenger evacuation optimization
Passenger evacuation assessment

ABSTRACT

During ship emergencies, a reliable and efficient evacuation system is able to guide passengers to the appropriate muster stations as quickly as possible. The majority of the existing indoor evacuation systems provide emergency guidance for people trapped in general buildings. However, those systems fail to consider the unique challenges of ship passenger evacuation, such as the effect of ship motion on pedestrian motion and the feedback of pedestrian motion on ship inclination state. Consequently, evacuation guidance provided by these schemes may not always be optimal or may even make the evacuation worse due to the differences in the critical factors influencing emergency guiding between land-based buildings and passenger ships. This paper presents a systematic literature overview of recent advances in building evacuation, followed by a description of the challenges unique to evacuating passengers on vessels. Furthermore, the existing ship evacuation research is reviewed from three aspects, i.e., passenger behavior study, ship evacuation optimization, and evaluation of evacuation on passenger ships. A discussion of land-based evacuation schemes and prospects for ship evacuation is also presented.

1. Introduction

Over the past few years, passenger ships have become one of the most popular means of marine transportation and tourism (Fowler and Sorgaard, 2000; Yang et al., 2020). According to the data from Cruise Lines International Association (CLIA), the worldwide ocean cruise passenger capacity had a compound annual growth rate of 6.6% from 1990 to 2021 (Chiou et al., 2021). Fig. 1 shows the worldwide passengers carried from 1990 to 2021. Although modern cruise ships have made continuous progress in their structural designs, operating practices, marine technologies, and regulations in the past 20 years, passenger ship accidents still occurred with catastrophic consequences, e.g., the Costa Concordia disaster in 2012, which leads to 32 passengers/crew dead and more than 4000 injured (Mileski et al., 2014; Liu et al., 2022). According to Lloyds Register accident statistics, there were close to a hundred thousand deaths and injuries of vessels worldwide from 2000 to 2020, of which more than 5% were associated with inappropriate evacuation (Wang et al., 2022; Statistics, 2020). Therefore, an efficient evacuation scheme should be a favorable measure to reduce the losses of human lives in such catastrophes.

The existing evacuation works focus on designing land-based evacuation schemes (Li et al., 2019). As shown in Fig. 2, there are four

kinds of guidance systems for evacuation in buildings on the land: (1) Signage-based evacuation scheme, (2) Leader-based evacuation scheme, (3) Mobile equipment (ME)-based evacuation scheme, and (4) Wireless Sensor Network (WSN)-based evacuation scheme. Earlier studies focused on the design of evacuation signage, including fixed and variable signage. The former is predetermined and does not respond to environmental dynamics, while the latter can adapt to changing hazard status or pedestrian flow to guide occupants (Chu et al., 2017). People may panic in emergency situation, especially when they are unfamiliar with the environment, leading to a poor understanding of evacuation signs, potentially resulting in a stampede and subsequent casualties. The deployment of evacuation leaders is an effective method to improve evacuation safety and efficiency. There are two types of leaders: human and robotic leaders. A mobile robot plays a role similar to that of a human leader in guided crowd evacuation. Moreover, mobile robots could be more advantageous in certain emergency cases where human leaders cannot be assigned to guide people out. Rapid development in intelligent wearable devices and mobile communication technologies has made ME-based evacuation possible. ME-based schemes typically assume the location information of people is available, which may not always be available in many

* Corresponding author.

E-mail addresses: kzliu@whut.edu.cn (K. Liu), 278827@whut.edu.cn (Y. Ma), chenmz@whut.edu.cn (M. Chen), kehao.wang@whut.edu.cn (K. Wang), kzheng@whut.edu.cn (K. Zheng).

<https://doi.org/10.1016/j.oceaneng.2022.112403>

Received 11 May 2022; Received in revised form 18 August 2022; Accepted 22 August 2022

Available online 5 September 2022

0029-8018/© 2022 Elsevier Ltd. All rights reserved.

realistic situations (Fujihara and Yanagizawa, 2015; Mulloni et al., 2011; Gelenbe and Bi, 2014; Ikeda and Inoue, 2016; Iizuka and Iizuka, 2015; Wada and Takahashi, 2013; Fujihara and Miwa, 2012; Inoue et al., 2008; Chu and Wu, 2011; Chen et al., 2015; Chittaro and Nadalutti, 2008). The follow-up studies enable users to bootstrap their indoor evacuation services by themselves, avoiding the dependency on a pre-deployed localization system (Zheng et al., 2017; Shu et al., 2015; Yin et al., 2016; Dong et al., 2019; Teng et al., 2019; Li et al., 2020; Pan and Li, 2019). The ME-based systems neglect environmental dynamics, which may navigate users to hazardous areas. WSNs, capable of automatically monitoring environmental dynamics, should be incorporated into evacuation systems (Wang et al., 2014a). The WSN-assisted scheme can be divided into two categories: sensor-centric scheme, which is to find a direction for every single sensor, and user-centric scheme, which aims to provide customized guidance for each evacuee (Wu, 2017).

The above systems can effectively mitigate potential harm to building occupants in case of emergency. However, evacuating people on passenger vessels is still very challenging due to the unique characteristics of ship evacuation. For example, the impact of dynamic ship motion on pedestrian movement and the feedback of pedestrian movement on ship motion. Compared with the relatively mature land-based evacuation, the research on ship evacuation only started lately. There are mainly three kinds of research focusing on ship evacuation in terms of study intentions: (1) Investigating and analyzing the likely behavior of ship passengers in emergency situations; (2) Optimizing evacuation strategy for trapped passengers; (3) Evaluating ship evacuation performance. The first kind of research examines the characteristics of passengers (e.g., passengers' likely behavior when hearing an evacuation alarm) by conducting experiments, questionnaire surveys, or model-based simulations (Chen et al., 2016a; Wang et al., 2020; Valanto, 2006; Sun et al., 2018a). With respect to passenger evacuation optimization, most researchers focus on planning escaping routes (Ng et al., 2021), optimizing the staircase layout (Wang et al., 2022), and scheduling the time for issuing evacuation orders (Xie et al., 2020c). Ship passenger evacuation can be evaluated in two ways: advanced analyses and simplified analyses (Ni et al., 2017; Kang et al., 2019; Vilen et al., 2020; Galea et al., 2015; Wang et al., 2022; Cho et al., 2016; Sarshar et al., 2013; Xie et al., 2020b; Kana and Droste, 2019; Hifi, 2017; Vanem and Skjong, 2006). The simplified analysis considers a large passenger group as a whole. In contrast, every passenger is regarded as an individual with his/her characteristics in the advanced analysis.

This paper provides an analysis of ship passenger evacuation. The main contributions of our work are summarized as follows:

- A thorough analysis and comparison in recent advances in land-based indoor evacuation systems based on signage, leader, ME, and WSN, is presented.
- The specificities of passenger vessels, which result in the inapplicability of these land-based systems on ship passenger evacuation, are analyzed.
- The research about the evacuation on passenger vessels is reviewed from three perspectives, i.e., the likely behavior of passengers in emergency situations, the optimization of ship evacuation, and the evaluation of evacuation on passenger ships.
- Some comments on the land-based evacuation and the future research directions for the area of ship passenger evacuation are discussed.

This paper is organized as follows. Section 2 reviews the work pertaining to land-based evacuation with signage, leader, ME, and WSN. In Section 3, the unique characteristics and the recent research efforts about ship passenger evacuation are discussed, respectively. Finally, Section 4 presents our comments on the land-based evacuation schemes and the prospects for evacuating passengers on ships. The organization of our paper is illustrated in Fig. 3.

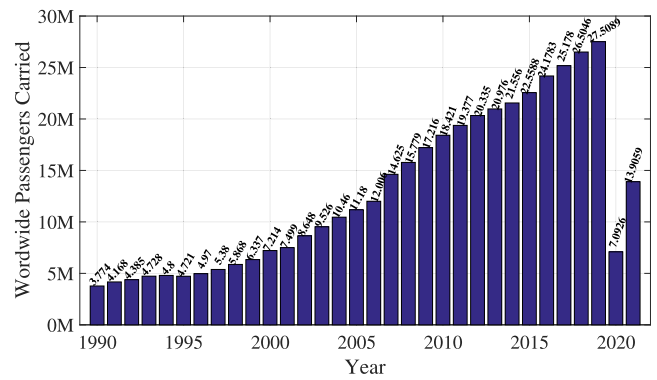


Fig. 1. Worldwide passengers carried from 1990 to 2021.

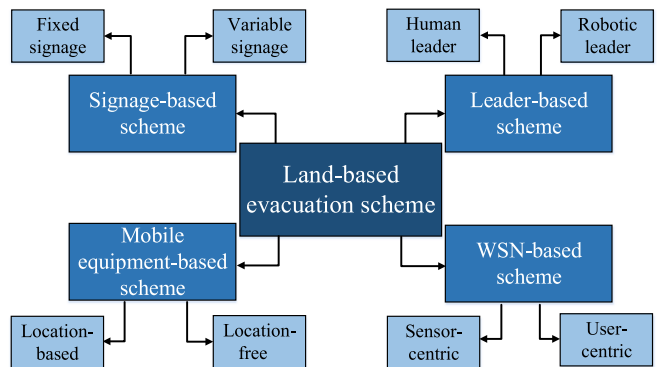


Fig. 2. Different types of crowd evacuation schemes.

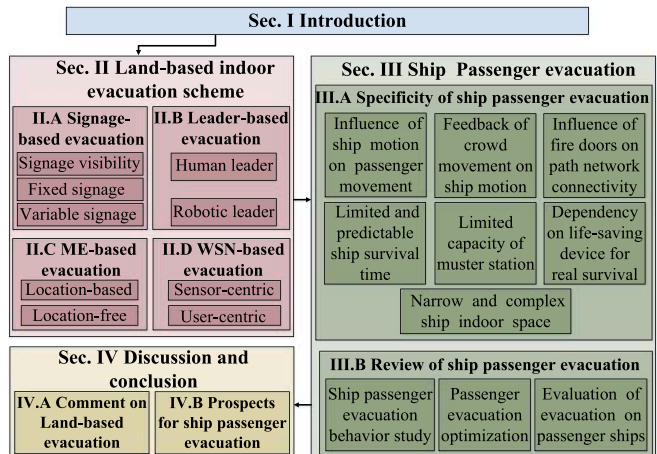


Fig. 3. Organization of this paper.

2. Land-based indoor evacuation scheme

A number of evacuation schemes for general buildings have been proposed, which can be classified into four groups, according to their guidance pattern: signage-based evacuation scheme, leader-based evacuation scheme, ME-based evacuation scheme, and WSN-based evacuation scheme (see Fig. 2). This section describes these different types of land-based indoor evacuation schemes.

2.1. Signage-based evacuation scheme

Signage systems are widely applied to large buildings such as urban rail transit stations, office buildings, and supermarkets. As a sort of

Table 1
Crowd evacuation with static signage.

Related work	Year	Optimization objective	Technique	Algorithm/Model	Scenario
Chen et al. (2009)	2009	Sign location	MCLP	Lagrangian relaxation algorithm	Single-floor supermarket
Chu and Yeh (2012)	2012	Sign location and number	MCLP with side constrains	Visibility graph	A transportation terminal
Motamedi et al. (2017)	2017	Sign location	Simulation	Grid-based model	SenriChuo station, A 440 m ² rectangle area
Zhou et al. (2020)	2020	Sign location	Simulation	SF model	Beijing Subway Station
Yuan et al. (2018)	2018	Mixed layout of WS and GS	Simulation	SF model	A smoky hall

way-finding facility, the signage system does not only provide guidance to occupants who are unfamiliar with the layout of the building in normal situations, it also can offer safety information for evacuees in case of emergencies. Many studies have shown that the arrangement of signage is a feasible way to improve the efficiency of an emergency evacuation in most situations (Tang et al., 2009; Liu et al., 2011; Ronchi et al., 2012; Wang et al., 2014b; Cosma et al., 2016). Based on the response to contemporary evacuation situations, the existing signage-based evacuation system can be divided into fixed signage-based and variable signage-based guidance. The former is predetermined and cannot vary with the status of hazards and congestion, while the latter can respond to dynamic emergency conditions. This section presents a thorough review of the above-mentioned signage-based evacuation scheme.

2.1.1. Fixed signage-based evacuation scheme

The majority of existing signage-based evacuation schemes utilize static signs to provide stabilized guidance to evacuees unfamiliar with the building environment. Table 1 summarizes the previous work on crowd evacuation with static signs. Chen et al. formulated the location optimization for evacuation signs as a maximal-coverage location problem (MCLP) (Chen et al., 2009). Results showed that the proposed guidance arrangement scheme improved evacuation efficiency. However, it is not effective to simply optimize signage placement based on sign locations and visibility while ignoring the associated evacuation routes. Chu et al. found the position of signs that maximized coverage and constituted connected shortest paths by solving a maximum-coverage problem with side constraints (Chu and Yeh, 2012).

In addition, many researchers used simulations to reach efficient signage placement. Motamedi et al. utilized a Building Information Model (BIM) and a grid-based game engine to simulate the movement of pedestrians. Then the efficiency of the signage system design was investigated and optimized (Motamedi et al., 2017). Based on an improved social force model (SF), Yuan et al. proposed a mixed layout scheme of wall signs (WS) and ground signs (GS) with high evacuation efficiency in fire smoke (Yuan et al., 2018). Zhou et al. incorporated a perception probability model that quantified the probability pedestrians could notice and comprehend signs into a modified SF model to investigate crowd evacuation dynamics under the effects of different signage distribution schemes (Zhou et al., 2020).

2.1.2. Variable signage-based evacuation scheme

Since fixed signage cannot respond to the contemporary population density, it would more likely result in heavy congestion. Moreover, static guidance could also lead to pedestrians' frequent oscillations when hazards are on the evacuation routes predetermined by the fixed signs. Variable evacuation signage systems where signs change according to hazard status and pedestrian flow have attracted many researchers' attention in recent years (Tables 2 and 3). A series of studies have proved the effectiveness of the dynamic signage system. Hui et al. conducted experimental trials to test the comprehensibility and effectiveness of variable signs (Hui et al., 2014; Galea et al., 2017b,a). Considering the high cost of field experiments, Olyazadeh et al. exploited virtual environments (VEs) and questionnaires to investigate and evaluate dynamic signage for emergency evacuation (Olander et al., 2017; Galea et al., 2017a; Olyazadeh, 2013; Langner and Kray, 2014; Lin et al., 2017).

Some works take into account the effect of evolving emergencies and depend on the periodic recalculation of guidance information provided by signs to keep occupants safe (Veichtlbauer and Pfeiffenberger, 2011; Wang et al., 2008; Sharma et al., 2018; Luh et al., 2012; Cho et al., 2015a). Complying with the variable guidance, pedestrians can avoid hazardous areas and go out of the building with highest probability. However, frequent change in sign indications may cause possible confusion and reduce the credibility of guidance information disseminated by the signs. Wang et al. proposed that guidance should only be updated when emergency status varied significantly, as determined by emergency responders' subjective judgments (Wang et al., 2009). Desmet et al. scheduled the dynamic pointing directions of signage according to a capacity-reservation routing algorithm. Future capacity reservations can effectively forecast congestion and then assist subsequent path assignment (Desmet and Gelenbe, 2014). Chu et al. proposed a bi-level optimization approach to determine variable pedestrian evacuation guidance in buildings with convex polygonal interior spaces (Chu et al., 2017). The lower-level model utilized a modified floor field cellular automata model (FFCA) to predict congestion and passed the prediction to the upper-level model which used a decreased order of time (DOT) algorithm to calculate variable guidance.

2.2. Leader-based evacuation scheme

Many studies have proved that the staffing of trained evacuation leaders with complete knowledge of the layout of a building can guide evacuees to expected exits and significantly reduce the casualties (Spartalis et al., 2014; Yang et al., 2014; Wang et al., 2015b; Ma et al., 2017; Li et al., 2016; Yang et al., 2015; Vihás et al., 2012; Zhou et al., 2019b).

2.2.1. Human leader-based evacuation scheme

A trained human leader can issue guidance information and spread positive emotion. Over the past decades, several follow-the-leader evacuation models (e.g., SF model (Fig. 4a), vector field model (VF) (Fig. 4b), multi-grid model (Fig. 4c), and cellular automata model (CA) (Fig. 4d)) have been proposed, which can be used in leader effect understanding and leader distribution optimization (Tables 4 and 5).

Utilizing an extended dynamic communication field model (DCF), Wang et al. found the centripetal effect of evacuation assistants (Wang et al., 2015b). Yang et al. proposed a modified SF model to simulate guided crowd evacuation dynamics. Some phenomena, for example, pedestrians following the leader can escape with a faster velocity than those walking independently, were observed in the simulation results (Yang et al., 2014). Based on a CA-based model, Spartalis et al. discovered that a trained leader could not only trigger herding formations of crowds but activate alternative routes, which decreased congestion levels in specific passages and exits (Spartalis et al., 2014; Vihás et al., 2012). However, the effects of the staffing of guides are not always positive. Ma et al. found the dual effect of guides on pedestrian evacuation under limited visibility via an extended SF model (Ma et al., 2017). On the one hand, a few guides could already facilitate pedestrian evacuation when the neighbor density within the visual field was moderate. On the other hand, when the neighbors within the visual field were too many or too few, the effect of guides was usually negative.

Evacuation performance strongly correlates with the distribution and action of guiders. Yuan et al. proved the impact of the number

Table 2
Evaluating crowd evacuation with variable signage.

Related work	Year	Evaluation goal	Technique	Technique description	Scenario	Participant
Hui et al. (2014)	2014	Comprehensibility and Detectability	Survey, Experiment	An international web based survey, Field experiment	Queen Anne building	68
Olyazadeh (2013)	2013	Response time to dynamic signs, Effectiveness of exit signs, Realism of VR experiment	Experiment, Questionnaire	Immersive video environment	Three back projected wall (140 degree)	10
Lin et al. (2017)	2017	Effectiveness in evacuating through emergencies	Simulation	Agent-based model	Underground parking lot	110
Langner and Kray (2014)	2014	Impact on Mass Evacuation	Simulation	SF model	SC Preußen 06 e. V.	12,500
Olander et al. (2017)	2017	Impact on effectiveness of dissuasive exit signage	Questionnaire	Theory of affordances	An egress door within a virtually simulated office	46
Galea et al. (2017a)	2017	Effectiveness of ADSS, Most effective signage type	Experiment, Survey	An international web based survey, Field experiment	A rail station	200
Galea et al. (2017b)	2017	Effectiveness of improved ADSS	Experiment	Field experiment	Sant Cugat station	139

Table 3
Optimizing crowd evacuation with variable signage.

Related work	Optimization goal	Method	Method description	Validation
Cho et al. (2015b)	Shortening safe egress	Dijkstra algorithm	Reverse and simplify start and end nodes of Dijkstra algorithm by adding a virtual node	Simulation
Luh et al. (2012) and Wang et al. (2008, 2009)	Mitigating blocking	Divide-and-conquer	Dynamic programming method for each group subproblem, Lagrangian relaxation framework for Inter-group coordination	Numerical example, Simulation
Chu et al. (2017)	Reducing evacuation time	Bi-level optimization	FFCA for lower-level problem, DOT algorithm for upper-level problem	Numerical example
Sharma et al. (2018)	Supporting real-time reactive signage, Extensible, Energy-efficient, Scalable	DSS-SL	SDN forwarding devices, LED-based visible light communication scheme	–
Desmet and Gelenbe (2014)	Reducing evacuation time	Capacity-reservation algorithm	CPN, CCRP	Simulation

Table 4
The effect of human leader on crowd evacuation.

Related work	Year	Model	Scenario	Exit number	Exit size
Spartalis et al. (2014)	2014	CA model	20 m × 30 m retirement house	Three	0.8 m, 1.2 m
Yang et al. (2014)	2014	SF model	50 m × 50 m room	One	1 m
Li et al. (2016)	2016	Trace Model	Indoor classroom	Two	–
Vihás et al. (2012)	2012	CA model	A two-dimensional space with 17 sectors, a cubic space with 4 sectors	–	–
Wang et al. (2015b)	2015	Extended DCF model	26 m × 26 m room	One	0.8 m
Ma et al. (2017)	2017	SF model	15 m × 15 m room	One	4 m
Zhou et al. (2019b)	2019	SF model	Beijing's urban rail transit station	Three	3.4 m

of guiders on evacuation by using a CA-based model (Yuan and Tan, 2009). Hou et al. discovered that for evacuation under a single-exit scenario, only one or two leaders could exert a remarkable impact, while more leaders are expected for configurations with multi-exits (Hou et al., 2014). Wang et al. optimized the position of leaders while minimizing their number and observed that except for the distribution of leaders, other factors such as the number of evacuees guided by a leader, the visibility range of environments, and the leaders' speeds significantly affect evacuation efficiency (Wang et al., 2012; Zhang et al., 2021; Wang et al., 2015c, 2016). In addition, Cao et al. did not only derive the appropriate distribution of leaders but also optimized their guidance strategy (Cao et al., 2016; Zhou et al., 2019a; Yang et al., 2013).

2.2.2. Robotic leader-based evacuation scheme

Human leaders may arrive at the emergency site too late to assist crowd evacuation. In addition, they cannot be sent to guide evacuees out in some accidents like nuclear leakage because of security concerns. In such cases, the usage of robotic leaders could be attractive. Many simulators have been used to model robots and crowds to demonstrate the effectiveness of using robots for aiding emergency evacuations (Sakour and Hu, 2017).

Earlier works focused on indirectly evacuating evacuees utilizing autonomous robots, not involving human–robot interaction (Shell et al., 2005; Ferranti and Trigoni, 2008). Shell et al. described a multi-robot-based navigational aid deployment strategy with which a network of directional audio aids can be deployed automatically following an emergency with the assistance of a team of robots (Shell et al., 2005). Ferranti et al. devised two robot-assisted evacuation route discovery (ERD) mechanisms, namely Agent-to-Tag-ERD and Tag-to-Tag-ERD, with which robots can search for the shortest evacuation routes as soon as possible in parallel with their exploration of an unknown hazardous area (Ferranti and Trigoni, 2008).

Recently, the improvement in the trust in human–robot interaction makes it possible to guide occupants directly using emergency evacuation robots. Kim et al. designed a portable fire evacuation guide robot that can be thrown into fire scenes to explore the information about environmental conditions and trapped occupants, which would be transmitted to firefighters to determine a guide strategy that could be broadcast through the microphone and speaker system on the robot (Kim et al., 2009). Robinette et al. devised robots incorporating a model of human panic behavior to navigate evacuees safely to appropriate exits (Robinette and Howard, 2011). The above-mentioned robot-assisted evacuation systems require control and decision support from human operators. With the advance in integration techniques

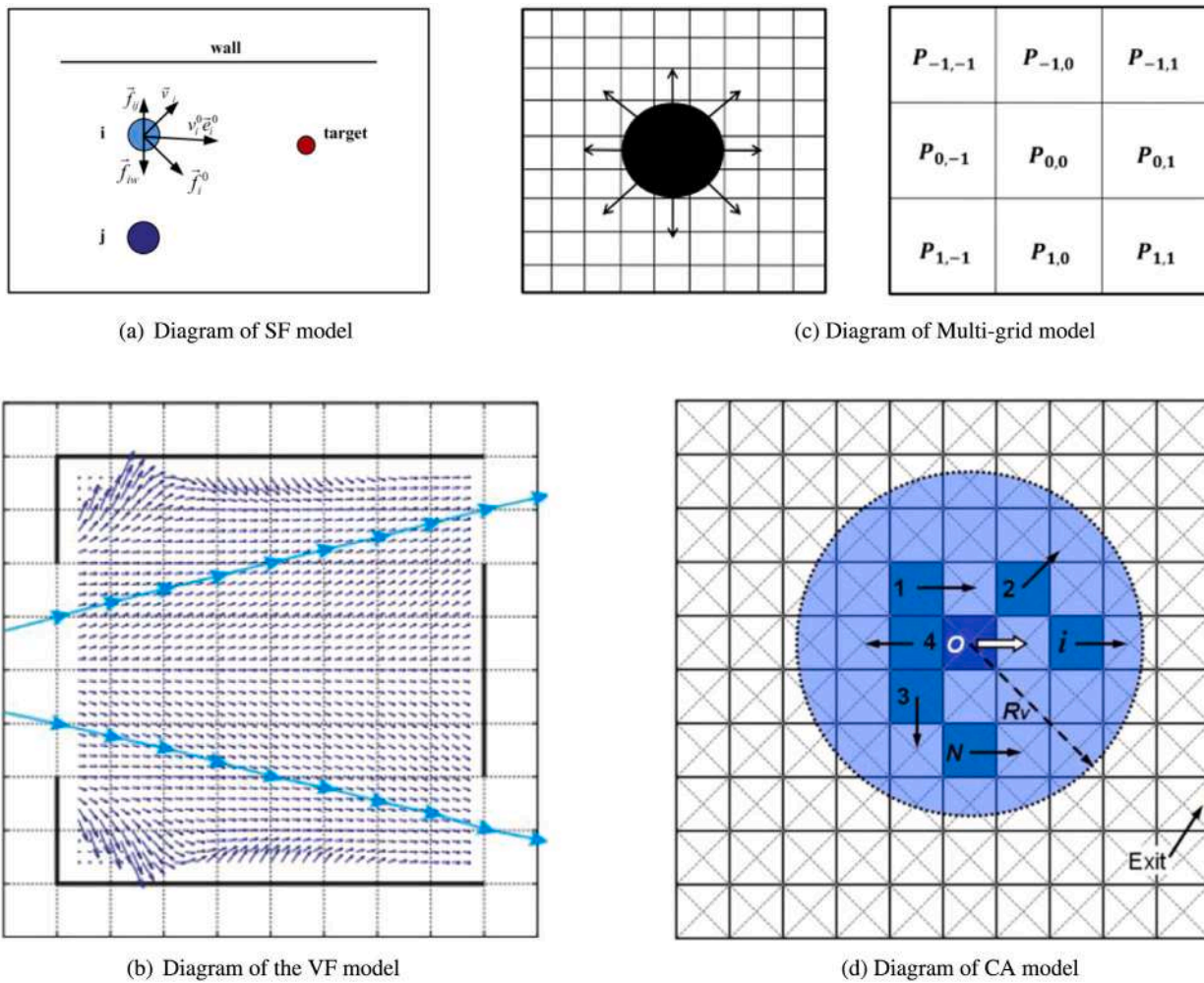


Fig. 4. Diagram of classical follow-the-leader evacuation model (Yuan and Tan, 2009; Okada and Ando, 2011; Cao et al., 2016; Yang et al., 2014).

Table 5
The influencing factors of human leader-based evacuation.

Related work	Year	Model	Influencing factor	Scenario	Exit number	Exit size
Okada and Ando (2011)	2011	VF model	Location, number	A room	Two	-
Ma et al. (2016)	2016	SF model	Location, number, visibility, distribution range of evacuees	20 m × 20 m room	One	1 m–20 m
Yuan and Tan (2009)	2009	CA model	Visibility, number	20 m × 20 m room	One	2 m
Wang et al. (2012)	2012	CA model, CF model	Location, number	26 m × 26 m room	One	0.4 m
Hou et al. (2014)	2014	SF model	Location, number, velocity, visibility	20 m × 20 m room	One, two, four	2 m
Cao et al. (2016)	2016	Multi-grid model	Guidance strategy, guider type, number and distribution	20 m × 10 m room	Two	1 m
Wang et al. (2015c)	2015	CA model, CF model	Walking speed, information transmission radius	26 m × 26 m room	One	0.8 m
Yang et al. (2015)	2015	SF model	Location, number	50 m × 50 m room	One	1 m
Wang et al. (2016)	2016	Multi-Information CF model	Sensing radius	0.4 m × 10 m T-shaped channel, 2 m × 24 m T-shaped channel	Two	2 m
Yang et al. (2013)	2013	Multi-agent model	Guiding route	80 × 80 area	Three	Radius 15, 10, 5
Zhou et al. (2019a)	2019	Hybrid bi-level model	Location, number, route	Beijing's urban rail transit station	Three	3.4 m
Zhang et al. (2021)	2021	E-AECM	Location	Spring city square of Jinan	-	-

and computing power, robots can evacuate occupants independently. Jiang et al. presented an adaptive dynamic programming approach (ADP) to control the motion of a robot for a desirable collective velocity (Jiang et al., 2017). Boukas et al. trained the intelligent emergency evacuation robots to attract evacuees heading towards saturated exits and redirect them to less blocked ones to ensure a faster and safer evacuation (Boukas et al., 2015; Tang et al., 2016; Wan et al., 2020; Zhang and Guo, 2015; Garrell et al., 2009).

2.3. ME-based evacuation scheme

Typical ME for assisting crowd evacuation includes smartphones and Augmented Reality (AR) headsets. This kind of equipment can present more useful and intuitive evacuation information than that provided by traditional techniques based on audio alarms and paper maps. In addition, with the fast development of AR and Virtual Reality (VR) technology, AR/VR-based wearable hardware such as the

Table 6
Crowd evacuation with ME.

Source	Location-based	Localization technique	Track-based	Tracking technique	Floor plan-based	Central server-based	Optimization objective	Capacity aware	Clustering aware
Iizuka and Iizuka (2015) and Wada and Takahashi (2013)	✓	GPS	×		✓	×	Evacuation time	×	×
Fujihara and Miwa (2012)	✓	GPS	×		✓	×	Evacuation time	✓	×
Ikeda and Inoue (2016)	✓	GPS	×		✓	✓	Evacuation time	×	×
Gelenbe and Bi (2014)	✓	Built-in camera	×		✓	✓	Survival rate	×	✓
Diao and Shih (2018) and Zhang et al. (2020c)	✓	Built-in camera	×		✓	✓	Evacuation time	×	×
Stigall and Sharma (2017)	✓	Built-in camera	×		✓	✓	Evacuation distance	×	×
Ahn and Han (2011)	✓	Built-in sensors	×		✓	✓	Evacuation time	×	×
Chen and Chung (2017) and Chen and Liu (2021)	✓	iBeacon	×		✓	✓	Evacuation time	✓	✓
Fujihara and Yanagizawa (2015)	✓	iBeacon	×		✓	×	True positive detection rate of guidance	×	×
Mulloni et al. (2011)	✓	Info points	×		✓	×	Evacuation distance	×	×
Fujihara and Miwa (2012)	✓	Wi-Fi	×		✓	×	Evacuation time	✓	×
Chen et al. (2015)	✓	RFID, iBeacon, RSSI-based	×		✓	✓	Evacuation time	✓	×
Chu (2010)	✓	NFC, RFID	×		✓	✓	Evacuation time	×	×
Nadalutti and Chittaro (2008) and Chittaro and Nadalutti (2008)	✓	RFID	×		✓	×	Navigation error, stops	×	×
Chu and Wu (2011)	✓	RFID	×		✓	✓	Distance, congestion, temperature	✓	×
Inoue et al. (2008)	✓	Radio beacon	×		✓	✓	Evacuation distance	×	×
Zheng et al. (2017)	×		✓	Image, IMU, WiFi	×	×	Spatial error, energy saving, path distance	×	×
Shu et al. (2015)	×		✓	IMU	×	×	Spatial error, energy saving	×	×
Zhang et al. (2020b) and Yin et al. (2016)	×		✓	WiFi, IMU	×	×	Spatial error, deviation detection time	×	×
Dong et al. (2019)	×		✓	Visual SLAM	×	×	Navigation success rate	×	×
Li et al. (2020)	×		✓	WiFi, IMU	×	×	Space error	×	×
Dong et al. (2020)	×		✓	Visual SLAM	×	✓	Navigation success rate, space error	×	×
Pan and Li (2019)	×		✓	IMU, iBeacon	×	✓	Navigation distance, navigation deviation, notification delay	×	×
Teng et al. (2019)	×		✓	Point clouds, IMU	×	✓	Tracking error, navigation success rate	×	×

wireless head-mounted display (HMD) has been introduced to study human evacuation behavior and train occupants. Using HMD-based VR experiments, Feng et al. investigated the response of evacuees to different types of information (e.g., crowd flow and exit signs) (Feng et al., 2021; Lin et al., 2020). Lin et al. examined the effect of repeated exposures to indoor environments on people's indoor wayfinding performance (Lin et al., 2019). In addition, Lovreglio et al. trained occupants to cope with emergencies in an earthquake or fire by using VR-based simulators (Lovreglio et al., 2018; Xu et al., 2014).

Based on the dependency on the pre-knowledge of user locations, the ME-based evacuation schemes are classified into two categories: location-based and location-free evacuation schemes using ME (Table 6). This section presents the review of the two schemes.

2.3.1. Location-based evacuation scheme using ME

Most of the existing ME-based evacuation schemes rely on the availability of location information on each user. Ikeda et al. exploited

the built-in Global Positioning System (GPS) function to provide the position of smartphones (Ikeda and Inoue, 2016; Iizuka and Iizuka, 2015; Wada and Takahashi, 2013; Fujihara and Miwa, 2012). But it is challenging to receive satellite signals within a modern building. Therefore other location awareness systems become necessary for location-based indoor evacuation using ME. Chen et al. proposed that the location of each person can be periodically detected by his/her smartphone through signal strength-based localization or infrastructure-based positioning (e.g., radio-frequency ID (RFID) and iBeacon) (Chu, 2010; Nadalutti and Chittaro, 2008; Chittaro and Nadalutti, 2008; Chen et al., 2015; Chu and Wu, 2011; Shin et al., 2011). Gelenbe et al. identified evacuees' positions by the camera or sensors built in smartphones or AR headsets (Gelenbe and Bi, 2014; Zhang et al., 2020c; Ahn and Han, 2011; Stigall and Sharma, 2017). In addition, Mulloni et al. exploited activity-based instructions to guide users from one info point to the next (Mulloni et al., 2011). In this system, only sparse 3D localization at selected info points in a building is necessary.

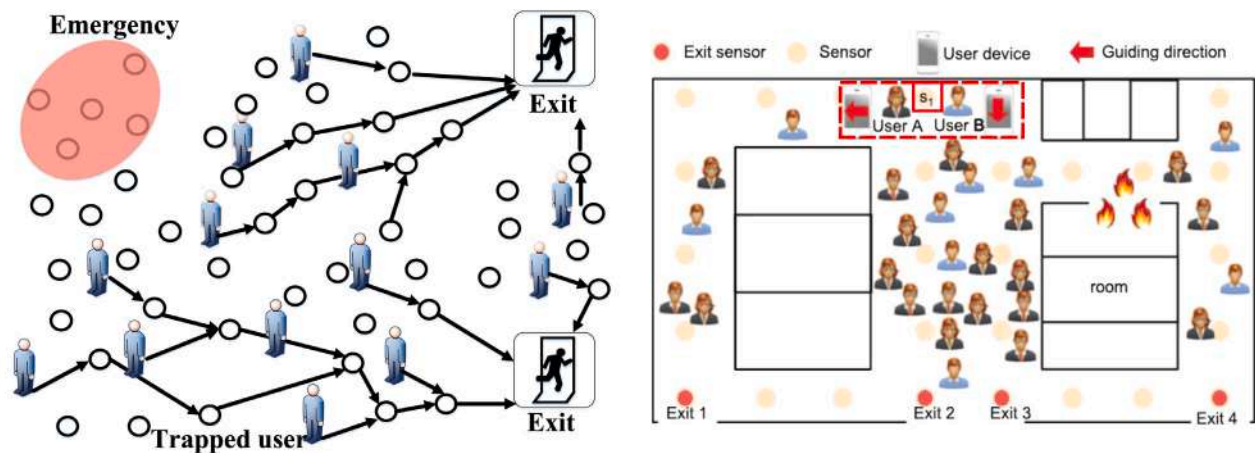


Fig. 5. The typical sensor-centric and user-centric evacuation scheme using WSN (Wang et al., 2017). In (b), sensor s_1 can provide different guiding directions for the User A and User B even though both of them are located nearby s_1 .

Fig. 5. The typical sensor-centric and user-centric evacuation scheme using WSN (Wang et al., 2017). In (b), sensor s_1 can provide different guiding directions for the User A and User B even though both of them are located nearby s_1 .

2.3.2. Location-free evacuation scheme using ME

The location information may not always be available in many realistic situations where emergency guidance is needed. Zheng et al. designed Peer-to-Peer (P2P) navigation systems on mobile phones, which enabled efficient navigation without resorting to pre-deployed location service and the availability of indoor maps (Zheng et al., 2017; Shu et al., 2015; Dong et al., 2019; Zhang et al., 2020b; Yin et al., 2016). In this kind of system, guiders recorded their traces in a variety of forms (e.g., pathway images, geomagnetic fields, or WiFi signals) and transmitted them to followers so that they could get prompt path instructions through their phones. However, P2P mode suffers from path deficiency in large complex indoor scenarios, which significantly hampers its application. Teng et al. merged the paths of different guiders into a global map by introducing a crowdsourcing scheme (Teng et al., 2019; Li et al., 2020; Pan and Li, 2019; Dong et al., 2020).

2.4. WSN-based evacuation scheme

WSN is a natural choice for supporting emergency evacuation, given the ubiquitous sensing and communication capability. Previous researches verified the effectiveness of WSN-assisted guiding mechanisms using simulations and real test-bed implementation approaches (Ahmed et al., 2015; Yin, 2015; Lung et al., 2016; Stigen, 2019). Fig. 5 shows the typical WSN-assisted emergency evacuation system. A number of sensor nodes are deployed in a building to monitor the time-varying environmental conditions, calculate guiding paths and send them to nearby evacuees equipped with radio modules. Existing WSN-assisted evacuation schemes can be divided into two classifications: the sensor-centric guiding scheme (Fig. 5(a)) and the user-centric guiding scheme (Fig. 5(b)). This section reviews the two types of evacuation schemes.

2.4.1. Sensor-centric evacuation scheme

In sensor-centric scheme, all people associated with the same sensor are provided with the same direction. Table 7 summarizes previous work on evacuation with WSNs. Some research assumed the availability of global knowledge about path topology and used global exhaustive search algorithms to determine optimal guiding routes. Buragohain et al. carried out a Breadth-First-Search (BFS) to calculate an optimal path. In addition, in order to reduce communication expenses, an adaptive skeleton graph was constructed in a distributed fashion (Buragohain et al., 2016). Filippopolitis et al. used the Dijkstra algorithm to calculate the path with the minimum effective length (Filippopolitis and Gelenbe, 2009). Wang et al. proposed a novel metric

of path planning named Expected Number of Oscillations (ENO) to quantify the dynamics of emergency. Based on ENO information, the path minimizing the probability of oscillation was found using a global exhaustive search algorithm (Wang et al., 2014a). Chen et al. provided the fastest routes for people to reach exits based on the evacuation time estimated by an analytical model that took into account corridor capacity and length, exit capacity, and concurrent movement and distribution of people (Chen et al., 2012b). Shen et al. employed the Dinic Algorithm to provide evacuees with navigation service, which reduced congestion and increased the evacuated ratio in a short time (Shen et al., 2011).

Instead of global search, Tseng et al. executed path planning based on local search algorithms (Tseng et al., 2006; Zhou et al., 2012; Chen et al., 2012a; Wang et al., 2017, 2013, 2015a; Li et al., 2003; Chen et al., 2011, 2008; Pan et al., 2006; Chen et al., 2016b; Park and Corson, 1997; Pooja et al., 2019). Wang et al. computed an artificial potential field for the corresponding state to generate optimal guiding direction (Wang et al., 2017; Li et al., 2003; Chen et al., 2008, 2011; Pooja et al., 2019). Chen et al. assigned sensor nodes temporally ordered sequence numbers to construct a directed navigation graph in a localized manner (Tseng et al., 2006; Chen et al., 2012a; Zhou et al., 2012; Chen et al., 2016b; Park and Corson, 1997; Pan et al., 2006). Wang et al. sought for a global or local topological structure as a public infrastructure to provide navigation information for internal queries, through which unnecessary overhead of individually path planning is avoided (Wang et al., 2015a, 2013).

2.4.2. User-centric evacuation scheme

The user-centric guiding system provides navigation directions for each individual user rather than for each sensor. As shown in Fig. 5(b), the sensor s_1 can provide different guiding directions for User A and User B even though both of them are nearby s_1 . The user-centric evacuation scheme relaxes the constraint on the number of guiding directions provided by a single sensor, which opens up more opportunities to optimize overall evacuation time. Wu et al. proposed a localized user-centric guiding protocol where the overall evacuation time is minimized with the consideration of the effect of hazards and the limited capacity of a certain sensor at a certain time slot (Wu, 2017).

3. Ship passenger evacuation

The consequences of an accident could be destructive for passenger ships, especially for luxury cruises. For example, thirty-two people were

Table 7
Crowd evacuation with WSNs.

Related work	Location-based/Location-free	Global/Local search	Method	Congestion-aware	Path metric
Buragohain et al. (2016)	Location-based	Global	BFS	×	Path length
Shen et al. (2011)	Location-based	Global	Dinic algorithm	✓	Evacuation time
Wang et al. (2014a)	Location-free	Global	OPEN	×	ENO
Chen et al. (2012b)	Location-based	Global	TORA	✓	Evacuation time
Pan et al. (2006), Tseng et al. (2006), Chen et al. (2012a) and Park and Corson (1997)	Location-based	Local	TORA	×	Path length
Zhou et al. (2012) and Chen et al. (2016b)	Location-based	Local	TORA	✓	Evacuation time
Filippopolitis and Gelenbe (2009)	Location-based	Global	Dijkstra algorithm	×	Effective length
Li et al. (2003)	Location-free	Local	Artificial potential field	×	Distance to dangers
Chen et al. (2008)	Location-based	Local	Artificial potential field	✓	Evacuation time
Chen et al. (2011)	Location-free	Local	Artificial potential field	✓	Evacuation time
Wang et al. (2017) and Pooja et al. (2019)	Location-free	Local	Artificial potential field	✓	Distance to dangers
Wang et al. (2015a)	Location-free	Local	Level set method	✓	Congestion level, Path length
Wang et al. (2013)	Location-free	Local	Road map	×	Distance to dangers

killed when the Costa Concordia capsized in 2012. In case of such a catastrophe, an appropriate evacuation strategy should be applied to reduce casualties. The land-based indoor evacuation approaches mentioned in Section 2 cannot be used directly to guide evacuees on passenger ships due to the specificities of ships' internal structure and passengers' behavior during evacuation. Compared with the mature land-based indoor evacuation, the research on evacuation on passenger ships is relatively limited and mainly focuses on three aspects from the view of intentions: (1) Investigation of the likely evacuation behavior of passengers; (2) Optimization of passenger evacuation for decreasing casualties; (3) Evaluation of evacuation on passenger ships. This section first presents the latest guideline on evacuation analysis for passenger ships, issued by International Maritime Organization (IMO), and then analyze the unique characteristics of ship passenger evacuation. Finally, a survey of existing research efforts on the evacuation of passenger ships is given.

3.1. Evaluation of the IMO guideline on ship evacuation

The international regulation "Safe Return to Port" specifies the design criteria that guarantee the return of the ship to the port when a casualty occurs. In such a case, passengers should move to the so-called Safe Areas. If the given threshold of damage is exceeded, it is necessary to abandon the ship and evacuate passengers to survival crafts. In both cases, the evacuation analysis must be performed. The latest guidelines concerning evacuation analysis for passenger ships are dictated by IMO in MSC.1/Circ.1533 (IMO, 2007). The guidelines allow evacuation analysis by either the simplified or the advanced method. The simplified analysis is based on a macroscopic model, treating passengers as the fluid that runs through corridors and stairs as if they are tubes. In this sort of analysis, the geometry of doorways, stairs and corridors, and the initial density of passengers are considered to calculate the total evacuation duration and identify the possible bottlenecks (Nasso et al., 2019). The advanced method simulates individual passengers, taking into account the particular features of passengers, such as the walking speed and the reaction time to an emergency. In this method, IMO-certified software (e.g., EVI and AENEAS), based on VR, is used to calculate the travel duration, including the response duration.

The regulations on safe return to port and evacuation analysis are of primary importance in the early stage of design for passenger ships to upgrade the intrinsic ship safety in event of casualties. In addition, these regulations provide standard scenarios and indexes for the evaluation of ship evacuation systems. The performance of a proposed ship evacuation scheme should be evaluated in day and night scenarios, in which the initial distribution of passengers on board is different. The

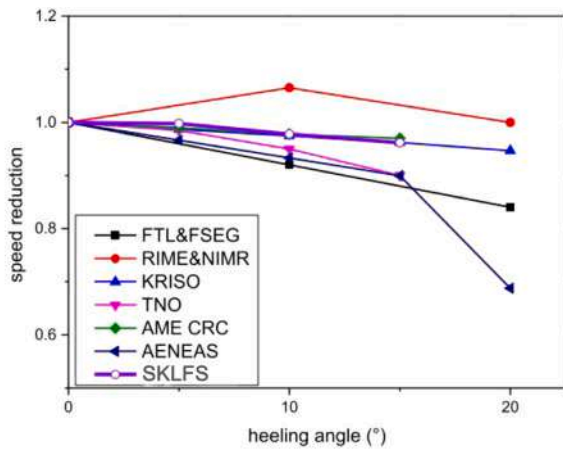
evacuation performance of a scheme should be measured in terms of the traversal time required for passengers to arrive at the Safe Areas when it is assumed that the accident does not exceed a fixed threshold. Otherwise, it should be measured by the duration until the launch of survival crafts.

3.2. Specificity of ship passenger evacuation

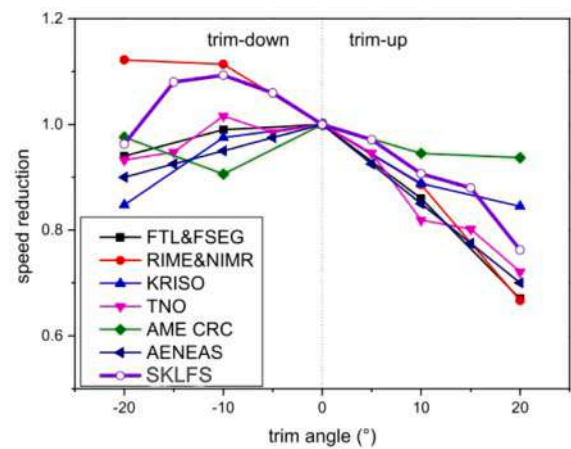
Based on the analysis of maritime accident investigation reports and case studies, as well as the data collection on a real passenger ship, this section describes the specificities of the evacuation environment and crowd behaviors during the emergency evacuation on passenger ships.

3.2.1. The influence of ship motion on passenger movement

The movement pattern of passengers on board is significantly different from that on the static ground because of the effect of ship inclination and motion. Many simulations and experiments have been performed to quantify the influence of ship inclination or motion on pedestrian speed. Fig. 6 presents the speed reduction data due to ship inclination from various international research projects (i.e., Fleet Technology Limited (FTL) and Fire Safety Engineering Group (FSEG) in the University of Greenwich, Research Institute of Marine Engineering of Japan (RIME) and National Maritime Research Institute of Japan (NIMR), Korea Research Institute of Ship and Ocean Engineering (KRISO), the Netherlands Organization for Applied Scientific Research (TNO), Australian Maritime Engineering Cooperative Research Centre (AME CRC), TraffGo HT GmbH using evacuation software AENEAS, and the Skate Key Laboratory of Fire Science in the University of Science and Technology of China (SKLFS)). In addition, Valanto et al., by means of evacuation software AENEAS, presented speed reduction factors in laterally and longitudinally tilted staircases as the function of ship inclination angle (see Eqs. (2)–(4)) (Valanto, 2006). ϕ denoted the slope angle; r_{trans} indicated the reduction factor in laterally tilted staircases; r_{longu} and r_{longd} were reduction factors when walking up and down longitudinally tilted staircases, respectively. Sun et al. exploited a ship corridor simulator to investigate the effect of heeling and trim on individual walking speed and group walking speed, respectively (Sun et al., 2018a,b). Chen et al. investigated the coupled-forced pedestrian movement features as a result of ship swaying using an agent-based pedestrian model (Chen et al., 2016a). Wang et al. carried out a series of walking experiments on a real ship to quantitatively evaluate the effect of different rolling angles on individual walking speed both on



(a) Speed reduction as a function of transverse slope in a corridor



(b) Speed reduction as a function of longitudinal slope in a corridor

Fig. 6. Speed reduction data under different situations from various international research projects.

flat terrains and staircases (Wang et al., 2021a).

$$r_{trans} = \begin{cases} -0.005\phi + 1 & 0^\circ \leq \phi < 20^\circ \\ -0.085\phi + 2.6 & 20^\circ \leq \phi < 30^\circ \\ 0.05 & 30^\circ \leq \phi \leq 40^\circ \\ 0 & 40^\circ < \phi \end{cases} \quad (1)$$

$$r_{longu} = \begin{cases} 0 & \phi < -45^\circ \\ 0.038\phi + 1.76 & -45^\circ \leq \phi < -20^\circ \\ 1 & -20^\circ \leq \phi < 0^\circ \\ -0.015\phi + 1 & 0^\circ \leq \phi \leq 20^\circ \\ -0.065\phi + 2 & 20^\circ \leq \phi < 30^\circ \\ 0.05\phi + 2.1 & 30^\circ \leq \phi \leq 45^\circ \\ 0 & 45^\circ < \phi \end{cases} \quad (2)$$

$$r_{longd} = \begin{cases} 0 & \phi < -45^\circ \\ 0.05 & -45^\circ \leq \phi < -30^\circ \\ 0.065\phi + 2 & -30^\circ \leq \phi < -20^\circ \\ 0.015\phi + 1 & -20^\circ \leq \phi < 0^\circ \\ 1 & 0^\circ \leq \phi < 15^\circ \\ -0.032\phi + 1.48 & 15^\circ \leq \phi \leq 45^\circ \\ 0 & 45^\circ < \phi \end{cases} \quad (3)$$

3.2.2. The feedback of crowd movement on ship motion

Crowd movement, in turn, can affect the motion of a ship. On September 26, 2002, MV Le Joola capsized off the coast of The Gambia with 1863 deaths (Rothe et al., 2006). The ship was submerged in just five minutes. According to the analysis of the relative maritime accident investigation reports, it is found that lopsided crowd movement is one of the main reasons for such fast sinking, which dramatically decreased the allowable evacuation time. There were about five hundred passengers on the upper deck before the disaster occurred, which ascended the ship's center of gravity and thus reduced ship stability. It was, therefore, more vulnerable to severe weather and sea states. Moreover, passengers on the upper deck swarmed to the port side to avoid storms from the starboard side, which undeniably accelerated the capsizing of MV Le Joola. The sinking of Phoenix PC Diving also revealed that it was critical for an evacuation scheme to take into account the feedback of crowd movement on ship motion. When danger arose, passengers on Phoenix PC Diving stampeded to the starboard side, which sped up the ship's overturning. Within only three minutes, it sank in the ocean near Phuket, Thailand, causing 47 deaths (Chen, 2021).

3.2.3. The influence of fire doors on path network connectivity

Fire doors with different fire resistance ratings are installed to reduce the spread of fire and smoke between separate components of a passenger ship to enable safe egress from a vessel (Perez Villalonga, 2005). Certain fire doors on vessels are hidden in normal situations and can be closed in the event of a fire, which is different from the fire doors in general buildings. Once the fire door is closed, it can only be opened from one side of the door. That is to say, certain corridors on vessels are unidirectionally passable due to the existence of fire doors, which makes the evacuation scenario on a passenger ship distinguishing. In addition, it takes a certain amount of time to open the fire doors, so the calculation of the traversal time on the related passageways is different from common ones.

3.2.4. Limited and predictable ship survival time

A passenger ship is required to have sufficient hydrostatic stability to survive certain damage cases. However, the required stability cannot guarantee the survival of the ship in all cases, especially if the accident takes place in unfavorable weather conditions or sea states. In such cases, the survival time until capsizing for the ship is limited. In order to survive, passengers must flee from the damaged ship within the limited ship survival time. The value of ship survival time depends on the loading condition of a vessel, the type, location, and extent of damage, and the probable weather condition and sea state in an operation area. Valanto et al. determined a method to estimate the survival time (Valanto, 2006). Firstly, when the significant wave height is great than or equal to 4.5 m, the survival time can be obtained with the help of the numerical simulation of ship motion. Fig. 7 shows some typical examples of simulated ship roll motion until capsizing, where angle 30° is considered as the capsizing criterion. The estimation of the survival time for the significant wave height lower than 4.5 m using numerical simulation is very ineffective in terms of computation time. In such cases, the survival time can be extrapolated with the following formula:

$$T_c = T_s \times e^{A + \frac{B}{h^2}} \quad (4)$$

where T_c represents the survival time of a vessel. T_s and h indicate the significant wave period and height, respectively. The constants A and B can be calculated by numerical simulation for higher wave height with the same wave period.

3.2.5. Limited capacity of muster station

A passenger ship has multiple muster stations that are the equivalent of evacuees' destinations (Bucci et al., 2016). Different from the land building evacuation, the muster stations on passenger ships give a

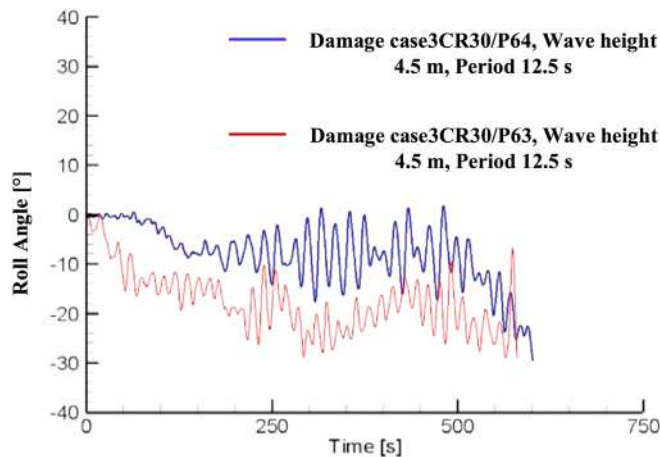


Fig. 7. Typical examples of simulated ship roll motion until capsizing.

limitation for routing selection due to the limited number of lifeboats and rafts in the stations (Qiao et al., 2014). When the embarkation and muster stations are not coincident, the capacity of each muster station is also limited due to the space limitation, which is determined in the ship design stage. Without considering the limited capacity of muster stations, passengers are likely to be guided to the stations that have no space to accommodate more evacuees, which would lead to a reassignment to another station, and thus inevitably prolongs the period required to navigate passengers to safety. Considering the resultant longer evacuation time, it is increasingly likely that passengers will eventually miss the limited ship survival time and consequently lose their lives when abandoning the ship becomes necessary.

3.2.6. Dependency on life-saving equipment for real survival

In case the damaged ship must be abandoned, passengers will be required to arrive at boarding stations and embark on lifeboats or rafts or jump into the water (Yoshida et al., 2001). In such cases, passengers need to equip themselves with life-saving equipment such as life vests and lifebuoys, which increases passengers' feelings of safety and their chance of survival. The minimum number of different life-saving equipment is defined in Safety of Life at Sea (SOLAS) regulations based on the size and passenger capacity of the ship (Ahola et al., 2014). Specifically, there are two life jackets in each passenger room, and at other specific locations (e.g., outside decks), a certain number of lifebuoys or jackets are distributed. If a passenger is not in the room when an emergency happens, it would be vital to consider the distribution of life-saving equipment in the path planning. For example, should they return to their cabins to collect life jackets, or should they head for other locations where pertinent appliances are placed?

3.2.7. Narrow and complex ship indoor space

The internal structure of a passenger ship is very complex, especially for state-of-the-art passenger ships with theaters, shops, swimming pools, and gyms (Stefanidis et al., 2019). Moreover, the width of corridors in cruises ranges from 1 m to 3 m, only allowing one or two passengers to pass simultaneously. However, with the increase in passenger capacity, there may be thousands of passengers on a cruise ship, which gives rise to congestion points. Without considering the heavy congestion and even blocking and trampling due to capacity constraints of pathways, it is likely to aggravate the extent of injuries and casualties.

3.3. Studies of ship passenger evacuation

There are three kinds of research focusing on ship passenger evacuation from the view of intentions, i.e., evacuation behavior study, passenger evacuation optimization, and evaluation of evacuation on passenger ships. Previous research on ship passenger evacuation is summarized in Table 8.

3.3.1. Passenger behaviors during evacuation

It is critical to study passengers' behaviors during a ship evacuation process. Valanto et al. investigated the moving characteristics of passengers considering the effect of ship inclination and motion (Valanto, 2006; Sun et al., 2018a; Chen et al., 2016a; Sun et al., 2018b; Wang et al., 2021a). Sun et al. investigated the effect of heeling and trim on individual walking speed using a ship corridor simulator (Sun et al., 2018a). Results showed that compared with trim angles, heeling angles had less impact on individual walking speed. Lu et al. explored the movement pattern of single file passengers under ship trim and heeling conditions (Sun et al., 2018b). Results indicated that as with individual walking speed, group speed was more vulnerable to heeling angles compared with trim angles. Moreover, the larger the inclination angle, the more the velocity between adjacent experimental subjects correlated. Chen et al. established an agent-based evacuation model taking into account the forced pedestrian movement pattern (Chen et al., 2016a). Simulations of single pedestrian movement indicated that pedestrian movement was significantly affected by the angle between pedestrian movement direction and ship swaying direction. Based on the primary data from a series of walking experiments on a real ship, Wang et al. analyzed the individual walking speed under different rolling conditions in two scenarios, i.e., flat terrains and staircases (Wang et al., 2021a). Other behaviors including cooperation with others, perception of wayfinding tools, proactive response to evacuation alarms, compliance with the crew, observation on others' actions, obedience to evacuation instructions, patient queuing, and return to the cabin when their families are left behind, were also investigated (Kwee-Meier et al., 2017; Wang et al., 2021b; Zhang et al., 2020a). In addition, Wang et al. addressed the demographic differences among these behaviors (Wang et al., 2020).

Some research focused on the factors affecting passengers' evacuation behaviors (Li et al., 2021). With the help of hypothesis testing, Zhang et al. analyzed the relationship between personnel characteristics (e.g., blood type and personality type) and evacuation behaviors (e.g., the first response to a fire alarm and the possibility of return for properties) (Zhang et al., 2020a). Ahola et al. conducted user studies in an authentic environment to assess the themes pertaining to passenger perception of safety (Ahola et al., 2014; Ahola and Mugge, 2017). Based on ship accident investigation reports, Nevalainen et al. found that both external stimuli, including alarm sound, abnormal noise, and the darkness caused by a blackout, and inner emotion could affect how passengers process and interpret environmental cues under emergencies (Nevalainen et al., 2015).

3.3.2. Passenger evacuation optimization

Regarding passenger evacuation optimization, the plan of escaping routes, the optimization of staircase layout, and the schedule of the time for issuing evacuation orders have attracted the attention of many researchers. Casareale et al. demonstrated the effectiveness of wayfinding systems in improving evacuation on cruise ships (Casareale et al., 2017). Ni et al. applied a goal-driven decision-making model to create a concrete escape plan (Ni et al., 2017). Ng et al. iteratively utilized a modification of the scheduling algorithm introduced by Leung and Ng to find a schedule for different groups at risk, which minimized the time of evacuating all people with the least total cost (Ng et al., 2021). Based on a SF model, Wang et al. optimized the staircase layout on a Ro-Ro vessel to reduce evacuation time (Wang et al., 2022). Xie proposed a surrogate-based optimization method to determine the time for issuing evacuation orders so that the assembly time could be minimized (Xie et al., 2020c).

Table 8
Ship passenger evacuation.

Research intentions	Research content	Technique	Implemented in
Passenger evacuation behavior	Moving characteristic	Simulation with agent-based models, Full-scale experiment on ships, Experiment with simulators	Valanto (2006), Sun et al. (2018a), Chen et al. (2016a), Sun et al. (2018b) and Wang et al. (2021a)
	Perception of wayfinding tools	Experiment in simulated conditions, Questionnaire survey	Wang et al. (2020), Kwee-Meier et al. (2017) and Wang et al. (2021b)
	External and internal factors affecting passengers' behaviors	Experiment in simulated conditions, Passenger ship accident investigation reports, Full-scale experiments on ships, Questionnaire survey	Ahola et al. (2014), Nevalainen et al. (2015), Ahola and Mugge (2017) and Zhang et al. (2020a)
Passenger evacuation optimization	Effectiveness of wayfinding solutions	Simulation with SF model	Casareale et al. (2017)
	Staircase layout optimization	Simulation with SF model	Wang et al. (2022)
	Optimization of issuance of passenger evacuation orders	Genetic algorithm	Xie et al. (2020c)
	Optimization of evacuation path	BFS, Leung–Ng fast approximation scheduling algorithm	Ni et al. (2017) and Ng et al. (2021)
Passenger evacuation evaluation	Reliability of evacuation	Bayesian network parameter learning method, Risk-based methodology, K2 structure learning algorithm	Wang et al. (2021c) and Vanem and Skjong (2006)
	Evacuation process estimation	Simulation with SF model, Modeling with Batch NHPP, Simulation with grid-based model, Dynamic Bayesian network, Markov decision process, Polynomial chaos expansion	Kang et al. (2019), Ni et al. (2017), Hifi (2017), Vilen et al. (2020), Galea et al. (2015), Sarshar et al. (2013), Kana and Droste (2019) and Xie et al. (2020a,b)

3.3.3. Evaluation of evacuation on passenger ships

The evacuation process can be analyzed in two ways: advanced analyses and simplified analyses. The advanced analysis treats each passenger as an individual with his/her characteristic and behavior. Ni *et al.* proposed an extended SF model that considered the resistance force from obstacles in cabins to govern the movement of passengers (Ni *et al.*, 2017). Kang *et al.* incorporated the psychological tendency of pedestrians to slip downhill into the SF model to simulate evacuation behaviors on inclined shipwrecks (Kang *et al.*, 2019). Vilen *et al.* evaluated two advanced evacuation analysis software packages, i.e., Evi and Pathfinder, in terms of numerical results and user experience (Vilen *et al.*, 2020). Galea *et al.* did an experimental validation of the evacuation model maritimeEXODUS using two data sets generated from semi-unannounced assembly trials on a RO-PAX ferry and a cruise ship (Galea *et al.*, 2015). Results showed that the model was capable of predicting the assembly process for the two vessels to a specified level of accuracy. In addition, Hifi *et al.* described a set of scenarios for performing advanced evacuation analysis and recommended a survey of population composition and ship familiarity before the evacuation analysis to improve analysis accuracy (Wang *et al.*, 2022; Hifi, 2017). However, the advanced analysis is very time-consuming, and thus when a fast assessment of evacuation time is needed, it is not a suitable option. Cho *et al.* developed a simplified analysis solution that took a macroscopic view of the evacuation process, treating passengers as homogeneous particles in a fluid (Cho *et al.*, 2016). Sarshar *et al.* developed a dynamic Bayesian network model that considered the most vital factors influencing congestion (e.g., panic, age, sex, and the presence of rescue personnel) to predict the probability of congestion during the entire process of an evacuation (Sarshar *et al.*, 2013). Xie *et al.* established a surrogate model using a coupling technique of nested sampling and polynomial chaos expansion method to estimate passenger travel time uncertainty with acceptable accuracy (Xie *et al.*, 2020b,a). Kana *et al.* presented a ship-centric Markov decision process model for evaluating the evacuation during the preliminary design phase of a passenger ship (Kana and Droste, 2019). The simplified analysis ignored the different elements of an evacuation process and thus could not mirror passengers' movement. Hifi *et al.* developed a parametric model that could produce a fast estimate of evacuation time while capturing the factors influencing the evacuation to satisfactory accuracy (Hifi, 2017).

The quantitative evaluation of evacuation on ships is also essential. Wang *et al.* investigated the main factors leading to evacuation failure and established a model using the K2 structure learning algorithm and the Bayesian network parameter learning method to quantify the probability of a successful evacuation (Wang *et al.*, 2021c). Vanem *et al.* developed a risk-based approach to evaluate the evacuation performance associated with a specific passenger ship using the proposed set of evacuation scenarios (Vanem and Skjong, 2006).

4. Discussion and future directions

This section evaluates the above land-based evacuation schemes and delineates our insights into the future research perspectives for ship passenger evacuation.

4.1. Comment on land-based evacuation

Significant research works on building evacuation have been carried out. Based on different types of guidance patterns, a classification of land-based evacuation schemes is proposed, including signage-based evacuation, leader-based evacuation, ME-based evacuation, and WSN-based evacuation.

In Section 2.1, the review of land-based indoor evacuation with fixed and variable signage is provided. The latter can respond to contemporary environmental conditions and present up-to-date guiding information. However, pedestrians may not find signs in smoky conditions. Even under clear conditions, they are likely to neglect the signs at specific locations or cannot fully understand the content of signs during emergencies due to their anxiety and panic. In such emergencies, evacuation leaders with complete knowledge of the layout of a building can provide guiding instructions for occupants and significantly reduce casualties. Compared with human leaders, robotic leaders can be sent to guide evacuees out in several special accidents like nuclear leakage. An emergency evacuation system is requested to provide a time-critical guiding service. But for the leader-based evacuation system, it will take a significant amount of time to arrange leaders to appropriate locations. Therefore, evacuating through the equipped device (e.g., smartphone) regularly used in everyday life for all pedestrians is very attractive. However, the downsides to the three kinds of evacuation schemes are as follows: (1) Without real-time indoor environment monitoring, evacuation routes provided by these schemes are not necessarily passable due

to the encroachment of hazards; (2) Passengers observing the same sign or leader or near the same beacon will escape along the same direction, which inevitably causes heavy congestions, trampling and possible injuries and casualties. The WSN-based evacuation scheme is capable of exploring dynamic environmental conditions by means of the collaborative detection of sensor nodes. But sensor-centric WSN-based evacuation scheme is only effective on the first downside mentioned above, while powerless to solve the second problem. Therefore, a user-centric WSN-based evacuation scheme will be a good choice for a modern building.

4.2. Prospects for ship passenger evacuation

Compared with the land-based evacuation, there are some specific features for passenger ship evacuation due to the uniqueness of ship structure, passenger behaviors onboard, and evacuation requirements at sea. Therefore, personalized evacuation approaches for ship passengers are indispensable. However, in contrast to the relatively mature land-based evacuation schemes, the research on ship evacuation is still in its infancy and focuses on investigating the likely behaviors of passengers. Design or optimization of evacuation routes targeting ship passengers is also critical but scarce. Drawing from the four types of land-based evacuation schemes mentioned in Section 2, the prospects for the evacuation system of modern cruise ships are discussed in this section.

A WSN with functionally-separated sensors like tilt sensors, hydraulic pressure sensors, temperature sensors, and smoke sensors is deployed on a modern cruise ship. When an emergency takes place, the sensors will initiate a danger alarm and transmit the current locations and levels of hazards to a path planning server. In addition, the current position of each passenger is detected using the received strength of wireless signals on his/her smartphone, and the sensor ID with the strongest signal strength is used to determine the passenger's position in the blueprint database of sensor deployment. That is to say, the proposed scheme does not require accurate location information on each passenger. The smartphone periodically sends the determined position to the path planning server. According to the obtained information, the server will compute a dedicated escape route for each individual and broadcast it to his/her smartphone. The reason for selecting smartphones as guides during emergencies is that nowadays almost everyone has a smartphone and familiarity with their own smartphones can increase passengers' feelings of safety. Fig. 8 shows the system architecture of our proposed emergency guiding scheme for ship passengers. Red rectangles represent sensor nodes deployed at muster stations, doors, and crossing points among corridors and/or doors on a passenger ship in advance. The Wi-Fi access point is used for maintaining the communication between the smartphones and the path planning server. The following is a list of properties of evacuation routes provided to passengers:

- The path is apart from hazardous regions and through which a passenger can arrive at a specific exit before the ship capsizes under all circumstances.
- The total evacuation time of passengers should be reduced as much as possible. To realize this goal, an evacuation system has to consider not just the relative distance from the passenger to the muster station, but the movement speed on the route, the capacity of the route, and the up-to-date distribution as well as the spatial-temporal mobility of all passengers.
- The evacuation routes should be provided to passengers in a real-time manner.
- Escaping along the provided route, each passenger would have obtained a piece of saving-life equipment when arriving at the muster station.
- Following the offered direction would not speed up the ship leaning to one side.

- Passengers would not be guided to a muster station that cannot accommodate more evacuees.
- Except for guaranteeing passengers' safety, the evacuation system should also maintain the integrity of a passenger ship as much as possible.

The proposed architecture is attractive but challenging, due to the restricted battery power of low-cost sensor nodes and the ad-hoc routing protocol of a WSN in a large and complicated ship indoor space. Specifically, as the information regarding the environment is forwarded over multiple hops towards a gateway, some sensors get more congested than others, depending on their location. Therefore, they deplete their batteries quickly, shortening the overall network lifetime. In addition, considering the dynamics of the hazardous environment, the routing protocol in WSN functions poorly in the evacuation application. Because in order to ensure passengers' safety, frequent flooding is required to update the escaping paths in the rapidly changing environment, which may trigger many simultaneous bursts of broadcast packets throughout the network and thus cause a large number of packet collisions. The calculation of all routes is performed in the path planning server. So in case it malfunctions during the emergency, our evacuation system will break down. Moreover, while the potential of our proposed architecture to improve access to real-time monitoring and even intuitive and reliable navigation instruction can be provided to evacuees, concerns about personal data privacy remain. User data may be inadequately disclosed or transmitted to commercial entities by smartphone applications (apps) for ship passenger evacuation.

With the emergence of Low Power Wide Area Network (LPWAN) technologies, one type of WSN, which is designed for long-range Internet of Things (IoT) services, the above challenges from WSNs will hopefully bear solved. LPWAN IoT devices consume low transmission power but have a communication distance of several kilometers, so they can directly transmit the information pertaining to the environment to the path planning server and thus avoid the network breakdown caused by packet collisions. In addition, benefiting from the development of edge computing, in the future the distributed approach can be used to provide paths for passengers so as to reduce and even release the dependency on the path planning server. Moreover, given the negative impacts of inadequate privacy disclosures, data protection becomes particularly important. On the one hand, the anonymization technology can be adopted for the utilization of the results of analysis of the exchanged data, which includes passengers' sensitive personalized contexts (e.g., information about passengers' physical and psychological status) (Shinzaki et al., 2016). On the other hand, government regulation and up-to-date technical scrutiny are also essential for avoiding privacy leakages (Huckvale et al., 2019).

In addition, with the development of Extended Reality (XR) technology, VR-based or AR-based experiments can be introduced as an alternative method of post-emergency investigation and hypothetical survey to study passenger behavior during ship emergencies. XR-based experiments can arouse passengers' behavioral responses to virtual emergencies and thus provide the opportunity to collect evacuation behavior data with relatively high ecological validity. Taking into account passengers' behaviors, the designed evacuation system will be more effective at ensuring the safety and reliability of evacuation in reality. Moreover, it is possible to develop VR-based Serious Games (SGs) to train passengers to utilize the proposed evacuation scheme to escape, which is an effective approach to acquiring and retaining evacuation knowledge. It is also possible to substitute smartphones in the proposed architecture with AR devices that can provide more intuitive guidance for passengers.

5. Conclusion

This paper provides a survey of research efforts on crowd evacuation both in general buildings and on passenger ships. A comprehensive

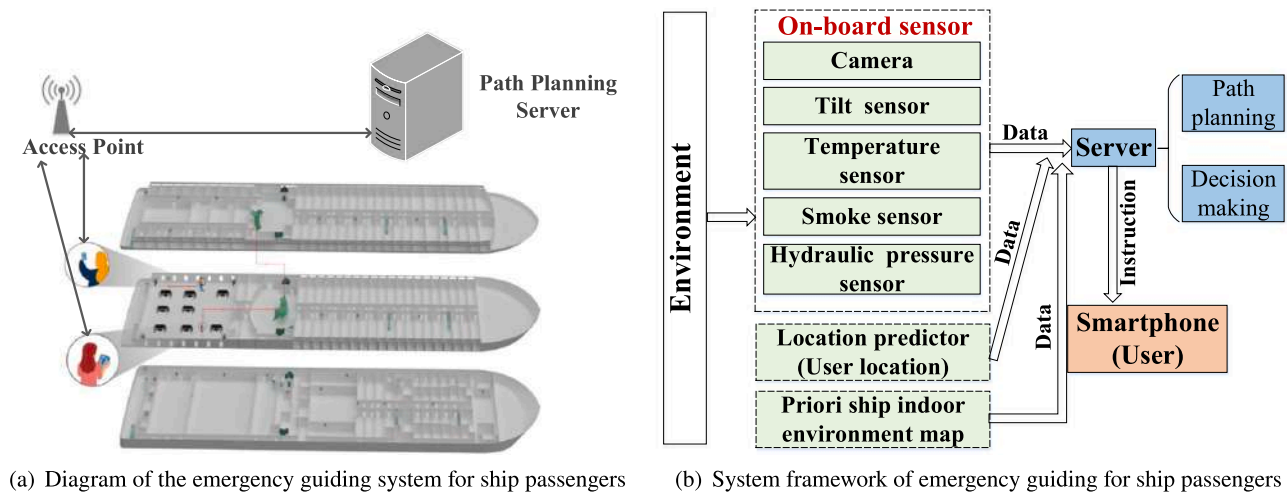


Fig. 8. System architecture of the emergency guiding scheme for ship passengers. (For interpretation of the references to color in this figure legend, the reader is referred to the web version of this article.)

analysis and synthesis of different kinds of guidance patterns for evacuation in land-based buildings, including signage-based, leader-based, ME-based, and WSN-based evacuation schemes, is presented. Those schemes are not used directly for ship passenger evacuation due to the unique challenges of guiding passengers on vessels. Section 3 analyzes the specificities of both evacuation environment and crowd behavior during the emergency evacuation on passenger ships. In addition, the existing work on evacuation for passenger ships are reviewed. Comments on land-based evacuation schemes and future research directions on ship passenger evacuation are also discussed. In the future, more intelligent and personalized guidance systems will be designed and implemented to improve the safety and efficiency of ship passenger evacuation.

Declaration of competing interest

The authors declare that they have no known competing financial interests or personal relationships that could have appeared to influence the work reported in this paper.

Data availability

Data will be made available on request.

Acknowledgments

The authors thank the anonymous reviewers for their insightful comments. This work was partially supported by the National Natural Science Foundation of China (NSFC) under Grant 51979216, and partially by the Natural Science Foundation of Hubei Province, China, under Grant 2021CFA001.

References

- Ahmed, A.A., Al-Shaboti, M., Al-Zubairi, A., 2015. An indoor emergency guidance algorithm based on wireless sensor networks. In: 2015 International Conference on Cloud Computing. ICC3, IEEE, pp. 1–5.
- Ahn, J., Han, R., 2011. Rescueme: An indoor mobile augmented-reality evacuation system by personalized pedometry. In: 2011 IEEE Asia-Pacific Services Computing Conference. IEEE, pp. 70–77.
- Ahola, M., Mugge, R., 2017. Safety in passenger ships: The influence of environmental design characteristics on people's perception of safety. *Applied Ergon.* 59, 143–152.
- Ahola, M., Murto, P., Kujala, P., Pitknen, J., 2014. Perceiving safety in passenger ships—User studies in an authentic environment. *Saf. Sci.* 70, 222–232.
- Boukas, E., Kostavelis, I., Gasteratos, A., Sirakoulis, G.C., 2015. Robot guided crowd evacuation. *IEEE Trans. Autom. Sci. Eng.* 12 (2), 739–751.

- Bucci, V., Marino, A., Mauro, F., Nabergoj, R., Nasso, C., 2016. On advanced ship evacuation analysis. In: *Engineering Mechanics 2016-22nd International Conference*. Institute of Thermomechanics Academy of Science of the Czech Republic, pp. 105–112.
- Buragohain, C., Agrawal, D., Suri, S., 2010. Distributed navigation algorithms for sensor networks. In: *Proceedings of the 25th International Conference on Computer Communications*. IEEE, pp. 1–10.
- Cao, S., Song, W., Lv, W., 2016. Modeling pedestrian evacuation with guiders based on a multi-grid model. *Phys. Lett. Sect. A: Gen. At. Solid State Phys.* 380 (4), 540–547.
- Casareale, C., Bernardini, G., Bartolucci, A., Marincioni, F., D'Orazio, M., 2017. Cruise ships like buildings: Wayfinding solutions to improve emergency evacuation. *Build. Simul.* 10 (6), 989–1003.
- Chen, L., 2021. Research on the differences of disaster reports in Chinese and American media from the cross-cultural perspective. In: *2021 4th International Conference on Humanities Education and Social Sciences (ICHESS 2021)*. Atlantis Press, pp. 2716–2721.
- Chen, W.-T., Chen, P.-Y., Wu, C.-H., Huang, C.-F., 2008. A load-balanced guiding navigation protocol in wireless sensor networks. In: *IEEE GLOBECOM 2008-2008 IEEE Global Telecommunications Conference*. IEEE, pp. 1–6.
- Chen, L.-W., Cheng, J.-H., Tseng, Y.-C., 2012b. Evacuation time analysis and optimization for distributed emergency guiding based on wireless sensor networks. In: *2012 International Conference on Connected Vehicles and Expo. ICCVE, IEEE*, pp. 130–135.
- Chen, L.W., Cheng, J.H., Tseng, Y.C., 2015. Optimal path planning with spatial-temporal mobility modeling for individual-based emergency guiding. *IEEE Trans. Syst. Man Cybern.: Syst.* 45 (12), 1491–1501.
- Chen, L.W., Cheng, J.H., Tseng, Y.C., 2016b. Distributed emergency guiding with evacuation time optimization based on wireless sensor networks. *IEEE Trans. Parallel Distrib. Syst.* 27 (2), 419–427.
- Chen, L.-W., Chung, J.-J., 2017. Mobility-aware and congestion-relieved dedicated path planning for group-based emergency guiding based on internet of things technologies. *IEEE Trans. Intell. Transp. Syst.* 18 (9), 2453–2466.
- Chen, P.Y., Kao, Z.F., Chen, W.T., Lin, C.H., 2011. A distributed flow-based guiding protocol in wireless sensor networks. In: *Proceedings of the International Conference on Parallel Processing*. IEEE, pp. 105–114.
- Chen, C., Li, Q., Kaneko, S., Chen, J., Cui, X., 2009. Location optimization algorithm for emergency signs in public facilities and its application to a single-floor supermarket. *Fire Saf. J.* 44 (1), 113–120.
- Chen, L.W., Liu, J.X., 2021. Time-efficient indoor navigation and evacuation with fastest path planning based on internet of things technologies. *IEEE Trans. Syst. Man Cybern.: Syst.* 51 (5), 3125–3135.
- Chen, J., Ma, J., Lo, S., 2016a. Modelling pedestrian evacuation movement on a swaying ship. In: *Traffic and Granular Flow'15*. Springer, pp. 297–304.
- Chen, D., Mohan, C.K., Mehrotra, K.G., Varshney, P.K., 2012a. Distributed in-network path planning for sensor network navigation in dynamic hazardous environments. *Wirel. Commun. Mob. Comput.* 12 (8), 739–754.
- Chiou, M.-R., Chao, S.-L., Hsieh, H.-Y., 2021. The moderating role of service recovery on customer loyalty in the context of cruise passengers. *Marit. Policy Manag.* 48 (2), 150–166.
- Chittaro, L., Nadalutti, D., 2008. A mobile RFID-based system for supporting evacuation of buildings. In: *International Workshop on Mobile Information Technology for Emergency Response*. Springer, pp. 22–31.
- Cho, Y.-O., Ha, S., Park, K.-P., 2016. Velocity-based egress model for the analysis of evacuation process on passenger ships. *J. Mar. Sci. Technol.* 24 (3), 12.

- Cho, J., Lee, G., Lee, S., 2015a. An automated direction setting algorithm for a smart exit sign. *Autom. Constr.* 59, 139–148.
- Cho, J., Lee, G., Lee, S., 2015b. An automated direction setting algorithm for a smart exit sign. *Autom. Constr.* 59, 139–148.
- Chu, L., 2010. A RFID-based hybrid building fire evacuation system on mobile phone. In: *Proceedings of the 6th International Conference on Intelligent Information Hiding and Multimedia Signal Processing, IHHMSP 2010*. IEEE, pp. 155–158.
- Chu, J.C., Chen, A.Y., Lin, Y.-F., 2017. Variable guidance for pedestrian evacuation considering congestion, hazard, and compliance behavior. *Transp. Res. C* 85, 664–683.
- Chu, L., Wu, S.J., 2011. A real-time decision support with cloud computing based fire evacuation system. In: *Proceedings of the 16th North-East Asia Symposium on Nano, Information Technology and Reliability, NASNIT 2011*. IEEE, pp. 45–48.
- Chu, J.C., Yeh, C.-Y., 2012. Emergency evacuation guidance design for complex building geometries. *J. Infrastruct. Syst.* 18 (4), 288–296.
- Cosma, G., Ronchi, E., Nilsson, D., 2016. Way-finding lighting systems for rail tunnel evacuation: A virtual reality experiment with Oculus Rift. *J. Transp. Saf. Secur.* 8 (sup1), 101–117.
- Desmet, A., Gelenbe, E., 2014. Capacity based evacuation with dynamic exit signs. In: *2014 IEEE International Conference on Pervasive Computing and Communication Workshops (PERCOM WORKSHOPS)*. IEEE, pp. 332–337.
- Diao, P.-H., Shih, N.-J., 2018. MARINS: A mobile smartphone AR system for pathfinding in a dark environment. *Sensors* 18 (10), 3442.
- Dong, E., Liang, J., Wang, Z., Xu, J., Shangquan, L., Ma, Q., Yang, Z., 2020. Improving the applicability of visual peer-to-peer navigation with crowdsourcing. In: *Proceedings of the 26th International Conference on Parallel and Distributed Systems (ICPADS)*. pp. 188–195.
- Dong, E., Xu, J., Wu, C., Liu, Y., Yang, Z., 2019. Pair-navi: Peer-to-peer indoor navigation with mobile visual slam. In: *IEEE Conference on Computer Communications. INFOCOM, IEEE*, pp. 1189–1197.
- Feng, Y., Duives, D.C., Hoogendoorn, S.P., 2021. Using virtual reality to study pedestrian exit choice behaviour during evacuations. *Saf. Sci.* 137, 105158.
- Ferranti, E., Trigoni, N., 2008. Robot-assisted discovery of evacuation routes in emergency scenarios. In: *Proceedings of the International Conference on Robotics and Automation. IEEE*, pp. 2824–2830.
- Filippopolitis, A., Gelenbe, E., 2009. A distributed decision support system for building evacuation. In: *Proceedings of the 2nd Conference on Human System Interactions. IEEE*, pp. 323–330.
- Fowler, T.G., Sorgaard, E., 2000. Modeling ship transportation risk. *Risk Anal.* 20 (2), 225–244.
- Fujihara, A., Miwa, H., 2012. Effect of traffic volume in real-time disaster evacuation guidance using opportunistic communications. In: *Proceedings of the 4th International Conference on Intelligent Networking and Collaborative Systems (INCoS)*. IEEE, pp. 457–462.
- Fujihara, A., Yanagizawa, T., 2015. Proposing an extended ibeacon system for indoor route guidance. In: *2015 International Conference on Intelligent Networking and Collaborative Systems. IEEE*, pp. 31–37.
- Galea, E.R., Deere, S., Brown, R., Filippidis, L., 2015. An experimental validation of an evacuation model using data sets generated from two large passenger ships. *Trans. Soc. Naval Archit. Mar. Eng.* 121 (3), 370–385.
- Galea, E., Xie, H., Deere, S., Cooney, D., Filippidis, L., 2017a. An international survey and full-scale evacuation trial demonstrating the effectiveness of the active dynamic signage system concept. *Fire Mater.* 41 (5), 493–513.
- Galea, E.R., Xie, H., Deere, S., Cooney, D., Filippidis, L., 2017b. Evaluating the effectiveness of an improved active dynamic signage system using full scale evacuation trials. *Fire Saf. J.* 91 (2001), 908–917.
- Garrell, A., Sanfeliu, A., Moreno-Noguer, F., 2009. Discrete time motion model for guiding people in urban areas using multiple robots. In: *2009 IEEE/RSJ International Conference on Intelligent Robots and Systems (IROS)*. pp. 486–491.
- Gelenbe, E., Bi, H., 2014. Emergency navigation without an infrastructure. *Sensors* 14 (8), 15142–15162.
- Hifi, Y., 2017. Probabilistic Modelling of the Process of Evacuation for Ship Crises Management (Ph.D. thesis). University of Strathclyde.
- Hou, L., Liu, J.-G., Pan, X., Wang, B.-H., 2014. A social force evacuation model with the leadership effect. *Physica A* 400, 93–99.
- Huckvale, K., Torous, J., Larsen, M.E., 2019. Assessment of the data sharing and privacy practices of smartphone apps for depression and smoking cessation. *JAMA Netw. Open* 2 (4), e192542.
- Hui, X., Galea, E.R., Lawrence, P.J., 2014. Experimental and survey studies on the effectiveness of dynamic signage systems. *Fire Saf. Sci.* 11, 1129–1143.
- Iizuka, Y., Iizuka, K., 2015. Disaster evacuation assistance system based on multi-agent cooperation. In: *2015 48th Hawaii International Conference on System Sciences. IEEE*, pp. 173–181.
- Ikeda, Y., Inoue, M., 2016. An evacuation route planning for safety route guidance system after natural disaster using multi-objective genetic algorithm. *Procedia Comput. Sci.* 96, 1323–1331.
- IMO, 2007. Guidelines for Evacuation Analysis for New and Existing Passenger Ships. MSC. 1/Circ. 1238, International Maritime Organization, London, UK.
- Inoue, Y., Sashima, A., Ikeda, T., Kurumatani, K., 2008. Indoor emergency evacuation service on autonomous navigation system using mobile phone. In: *2008 Second International Symposium on Universal Communication. IEEE*, pp. 79–85.
- Jiang, C., Ni, Z., Guo, Y., He, H., 2017. Learning human–robot interaction for robot-assisted pedestrian flow optimization. *IEEE Trans. Syst. Man Cybern.: Syst.* 49 (4), 797–813.
- Kana, A.A., Droste, K., 2019. An early-stage design model for estimating ship evacuation patterns using the ship-centric Markov decision process. *Proc. Inst. Mech. Eng. M* 233 (1), 138–149.
- Kang, Z., Zhang, L., Li, K., 2019. An improved social force model for pedestrian dynamics in shipwrecks. *Appl. Math. Comput.* 348, 355–362.
- Kim, Y.D., Kim, Y.G., Lee, S.H., Kang, J.H., An, J., 2009. Portable fire evacuation guide robot system. In: *2009 IEEE/RSJ International Conference on Intelligent Robots and Systems (IROS)*. IEEE, pp. 2789–2794.
- Kwee-Meier, S.T., Mertens, A., Schlick, C.M., 2017. Age-related differences in decision-making for digital escape route signage under strenuous emergency conditions of tilted passenger ships. *Applied Ergon.* 59, 264–273.
- Langner, N., Kray, C., 2014. Assessing the impact of dynamic public signage on mass evacuation. In: *Proceedings of the 3rd ACM International Symposium on Pervasive Displays*. pp. 136–141.
- Li, Y., Cai, W., Kana, A.A., 2019. Design of level of service on facilities for crowd evacuation using genetic algorithm optimization. *Saf. Sci.* 120, 237–247.
- Li, Y., Cai, W., Kana, A., Atasoy, B., 2021. Modelling route choice in crowd evacuation on passenger ships. *Int. J. Marit. Eng.* 163 (A2).
- Li, Q., De Rosa, M., Rus, D., 2003. Distributed algorithms for guiding navigation across a sensor network. In: *Proceedings of the 9th Annual International Conference on Mobile Computing and Networking*. pp. 313–325.
- Li, T., Han, D., Chen, Y., Zhang, R., Zhang, Y., Hedgpath, T., 2020. IndoorWaze: A crowdsourcing-based context-aware indoor navigation system. *IEEE Trans. Wireless Commun.* 19 (8), 5461–5472.
- Li, W., Li, Y., Yu, P., Gong, J., Shen, S., 2016. The Trace Model: A model for simulation of the tracing process during evacuations in complex route environments. *Simul. Model. Pract. Theory* 60, 108–121.
- Lin, J., Cao, L., Li, N., 2019. Assessing the influence of repeated exposures and mental stress on human wayfinding performance in indoor environments using virtual reality technology. *Adv. Eng. Inform.* 39, 53–61.
- Lin, H.-M., Chen, S.-H., Kao, J., Lee, Y.-M., Hsiao, G.L.-K., Lin, C.-Y., 2017. Applying active dynamic signage system in complex underground construction. *Int. J. Sci. Eng. Res.* 8 (2).
- Lin, J., Zhu, R., Li, N., Becerik-Gerber, B., 2020. Do people follow the crowd in building emergency evacuation? A cross-cultural immersive virtual reality-based study. *Adv. Eng. Inform.* 43, 101040.
- Liu, J., Zhang, J., Yan, X., Soares, C.G., 2022. Multi-ship collision avoidance decision-making and coordination mechanism in Mixed Navigation Scenarios. *Ocean Eng.* 257, 111666.
- Liu, M., Zheng, X., Cheng, Y., 2011. Determining the effective distance of emergency evacuation signs. *Fire Saf. J.* 46 (6), 364–369.
- Lovreglio, R., Gonzalez, V., Feng, Z., Amor, R., Spearpoint, M., Thomas, J., Trotter, M., Sacks, R., 2018. Prototyping virtual reality serious games for building earthquake preparedness: The Auckland City Hospital case study. *Adv. Eng. Inform.* 38, 670–682.
- Luh, P.B., Wilkie, C.T., Chang, S.C., Marsh, K.L., Olderman, N., 2012. Modeling and optimization of building emergency evacuation considering blocking effects on crowd movement. *IEEE Trans. Autom. Sci. Eng.* 9 (4), 687–700.
- Lung, C., Sabou, S., Buchman, A., 2016. Wireless sensor networks as part of emergency situations management system. In: *2016 IEEE 22nd International Symposium for Design and Technology in Electronic Packaging (SIITME)*. IEEE, pp. 240–243.
- Ma, Y., Lee, E.W.M., Shi, M., 2017. Dual effects of guide-based guidance on pedestrian evacuation. *Phys. Lett. Sect. A: Gen. At. Solid State Phys.* 381 (22), 1837–1844.
- Ma, Y., Yuen, R.K.K., Lee, E.W.M., 2016. Effective leadership for crowd evacuation. *Physica A* 450, 333–341.
- Mileski, J.P., Wang, G., Beacham IV, L.L., 2014. Understanding the causes of recent cruise ship mishaps and disasters. *Res. Transp. Bus. Manag.* 13, 65–70.
- Motamedi, A., Wang, Z., Yabuki, N., Fukuda, T., Michikawa, T., 2017. Signage visibility analysis and optimization system using BIM-enabled virtual reality (VR) environments. *Adv. Eng. Inform.* 32, 248–262.
- Mulloni, A., Seichter, H., Schmalstieg, D., 2011. Handheld augmented reality indoor navigation with activity-based instructions. In: *Mobile HCI 2011 - 13th International Conference on Human-Computer Interaction with Mobile Devices and Services*. pp. 211–220.
- Nadalutti, D., Chittaro, L., 2008. Presenting evacuation instructions on mobile devices by means of location-aware 3D virtual environments. In: *Proceedings of the 10th International Conference on Human Computer Interaction with Mobile Devices and Services*. pp. 395–398.
- Nasso, C., Bertagna, S., Mauro, F., Marino, A., Bucci, V., 2019. Simplified and advanced approaches for evacuation analysis of passenger ships in the early stage of design. *Brodogr.: Teor. Praksa Brodogr. Pomor. Teh.* 70 (3), 43–59.
- Nevalainen, J., Ahola, M.K., Kujala, P., 2015. Modeling passenger ship evacuation from passenger perspective. In: *RINA, Royal Institution of Naval Architects - Marine Design 2015, Papers*. pp. 121–129.
- Ng, C.T., Cheng, T.C., Levner, E., Krieheli, B., 2021. Optimal bi-criterion planning of rescue and evacuation operations for marine accidents using an iterative scheduling algorithm. *Ann. Oper. Res.* 296 (1–2), 407–420.

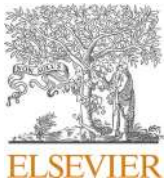
- Ni, B., Li, Z., Zhang, P., Li, X., 2017. An evacuation model for passenger ships that includes the influence of obstacles in cabins. *Math. Probl. Eng.* 2017, 1–21.
- Okada, M., Ando, T., 2011. Optimization of personal distribution for evacuation guidance based on vector field. In: *IEEE International Conference on Intelligent Robots and Systems*. IEEE, pp. 3673–3678.
- Olander, J., Ronchi, E., Lovreglio, R., Nilsson, D., 2017. Dissuasive exit signage for building fire evacuation. *Applied Ergon.* 59, 84–93.
- Olyazadeh, R., 2013. Evaluating Dynamic Signage for Emergency Evacuation using an Immersive Video Environment (Ph.D. thesis). Citeseer.
- Pan, M.-S., Li, K.-Y., 2019. EzNavi: an easy-to-operate indoor navigation system based on pedestrian dead reckoning and crowdsourced user trajectories. *IEEE Trans. Mob. Comput.* 20 (2), 488–501.
- Pan, M.S., Tsai, C.H., Tseng, Y.C., 2006. Emergency guiding and monitoring applications in indoor 3D environments by wireless sensor networks. *Int. J. Sensor Netw.* 1 (1–2), 2–10.
- Park, V.D., Corson, M.S., 1997. A highly adaptive distributed routing algorithm for mobile wireless networks. In: *Proceedings of the 97th International Conference on Computer Communications*, Vol. 3. INFOCOM, IEEE, pp. 1405–1413.
- Perez Villalonga, F.J., 2005. Dynamic Escape Routes for Naval Ships (Ph.D. thesis). Monterey California. Naval Postgraduate School.
- Pooja, S., Vandhana, P., Rakshana, A., Babiyola, A., 2019. MSEND: Modified situation-aware emergency navigation algorithm in wireless sensor networks. *Internat. J. Engrg. Sci.* 21129.
- Qiao, Y., Han, D., Shen, J., Wang, G., 2014. A study on the route selection problem for ship evacuation. In: *2014 IEEE International Conference on Systems, Man, and Cybernetics*. SMC, IEEE, pp. 1958–1962.
- Robinette, P., Howard, A.M., 2011. Incorporating a model of human panic behavior for robotic-based emergency evacuation. In: *Proceedings of the International Workshop on Robot and Human Interactive Communication*. IEEE, pp. 47–52.
- Ronchi, E., Nilsson, D., Gwynne, S.M., 2012. Modelling the impact of emergency exit signs in tunnels. *Fire Technol.* 48 (4), 961–988.
- Rothe, D., Muzzatti, S., Mullins, C.W., 2006. Crime on the high seas: Crimes of globalization and the sinking of the Senegalese Ferry Le Joola. *Crit. Criminol.* 14 (2), 159–180.
- Sakour, I., Hu, H., 2017. Robot-assisted crowd evacuation under emergency situations: A survey. *Robotics* 6 (2), 8.
- Sarshar, P., Radianti, J., Granmo, O.C., Gonzalez, J.J., 2013. A dynamic Bayesian network model for predicting congestion during a ship fire evacuation. *Lect. Notes Eng. Comput. Sci.* 1, 29–34.
- Sharma, P.K., Kwon, B.W., Park, J.H., 2018. DSS-SL: Dynamic signage system based on SDN with LiFi communication for smart buildings. *Lect. Notes Electr. Eng.* 474, 805–810.
- Shell, D.A., Matari, C., Maja, J., 2005. Insights toward robot-assisted evacuation. *Adv. Robot.* 19 (8), 797–818.
- Shen, L., Andong, Z., Xiaobing, W., Panlong, Y., Guihai, C., 2011. Efficient emergency rescue navigation with wireless sensor networks. *J. Inf. Sci. Eng.* 27 (1), 51–64.
- Shin, H., Chon, Y., Cha, H., 2011. Unsupervised construction of an indoor floor plan using a smartphone. *IEEE Trans. Syst. Man Cybern. C* 42 (6), 889–898.
- Shinzaki, T., Morikawa, I., Yamaoka, Y., Sakemi, Y., 2016. IoT security for utilization of big data: Mutual authentication technology and anonymization technology for positional data. *Fujitsu Sci. Tech. J.* 52 (4), 52–60.
- Shu, Y., Shin, K.G., He, T., Chen, J., 2015. Last-mile navigation using smartphones. In: *Proceedings of the Annual International Conference on Mobile Computing and Networking (MOBICOM)*, 2015-September. pp. 512–524.
- Spartalis, E., Georgoudas, I.G., Sirakoulis, G.C., 2014. Ca crowd modeling for a retirement house evacuation with guidance. In: *International Conference on Cellular Automata*. Springer, pp. 481–491.
- Statistics, R.B., 2020. Table 1. US Department of Homeland Security and US Coast Guard.
- Stefanidis, F., Boulougouris, E., Vassalos, D., 2019. Ship evacuation and emergency response trends. *Des. Oper. Passeng. Ships*.
- Stigall, J., Sharma, S., 2017. Mobile augmented reality application for building evacuation using intelligent signs. In: *Proceedings of ISCA 26th International Conference on Software Engineering and Data Engineering (SEDE-2017)*. pp. 19–24.
- Stigen, M., 2019. Applying Swarm to Unknown and Dynamic Environments in Evacuation Planning (Master's thesis). NTNU.
- Sun, J., Guo, Y., Li, C., Lo, S., Lu, S., 2018a. An experimental study on individual walking speed during ship evacuation with the combined effect of heeling and trim. *Ocean Eng.* 166 (September 2017), 396–403.
- Sun, J., Lu, S., Lo, S., Ma, J., Xie, Q., 2018b. Moving characteristics of single file passengers considering the effect of ship trim and heeling. *Physica A* 490, 476–487.
- Tang, B., Jiang, C., He, H., Guo, Y., 2016. Human mobility modeling for robot-assisted evacuation in complex indoor environments. *IEEE Trans. Hum.-Mach. Syst.* 46 (5), 694–707.
- Tang, C.H., Wu, W.T., Lin, C.Y., 2009. Using virtual reality to determine how emergency signs facilitate way-finding. *Applied Ergon.* 40 (4), 722–730.
- Teng, X., Guo, D., Guo, Y., Zhou, X., Liu, Z., 2019. CloudNavi: Toward ubiquitous indoor navigation service with 3D point clouds. *ACM Trans. Sensor Netw.* 15 (1), 1–28.
- Tseng, Y.-C., Pan, M.-S., Tsai, Y.-Y., 2006. Wireless sensor networks for emergency navigation. *Computer* 39 (7), 55–62.
- Valanto, P., 2006. Time-dependent survival probability of a damaged passenger ship ii-evacuation in seaway and capsizing. In: *HSVA Report*. pp. 42–62.
- Vanem, E., Skjong, R., 2006. Designing for safety in passenger ships utilizing advanced evacuation analyses - A risk based approach. *Saf. Sci.* 44 (2), 111–135.
- Veichtlbauer, A., Pfeiffenberger, T., 2011. Dynamic evacuation guidance as safety critical application in building automation. In: *International Workshop on Critical Information Infrastructures Security*. Springer, pp. 58–69.
- Vihás, C., Georgoudas, I.G., Sirakoulis, G.C., 2012. Follow-the-leader cellular automata based model directing crowd movement. In: *International Conference on Cellular Automata*. Springer, pp. 752–762.
- Vilen, E., et al., 2020. Evaluation of Software Tools in Performing Advanced Evacuation Analyses for Passenger Ships (Master's thesis). Aalto University.
- Wada, T., Takahashi, T., 2013. Evacuation guidance system using everyday use smartphones. In: *2013 International Conference on Signal-Image Technology & Internet-Based Systems*. IEEE, pp. 860–864.
- Wan, Z., Jiang, C., Fahad, M., Ni, Z., Guo, Y., He, H., 2020. Robot-assisted pedestrian regulation based on deep reinforcement learning. *IEEE Trans. Cybern.* 50 (4), 1669–1682.
- Wang, X., Guo, W., Cheng, Y., Zheng, X., 2015b. Understanding the centripetal effect and evacuation efficiency of evacuation assistants: Using the extended dynamic communication field model. *Saf. Sci.* 74, 150–159.
- Wang, X.-L., Guo, W., Zheng, X.-P., 2015c. Effects of evacuation assistant's leading behavior on the evacuation efficiency: Information transmission approach. *Chin. Phys. B* 24 (7), 070504.
- Wang, X., Guo, W., Zheng, X., 2016. Information guiding effect of evacuation assistants in a two-channel segregation process using multi-information communication field model. *Saf. Sci.* 88, 16–25.
- Wang, L., He, Y., Liu, W., Jing, N., Wang, J., Liu, Y., 2014a. On oscillation-free emergency navigation via wireless sensor networks. *IEEE Trans. Mob. Comput.* 14 (10), 2086–2100.
- Wang, J., Li, Z., Li, M., Liu, Y., Yang, Z., 2013. Sensor network navigation without locations. *IEEE Trans. Parallel Distrib. Syst.* 24 (7), 1436–1446.
- Wang, C., Lin, H., Jiang, H., 2015a. CANS: Towards congestion-adaptive and small stretch emergency navigation with wireless sensor networks. *IEEE Trans. Mob. Comput.* 15 (5), 1077–1089.
- Wang, C., Lin, H., Zhang, R., Jiang, H., 2017. SEND: A situation-aware emergency navigation algorithm with sensor networks. *IEEE Trans. Mob. Comput.* 16 (4), 1149–1162.
- Wang, X., Liu, Z., Loughney, S., Yang, Z., Wang, Y., Wang, J., 2021a. An experimental analysis of evacuees' walking speeds under different rolling conditions of a ship. *Ocean Eng.* 233, 108–997.
- Wang, X., Liu, Z., Loughney, S., Yang, Z., Wang, Y., Wang, J., 2022. Numerical analysis and staircase layout optimisation for a Ro-Ro passenger ship during emergency evacuation. *Reliab. Eng. Syst. Saf.* 217, 108056.
- Wang, X., Liu, Z., Wang, J., Loughney, S., Zhao, Z., Cao, L., 2021b. Passengers' safety awareness and perception of wayfinding tools in a Ro-Ro passenger ship during an emergency evacuation. *Saf. Sci.* 137, 105–189.
- Wang, X., Liu, Z., Zhao, Z., Wang, J., Loughney, S., Wang, H., 2020. Passengers' likely behaviour based on demographic difference during an emergency evacuation in a Ro-Ro passenger ship. *Saf. Sci.* 129 (1), 104–803.
- Wang, W.L., Lo, S.M., Liu, S.B., Kuang, H., 2014b. Microscopic modeling of pedestrian movement behavior: Interacting with visual attractors in the environment. *Transp. Res. C* 44, 21–33.
- Wang, P., Luh, P.B., Chang, S.C., Marsh, K.L., 2009. Efficient optimization of building emergency evacuation considering social bond of evacuees. In: *2009 IEEE International Conference on Automation Science and Engineering, CASE 2009*. IEEE, pp. 250–255.
- Wang, P., Luh, P.B., Chang, S.-C., Sun, J., 2008. Modeling and optimization of crowd guidance for building emergency evacuation. In: *2008 IEEE International Conference on Automation Science and Engineering*. IEEE, pp. 328–334.
- Wang, Y., Wang, K., Wang, T., Li, X.Y., Khan, F., Yang, Z., Wang, J., 2021c. Reliabilities analysis of evacuation on offshore platforms: A dynamic Bayesian network model. *Process Saf. Environ. Prot.* 150, 179–193.
- Wang, X., Zheng, X., Cheng, Y., 2012. Evacuation assistants: An extended model for determining effective locations and optimal numbers. *Physica A* 391 (6), 2245–2260.
- Wu, F.-J., 2017. A sensor-assisted emergency guiding system: sensor-centric or user-centric? *IEEE Trans. Veh. Technol.* 67 (2), 1598–1611.
- Xie, Q., Li, S., Ma, C., Wang, J., Liu, J., Wang, Y., 2020a. Uncertainty analysis of passenger evacuation time for ships' safe return to port in fires using polynomial chaos expansion with Gauss quadrature. *Appl. Ocean Res.* 101, 102190.
- Xie, Q., Wang, P., Li, S., Wang, J., Lo, S., Wang, W., 2020b. An uncertainty analysis method for passenger travel time under ship fires: A coupling technique of nested sampling and polynomial chaos expansion method. *Ocean Eng.* 195, 106604.
- Xie, Q., Zhang, S., Wang, J., Lo, S., Guo, S., Wang, T., 2020c. A surrogate-based optimization method for the issuance of passenger evacuation orders under ship fires. *Ocean Eng.* 209 (March), 107–456.
- Xu, Z., Lu, X., Guan, H., Chen, C., Ren, A., 2014. A virtual reality based fire training simulator with smoke hazard assessment capacity. *Adv. Eng. Softw.* 68, 1–8.

- Yang, Y., Dimarogonas, D.V., Hu, X., 2013. Optimal leader-follower control for crowd evacuation. In: Proceedings of the IEEE Conference on Decision and Control. IEEE, pp. 2769–2774.
- Yang, X., Dong, H., Wang, Q., Chen, Y., Hu, X., 2014. Guided crowd dynamics via modified social force model. *Physica A* 411, 63–73.
- Yang, X., Dong, H., Yao, X., Sun, X., Wang, Q., Zhou, M., 2015. Necessity of guides in pedestrian emergency evacuation. *Physica A* 442, 397–408.
- Yang, D., Zhang, L., Luo, M., Li, F., 2020. Does shipping market affect international iron ore trade?—An equilibrium analysis. *Transp. Res. E* 144, 102107.
- Yin, K., 2015. Fire evacuation simulation for the case of a non-symmetrical metro station using wireless sensor network. In: 2015 5th International Conference on Information Science and Technology, ICIST 2015. IEEE, pp. 141–146.
- Yin, Z., Wu, C., Yang, Z., Lane, N., Liu, Y., 2016. PpNav: Peer-to-peer indoor navigation for smartphones. In: 2016 IEEE 22nd International Conference on Parallel and Distributed Systems. ICPADS, IEEE, pp. 104–111.
- Yoshida, K., Murayama, M., Itakaki, T., 2001. Study on Evaluation of Escape Route in Passenger Ships by Evacuation Simulation and Full-Scale Trials. Research Institute of Marine Engineering, Japan.
- Yuan, Z., Jia, H., Zhang, L., Bian, L., 2018. A social force evacuation model considering the effect of emergency signs. *Simulation* 94 (8), 723–737.
- Yuan, W., Tan, K.H., 2009. Cellular automata model for simulation of effect of guiders and visibility range. *Curr. Appl. Phys.* 9 (5), 1014–1023.
- Zhang, S., Guo, Y., 2015. Distributed multi-robot evacuation incorporating human behavior. *Asian J. Control* 17 (1), 34–44.
- Zhang, Z., He, S., Shu, Y., Shi, Z., 2020b. A self-evolving WiFi-based indoor navigation system using smartphones. *IEEE Trans. Mob. Comput.* 19 (8), 1760–1774.
- Zhang, Z., Liu, H., Jiao, Z., Zhu, Y., Zhu, S.-C., 2020c. Congestion-aware evacuation routing using augmented reality devices. In: 2020 IEEE International Conference on Robotics and Automation. ICRA, IEEE, pp. 2798–2804.
- Zhang, G., Lu, D., Liu, H., 2021. IoT-based positive emotional contagion for crowd evacuation. *IEEE Internet Things J.* 8 (2), 1057–1070.
- Zhang, J., Zhao, J., Song, Z., Gao, J., 2020a. Evacuation performance of participants in an offshore platform under smoke situations. *Ocean Eng.* 216, 107–739.
- Zheng, Y., Shen, G., Li, L., Zhao, C., Li, M., Zhao, F., 2017. Travi-navi: Self-deployable indoor navigation system. *IEEE/ACM Trans. Netw.* 25 (5), 2655–2669.
- Zhou, M., Dong, H., Wang, X., Hu, X., Ge, S., 2020. Modeling and simulation of crowd evacuation with signs at subway platform: A case study of Beijing subway stations. *IEEE Trans. Intell. Transp. Syst.* 1–13.
- Zhou, M., Dong, H., Zhao, Y., Ioannou, P.A., Wang, F.Y., 2019a. Optimization of crowd evacuation with leaders in urban rail transit stations. *IEEE Trans. Intell. Transp. Syst.* 20 (12), 4476–4487.
- Zhou, M., Liu, J., Ge, S., Dong, H., 2019b. Passenger cooperative guidance system for urban rail transit stations. In: 2019 Chinese Automation Congress. CAC, IEEE, pp. 2985–2990.
- Zhou, J., Wu, C.-C., Yu, K.-M., Tsao, Y., Lei, M.-Y., Chen, C.-J., Cheng, S.-T., Huang, Y.-S., 2012. Crowd guidance for emergency fire evacuation based on wireless sensor networks. In: The 5th IET International Conference on Ubi-Media Computing (U-Media). pp. 303–308.

ARTICLES FOR FACULTY MEMBERS

RESCUE VESSEL OPERATION FOR FLOOD EVACUATION PROTOCOL

Title/Author	An autonomous coverage path planning algorithm for maritime search and rescue of persons-in-water based on deep reinforcement learning / Wu, J., Cheng, L., Chu, S., & Song, Y.
Source	<i>Ocean Engineering</i> Volume 291 (2024) 116403 Pages 1-21 https://doi.org/10.1016/J.OCEANENG.2023.116403 (Database: ScienceDirect)



An autonomous coverage path planning algorithm for maritime search and rescue of persons-in-water based on deep reinforcement learning

Jie Wu^a, Liang Cheng^{a,b,c,d,*}, Sensen Chu^{a,b,c}, Yanjie Song^e

^a School of Geography and Ocean Science, Nanjing University, Nanjing, China

^b Jiangsu Provincial Key Laboratory of Geographic Information Science and Technology, Nanjing University, Nanjing, China

^c Collaborative Innovation Center for the South Sea Studies, Nanjing University, Nanjing, China

^d Collaborative Innovation Center of Novel Software Technology and Industrialization, Nanjing University, Nanjing, China

^e College of Systems Engineering, National University of Defense Technology, Changsha, China

ARTICLE INFO

Handling Editor: Prof. A.I. Incecik

Keywords:

Persons-in-water
Drift trajectory prediction
Maritime search and rescue
Coverage path planning
Deep reinforcement learning

ABSTRACT

The prevalence of maritime transportation and operations is increasing, leading to a gradual increase in drowning accidents at sea. In the context of maritime search and rescue (SAR), it is essential to develop effective search plans to improve the survival probability of persons-in-water (PIWs). However, conventional SAR search plans typically use predetermined patterns to ensure complete coverage of the search area, disregarding the varying probabilities associated with the PIW distribution. To address this issue, this study has proposed a maritime SAR vessel coverage path planning framework (SARCPPF) suitable for multiple PIWs. This framework comprises three modules, namely, drift trajectory prediction, the establishment of a multilevel search area environment model, and coverage search. First, sea area-scale drift trajectory prediction models were employed using the random particle simulation method to forecast drift trajectories. A hierarchical probability environment map model was established to guide the SAR of multiple SAR units. Subsequently, we integrated deep reinforcement learning with a reward function that encompasses multiple variables to guide the navigation behavior of ship agents. We developed a coverage path planning algorithm aimed at maximizing the success rates within a limited timeframe. The experimental results have demonstrated that our model enables vessel agents to prioritize high-probability regions while avoiding repeated coverage.

1. Introduction

With continuous development of the global economy, maritime transportation has emerged as the primary mode for transporting international goods. With increasing human exploration and production activities at sea, offshore operations have become increasingly common. The marine environment is complex and dynamic, with natural disasters such as strong winds, high waves, storms, lightning strikes, and tsunamis potentially occurring. These events can increase the number of maritime accidents (Yang et al., 2020; Zhang et al., 2017; Zhou et al., 2020a, 2020b; Zhou, 2022). Maritime accidents often result in drowning and casualties. Therefore, the timely development of effective search plans and improvements in the efficiency of maritime search and rescue have become a key research focus (Koopman, 1956a, 1956b, 1957; Peng et al., 2022; Rani et al., 2022; Sendner, 2022). This is critical for enhancing the likelihood of survival among PIWs.

Maritime SAR comprises two essential components, that is, search and rescue, with search serving as a prerequisite for rescue (Carneiro, 1988; Haga and Svanberg, 2022; IAMSAR, 2016; International Maritime Organization, 1979). In maritime SAR, the scarcity of search resources and adverse meteorological conditions are the two primary factors that impede the SAR process (Zhou, 2022). This forces search planners to minimize the search area and maximize the chances of locating the search object (Tapkin and Temur, 2022). Search optimization is necessary to achieve maximum success rates while considering the correlation between time and resource constraints. Given the vulnerability of PIWs in maritime environments, rescuers must locate them immediately. Therefore, searching for PIWs includes three main tasks: (1) accurately and quickly predicting the drift trajectory of PIWs (Brushett et al., 2017; Chen et al., 2017, 2022; Wu et al., 2023); (2) determining the optimal search area to ensure full coverage of the possible distribution range; and (3) planning the search path for the SAR units and maximizing the

* Corresponding author. School of Geography and Ocean Science, Nanjing University, Nanjing, 210023, China.

E-mail addresses: 1936063643@qq.com (J. Wu), lcheng@nju.edu.cn (L. Cheng), chusensen@163.com (S. Chu), songyj_2017@163.com (Y. Song).

cumulative probability of success (POS) of the entire search process (Brown, 1980; Kratzke et al., 2010; Lin and Goodrich, 2014; Mou et al., 2021; Washburn, 1983).

When the rescue units arrive at their initial position in maritime SAR, the PIWs continue to drift owing to the combined influence of surface currents, sea waves, and wind. The complexity of the maritime environment, along with numerous uncertain factors influencing the drifting process, amplifies the challenge of locating PIWs. It also increases the complexity of search path planning, thereby rendering the search more intricate. The prediction of drift trajectories involves the consideration and quantification of factors that affect the drift process, including the submersion scene, maritime conditions, and prediction modeling. In marine accidents involving PIWs, the drift characteristics vary depending on the posture, including whether the PIWs are upright, seated, or face down, or the load conditions (Wu et al., 2023). First proposed by Allen and Plourde (1999) to quantify the drift of objects, the Leeway model has been widely used to help plan national searches such as the French MOTHY (Daniel et al., 2003), Canadian CANSARP (Canadian Coast Guard College CANSARP Development Group Web site, 2009), and U.S. Coast SAROPS (Kratzke et al., 2010). Sea-based drift tests are widely recognized as the most commonly used and highly dependable approach for determining leeway coefficients (Breivik et al., 2012; Kasyk et al., 2021; Meng et al., 2021; Sutherland et al., 2020; Tu et al., 2021; Wu et al., 2023; Zhu et al., 2019).

Path-planning methods can be classified into two categories, that is, traditional and intelligent algorithmic. Traditional path planning algorithms include the dijkstra algorithm (Dijkstra, 1959; Wang et al., 2011), the A* algorithm and its improved versions (Chabini and Lan, 2002; Hart et al., 1972; Nash and Koenig, 2013), the D* algorithm and its improved versions (Koenig and Likhachev, 2005; Marija and Ivan, 2011; Stentz, 1994), the artificial potential field method (Zhang et al., 2012), the probabilistic path graph method (Kavraki et al., 1996), and the rapid exploration of random trees method (RRT) (Lavalle, 1998). Intelligent path planning algorithms include genetic algorithms (Prins, 2004), ant colony algorithms (Luo et al., 2020) and particle swarm algorithms (Masehian and Sedighzadeh, 2010). The reinforcement learning (RL) method (Wiering and Van, 2012) is an important approach in machine learning. In contrast with other intelligent algorithms for machine learning, RL focuses on the acquisition of system mapping from the environment to the behavior. It does not rely on labeled interactions as seen in supervised learning; instead, it learns from its own experiences. The objective of RL is not to discover hidden structures but rather to maximize rewards. The most used reinforcement learning methods include Q learning, SARSA learning, TD learning, and adaptive dynamic programming algorithms. Recently, significant advancements have been made in combining path planning with reinforcement learning (Busoniu et al., 2008; Xi et al., 2022; Xie et al., 2021).

Full-coverage path planning (CPP) is a specialized technique in robotics for generating a continuous path that passes through all accessible points within a given area with a minimum repetition rate and maximum coverage rate. This can be achieved using either random or environment-based models (Galceran and Carreras, 2013). To ensure comprehensive coverage, most existing CPP methods divide the target area and the surrounding space into cells using exact or approximate cell division techniques. CPPs have a wide range of applications in autonomous underwater vehicles (AUVs), including seabed mapping, mine detection, and oil spill cleanup (Englot and Hover, 2013; Shen et al., 2019; Song et al., 2013). CPP have also been extensively used in other fields, including photogrammetry for unmanned aerial vehicles (UAVs), agriculture, fire, disaster management, and vacuum-cleaning robots (Fevgas et al., 2022; Galceran and Carreras, 2013; Seraj et al., 2022). Recently, researchers have begun to consider using reinforcement learning in CPP. Theile et al. (2020) used deep reinforcement learning algorithms for UAV CPP under different power constraints. Kyaw et al. (2020) used a new approach for solving CPP problems in large complex environments based on the traveling salesman problem (TSP) and deep

reinforcement learning. Xi et al. (2022) integrated ocean information for a regional ocean simulation system combined with RL to generate AUV path-planning solutions. Jonnarth et al. (2023) used an end-to-end RL approach based on a continuous state and action space to address online CPP problems in unknown environments.

In the field of maritime SAR path planning, the primary objective is to optimize the shortest route from the starting point to the destination while avoiding potential obstacles along the path (Cao et al., 2019; Li et al., 2021; Liu et al., 2017; Xi et al., 2022; Yang et al., 2020; Zhang et al., 2019, 2020). However, accurately determining the location of individuals in distress during maritime accidents is challenging because of the varying postures of PIW and complex and constantly changing marine environments. Therefore, it is crucial to establish a search area and plan a path that ensures full coverage of the entire region. This is known as maritime full coverage search path planning (Ai et al., 2021). Compared with traditional CPP problems, the maritime search and rescue coverage path planning (MCCPP) problem presents unique challenges. In addition to achieving complete coverage of the search area and avoiding path overlaps and obstacles, priority must be given to searching for high-probability areas.

To achieve this objective, traditional SAR operations used methods such as parallel track, crawl line, extended square, and sector searches (IAMSAR, 2016; Koopman, 1957). Recently, there has been a surge in research aimed at enhancing traditional search methods. Ramirez et al. (2011) used a collaborative model of UAVs and unmanned boats for maritime rescue coordination, which proved to be highly effective in completing rescue missions. Karakaya (2014) used an ant colony system optimization algorithm for route planning, aiming to efficiently cover the maximum search area with a limited number of UAVs. Xiong et al. (2021) introduced a helicopter maritime SAR path-planning method based on the minimum outer rectangle and k-means clustering algorithm. Cho et al. (2021) presented a mixed-integer linear programming (MILP) model that used a hexagonal grid decomposition approach to efficiently generate search paths for multiple heterogeneous UAVs within the shortest possible timeframe. Ouelmokhtar et al. (2022) used a multi-objective evolutionary algorithm, namely, the non-dominated sorting genetic algorithm II (NSGA-II) and Pareto evolutionary strategy (PAES), to solve the dual-objective CPP problem, that is, minimizing energy consumption and maximizing coverage, for UAV maritime monitoring. However, these methods have not considered the variability in the probability distribution of personnel in distress (PIWs) within the search area. Given that rescue time is critical for ensuring personnel safety, incorporating the PIW probability distribution can substantially enhance survival rates. Therefore, it is imperative to devise a path that maximizes SAR cumulative success rates (Ai et al., 2021; Bourgault et al., 2003; Cho et al., 2021; Frost, 2001; Yao et al., 2019).

Most current studies have primarily focused on single drowning person scenarios in search and rescue (SAR) operations. However, it is crucial to consider SAR scenarios involving multiple individuals in varying postures, such as the upright and face down positions, particularly during maritime accidents. For large-scale drowning accidents, the range of maritime SAR is large and requires the establishment of a multidimensional search and rescue area and multi-agent coverage path planning. One strategy for promoting collaboration among agents is to partition regions into distinct blocks and assign each agent a responsibility to a specific block (Xiong et al., 2021). The second approach is cooperative path planning for multiple agents (Binney et al., 2010; Cho et al., 2021; Mou et al., 2021). Throughout the search process, UAVs encounter several limitations, including a restricted battery life, vulnerability to adverse environmental conditions, limited search ranges, and challenges in detecting diminutive targets within water bodies (Hou et al., 2020). The Automatic Identification System (AIS) can provide information on vessels in proximity to the distress area, facilitating the allocation of ship resources for search and rescue operations. Therefore, it is imperative to investigate the planning of maritime coverage paths for vessel agents.

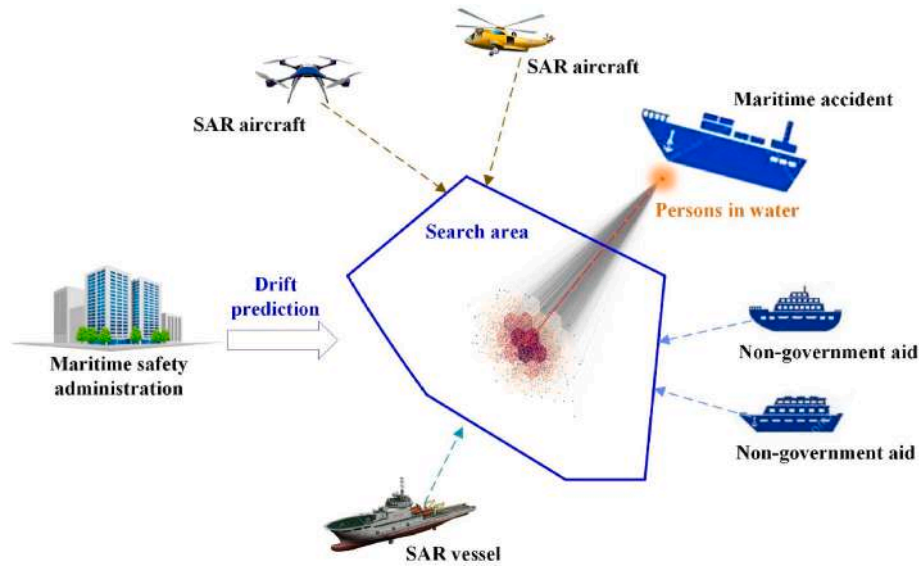


Fig. 1. Maritime SAR concept for PIWs.

This study integrated deep reinforcement learning techniques into the planning process of SAR coverage paths. First, sea-area-scale drift trajectory prediction models were used to predict the trajectories of persons in various sea areas. A random particle simulation algorithm was used to simulate the drift paths for different postures. Subsequently, a hierarchical probability map was established. By integrating deep reinforcement learning into the design of the covering path-planning algorithm, an improved success rate within a limited timeframe was achieved.

The main innovations of this study can be summarized as follows:

- (1) A maritime search and rescue vessel path planning framework (SARCPPF) was proposed, which includes the prediction of the drift trajectory at the sea area scale, establishment of a hierarchical environment map of the search area for persons in water with multiple attitudes, and planning of the covering path.
- (2) Developed a coverage path planning system with a multi-objective reward function based on deep reinforcement learning for maritime SAR. State and dynamically adjusted action-selection strategies applicable to specific maritime SAR scenarios were designed.
- (3) For specific scenarios of maritime search and rescue, deep learning was introduced into search path planning, which achieves the goal of maximizing the cumulative success rate of search and rescue and provides a demonstration case for search path planning in high-dimensional state and action spaces.

The remainder of this study is organized as follows: In Section 2, the maritime optimal search theory, variables in search planning, and SARCPPF for this study are presented. Section 3 describes the sea-area-scale drift-trajectory prediction models and the drift prediction method. Section 4 introduces the modeling of the SAR environment. Section 5 introduces the SAR path planning algorithm combined with reinforcement learning. Section 6 presents a drift experiment of actual PIWs as a case study to perform a comparative analysis of the experimental results. Finally, Section 7 presents conclusions and prospects.

2. Maritime optimal search theory and maritime SARCPPF

Maritime optimal search theory serves as the foundation for determining search areas, dispatching SAR units, and assigning search tasks. Soza Company Ltd. (1996) and Frost (1997, 2001) distilled this theory into three critical components, that is, probability of containment

(POC), probability of detection (POD), and probability of successful search (POS).

Maritime SAR aims to develop search plans and improve POS within the shortest possible time with limited search resources. POS relies mainly on POC and POD (Xiong et al., 2020):

$$POS = POC \times POD \quad (1)$$

Therefore, maritime SAR aided decision-making involves two key issues: (1) optimal maritime SAR area determination, namely, full consideration and quantification of all influencing factors, such as distress waters, distress targets, and marine environmental conditions, in the drift process to predict the target trajectories and their final location probability distribution, and to determine the optimal search and rescue region, and (2) optimal planning of the maritime SAR, that is, based on SAR area determination, an optimal allocation scheme of SAR resources in time and space should be sought to improve the POS. The concept of maritime SAR for PIWs is illustrated in Fig. 1.

2.1. POC

Referring to the likelihood of an object being present within a search area, POC is a critical factor in search planning. Search planners need to allocate resources effectively to maximize their discovery potential. POC is expressed as a percentage and increases with larger search areas. When all particles can be contained within the region, POC reaches 100%. In actual maritime SAR missions, SAR units are often restricted in number, which requires SAR units to prioritize areas with high POC. Therefore, the search area is often subdivided into equally sized $A \times B$ square grids, with the size of the grid cells depending on the capability of the SAR detection equipment. The possibility of a SAR target being present in each subgrid was quantified by calculating the POC of each grid cell.

The specific equation for the calculation can be described as follows:

$$POC = m_i / M \quad (2)$$

where m_i is the number of particles falling in cell i , and M is the number of particles contained in the overall distribution area.

2.2. POD

POD represents the probability of detection, indicating the likelihood that a search unit can detect a SAR target, and it is a crucial metric for

Table 1
Weather correction coefficients for generic search targets.

Winds (km/h) or currents (m)	Objects	
	PIW, life raft, or ship <10 m (33 ft)	Other objects
0–28 km/h or 0–1 m	1.0	1.0
28–46 km/h or 1–1.5 m	0.5	0.9
>46 km/h or > 1.5 m	0.25	0.9

Table 2
Sweep width tables of vessels.

Objects	Meteorological visibility (km)				
	6	9	19	28	37
PIW	0.7	0.9	1.1	1.3	1.3

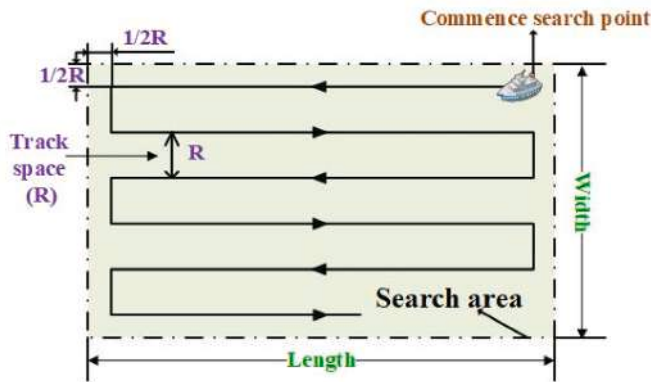


Fig. 2. Parallel line search for maritime search and rescue.

evaluating the effectiveness of an SAR detector in the search area (Abi-Zeid and Frost, 2005). Calculating the POD involves two important concepts, that is, sweep width and coverage rate. Sweep width refers to the effective distance within which the detector can locate the search object in a given search area. In this study, it serves as an indicator of the vessel’s search capability.

Accurately determining the sweep width of the equipment requires statistical analysis of extensive experimental and practical samples, because different SAR targets in various search environments exhibit distinct horizontal range curves for each piece of equipment. Typically, a lateral curve can be plotted by analyzing large amounts of experimental data to assess the performance of a given device (Ai et al., 2019; Washburn and Kress, 2009; Wu and Zhou, 2015). Given that the actual sweep width can be affected by the performance of the SAR equipment, such as sensor performance, the characteristics of the search target, that is, physical characteristics such as size and color, and the maritime environment, such as wind, sea conditions, visibility, and sunlight reflection, it needs to be adjusted according to the actual situation.

IAMSAR (2016) provides the sweep width of the universal SAR equipment for generic search targets and the correction coefficient under different environmental conditions (Table 1). The sweep widths of the vessels are listed in Table 2. This table was compiled in the 1980s by the United States Coast Guard, which has conducted a large number of maritime SAR experiments according to the actual SAR environment. They measured the sweep widths of different search facilities under various conditions for different search targets (Anderson et al., 2006; Engel and Weisinger, 1988).

Coverage (C) is a measure of the degree to which a SAR unit’s search area is covered during an operation (Burciu, 2010; Frost, 1997). This can

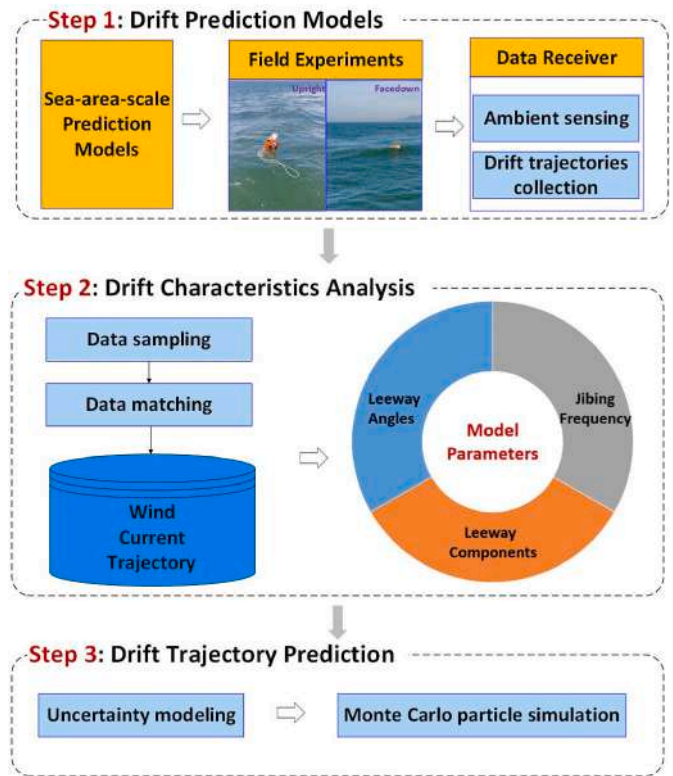


Fig. 3. Framework for drift prediction.

be expressed as the effective coverage divided by the total search area. It is generally assumed that a vessel chooses to search using the parallel-line method, which requires fewer turns and is applicable to complex search scenarios (Fig. 2). The equation is as follows:

$$C = \frac{W \times S}{A} = \frac{W}{R} \quad (3)$$

where W is the sweep width, S is the effective path length, A is the size of the search area, and R is the route spacing.

There is a close functional relationship between POD and coverage. Three models have been identified to describe this relationship, that is, fixed distance detection, inverse cube, and the random detection model (Abi-Zeid et al., 2011). Among them, the random detection model has been used to estimate the POD in a complex maritime SAR environment. Therefore, we used a random detection model in our study as follows:

$$POD = 1 - e^{-C} \quad (4)$$

2.3. Maritime SARCPPF

This paper presents a coverage path planning algorithm for search and rescue (SAR) vessels in maritime drowning accidents based on optimal SAR theory. The proposed SARCPPF consists of three modules, that is, drift trajectory prediction, SAR environment modeling, and coverage search. To predict the drift trajectories of PIWs with different postures in different sea areas, sea-area-scale drift trajectory prediction models (Wu et al., 2023) were used along with a random particle simulation method. All the predicted positions of the PIWs were then fused to generate a new prediction area. The search path planning region was determined based on the minimum bounding rectangle, and a hierarchical probability environment map was established to realize the SAR of multiple SAR units. A covering path planning algorithm combining deep reinforcement learning was proposed to enable rescue

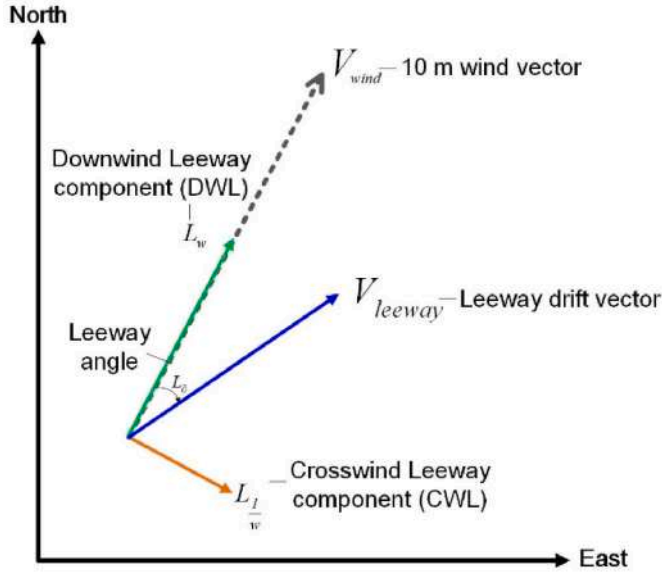


Fig. 4. Relationships between the leeway, leeway angle, and the DWL and CWL components of the leeway (Breivik and Allen, 2008).

units to achieve fast arrival and high cumulative POS coverage, thereby increasing the SAR success rate in a limited time.

3. Predicting maritime drift trajectories

Drift theory investigates the impact of meteorological and oceanographic factors on object motion in marine environments and forms the basis for the mathematical methods used to determine search areas and routes in maritime SAR (Frost and Stone, 2001). In this study, sea-area-scale drift prediction models (Wu et al., 2023) were used to predict the trajectories of individuals with different postures in the Chinese sea areas, as illustrated in Fig. 3.

3.1. Drift prediction models for persons in the water

The Leeway model (Allen and Plourde, 1999; Allen, 2005; Allen et al., 2010; Breivik and Allen, 2008) was developed to analyze the impact of sea wind at a reference height of 10 m on the drift of various unpowered floating objects using Lagrangian particle simulation and probabilistic statistical analysis. Leeway is defined as “the motion of an object caused by wind and waves relative to currents (from depths ranging from 0.3 m to 1.0 m)” (Allen and Plourde, 1999; Breivik et al., 2013).

Marine environmental data can be used to compute the drift velocity vector of particles in water as follows:

$$\frac{dx}{dt} = v(x, t) \quad (5)$$

where dx is the change in the horizontal position of the floating object over time and $v(x, t)$ is the two-dimensional horizontal velocity.

$$v(x, t) = V_{F-current}(x, t) + V_{leeway}(x, t) + V_{F-wave}(x, t) \quad (6)$$

Among them, $V_{F-current}(x, t)$ represents the velocity caused by the current, that is, the sea surface velocity. $V_{leeway}(x, t)$ represents the wind-induced drift velocity. $V_{F-wave}(x, t)$ is the wave-induced drift speed. Generally, the effect of wave forces is believed to be negligible for most targets in distress at less than 30 m in length (Breivik et al., 2011). Therefore, wave-induced drift velocity was excluded from this study.

The wind-induced drift speed can be decomposed into two components, that is, downwind speed (DWL) and crosswind speed (CWL), which are linearly correlated with wind speeds 10 m above sea level

(Fig. 4), as demonstrated by Formula (7) in Allen (2005). The probability of +CWL and -CWL can be obtained from experimental statistics, where the CWL speed is deemed positive if it is to the right of the DWL. The direction of the crosswind speed changes from +CWL to -CWL or from -CWL to +CWL when the wind velocity falls within a specified range, which is referred to as jibing frequency (Allen and Plourde, 1999).

$$\begin{aligned} L_w &= c_w V_{wind} + b_w + \varepsilon_w \\ L_{w+} &= c_{w+} V_{wind} + b_{w+} + \varepsilon_{w+} \\ L_{w-} &= c_{w-} V_{wind} + b_{w-} + \varepsilon_{w-} \end{aligned} \quad (7)$$

Among them, L_w , L_{w+} , L_{w-} represent the leeway components, c_w , c_{w+} , c_{w-} are the linear regression slopes, b_w , b_{w+} , b_{w-} are intercepts, ε_w , ε_{w+} , ε_{w-} are the error terms. This equation is an unconstrained model, whereas the constrained method generates a linear fit with zero offset, as follows:

$$\begin{aligned} L_w &= c_w V_{wind} + b_w \\ L_{w+} &= c_{w+} V_{wind} + b_{w+} \\ L_{w-} &= c_{w-} V_{wind} + b_{w-} \end{aligned} \quad (8)$$

The leeway rate of each object at sea is highly specific and contingent on its exposure to wind, mass, and structures above and below the waterline. Simulating a person's drift is an intricate process owing to the numerous uncertainties involved. Maritime meteorological conditions are often complex and are characterized by small-scale turbulence, vortices, stratification, and shear in near-surface currents. These issues are intricate, not easily discernible, and frequently pose challenges for resolution.

Therefore, in this study, we used the sea-area scale prediction models developed by Wu et al. (2023), which divided the Chinese coastline into distinct regions. We conducted drift tests that involved releasing manikins integrated with GPS devices and ship tracking to observe maritime environmental elements. Based on field experiment data, they modeled the drift trajectory at the sea area scale and generated predictive models for PIWs exhibiting different postures.

3.2. Drift trajectory prediction

In areas with complex marine environments, the accuracy of the Last-Known-Position (LKP) can be compromised, leading to significant deviations in the drift trajectory prediction. Therefore, alternative methods should be explored to improve the reliability of location information used as a starting point. To address this issue, we used the Monte Carlo simulation method to simulate the LKP error (Shchekinova and Kumkar, 2015). According to Breivik and Allen (2008), uncertainty modeling of the leeway parameters was performed. In the case of DWL:

$$L_w = (c_w + \varepsilon_w/20) \times V_{wind} + \left(b_w + \frac{\varepsilon_w}{2}\right) \quad (9)$$

where, $\varepsilon_w = S_{yx} \times Z$; S_{yx} is the standard deviation; Z is a random number which is normally distributed $N(0, 1)$.

The maritime environmental data obtained may not accurately reflect real marine conditions owing to inherent limitations in measurement errors and other contributing factors. Therefore, a random walk model was used to effectively capture the uncertainty in marine environment data during the drift trajectory prediction process. Considering DWL as an example, the equation can be expressed as follows:

$$\begin{aligned} \mathbf{u}'_m &= (K)^{1/2} dw(t) \\ K &= \sigma_w^2 T \\ \mathbf{u}'_m &\equiv (u'_m, v'_m) \end{aligned} \quad (10)$$

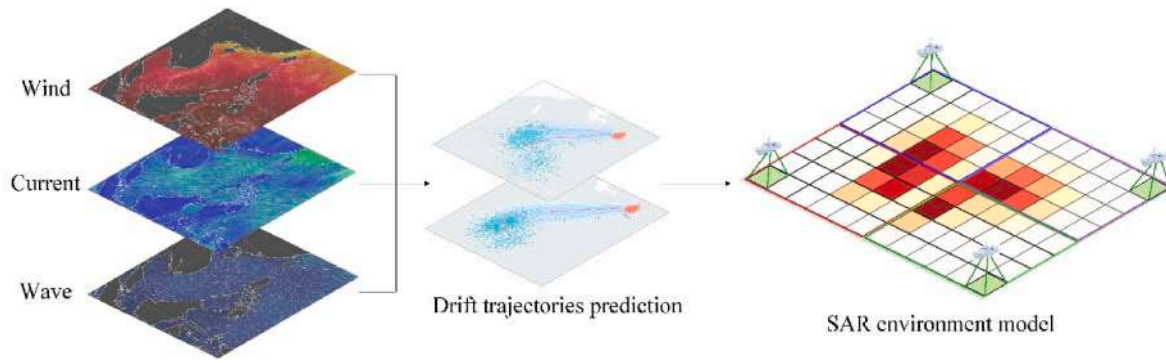


Fig. 5. Maritime search and rescue path planning environment modeling.

$$L_w = (c_w + \varepsilon_w/20) \times (\|V_{wind}\| + \mathbf{u}'_m) + \left(b_w + \frac{\varepsilon_w}{2}\right) \quad (11)$$

where K is the diffusion coefficient, $dw(t)$ is a general random variable satisfying a normal distribution with mean 0 and a second moment of $2dt$, σ_w^2 is the variance of wind or current speed, and T is the integral time scale, usually $T = dt/2$.

The drift speed of the PIWs at any given time can be calculated based on the wind and flow data using Eq. (6). The drift trajectory can be determined by integrating the drift speed as follows:

$$loc_i(t) - loc_i(0) = \int_0^t [V_{drift}(t')dt'] = \int_0^t [V_{Leeway}(t') + V_{F-current}(t')] dt' \quad (12)$$

where $loc_i(t)$ is the location of the PIW at a given time t , $loc_i(0)$ are LKPs.

In this study, distress sea areas and different leeway coefficients of different search objects were introduced because drifting objects of different types and distress sea areas have different leeway coefficients. Search planners need to determine the types of distress targets when making search plans. However, in an actual operation, it is difficult to determine the type of distress object because the accident information obtained is not always sufficiently comprehensive. This requires the search planner to make strategic judgment based on existing accident information. This study has introduced multi-object leeway coefficients for various possible distress objects to further plan the search prediction areas.

The corresponding sea-scale drift trajectory prediction model was selected for the upright and facedown drowning personnel, and the drift trajectory prediction was performed accordingly. In maritime SAR, the target search range and the output probability distribution of the drift prediction model have proven to be of considerable importance in guiding search path planning. For each simulation, particle tracking was conducted using the Monte Carlo method to generate 1000 particles.

4. Maritime SAR environment modeling

The complexity and variability of the marine environment, coupled with the diverse postures of PIWs, have heightened the challenges in search-path planning. There is an urgent need for robust environmental modeling to facilitate future path planning based on the multi-posture PIW drift prediction results. Based on the simulation results, a new drift prediction area was generated by integrating all the PIW particles in different positions to simulate the drifting conditions of large-scale PIWs during maritime accidents. This area was then used to determine the search zone and generate a model for the maritime SAR environment. A path-planning algorithm was developed to enable searching among multiple vessels. The modeling process is illustrated in Fig. 5.

4.1. Establishment of the minimum bounding rectangle (MBR)

The Graham scanning algorithm (Graham, 1972; Kong et al., 1990) was used to generate the minimum convex hull. This algorithm consists of the following six steps.

- (1) Find the bottom-left point from the point set that must be on the convex hull.
- (2) Rank the remaining points according to the polar angle and compare the distance to the pole when the polar angles are the same, with the one closer to the pole taking precedence.
- (3) Stack S was used to store the points on the convex hull, and the two smallest points sorted by pole angle and pole were pushed into the stack.
- (4) Scan each point to check whether the line segment formed by the first two elements on the top of the stack and this point “turns” to the right (cross product ≤ 0).

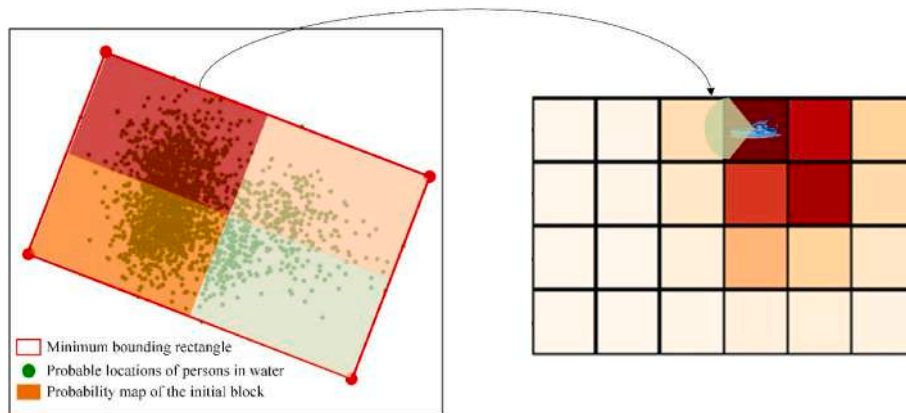


Fig. 6. Hierarchical probability map modeling.

- (5) If “yes,” pop up the top element of S and return to step (4) until “no,” then push this point onto S and proceed to step (5) for the other points.
- (6) Vertex sequence of the convex hull is an element of the final stack.

The direct use of convex polygons as search areas is not conducive to search-path planning. Therefore, an MBR containing convex polygons should be generated to facilitate search-path planning (Cheng et al., 2008; Xiong et al., 2021). The procedure was as follows:

- (1) Two points should be considered as the edge of the rectangle, using this edge as the base coordinate of the xy -axis.
- (2) All the points are rotated around this base coordinate to find the minimum and maximum x -coordinates and the maximum y -coordinates of all points based on this edge; then, the area value of the range and the boundary data are obtained.
- (3) Process (2) was repeated for each edge, and the MBR parameters with the minimum area were the output.

4.2. Hierarchical probability map modeling

In a scenario where multiple people fall into the water, the final search area may be relatively large, and multiple search and rescue forces are required to search simultaneously. Therefore, it is necessary to divide the search and rescue areas and conduct search and rescue path planning for each sub-area. In previous studies, the search area was primarily divided through a continuous expansion centered on the grid cell with the highest POC, potentially leading to locally optimal solutions. To address this issue, this study has proposed a new MBR and hierarchical path-planning algorithm based on the assumption of sufficient SAR units. The search area was determined based on the minimum bounding rectangle (MBR) by considering the integrated position distribution of the simulated particles at different PIW times. A hierarchical probability map was established, and each search and rescue unit proceeded directly to the highest probability area within its corresponding block for simultaneous search and rescue operations.

As shown in Fig. 6, the overall area was initially divided into large blocks of equal size, and the probability distribution of the particles in each block was calculated. A SAR unit was deployed for each block simultaneously. Subsequently, each block was divided into equal-sized $A \times B$ regular grids (Agbissoh Otote et al., 2019), with the grid cell size dependent on the sweeping width of the search ships (Galceran and Carreras, 2013). The POC was then calculated and colors were assigned to different grid cells according to their respective POC values, thereby generating a probability distribution map (Agbissoh Otote et al., 2019; Ai et al., 2019; Lee and Morrison, 2015; Xiong et al., 2020). In this study, we assumed that the environmental state was stable at a given time. Once the search area was defined, it remained unchanged with the development of the SAR process.

5. Maritime SAR coverage path planning based on deep reinforcement learning

In this study, we have proposed an autonomous coverage path-planning algorithm for multiship search and rescue (SAR) units based on deep reinforcement learning. Prior research (Wu et al., 2023) demonstrated the superior trajectory prediction accuracy and search area of the sea-area-scale drift trajectory prediction model. Therefore, in our study, each SAR unit navigates directly to the highest probability grid of its corresponding block using an environmental map established from the drift simulation results at a given time. Search path planning is the process of selecting navigation actions according to the current SAR environment information.

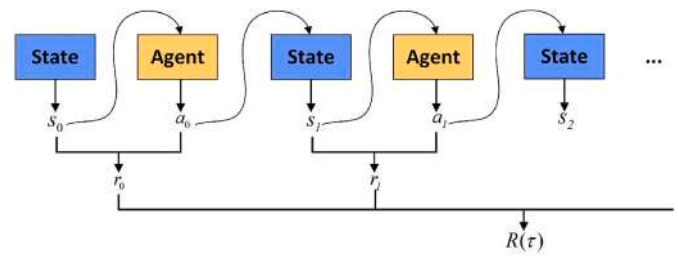


Fig. 7. Markov decision process diagram.

Table 3

The symbols and the corresponding explanations of the maritime SAR path planning model.

List of symbols	Explanations
S	The state space of the environment.
A	The action space of the SAR unit.
P	The state transition model.
R	The reward value function.
γ	The discount factor.
s_t	The state at time t .
S_{done}	The state when the agent passes the whole area.
a_t	The action taken at time t .
r_t	The reward value at time t .
R_t	The cumulative reward value.
R_{POC}	The reward value of POC.
R_{search}	The reward value if the next state $S_{t+1} \notin H$.
R_{done}	The reward value that the agent passes the whole area.
POC_i	The POC value at step i .
$step_i$	The number of steps experienced at step i .
T	The maximum number of steps that the agent can take.
Π	The strategy of the agent.
$\Pi(a s)$	The action selection strategy.
H	The set of grid units searched by the agents.
U	The set of grid units has not been searched by the agents.
F	The set of grid units whose POC value is 0.
ϵ	The probability that a random action selection is conducted.
A^*	The action with the highest Q value at the current state.
A_{choose}	The set of available actions under the current state.
$V_{\Pi}(s)$	The state value function.
$Q_{\Pi}(s, a)$	The action value function.

5.1. Overall maritime SAR path planning process

When planning maritime SAR routes, the next stage of the SAR unit depends only on the previous state and action, which can be expressed as a Markov Decision Process (MDP) (Sutton and Barto, 1998; Mnih et al., 2013). An MDP process is an interaction process between the environment and the agent, which includes three signals, namely, state (S), action (A), and reward (R). It provides direct feedback on the results generated by interactions with the environment (E). The agent receives the states at each discrete time step and selects the corresponding actions to transform them into new states. This transformation process then generates an evaluation value reward. The new state is acquired by the agent, and the cycle is repeated, as shown in Fig. 7.

5.2. Algorithm structure

5.2.1. The Markov decision process of maritime SAR path planning

The expression for maritime SAR path planning includes a vessel agent and two sets (state set S and action set A). By selecting and executing an action from the action set A , the agent completes a state transition. During reinforcement learning (RL), the vessel’s goal is to maximize the cumulative reward. This process mainly contains quintuples (s, a, p, r, γ). The symbols and their corresponding explanations are listed in Table 3.

S is the state space of the environment, that is, the limited state that the SAR unit can achieve (Minsky, 1967). A is the action space of the SAR unit, which consists of all possible actions that the vessel agent can choose through strategy selection in each environmental state. In this study, the action space of the vessel agent is discretized, meaning that, from one grid to another, there are only four actions to reduce the negative impact of irregular searches on the security of searches (IAM-SAR, 2016). P is the state transition model; that is, the probability that in the current state s of the environment, where an agent causes this s to transfer to another state s' . R is the reward value function fed back to the agent by the environment in the form of encouragement or punishment. The strategy of agent Π is to map S to A . If state $s_t \in S$, the agent takes action $a_t \in A$, and moves to the next state s_{t+1} according to P , meanwhile receives a reward value $r_t \in R$. The discount factor γ is used to calculate the cumulative value of returns over time. We have provided a detailed description of reward and action selection policies.

- Reward function

A suitable reward function is required to specify the training objective. The advantages and disadvantages of a vessel agent in the learning process can be determined using the reward function. This enables it to achieve its goal in the shortest time. In maritime SAR coverage path planning, a ship agent is required to search the overall SAR area under the conditions of prioritizing search areas with high probability and ensuring that no duplicate paths are taken.

Sets H and U are introduced to mark the position information of the grid units that the agent has searched for and has not searched for. At model initialization, set $H = \{s_0\}$ and $U = \{s_1, s_2, s_3, \dots, s_n\}$. Grid units in the hierarchical environment map with a POC value of 0 were not searched and were denoted as set F to reduce the search time. Set F is then added to set H and it is removed simultaneously from set U .

After the ship's agent selects an action according to the action selection strategy, it arrives at state s_{t+1} and determines whether s_{t+1} is already in set H . If $s_{t+1} \notin H$, positive rewards R_{search} is feedback, and the state s_{t+1} is then added to set H while being removed from set U . This can guide the agents to cover all the SAR areas. The reward function design should consider the priority search of high-probability grids, namely, the POC reward, which is calculated using the following equation:

$$R_{POC} = \frac{1}{step_i} POC_i \times 1000i \in (0, T) \quad (13)$$

where T is the maximum number of steps that the vessel agent can take in each iteration; POC_i is the POC value of the SAR grid in the next state that the agent reaches; and $step_i$ is the number of steps experienced by the ship agent in the current state. As the number of steps increases, R_{POC} decreases, thereby guiding the ship agent to search the high-probability region first.

R_{done} is given once the ship agent passes through the entire search area, and they enter the termination state S_{done} . The reward function was set as follows:

$$R = \begin{cases} R_{search} + R_{POC} & s_{t+1} = S_{done} \&\& s_{t+1} \notin H \\ R_{done} & s_{t+1} = S_{done} \\ 0 & else \end{cases} \quad (14)$$

- Action selection policy

In reinforcement learning, the two crucial concepts of exploitation and exploration need to be balanced. Exploitation involves selecting the optimal action for the vessel agent by maximizing the value of all known state-action pairs. However, if the vessel agent chooses randomly from its set of actions, it is referred to as exploration. While exploitation helps maximize the expected rewards in real time, it may lead to local optima. By contrast, exploration helps maximize total returns in the long run.

In this study, we have proposed an action selection strategy that balances exploitation and exploration to achieve a global optimal solution. In the early stages of reinforcement learning, the vessel agent prioritizes exploration with a high probability. As the number of learning episodes increases, the probability of exploration gradually decreases, whereas the probability of exploitation increases. In this study, a ϵ -greedy strategy was used (Tokic, 2010). A random action selection is conducted with the probability of ϵ to explore the new environment. Meanwhile, action a with the highest Q value is selected with the probability of $1 - \epsilon$. The equation used is as follows:

$$A^* \leftarrow \arg \max_a Q(s, a) \quad (15)$$

$$\Pi(a|s) \leftarrow \begin{cases} 1 - \epsilon + \frac{\epsilon}{|A(s)|} & \text{if } a = A^* \\ \frac{\epsilon}{|A(s)|} & \text{if } a \neq A^* \end{cases} \quad (16)$$

where $|A(s)|$ denotes the number of actions performed in the current state.

During learning, a random number $rand$, $rand \in (0, 1)$ is generated. If $rand < \epsilon$, the action is selected at random, and if $rand > \epsilon$, the action with the highest Q value in the current state is selected. To ensure model stability and obtain the global optimal solution, the value of ϵ is dynamically adjusted in the iterative calculation as follows:

$$\epsilon = 1 - episode / L \quad (17)$$

where $episode$ is the current episode number and L is the maximum learning episode.

Boundary assessment, repeated search assessment, and termination conditions were added to the action selection process to prevent the model from looping endlessly. Each time a new state s_t is reached, the set of available actions A_{choose} under the current state is initialized as $[True, True, True, True]$, and the action a_t is selected using an ϵ -greedy approach. Upon reaching the next state s_{t+1} , if the current state s_t is located at the boundary of the search area and the state s_{t+1} is beyond the SAR area, or if $s_{t+1} \in H$, the action is reselected and the corresponding action in A_{choose} is marked as False. If $A_{choose} = [False, False, False, False]$, the termination condition is reached and the current episode ends.

The objective of reinforcement learning is to optimize the long-term cumulative reward for vessel navigation, rather than focusing on short-term rewards. With the introduction of $\gamma \in [0, 1)$, the feedback value can be described as follows:

$$R_t = r_{t+1} + \gamma r_{t+2} + \gamma^2 r_{t+3} + \dots = \sum_{k=0}^{\infty} \gamma^k r_{t+k+1} \quad (18)$$

The state value function $V_{\Pi}(s)$ is the evaluation of the quality of the current state. Each state's value depends not only on its current state, but also on its subsequent states. The value of the $V_{\Pi}(s)$ of the current s is obtained by calculating the expectation of the accumulated reward R_t of the state:

$$V_{\Pi}(s) = E_{\Pi}[R_t | s_t = s] \quad (19)$$

The action value function of the state-action couple (s, a) , denoted as $Q_{\Pi}(s, a)$, evaluates the long-term payoff to the agent through the use of strategy Π :

$$Q_{\Pi}(s, a) = E_{\Pi}[R_t | s_t = s, a_t = a] \quad (20)$$

The optimal decision sequence of the MDP is solved using the Bellman equation, which is the transformation relation of the value function:

$$V_{\Pi}(s) = \sum_a \Pi(s, a) \sum_{s'} P_{ss'}^a [R_{ss'}^a + \gamma V_{\Pi}(s')] \quad (21)$$

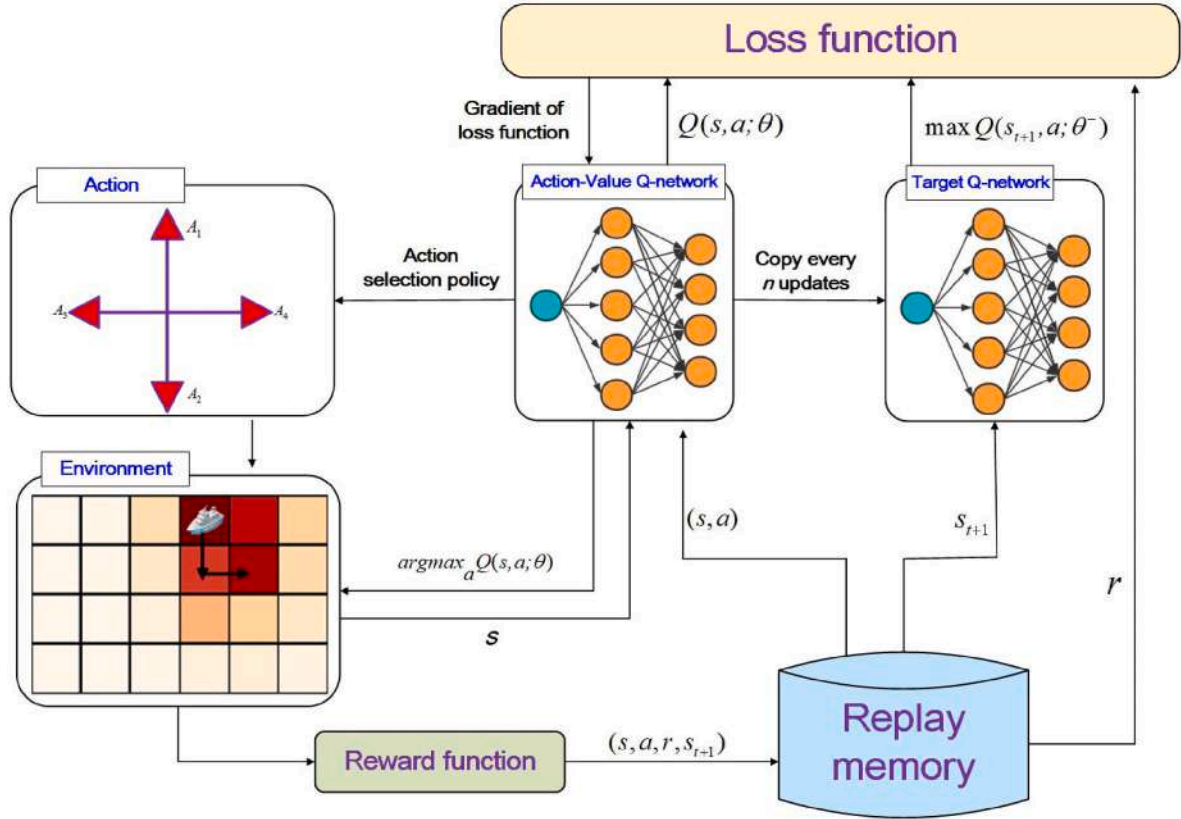


Fig. 8. The path planning model based on DQN.

$$Q_{\Pi}(s, a) = \sum_s P_{ss}^a \left[R_{ss}^a + \gamma \sum_{a'} Q_{\Pi}(s', a') \right] \quad (22)$$

where, $P_{ss}^a = P(s_{t+1} = s' | s_t = s, a_t = a)$, $R_{ss}^a = E[r_{t+1} | s_t = s, a_t = a, s_{t+1} = s]$.

Monte Carlo learning and time difference learning (TD) are used to approximate the solution of the Bellman equation, while continuously optimizing of the value function to improve Π . Watkins first proposed the Q-learning algorithm (Watkins, 1989; Watkins and Dayan, 1992), combining the Bellman equation, MDP, and other theories with TD learning. TD Learning combines a Monte Carlo sampling method with a dynamic programming method, estimating the current value function from the value function of the subsequent state. The value function was computed as follows:

$$V_{\Pi}(s) \leftarrow V_{\Pi}(s) + \delta (R_{t+1} + \gamma V_{\Pi}(s') - V_{\Pi}(s)) \quad (23)$$

where $R_{t+1} + \gamma V_{\Pi}(s')$ is the TD target, $\delta_t = R_{t+1} + \gamma V_{\Pi}(s') - V_{\Pi}(s)$ is the TD bias, δ is the learning rate.

5.2.2. Maritime coverage path planning model based on deep reinforcement learning

RL has an edge in decision-making, and the deep learning approach combines low-level features to form more abstract high-level features or categories, approximating a nonlinear function, and excels in perception (Hinton et al., 2006). Combined with the characteristics of deep learning, the use of deep neural networks as function approximators can substantially improve RL performance of reinforcement learning. DRL integrates RL and deep learning to complement each other and provides a more effective solution to the perception and decision problems of the system. The Q-learning algorithm builds a Q-table to iterate over the values of all existing state-action pairs in the storage environment and then reads these values through queries. DQN uses a general function

approximator (artificial neural network) to replace the stored Q value. The main idea is to replace the traditional Q table with a deep neural network trained from stored experience samples, build a “memory” of selected experiences, and train the Q network on a subset of states rather than on all states that the agent sees. Given that there is no network, Q-learning is too dependent on the state and may lead to insufficient learning (Cao et al., 2019; Fang et al., 2021; Zhu and Zhang, 2021; Meng et al., 2021).

Most current studies consider a single person falling into water as an example to determine the search area and plan the search path. This study has considered the integrated search and rescue area of people falling into water using different gestures. In this context, the state space is two-dimensional and the action space is discrete. In future studies, large-scale drowning accidents caused by ship collisions, as well as the collaborative search and rescue of drones and ships involving a three-dimensional state space and continuous action space, will be further considered. In the study of high-dimensional problems, the amount of computation required for the traditional RL algorithm increases sharply with an increase in the number of inputs, and it is difficult to determine an effective strategy. When the environment expands, it may cause a memory burden and lead to a failure in obtaining the optimal solution. A DQN uses neural networks to estimate values and overcomes the shortcomings of Q learning.

Mnih et al. (2015) published their work on DQN in Nature using a convolutional neural network (Lecun et al., 1998) to express the action value function and train it based on rewards. The Q-network approximation of the Q-value calculation is expressed as

$$Q(s, a; \theta) \approx Q_{\Pi}(s, a) \quad (24)$$

The DQN used in this study consists of two fully connected layers. Feature extraction and nonlinear combinations are performed to obtain the Q-value evaluated by the network for each action. The main characteristics of a DQN are as follows (Zhu and Zhang, 2021):

Table 4
Pseudo-code of the DQN training.

Algorithm. Training algorithm of DQN

Input: initial state s_0 , maximum learning episode L , maximum step size T , threshold ϵ , size of batch B , memory length M , number of steps to copy the target Q-network n

Output: trained Q-network

1. Initialize the experience buffer pool D
2. Initialize the current Q-network, generate random parameters θ .
3. Initialize the target Q-network, parameters $\theta^- \leftarrow \theta$.
4. Set $episode = 1$
5. While ($episode \leq L$) do
6. Initialize state list s_0
7. Set time step $t = 0$
8. While ($t \leq T$) do
9. $rand \leftarrow \text{random}()$
10. $Q \leftarrow \text{predict}(s_t)$
11. Get the available task list AL under state s_t
12. $a_t \leftarrow \begin{cases} \text{Randomly taken a action from AL, } rand \leq \epsilon \\ \text{argmax}Q(A) | A \in \text{AL} & \text{others} \end{cases}$
13. Calculate reward r_t by Eq. 14
14. Transfer to state s_{t+1}
15. Add the experience set of (s_t, a_t, r_t, s_{t+1}) to the experience buffer pool D.
16. $t \leftarrow t + 1$
17. For $i = 1: \min(M, B)$ do
18. load a record (s_j, a_j, r_j, s_{j+1}) from experience buffer pool D
19. add the state s_j to the set H
20. $Q(s, a) \leftarrow \max(\text{predict}(s_{j+1}))$
21. If s_{j+1} is the terminal state, then
22. $\text{targets} \leftarrow r_j$;
23. Else
24. $\text{targets} \leftarrow r_j + \gamma * Q(s, a)$;
25. End If
26. Calculate loss using mean square loss function
27. Update the current Q-network θ using gradient descent algorithm.
28. End For
29. Copy the target Q-network every n step, update parameters $\theta^- \leftarrow \theta$.
30. End While
31. End While
32. **Return:** Q-network

Table 5

The experimental overview of maritime SAR simulation.

No.	Posture	Start position	Start time (UTC+8)	End time (UTC+8)	Wind speed (m/s)	Current speed (m/s)
1	upright	119.885°E	2021/04/17 09:45	2021/04/17 16:00	2.7–7.1	0.17–0.63
		25.455°N	2021/04/17 09:45	2021/04/17 16:00		
2	facedown	119.885°E	2021/04/17 09:45	2021/04/17 16:00	2.7–7.1	0.17–0.63
		25.455°N	2021/04/17 09:45	2021/04/17 16:00		

We used Taiwan Strait drift prediction models for PIW with upright and facedown postures, namely TS_I and TS_II. In this section, unconstrained models are used to predict drift trajectories.

(1) Target network

To mitigate the instability that arises during Q-function updates, a target network is introduced to obtain the Q value before updating the Q function. The new Q function is then used to update the target network; that is, every n steps, the parameter θ_i of the current Q network will be copied to the target Q network $Q(s', a'; \theta_i^-)$.

(2) Experience pool U (D)

The experience pool constructs a replay buffer, also known as a replay memory, to store and manage samples (s_t, a_t, r_t, s_{t+1}) . The experience replay mechanism was used, and minibatch (B) samples were randomly selected for training the Q-network.

The current Q-network parameters are updated using the gradient descent method, and their loss function is expressed as:

$$L(\theta_i) = \frac{1}{2} \left(r + \gamma \max_a Q(s', a'; \theta_i^-) - Q(s, a; \theta_i) \right)^2 \tag{25}$$

The derivative $\nabla_{\theta} L$ of the parameter θ in the loss function is calculated as follows:

$$\nabla_{\theta} L = \left[r + \gamma \max_a Q(s', a'; \theta_i^-) - Q(s, a; \theta_i) \right] \nabla_{\theta} Q(s, a; \theta_i) \tag{26}$$

The proposed DQN-based search path planning model obtains the optimal search path through interactive learning between agents and a maritime SAR environment model. The vessel agent arrives at the highest POC grid unit of each block and begins searching. The path planning model is illustrated in Fig. 8. Table 4 lists these algorithms.

Maritime SAR coverage path planning based on deep RL algorithms is divided into two phases, that is, training and testing. In the training phase, the time complexity of the DQN is $O(n_s * n_d)$ when forward propagation is performed. Here, n_s is the number of states and n_d denotes the state feature dimension. When backward propagation is performed, the time complexity of the DQN is also $O(n_s * n_d)$. Therefore, the time complexity is $O(n_s * n_d)$. When training $epoch$ rounds, the forward propagation time complexity is $O(epoch * n_s * n_d)$. In the testing phase, the time complexity of DQN is also $O(n_s * n_d)$.

6. Results and discussion

6.1. Maritime SAR experimental settings

To verify the validity of the proposed SARCPPE, a real offshore drift experiment was used as a case study for the calculations and analysis. On April 16–17, 2021, sea-drift experiments with manikins in different postures (upright and facedown) were conducted in the Pingtan waters of the Taiwan Strait. The experimental overview is presented in Table 5.

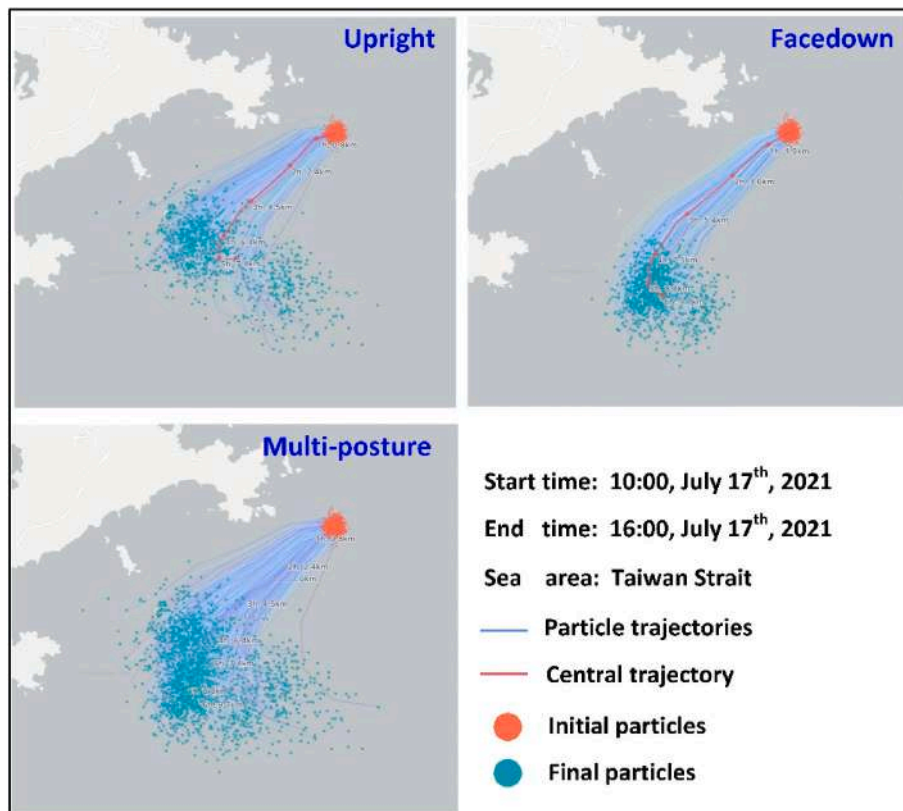


Fig. 9. Drift trajectory prediction results.

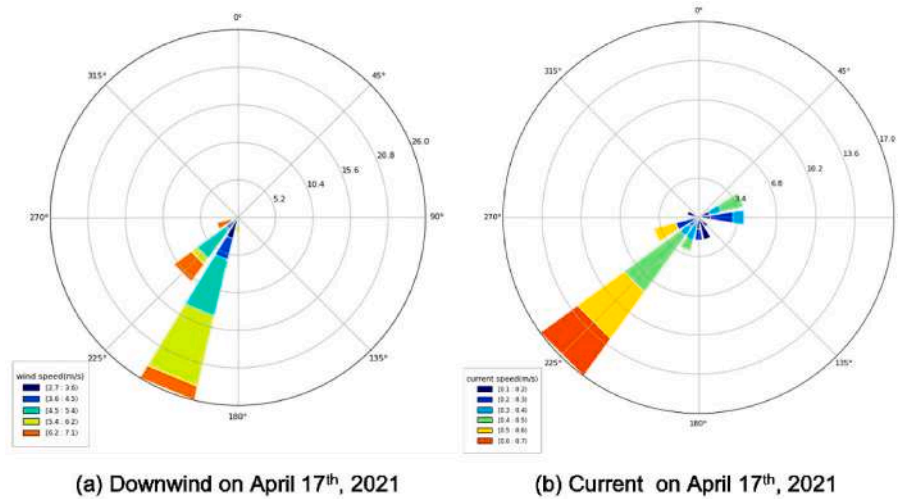


Fig. 10. The marine environment data used in the modeling process ((a) downwind speed and direction, (b) current speed and direction).

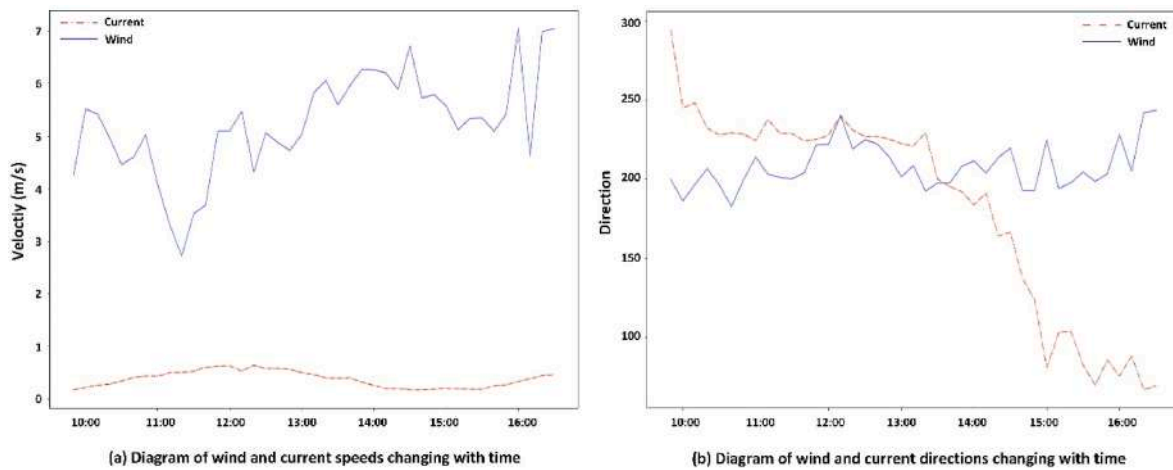


Fig. 11. The marine environment data and their changes with time used in the modeling process ((a) velocity changes, (b) direction changes).

6.2. Results of drift trajectory prediction

We took the release point of the manikins as the initial point and used the hydrometeorological data measured on April 17, 2021, the possible 6 h drift trajectories of PIWs in vertical and facedown postures were

calculated, as shown in Fig. 9. A 6 h drift trajectory and particle distribution map of PIWs was generated with the fusion of multiple postures. This was used to simulate the possible position distribution of survivors when SAR vessels arrive at the scene of multiple drownings in a maritime accident. In this study, it was assumed that the data of the possible position distribution were constant at the 6 h drift time.

The ranges of the wind and flow velocities measured (10 min average) during the experiment were counted, and a detailed statistical

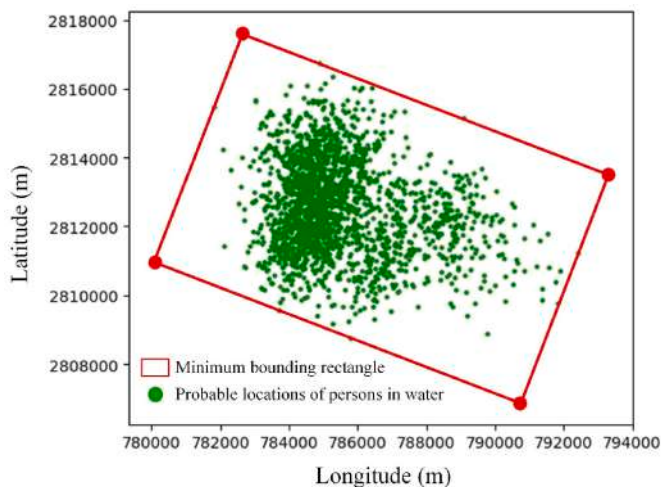


Fig. 12. The MBR of the area for SAR path planning.

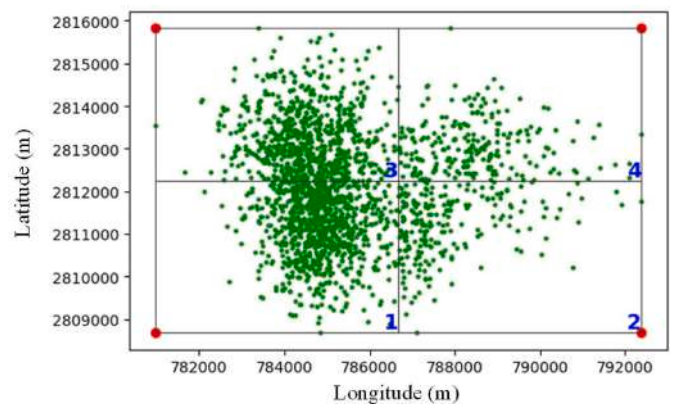


Fig. 13. The initial block division results.

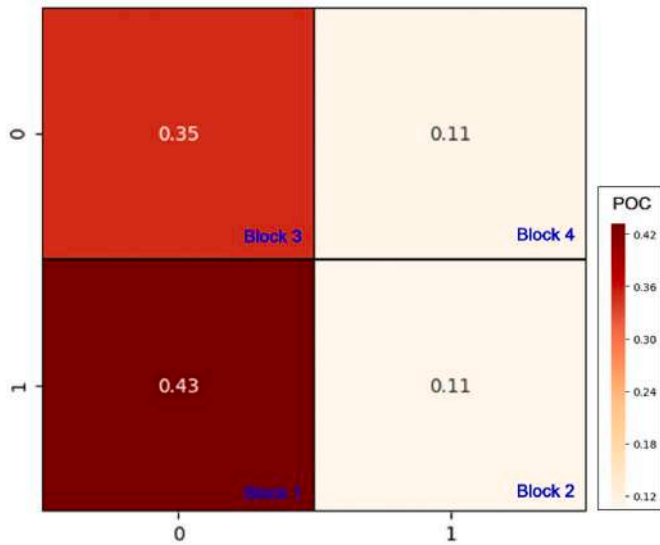


Fig. 14. The one-level hierarchical environment map.

analysis of the sea state was conducted. The wind speed range was 2.7–7.1 m/s, and the downwind direction varied in the southwest direction, and the variation range was less than 90° with relatively little fluctuation. The wind speed was divided according to wind conditions, and a rose diagram of the wind direction was drawn. The flow speed range was 0.17–0.63 m/s, and the flow direction varied from southwest to northeast with counterclockwise deflection over time. Based on the flow conditions, the flow speeds were divided, and a flow rose diagram was drawn. As shown in Figs. 10 and 11, the marine environment data and changes used in the modeling process are depicted.

Table 6

The parameters of the algorithm proposed in this study.

Parameter	Value	Description
L	5000	maximum learning episode
T	200	maximum step size
γ	0.5	discount factor
LR	0.1	learning rate
n	50	target network update frequency
ϵ	0.9	initial action selection strategy
B	32	batch size
M	1000	memory length
Layers	10	the number of neurons in each hidden layer
N_STATES	2	the input neurons
$N_ACTIONS$	4	the output neurons
Optimizer	Adam	optimizer

6.3. Results of maritime SAR environment modeling

6.3.1. Results of the establishment of MBR

The MBR of the area for SAR path planning according to the final particle distribution of the multi-posture PIWs is shown in Fig. 12. Assuming that four nearby vessels can be engaged in simultaneous search and rescue after rotation, the initial block-division results are as shown in Fig. 13.

6.3.2. Results of the hierarchical probability map

A one-level hierarchical environment map was generated. According to visibility reanalysis data from the European Center for Medium-Range Weather Forecasts (ECMWF), visibility in Pingtan was 18.5 km on April 17, 2021. Based on the sweep width table (Table 2), the sweeping width of the vessel agent was set to 1 km. From the measured marine environment data (Table 5 and Fig. 10), the value of the weather correction coefficient was 1. Therefore, the corrected sweep width of the vessel is the same as the unadjusted sweep width.

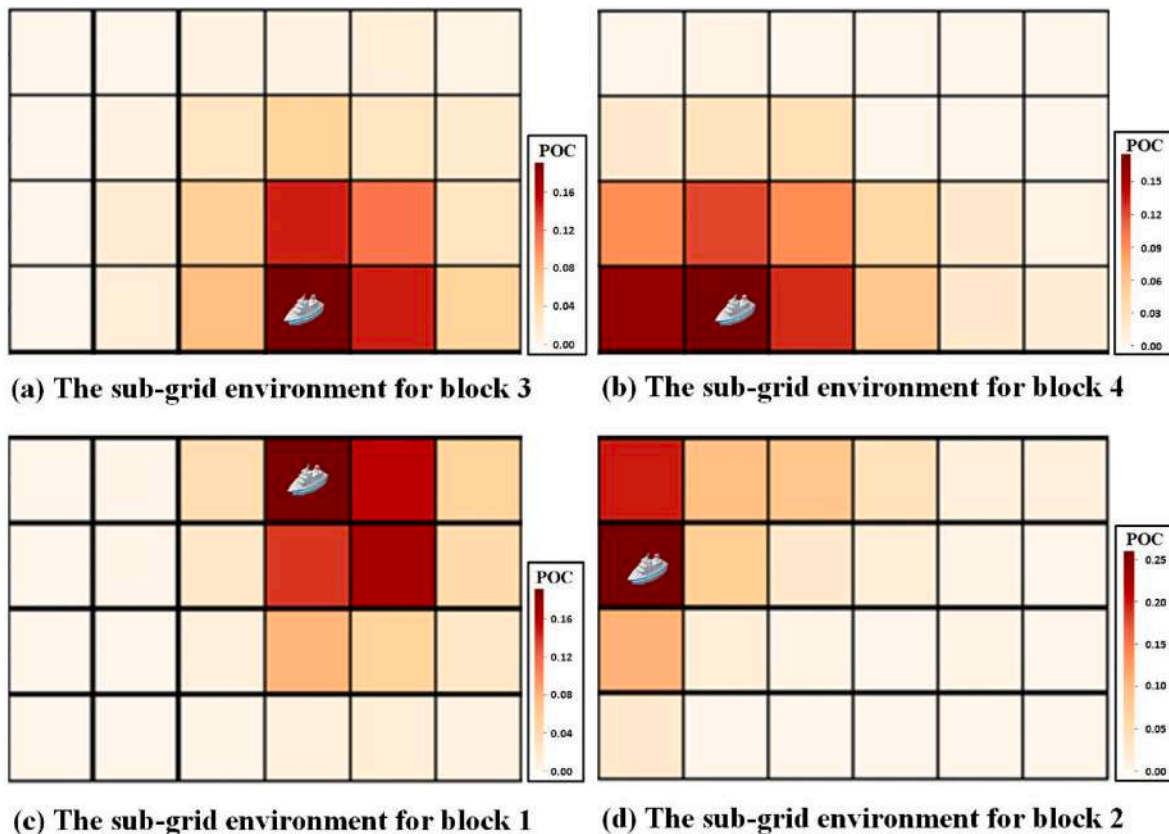


Fig. 15. The sub-grid hierarchical environment map.

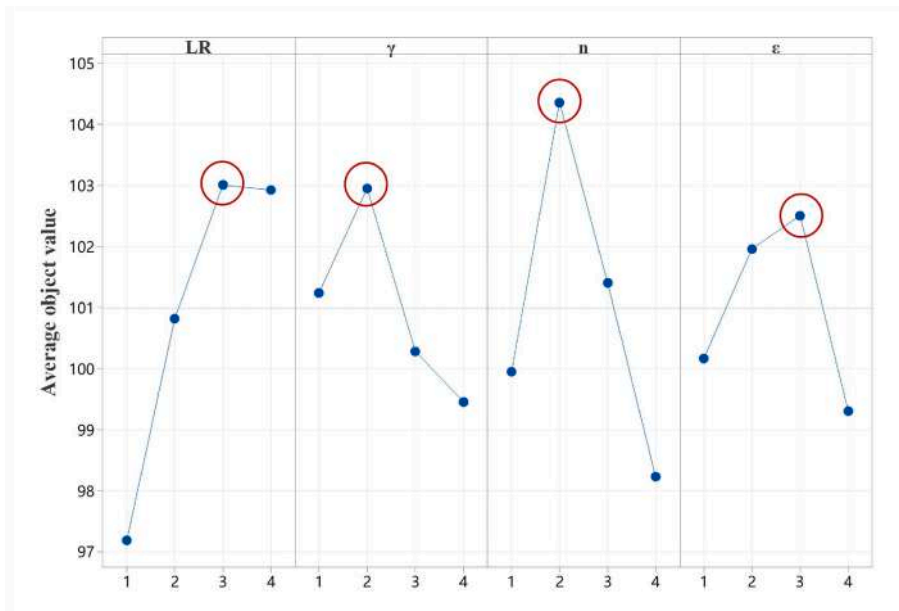


Fig. 16. The average results of our object for different parameter settings.

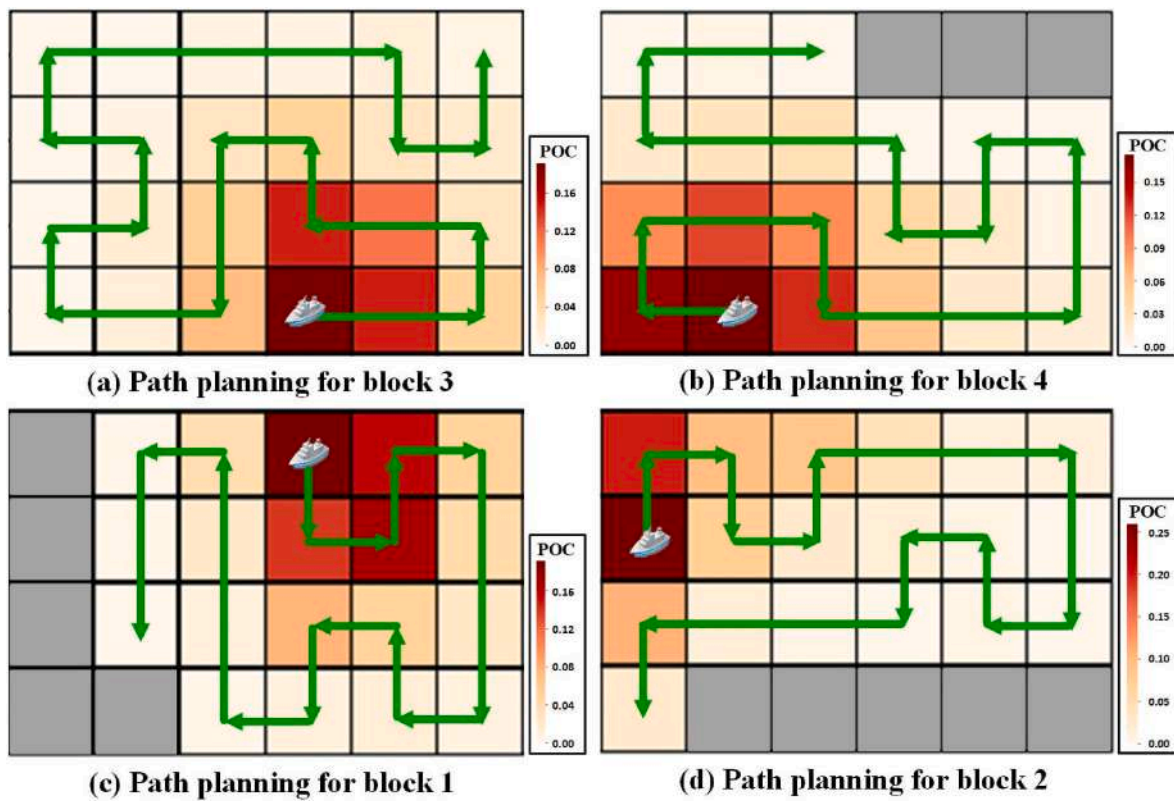


Fig. 17. The path planning results obtained by the model proposed in this study.

Based on the corrected sweep width, each initial block was partitioned into grid units to generate a hierarchical environmental map. The grid cell size and track spacing were determined using the corrected sweep-width. The simulated scene was situated in an open sea without natural or artificial obstacles. The hierarchical probability environment map and the initial position of the SAR vessels are shown in Figs. 14 and 15.

6.4. SAR coverage path planning results

- Experimental settings

Simulation Environment: All the simulation experiments in our study were conducted on a desktop computer with an Intel (R) Core (TM) i7-1260P 2.10 GHz CPU, 16 GB of RAM, and Windows 11 operating system, using the Python programming language.

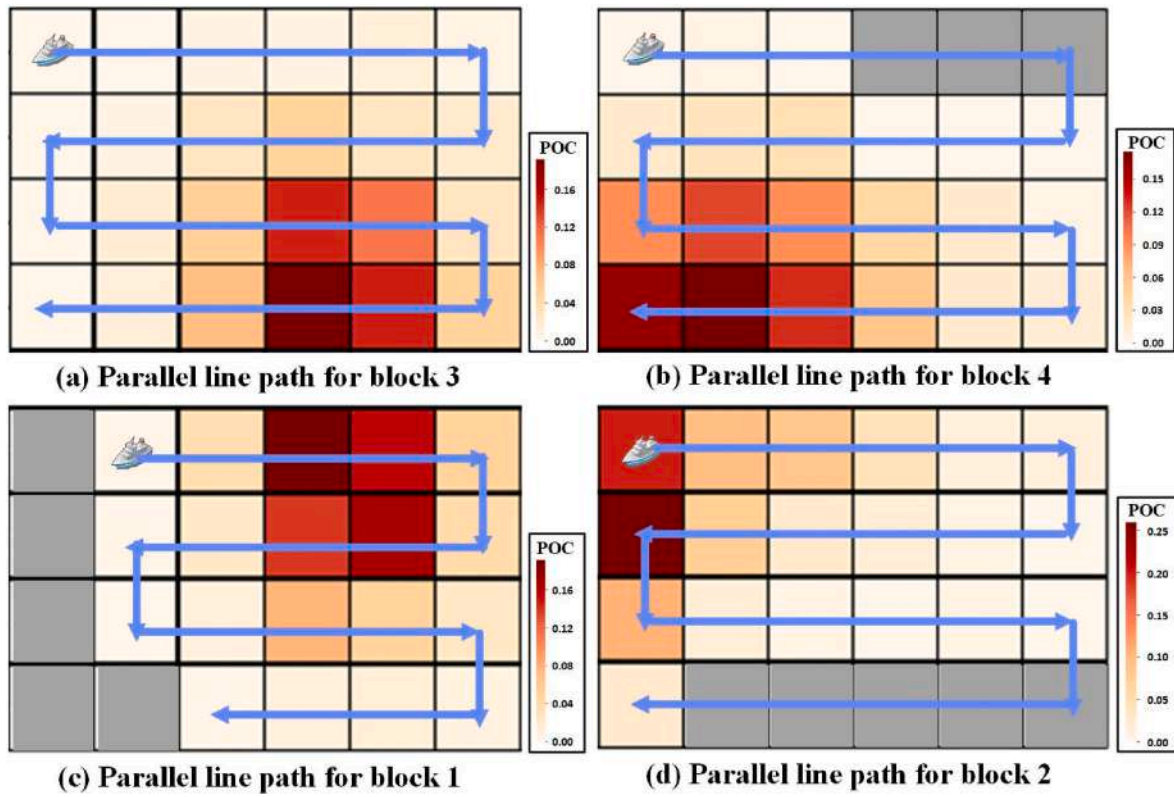


Fig. 18. Search starting points and routes of the traditional parallel line scanning algorithm (PA).

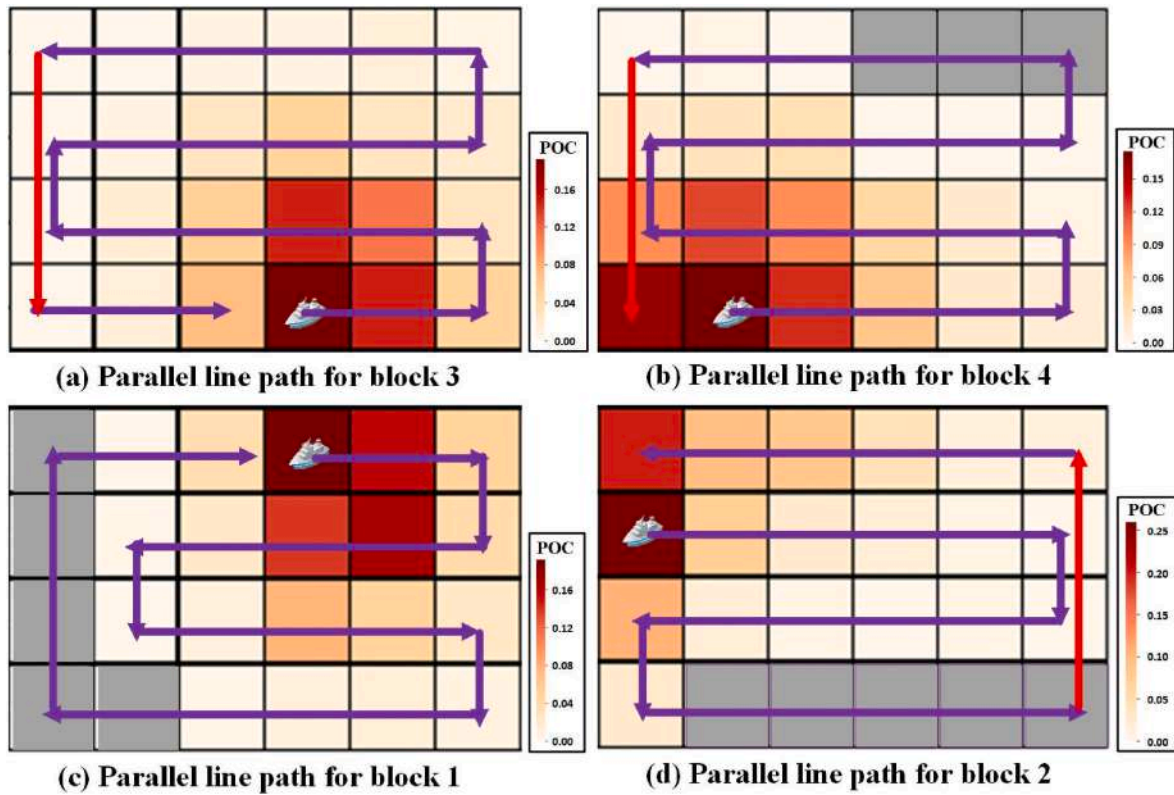


Fig. 19. Search starting points and routes of the traditional parallel line scanning algorithm starting from the highest heat grid (SPA) (the red line represents the overlapping path).

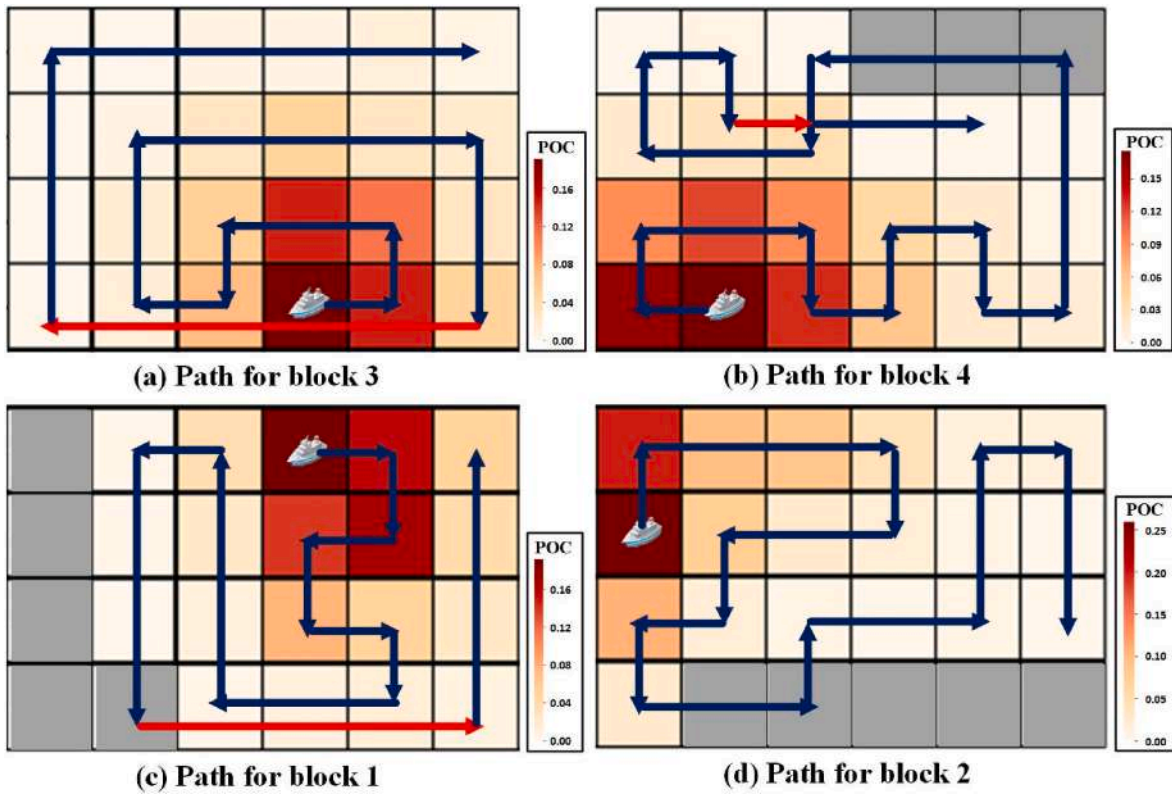


Fig. 20. Search starting points and routes of the BA* algorithm (the red line represents the overlapping path).

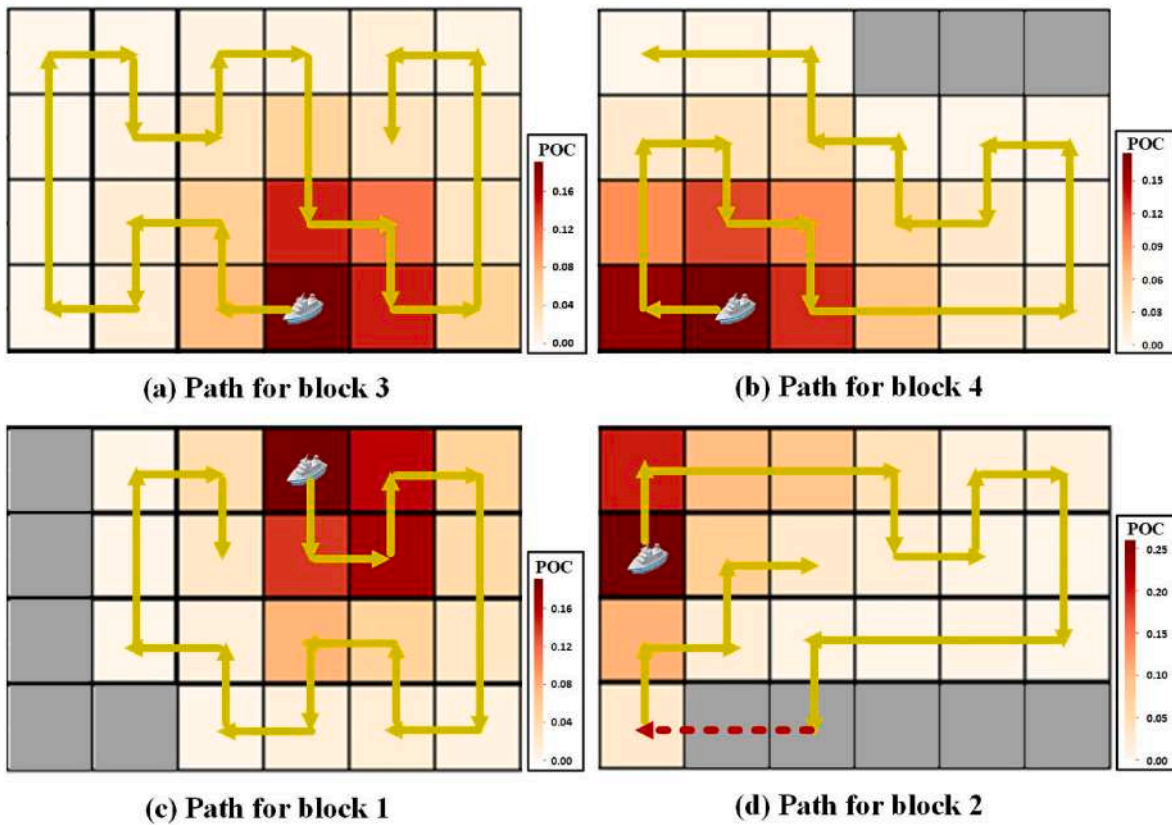


Fig. 21. Search start points and routes of the Q-learning algorithm.

Table 7

The repetition rate, coverage ratio, and the number of steps of SAR planning results.

Block	Algorithms	Repeated coverage (%)	Coverage (%)	Step
Block 1	Ours	0	100	18
	Q-learning	0	100	18
	PA	0	100	18
	SPA	0	100	23
	BA*	13.6	100	22
Block 2	Ours	0	100	18
	Q-learning	0	100	20
	PA	0	100	23
	SPA	8	100	25
	BA*	0	100	20
Block 3	Ours	0	100	23
	Q-learning	0	100	23
	PA	0	100	23
	SPA	8	100	25
	BA*	14.8	100	27
Block 4	Ours	0	100	20
	Q-learning	0	100	20
	PA	0	100	23
	SPA	8	100	25
	BA*	4	100	25

Algorithm Comparison: The proposed algorithm was compared with a search method commonly used in maritime SAR and a more advanced path-planning algorithm. Including the traditional parallel line scanning algorithm (PA) (IAMSAR, 2016), the parallel line scanning algorithm

starts from the highest heat grid (SPA), the BA* algorithm (Viet et al., 2013), and the Q-learning method (Ai et al., 2021). The BA* algorithm was used to solve an online complete coverage task for an autonomous cleaning robot in an unknown workspace based on boustrophedon motion and an A* search algorithm. The robot performed a boustrophedon motion to cover the unvisited area until it reached the critical point. The robot then detected the backtracking point based on its accumulated knowledge, determined the best backtracking point as the starting point for the next boustrophedon motion, and continued to cover the next unvisited region, thereby achieving complete coverage. We added a search strategy for prioritizing high-probability areas to the BA* algorithm and Q-learning method to ensure fairness.

Algorithm parameter settings: The parameters of the proposed algorithm are listed in Table 6. Among them, the Taguchi experimental design methodology was used to determine the four control parameters, that is, learning rate LR , discount factor γ , target network update frequency n , and the initial action selection strategy ϵ , in our maritime coverage path planning model. The levels of the four parameters are as follows:

$$LR = \{0.005, 0.001, 0.1, 0.15\}$$

$$\gamma = \{0.45, 0.5, 0.6, 0.8\}$$

$$n = \{20, 50, 80, 100\}$$

$$\epsilon = \{0.8, 0.85, 0.9, 0.95\}$$

At these parameter levels, orthogonal matrix $L_{16}(4^4)$ was used for the

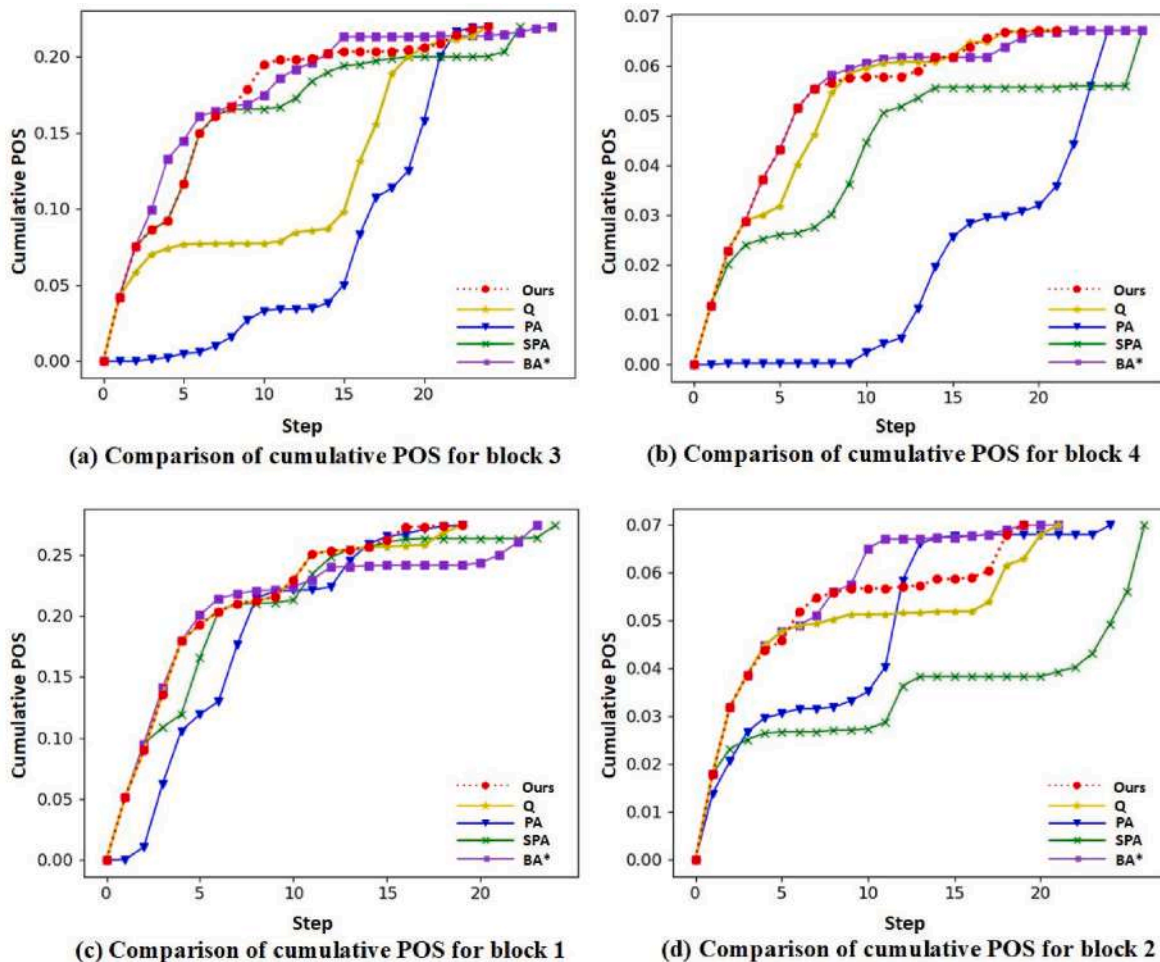


Fig. 22. Comparison of the cumulative changes in the POS between different methods for four hierarchical probability environments.

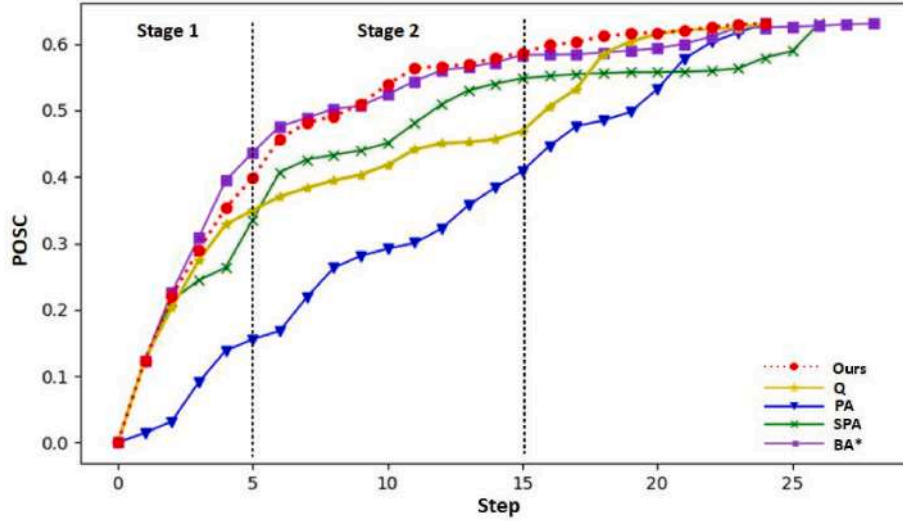


Fig. 23. Comparison of the cumulative changes in the POSC between different methods for the whole search area.

calibration experiment. To ensure equity, the algorithm was run 20 times independently for each parameter setting. The average results for our object for different parameter settings are shown in Fig. 16. The optimal control parameter settings were determined to be: $LR = 0.1$, $\gamma = 0.5$, $n = 50$, $\varepsilon = 0.9$.

Therefore, the control parameters used in this study were set as follows. The learning rate is 0.1, the γ coefficient is 0.5, the target network update frequency is 50 steps, the initial action selection strategy is 0.9, and the maximum learning episode is 5000.

• Results and analysis

The proposed method was tested in four hierarchical environments (Fig. 15), and the path-planning results are shown in Figs. 17–21. These algorithms can achieve full coverage of the search and rescue areas by setting search rules. However, the search path planning results of the SPA and BA* algorithms contained overlapping paths, whereas both the Q-learning algorithm and our model have the ability to achieve no duplicate path coverage. However, in some environments (grey grids in Fig. 21 d), the Q-learning algorithm passes through the region where the grid unit POC value is zero in the hierarchical probabilistic environment map, which may lead to an increase in search time.

To quantitatively assess the above methods, the repetition rate, coverage ratio, and number of path planning steps were computed, as shown in Table 7. The results have shown that the navigation route generated by our model performs more effectively than the other algorithms in terms of repetition and the number of steps. According to the calculation methods of POC and POD described in Section 2, they were evaluated from the perspective of the cumulative POS. As shown in Fig. 22, in the four sub environments, our model reached the maximum cumulative POS with the fewest steps, and the cumulative POS growth rate of our model was faster, indicating that the vessel agent in our model can prioritize covering high-probability regions.

The cumulative POS of the parallel line scanning algorithm and BA* algorithm increased rapidly at some point. However, the proposed algorithm still achieved the maximum cumulative POS with a relatively small number of steps, indicating that the proposed algorithm can still find higher-quality solutions after reaching a certain degree of search, demonstrating its superior exploitation ability. Although the BA* algorithm can achieve full coverage and rapid growth of cumulative POS in the short term, it performed poorly in balancing the two goals of non-duplicate paths and prioritizing the search for high probability zones. In some cases, it produced more duplicated searches in pursuit of high probability zone coverage (block 3), making it difficult to meet SAR

requirements in complex scenarios with large search areas. Although the Q-learning algorithm also showed strong performance in reaching the maximum cumulative POS with fewer steps, in some environments the cumulative POS growth rate was slower than that of our algorithm, and our algorithm showed better performance in preferentially covering high-probability regions.

Based on the hierarchical probability environment map, the cumulative POS for the overall SAR area (POSC) of each path-planning method was calculated based on the assumption that ships in the four subgrid hierarchical environments perform simultaneous searches at the same time and search speed. POSC can be calculated as follows:

$$POC_{mn} = POCT_{mn} * POC_m \quad (27)$$

$$POSC = \sum_{k=0}^N POS_k \quad (28)$$

$$POS_k = \sum_{m=1}^M POST_m \quad (29)$$

where POC_{mn} is the POC of each grid cell in the overall environment map, m is the block number, n is the grid cell number, $POCT_{mn}$ is the POC of grid cell n in the subgrid hierarchical environment, POC_m is the POC of block m in the one-level hierarchical environment map, k is the number of search steps of the current ship, N is the maximum number of search steps of each subgrid hierarchical environment map, POS_k is the POS of the entire SAR region in the current step, $POST_m$ is the POS of each subgrid hierarchical environment in the current step.

The POSC of the different path-planning methods are shown in Fig. 23. For the entire search and rescue area, both the Q-learning algorithm and our algorithm achieved the maximum POSC with the shortest number of steps and showed better search performance and convergence ability. The Q-learning algorithm also showed a high level of performance in the initial stage of the search (Stage 1). In the middle stage of the search (Stage 2), the cumulative POS growth was slow, indicating that our algorithm is superior to the Q-learning algorithm in exploration and can be used more effectively in conducting priority search in high-probability regions. Although the traditional PA algorithm can also achieve the fastest speed to complete the coverage search of the entire SAR area, it performs poorly in terms of the growth rate of POSC. The SPA algorithm achieves the improvement of search capability based on PA, and the BA* algorithm performed better in terms of prioritizing the search of high probability areas but performed poorly in terms of the time to complete the full-coverage search.

7. Conclusions

This study has integrated reinforcement learning into maritime SAR coverage path planning and establishes a maritime SARCPPF suitable for PIWs scenarios. This system comprises three modules, namely, drift trajectory prediction, hierarchical environment map modeling, and coverage search. Sea-area-scale drift prediction models of PIWs in the Chinese sea area were used based on the variations in PIWs across different sea areas and postures. A minimum bounding rectangle was used to establish a hierarchical probability environment map, facilitating the search for multiple SAR units. A coverage path planning algorithm that leverages deep reinforcement learning was devised. Comparative experiments have demonstrated that the proposed algorithm significantly enhances POS within a constrained timeframe.

However, this study has certain limitations, including that it was assumed that the search environment remained constant during path planning. In future studies, the algorithm should dynamically update the search environment based on the SAR task performance and drifting conditions to improve the search accuracy. This study was conducted based on the assumption that the number of SAR units was sufficient. In the future, a detailed analysis will be conducted on the number, location, search and rescue capabilities, as well as other characteristics of SAR forces, to optimize the division of search and rescue areas. In addition, coordinated searches using multiple SAR forces will also be studied.

Funding

This work was supported by the National Key Research and Development Program of China (2022YFB3903603) and National Natural Science Foundation of China (42001401).

CRedit authorship contribution statement

Jie Wu: Data curation, Methodology, Writing – original draft, Software. **Liang Cheng:** Conceptualization, Resources, Funding acquisition, Supervision. **Sensen Chu:** Visualization, Investigation. **Yanjie Song:** Validation, Writing – review & editing.

Declaration of competing interest

The authors declare that they have no known competing financial interests or personal relationships that could have appeared to influence the work reported in this paper.

Data availability

Data will be made available on request.

References

- Abi-Zeid, I., Frost, J.R., 2005. SARPlan: a decision support system for Canadian search and rescue operations. *Eur. J. Oper. Res.* 162, 630–653. <https://doi.org/10.1016/j.ejor.2003.10.029>.
- Abi-Zeid, I., Nilo, O., Lamontagne, L., 2011. A constraint optimization approach for the allocation of multiple search units in search and rescue operations. *Info. R.* 49, 15–30. <https://doi.org/10.3138/infor.49.1.015>.
- Agbissoh Otote, D., Li, B., Ai, B., et al., 2019. A decision-making algorithm for maritime search and rescue plan. *Sustainability* 11, 2084. <https://doi.org/10.3390/su11072084>.
- Ai, B., Jia, M., Xu, H., et al., 2021. Coverage path planning for maritime search and rescue using reinforcement learning. *Ocean Eng.* 241, 110098 <https://doi.org/10.1016/j.oceaneng.2021.110098>.
- Ai, B., Li, B., Gao, S., Xu, J., Shang, H., 2019. An intelligent decision algorithm for the generation of maritime search and rescue emergency response plans. *IEEE Access* 7, 155835–155850. <https://doi.org/10.1109/ACCESS.2019.2949366>.
- Allen, A.A., 2005. Leeway Divergence. U.S. Coast Guard Rep. CG-D-05-05, p. 128.
- Allen, A.A., Plourde, J.V., 1999. Review of Leeway: Field Experiments and Implementation. U.S. Coast Guard Rep. CG-D-08-99, p. 351.

- Allen, A.A., Roth, J.C., Maisondieu, C., et al., 2010. Field Determination of the Leeway of Drifting Objects. Norwegian Meteorological Institute, Oslo.
- Anderson, E., Greenbaum, H., McClay, T., et al., 2006. NSMRL. S.E.E./Rescue Project Target Detectability Testing, Modeling, and Analysis, vol. 2006. nsmrl see/rescue project target detectability testing modeling & analysis.
- Binney, J., Krause, A., Sukhatme, G.S., 2010. Informative Path Planning for an Autonomous Underwater Vehicle. *IEEE Publications*, pp. 4791–4796. <https://doi.org/10.1109/ROBOT.2010.5509714>.
- Bourgault, F., Furukawa, T., Durrant-Whyte, H.F., 2003. Coordinated decentralized search for a lost target in a Bayesian world. *Int. Conf. Intell. Robots Syst., Las Vegas* 48–53. <https://doi.org/10.1109/IROS.2003.1250604>.
- Breivik, Ø., Allen, A.A., 2008. An operational search and rescue model for the Norwegian Sea and the North Sea. *J. Mar. Syst.* 69, 99–113. <https://doi.org/10.1016/j.jmarsys.2007.02.010>.
- Breivik, Ø., Allen, A.A., Maisondieu, C., Olagnon, M., 2013. Advances in search and rescue at sea. *Ocean Dynam.* 63, 83–88. <https://doi.org/10.1007/s10236-012-0581-1>.
- Breivik, Ø., Allen, A.A., Maisondieu, C., Roth, J., Forest, B., 2012. The leeway of shipping containers at different immersion levels. *Ocean Dynam.* 62, 741–752. <https://doi.org/10.1007/s10236-012-0522-z>.
- Breivik, Ø., Allen, A.A., Maisondieu, C., Roth, J.C., 2011. Wind-induced drift of objects at sea: the leeway field method. *Appl. Ocean Res.* 33, 100–109. <https://doi.org/10.1016/j.apor.2011.01.005>.
- Brown, S.S., 1980. Optimal search for a moving target in discrete time and space. *Oper. Res.* 28, 1275–1289. <https://doi.org/10.1287/opre.28.6.1275>.
- Brushett, B.A., Allen, A.A., King, B.A., Lemckert, C.J., 2017. Application of leeway drift data to predict the drift of panga skiffs: case study of maritime search and rescue in the tropical pacific. *Appl. Ocean Res.* 67, 109–124. <https://doi.org/10.1016/j.apor.2017.07.004>.
- Burciu, Z., 2010. Bayesian methods in reliability of search and rescue action. *Pol. Marit. Res.* 17, 72–78. <https://doi.org/10.2478/v10012-010-0039-7>.
- Busoniu, L., Babuska, R., De Schutter, B.A., 2008. A Comprehensive survey of multiagent reinforcement learning. *IEEE Trans. Syst. Man Cybern. C.* 38, 156–172. <https://doi.org/10.1109/TSMCC.2007.913919>.
- Cao, X., Sun, C., Yan, M., 2019. Target search control of AUV in underwater environment with deep reinforcement learning. *IEEE Access* 7, 96549–96559. <https://doi.org/10.1109/ACCESS.2019.2929120>.
- Canadian Coast Guard, Canadian Coast Guard College CANSARP Development Group Web site, 2009. CANSARP User Manual. <http://loki.cgc.gc.ca/cansarp/cansarp-manualsept1609.pdf>.
- Carneiro, J.P., 1988. Maritime search and rescue. *IETE Tech. Rev.* 5, 111–114. <https://doi.org/10.1080/02564602.1988.11438248>.
- Chabini, L., Lan, S., 2002. Adaptations of the A* algorithm for the computation of fastest paths in deterministic discrete-time dynamic networks. *Intel. Transport. Syst. IEEE Trans.* 3 (1), 60–74. <https://doi.org/10.1109/6979.994796>.
- Chen, H.T., Xu, W.M., Sun, L.Y., et al., 2017. An example of AP98 Leeway drift model application: drift experiment of DongFangHong 2. *Trans. Oceanol. Limnol.* 6, 46–51.
- Chen, Y., Zhu, S., Zhang, W., Zhu, Z., Bao, M., 2022. The model of tracing drift targets and its application in the South China Sea. *Acta Oceanol. Sin.* 41, 109–118. <https://doi.org/10.1007/s13131-021-1943-7>.
- Cheng, P.F., Yan, H.W., Han, Z.H., 2008. An algorithm for computing the minimum area bounding rectangle of an arbitrary polygo. *J. Eng. Graph.* 29 (1), 122–126. <https://doi.org/10.1007/s11123-007-0067-1>, 2008.
- Cho, S.W., Park, H.J., Lee, H., Shim, D.H., Kim, S., 2021. Coverage path planning for multiple unmanned aerial vehicles in maritime search and rescue operations. *Comput. Ind. Eng.* 161, 107612 <https://doi.org/10.1016/j.cie.2021.107612>.
- Daniel, P., Marty, F., Josse, P., Skandrani, C., Benschila, R., 2003. Improvement of drift calculation in MOTHY operational oil spill prediction system. In: *International Oil Spill Conference Proceedings International Oil Spill Conference, Vancouver*, vol. 2003, pp. 1067–1072. <https://doi.org/10.7901/2169-3358-2003-1-1067>, 2003.
- Dijkstra, E.W., 1959. A note on two problems in connexion with graphs. *Numer. Math.* 1, 269–271. <https://doi.org/10.1007/BF01386390>.
- Engel, D.D., Weisinger, J.R., 1988. OR practice—estimating visual detection performance at sea. *Oper. Res.* 36, 651–659. <https://doi.org/10.1287/opre.36.5.651>.
- Englot, B., Hover, F.S., 2013. Three-dimensional coverage planning for an underwater inspection robot. *Int. J. Robot Res.* 32, 1048–1073. <https://doi.org/10.1177/0278364913490046>.
- Fang, Y., Pu, J., Zhou, H., et al., 2021. Attitude Control Based Autonomous Underwater Vehicle Multi-Mission Motion Control with Deep Reinforcement Learning. In: *5th International Conference on Automation, Control and Robots (ICACR)*, Nanning, China, pp. 120–129. <https://doi.org/10.1109/ICACR53472.2021.9605171>, 2021.
- Fevgas, G., Lagkas, T., Argyriou, V., Sarigiannidis, P., 2022. Coverage path planning methods focusing on energy efficient and cooperative strategies for unmanned aerial vehicles. *Sensors (Basel)* 22, 1235. <https://doi.org/10.3390/s22031235>.
- Frost, J.R., 1997. *The Theory of Search: a Simplified Explanation*. Soza Limited.
- Frost, J.R., 2001. *Review of Search Theory*. U. S. Coast Guard Office of Operations (G-OPR), 2001.
- Frost, J.R., Stone, L.D., 2001. *Review of Search Theory: Advances and Applications to Search and Rescue Decision Support*. U.S. Coast Guard Research and Development Center. Report No. CG-D-15-01.
- Galceran, E., Carreras, M., 2013. A survey on coverage path planning for robotics. *Robot. Autonom. Syst.* 61, 1258–1276. <https://doi.org/10.1016/j.robot.2013.09.004>.
- Graham, R.L., 1972. An efficient algorithm for determining the convex hull of a finite planar set. *Inf. Process. Lett.* 1 (1972), 132–133.

- Xiong, P., Liu, H., Tian, Y., et al., 2021. Helicopter maritime search area planning based on a minimum bounding rectangle and K-means clustering. *Chin. J. Aeronaut.* 34, 554–562. <https://doi.org/10.1016/j.cja.2020.08.047>.
- Xiong, W., van Gelder, P.H.A.J.M., Yang, K., 2020. A decision support method for design and operationalization of search and rescue in maritime emergency. *Ocean Eng.* 207, 107399 <https://doi.org/10.1016/j.oceaneng.2020.107399>.
- Yang, T., Jiang, Z., Sun, R., Cheng, N., Feng, H., 2020. Maritime search and rescue based on group mobile computing for unmanned aerial vehicles and unmanned surface vehicles. *IEEE Trans. Ind. Inf.* 16, 7700–7708. <https://doi.org/10.1109/TII.2020.2974047>.
- Yao, P., Xie, Z., Ren, P., 2019. Optimal UAV route planning for coverage search of stationary target in river. *IEEE Trans. Control Syst. Technol.* 27, 822–829. <https://doi.org/10.1109/TCST.2017.2781655>.
- Zhang, H., Sun, J., Yang, B., Shi, Y., Li, Z., 2020. Optimal search and rescue route design using an improved ant colony optimization. *Inf. Technol. Control* 49, 438–447. <https://doi.org/10.5755/j01.itc.49.3.25295>.
- Zhang, J.F., Teixeira, Á.P., Guedes Soares, C.G., Yan, X., 2017. Probabilistic modelling of the drifting trajectory of an object under the effect of wind and current for maritime search and rescue. *Ocean Eng.* 129, 253–264. <https://doi.org/10.1016/j.oceaneng.2016.11.002>.
- Zhang, Q., Chen, D., Chen, T., 2012. An obstacle avoidance method of soccer robot based on evolutionary artificial potential field. *Energy Proc.* 16 (5), 1792–1798. <https://doi.org/10.1016/j.egypro.2012.01.276>.
- Zhang, X., Wang, C., Liu, Y., Chen, X., 2019. Decision-making for the autonomous navigation of maritime autonomous surface ships based on scene division and deep reinforcement learning. *Sensors (Basel)*. 19, 4055. <https://doi.org/10.3390/s19184055>.
- Zhou, X., 2022. A comprehensive framework for assessing navigation risk and deploying maritime emergency resources in the South China Sea. *Ocean Eng.* 248, 110797 <https://doi.org/10.1016/j.oceaneng.2022.110797>.
- Zhou, X., Cheng, L., Li, W.D., et al., 2020a. A comprehensive path planning framework for patrolling marine environment. *Appl. Ocean Res.* 100, 102155 <https://doi.org/10.1016/j.apor.2020.102155>.
- Zhou, X., Cheng, L., Min, K., et al., 2020b. A framework for assessing the capability of maritime search and rescue in the South China Sea. *Int. J. Disaster Risk Reduc.* 47, 10568 <https://doi.org/10.1016/j.ijdrr.2020.101568>.
- Zhu, K., Mu, L., Tu, H.W., 2019. Exploration of the wind-induced drift characteristics of typical Chinese offshore fishing vessels. *Appl. Ocean Res.* 92, 101916 <https://doi.org/10.1016/j.apor.2019.101916>.
- Zhu, K., Zhang, T., 2021. Deep reinforcement learning based mobile robot navigation: a review. *Tsinghua Sci. Technol.* 26, 674–691. <https://doi.org/10.26599/TST.2021.9010012>.

ARTICLES FOR FACULTY MEMBERS


RESCUE VESSEL OPERATION FOR FLOOD EVACUATION PROTOCOL

Title/Author	Analysis of flood evacuation process in vulnerable community with mutual aid mechanism: An agent-based simulation framework / Wang, Z., Huang, J., Wang, H., Kang, J., & Cao, W.
Source	<i>International Journal of Environmental Research and Public Health</i> Volume 17 Issue 2 (2020) Pages 1-21 https://doi.org/10.3390/ijerph17020560 (Database: MDPI)



Article

Analysis of Flood Evacuation Process in Vulnerable Community with Mutual Aid Mechanism: An Agent-Based Simulation Framework

Zhiqiang Wang ^{1,2,*} , Jing Huang ^{1,2}, Huimin Wang ^{1,2,*}, Jinle Kang ^{1,2} and Weiwei Cao ^{1,2}

¹ State Key Laboratory of Hydrology-Water Resources and Hydraulic Engineering, Hohai University, Nanjing 210098, China; j_huang@hhu.edu.cn (J.H.); kjlhhu@hhu.edu.cn (J.K.); cww@hhu.edu.cn (W.C.)

² Institute of Management Science, Business School, Hohai University, Nanjing 211100, China

* Correspondence: zqwang@hhu.edu.cn (Z.W.); hmwang@hhu.edu.cn (H.W.); Tel.: +86-025-83787221 (H.W.)

Received: 5 November 2019; Accepted: 13 January 2020; Published: 15 January 2020



Abstract: Timely and secure evacuation of residents during flood disasters or other emergency events is an important issue in urban community flood risk management, especially in vulnerable communities. An agent-based modeling framework was proposed in order to indicate how the community properties (e.g., community density and percentage of vulnerable residents), residents' psychological attributes (e.g., flood risk tolerance threshold) and mutual aid mechanism affect the flood evacuation process. Results indicated that: (1) The community density negatively affected the flood evacuation efficiency. The greater the density of the community, the longer the evacuation time. (2) There was a negative correlation between the flood risk tolerance threshold of residents and evacuation efficiency. (3) The proportion of vulnerable resident agents had opposite effects on the evacuation efficiency of different types of communities, which was to negatively affect low-density communities and positively affect high-density communities. (4) Mutual aid mechanism can reduce evacuation time in low-density communities, and the effect was more pronounced with a higher proportion of vulnerable resident agents in the community. These findings can help managers to develop better emergency evacuation management for urban communities.

Keywords: flood evacuation; vulnerable community; mutual aid mechanism; agent-based model; simulation

1. Introduction

Flood disasters are a major threat to human society and economic systems, and they can easily wipe out the wealth accumulated in the past [1]. In recent years, the frequency and scope of flood disasters have increased significantly as well as the economic losses and human casualties caused by floods (<https://www.cred.be>). Actually, casualties and economic losses can be reduced or prevented if people arrive shelters and transfer the assets before the flood disasters. Therefore, timely and securely evacuation of residents is of great importance during flood disaster events [2]. Nowadays, with the acceleration of urbanization in China, people gather together in the form of communities. Therefore, emergency evacuation of urban communities is becoming more important and serious. Vulnerability theory has been widely applied in the research of natural disasters. Vulnerability is generally considered as the possibility that an individual or a group is exposed to and affected by natural disasters [3–5]. Individuals or groups have different vulnerabilities due to their own characteristics, such as exposure, coping ability, and adaptability. When faced with natural disasters, residents can be divided into vulnerable residents and non-vulnerable residents according to their ability to resist natural disasters. The vulnerable residents refer to those individuals or groups with weak ability to resist disasters,

such as the disabled, the elderly, children, etc. The proportion of vulnerable residents can be used to show the vulnerability of a community. The higher the proportion of vulnerable residents, the more vulnerable the community. In highly vulnerable communities (communities with many elderly and children), due to slow disaster response, insufficient response capacity and resources, the emergency evacuation of vulnerable communities is more prominent and severe. To mitigate the adverse effects of flood disasters on urban residents, better evacuation planning based on the results of emergency evacuation studies is becoming critical in flood risk management. Due to this, the study of community flood emergency evacuation has attracted more and more attention in recent years.

In general, emergency evacuation is considered as a traditional routing problem and many improved classical algorithms have been proposed to solve this problem [6,7]. In fact, the emergency evacuation is a complex problem and is affected by many factors such as psychology [8], demographics [9], human relations [10], risk warning [11,12], and so on. Therefore, at present, many studies recognize the emergency evacuation problem from the perspective of complex system and use computer models to simulate the evacuation process [13,14]. There is no doubt that the purpose of emergency evacuation is to evacuate people to the safe areas as quickly as possible. Therefore, evacuation time, evacuation distance, evacuation ratio and other indicators are used to evaluate the efficiency and capability of emergency evacuation, and these indicators are also the most concerned by decision-makers. As for the simulation models, in the existing studies, agent-based model (ABM) has been suggested as an appropriate tool to solve the kind of complex system problems such as emergency evacuation. ABM is a type of computational model that can provide the most natural description and simulation of complex adaptive systems, and implement the assumptions of model [15]. Through the simulation of the behaviors and interaction of autonomous agents in the ABM, the dynamic feedback of subsystem components, their inherent complexities and their effects on the system can be captured. The applications of ABM range across virtually all kinds of disaster evacuation problems and well beyond the usual ones for simulation [16]. For example, Zou et al. carried out an agent-based modeling of people from trains and platforms in a typical subway station. Parametric investigations found out the impacts of some key parameters on evacuation time and provided some valuable insights for understanding the potential causes of delay of evacuations [17]. D'Orazio et al. presented an agent-based model to describe phases and rules of motion for pedestrians and found that evacuation paths choice depending on configuration of environment and damage distribution after an earthquake [18]. Liang et al. developed a two-level regional disaster evacuation model by coupling two agent-based models to simulate hurricane evacuation traffic in New Orleans and confirmed that the proposed model performs well in terms of high model accuracy [19]. Mostafizi et al. proposed an agent-based modeling framework to evaluate vertical evacuation behavior and shelter locations for a near-field tsunami hazard and revealed that the non-linear correlation between the aforementioned characteristics of the vertical evacuation shelter on the expected mortality rate [20]. Wijerathne et al. presented an HPC enhanced agent-based model developed with the aim of quantitatively estimating the strategies for accelerating emergency mass evacuations, like tsunami evacuation. It is demonstrated that the system has high strong scalability up to 10 million agents was simulated [21]. Liu et al. proposed a shelter assignment and routing strategy for evacuating households at the 2011 Brisbane flood event and the results showed that communities located in the east and west of Brisbane are scarcely covered by existing shelters [22]. These simulations showed the whole procedure of an emergency evacuation, found out a number of evacuation problems and provided possible improvements for emergency response.

Although many studies have been conducted, most studies on emergency evacuation were restricted to single building [23,24] or large-scale evacuations [22,25], while few studies focused on community-scale evacuation [6]. In addition, in the existing study of emergency evacuation of urban communities, there are two important issues rarely considered by researchers. The first one is that communities in China's small and medium-sized cities are becoming increasingly vulnerable. It should be noted that in China, with the rapid economic and urbanization development, young labor force prefers to work in big cities, resulting in the phenomenon that some communities in small and

medium-sized cities are dominated by the elderly and children. That means this kind of communities are at an increasing risk of flooding in terms of lower emergency response ability. Emergency evacuation in vulnerable communities under flood disaster is becoming a more critical issue. Therefore, it is important and necessary to pay attention to the emergency evacuation of vulnerable communities in order to quickly and orderly evacuate vulnerable residents. The second one is the mutual aid behaviors among residents in the communities during flood emergency evacuation. According to the results of our several field investigations and questionnaire surveys in Jingdezhen, Jiangxi Province, China, it was found that during flood emergency evacuation, residents generally had the consciousness and behaviors of helping each other and going to shelter together [1]. Moreover, the behaviors of helping each other to evacuate to the shelter together can be motivated, encouraged by the local government. In this paper, the act of helping each other escape the effects of flood disasters was defined as mutual aid behaviors. Accordingly, encouraging and motivating residents to produce such behavior was defined as a mutual aid mechanism, and the proportion of non-vulnerable residents who are willing to help was used to show the strength of the mutual aid mechanism. Through analyzing and understanding the role of residents' mutual aid mechanism in emergency evacuation can help local decision-makers to perfect reasonable emergency evacuation plans. However, the relationship between mutual aid behavior and emergency evacuation efficiency has not received much attention in existing studies.

Considering the limitation of the existing studies and motivated by the two important issues mentioned above, this study presented an agent-based modeling framework to simulate the flood evacuation in vulnerable communities and this framework incorporated the resident psychological model and transportation network model. The aims of this study were to find out how the community properties (e.g., community density and percentage of vulnerable residents), resident's psychological attributes (e.g., flood risk tolerance threshold) [26,27] and mutual aid mechanism affect the emergency evacuation efficiency, summary the characteristics of emergency evacuation in vulnerable communities, and give corresponding improvement suggestions of better response to emergency evacuation. Specifically, the simulation results of this study can easily present spatial analysis and statistics results, such as evacuation time, average evacuation time, number of agents on the road, the congestion of the road, etc. Through analyzing the evacuation simulation results, this study can help decision-makers at the community level to better understand the dynamic characteristics of community evacuation behavior and make effective emergency evacuation plans. It is of great practical significance for community emergency evacuation and flood risk management. A case study of synthetic community was conducted to demonstrate the feasibility and applicability of the framework.

2. Methodology

2.1. Framework of Agent-Based Model

This evacuation process simulation mainly involved two components: agents and transportation network. Thus, the proposed agent-based model took both human components (community residents and staff, and their decision-making process) and evacuation transportation network into consideration.

The agent-based model framework was structured in three steps: model initiation, model runs, and model outputs (as shown in Figure 1). In the model initialization step, the agents' environment and the agents were created, and the flood risk warning was also issued. When the agent-based model running, evacuation decision-making, mutual aid decision-making, evacuation route searching, and other behavior rules were running to finish the simulation process. With regard to the model output step, some data results at system level were outputted, analyzed and visualized. The focus of the study was to investigate the impact of various factors on the flood evacuation efficiency (such as evacuation status, percentage of evacuated agents and evacuation time, etc.). Therefore, in the model statistical analysis step, some main issues were considered as below:

- The impacts of the community density on the evacuation process
- The impacts of the average flood risk tolerance threshold on the evacuation process

- The impacts of the percent of the vulnerable resident agents on the evacuation process
- The impacts of the community mutual aid mechanism on the evacuation process

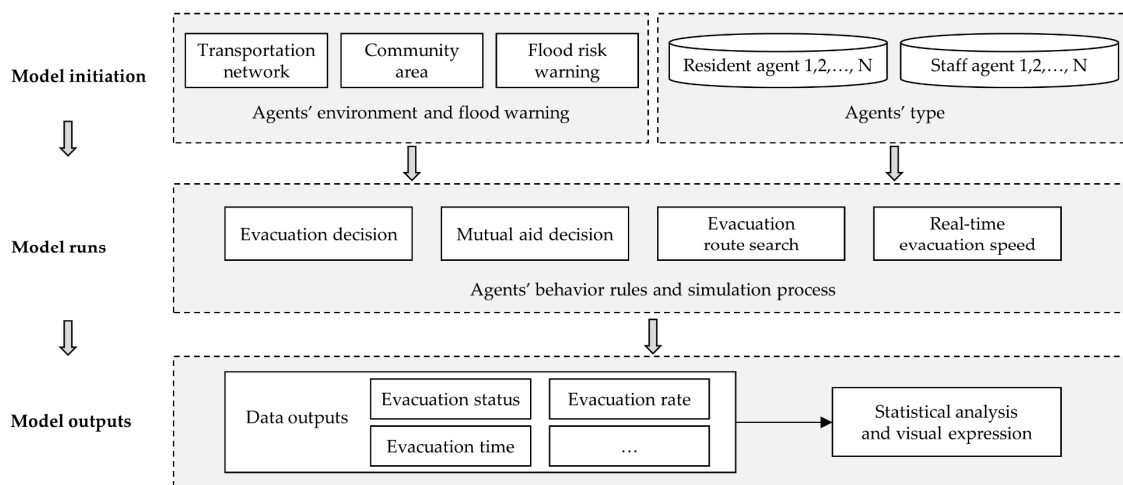


Figure 1. Framework of the agent-based model for flood evacuation process simulation. Each time step, the flood risk perception of agents was updated and agents took action.

2.2. Construction of the Agent-Based Model

2.2.1. Flood Risk Warning

In the mainland of China, the city local meteorological authority is responsible for the release of early flood risk warning signals within its administrative area. The flood risk warning signal is divided into four levels, which are represented by blue warning, yellow warning, orange warning and red warning. And the red flood risk warning signal is the highest level. When the red flood risk warning signal is issued, according to disaster management requirements, the community residents committee staff are required to inform and assist residents to evacuate, especially the vulnerable individuals.

In this study, let FRW_t denote the value of flood risk warning from authority department at time step t (i.e., $FRW_t \in [0, 1]$). The higher the value of FRW_t , the greater the flood risk. When the value of FRW_t is set to 1, it means the highest flood risk warning, and all the resident agents and community residents committee staff agents must evacuate to the shelter eventually. Since the authority department, in reality, broadcasts the flood risk warning information to all the residents and staff in its administrative area, all agents will receive the same flood risk warning information at each time step [26].

2.2.2. Resident Agents and Behavior Rules

An agent is defined by the attributes and behavior rules. Every agent’s response to the environment or other agents is based on its own attributes and behavior rules. The following sections introduced how to define the resident agent’s attributes and decision rules.

Resident Agent Attributes

There are various variables of resident that can affect the real evacuation process. It is difficult and challenging to completely include all of impact factors in one model when the empirical evacuation data is lacking. Therefore, in this study, only important factors of residents were taken into account [28]. The agents’ attributes were classified as physical attributes that were related to its evacuation process, and psychological attributes that were related to its response to flood warnings (as shown in Table 1).

Table 1. List of resident agents’ attributes.

Category	Variables	Description
Physical	<i>i</i>	Unique identification number of each agent
	ES	Evacuation status of agents
	GL	Geographical location of agents in the community
	CGN	Community grid number where agents live
	V_{max}	Agent’s max movement speed during the evacuation
	CAT	Agent’s categories (non-vulnerable resident and vulnerable resident)
Psychological	RT	Agent’s flood risk tolerance threshold
	FRP	Agent’s flood risk perception

In this study, the resident agents were divided into two categories: non-vulnerable resident agents and vulnerable resident agents (as shown in Table 2). The percentage of the vulnerable resident agents represented the extent of the vulnerability of the community. The moving speed of non-vulnerable resident was faster than vulnerable resident. Besides, the non-vulnerable resident agent can response to the flood event by themselves while the vulnerable resident only evacuates when the community staff inform them or other non-vulnerable resident help them to evacuate.

Table 2. Description of different categories of resident agent.

Category	Speed	Interaction Rules	Representative
Non-vulnerable resident agent	fast	- evacuate by themselves when its flood risk perception greater than the its flood risk tolerance threshold	Young adults
Vulnerable resident agent	slow	- evacuate when community staff find them and ask them to leave - evacuate when other non-vulnerable resident agent helps them to evacuate	Children, elderly, people with mobility problems

Resident Agents’ Flood Risk Perception

In this study, the flood risk perception of resident agents (denoted by a continuous variable $FRP_i, FRP_i \in [0, 1]$) referred to their feeling of the extent of flood risk in the community where they stay, which would affect their evacuation decision. In each time step, every resident agent’s flood risk perception was calculated and updated. If one resident agent’s flood risk perception exceeds its specified flood risk tolerance threshold, the resident agent would consider taking action to evacuate to the shelter. However, the flood risk perception can be affected by many factors, such as past flood experience, neighbors’ behavior and new information received [1,29,30].

In this study, the calculation of flood risk perception was based on factors identified through the literature review. When the community was hit by a flood event, the resident agent *i* mainly obtained flood risk information from the flood risk warning $I_{i,t}^W$ and neighbors’ flood risk perception $I_{i,t}^N$ (as shown in Equations (1) and (2), respectively). Some studies have also considered the impact of social media on flood risk perception [26,31]. However, this study argued that in small communities, the impact of government warning and neighbor behavior is far greater than that of social media.

$$I_{i,t}^W = FRW_t \tag{1}$$

$$I_{i,t}^N = \frac{\sum_{j=1}^n c_{i,j}FRP_{j,t}}{\sum_{j=1}^n c_{i,j}} \tag{2}$$

where FRW_t denotes the flood risk warning at time step t , $FRP_{j,t}$ denotes the flood risk perception of agent j , and if agent j and agent i are in the same community grid, the $c_{i,j}$ takes 1, otherwise $c_{i,j}$ takes 0. In other words, the $I_{i,t}^N$ is the average value of flood risk perception of resident agents in the same community grid.

Many previous studies using a set of weighting factors to formulate agents’ flood risk perception driven by multiple information sources. In this study, the approach was adopted and two main information influence parameters α_i and β_i were set to represent the influence of flood risk warning and neighbors’ flood risk perception for agent i , respectively. Thus, for agent i , the new flood risk information obtained from multiple sources can be represented by Equation (3).

$$\Delta I_{i,t} = \alpha_i I_{i,t}^W + \beta_i I_{i,t}^N \tag{3}$$

When new information on flood risk was obtained, the agent i would update its flood risk perception. However, because of past experience, information reliability, and information comprehensibility, different agents had different levels of trust in the new information. In this study, for agent i , a weight parameter ω_i was set to represent the extent of its willing to accept the new information it obtained at time step t . Therefore, the flood risk perception of agent i at time step t can be represented by Equation (4).

$$FRP_{i,t} = FRP_{i,t-1} + \omega_i \times \Delta I_{i,t} \tag{4}$$

So far, the process of how agents update their flood risk perception was modeled.

Resident Agents’ Evacuation Decision

At time step t , the agent would make an evacuation decision (denoted by a binary variable $ED_{i,t}$, $ED_{i,t} \in \{0, 1\}$) to evacuate or not when the flood risk warning was issued (as shown in Equation (5)). In this study, if one agent’s flood risk perception $FRP_{i,t}$ larger than its flood risk tolerance threshold $RT_{i,t}$ at time step t or the agent already on the way to the shelter in the last time step $t - 1$, the agent would decide to evacuate or continue to evacuate to the shelter. In other cases, the agent would stay at home.

$$ED_{i,t} = \begin{cases} 0 & \text{if } FRP_{i,t} < RT_{i,t} \\ 1 & \text{if } FRP_{i,t} > RT_{i,t} \text{ or } ED_{i,t-1} = 1 \end{cases} \tag{5}$$

Resident Agents’ Mutual Aid Process

For the non-vulnerable resident agents who willing to aid, if the mutual aid mechanism was on and they had decided to evacuate, they would check whether there were vulnerable resident agents in their same community grid. If there was at least one vulnerable resident agent did not evacuate, the non-vulnerable resident agents would move to their nearest vulnerable resident agent’s location and form one-on-one evacuation team. Then, they would move to the nearest road edge first and go to the shelter together through taking the shortest route. If there was no vulnerable resident agent in their community grid, the non-vulnerable resident agents would go to the shelter directly. For the non-vulnerable resident agents who did not want to afford help, they would go to the shelter directly regardless of the mutual aid mechanism was on or not. When the resident agents arrived at the shelter, they would change their evacuation status to ‘arrived shelter successfully’.

So far, the resident agents’ attributes and its behavior rules has been constructed. The simulation process end when the tick time agreed with the time set or all the resident agents arrived at the shelter. Figure 2 presented a completed decision-making process flowchart of the resident agents.

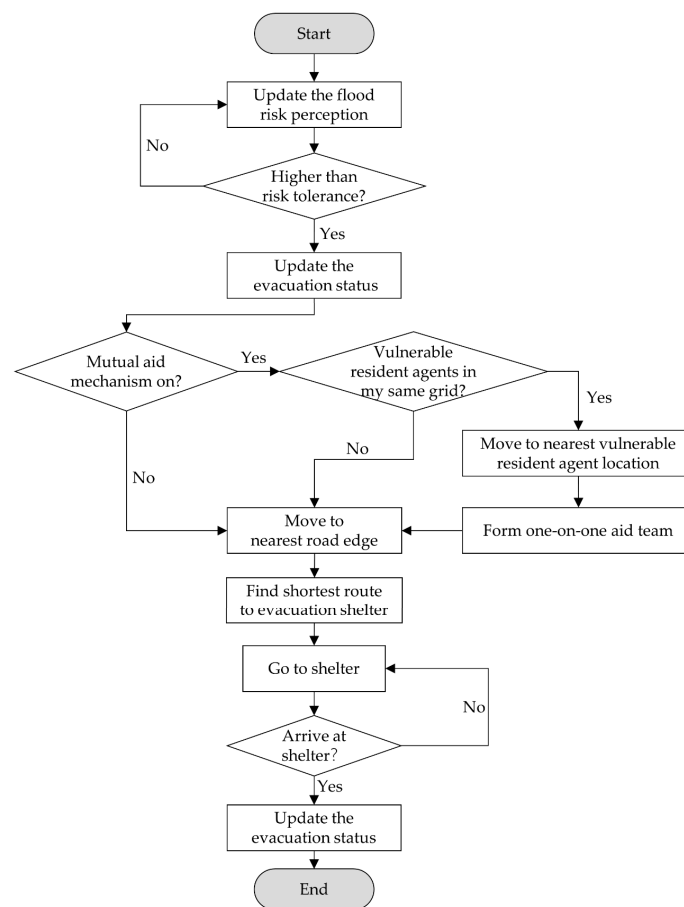


Figure 2. The decision-making process of resident agents.

2.2.3. Community Residents Committee Staff Agents and Behavior Rules

The staff agents represented the community residents committee staff in the real world. In each community grid, there were certain number of staff to responsible for the daily work in China. In the face of the flood risk, the community residents committee staff should inform and assist the residents to evacuate if the flood risk alert is red warning. In this study, the staff agents need to response to flood event and help the vulnerable resident agents to evacuate to the shelter. In this study, the attributes of the staff agents were the identification number, community grid number and evacuation status.

Figure 3 showed the completed flowchart of the decision-making process of the staff agents during the flood event. The staff agent firstly checked whether the flood risk warning was red alert, if yes, the staff agent would find the vulnerable resident agents in its same community grid and move to the nearest vulnerable resident agent location. Then, the staff and the vulnerable resident agent would go to the nearest road edge together. If there were no more vulnerable resident agents in its community grid, the staff agent and the vulnerable resident agent just found would go to the shelter directly. Otherwise, the staff would ask the vulnerable resident it found last time to go to the shelter alone by the shortest route, and the staff would go to find the next vulnerable resident in its community grid. After repeating the searching process several times, there were no more vulnerable resident agents, the staff agent would move to the shelter at last. All agents who arrived the shelter would update the evacuation status to “arrived shelter successfully”.

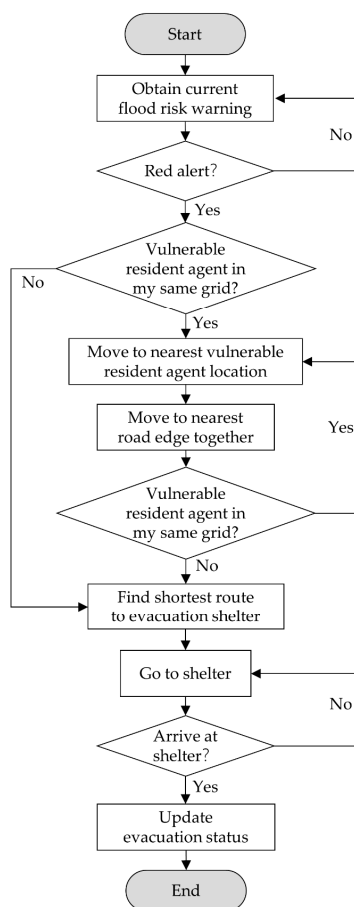


Figure 3. The decision-making process of community residents committee staff agents.

2.2.4. Road Network and Traffic Rules

The road network plays a key role in emergency evacuation and emergency management. A road network is a system of interconnecting lines and points (called edges and nodes in network science) that represent a system of streets or roads for a given area, and it describes a structure which permits either vehicular movement or flow of people [32]. Generally, the road network system includes road network, vehicles and people in the network and move rules that regulate the movements and interactions of vehicles and people. Thus, there were two main components in a road network system simulation: (1) the road network itself; and (2) the movement rules of the road network that all vehicles and people should follow. However, it is challenging to explicitly include all road network features in simulation model [28]. Therefore, many studies have suggested using a simplified road network which consists of a number of nodes, edges and edge weights [33,34]. A set of edges and nodes can be routed from one node to another in a road network. In this study, the road network was set to two-way road, and the Dijkstra's algorithm [35] was applied to find the shortest paths between nodes.

As for the movement rules, it stipulates the movement and interaction mechanisms of the vehicles and people in the road network. Among a variety of transportation network simulation methods, the Nagel–Schreckenberg model (N-S model) proposed by Nagel and Schreckenberg [36] is widely used to simulate the movement of the vehicle and the speed of the vehicle was adjusted by the road maximum limit speed, the speed of ahead vehicle, and a safe distance, etc. While regarding the short-distance evacuation process in a population-intensive community, people mainly evacuate by walking instead of using vehicles. Therefore, people's evacuation speed is mainly affected by their own walking speed and the density of people on the road. The calculation results of statistical data in many studies showed that the speed of pedestrians is 1–2 m/s, and the pedestrian walking speed would be increased or decreased under special circumstances. With regard to the density of people on

the road, it reflects the intensity of people in a certain space for each time step. Specifically, it refers to the value that the number of people on the road unit where you stay plus the number of people on ahead road unit, then divide it by 2. Although there are various models to study the relationship between the evacuation speed and the people density [10,37–39], they have similar general speed rules. In this study, the relationship between the speed of agent and agent density was referenced by the SGEM model [40] developed by Wuhan University and City University of Hong Kong (represented by Equation (6)).

$$v_i = \begin{cases} 1.4 & \text{if } \rho_i \leq 0.75 \\ 0.0412\rho_i^2 - 0.59\rho_i + 1.867 & \text{if } 0.75 < \rho_i \leq 4.2 \\ 0.1 & \text{if } \rho_i > 4.2 \end{cases} \quad (6)$$

where v_i denotes the speed of agent i , ρ_i denotes the agents density (*agents/road_unit*) on the road unit where agent i stay. The speed of all non-vulnerable resident agents and committee staff agents were v_i , and the speed of vulnerable resident agents was set to 0.8 times of v_i .

In order to find more detail information during the evacuation process, in this study, the road congestion index (RCI) was used to reflect the degree of crowdedness in the transportation network. It can be estimated by calculating the proportion of agents whose speeds reduce more than a certain percent at each time step (as shown in Equation (7)).

$$RCI = \frac{\sum_{i=1}^n SSA_i}{n} \quad (7)$$

where RCI denotes the extent of the road congestion, n denotes the total number of resident agents who are evacuating to the shelter, and the SSA_i is a binary function which is used to indicate whether the speed of agent i has decreased significantly, if its speed less than 50% of its max moving speed, SSA_i takes 1, otherwise SSA_i takes 0. In addition, the higher the RCI value, the more congested the road.

2.2.5. Model Assumptions and Outputs

It is very difficult to consider all the impact factors in one evacuation simulation model. Therefore, some main assumptions were set to simplify the model and ensure the availability and credibility of results. They were: all residents in the community were required to carry out emergency evacuation, and all residents were in their homes when the flood risk warning was issued; the evacuees were assumed to have good knowledge about the transportation network and they will head to the nearest road node first and then look for the shortest route to the shelter.

Besides, the community is a complex system due to it consists of residents, residents committee staff, roads, etc. When simulating the process of emergency evacuation, each agent interacted and influenced each other under certain rules. These interactions and influences happened in the process of flood risk perception update, evacuation decision, road congestion and other aspects. Actually, each agent makes different decisions during these interactions, and these behaviors were assumed to occur in a stochastic manner. Hence, the community evacuation system turns into highly randomness, nonlinear and noncontinuous. For such a system, obtaining the closed-form analytical solutions become very difficult.

In similar studies, numerical simulation methods were usually used by researchers to solve such problems [41–43]. Monte Carlo methods, which rely on repeated random sampling to obtain numerical results, are often used in physical and mathematical problems [44]. Therefore, in order to obtain stable numerical results, in this study, the Monte Carlo approach was applied to analyze the impacts of different agent variables on the evacuation process. The model was executed 500 times on the netlogo 6.0.4 platform per scenario to ensure the stabilization of numerical results. The 15% trimmed mean method was applied to further reduce the randomness and contingency of numerical results [45]. In addition, in order to improve the efficiency of the model, the model was optimized based on the method proposed by Steven et al. [46].

Multiple indicators were used to measure agents' evacuation behaviors at the system level (i.e., a community). These indicators were: (1) road congestion index RCI_t , representing the extent of the road congestion at time step t . (2) resident agents' evacuation status, where were the percentage of the resident agents with different status (i.e., start to evacuate, on the way to the shelter and successfully evacuated to the shelter) at time step t . (3) total evacuation time, representing the time cost to evacuate all the residents to the evacuation shelter; average evacuation time, representing the average value of all the resident agents' total evacuation time.

2.3. Synthetic Community and Scenario Design

2.3.1. Synthetic Community Design

In this study, the agent-based model proposed above was applied in a synthetic community (as shown in Figure 4), which was constructed according to the characteristics of urban communities' structure and the mechanism of community grid management in China. The synthetic community included a transportation network, nine community grids and an evacuation shelter in the bottom right. There were sixteen intersection nodes and twenty-four roads in the regular lattice road network, and the length of each road was 100 units. Each community grid contained a number of community residents committee staff and residents, and these community grids were connected by roads. In order to make the simulation more in line with the real situation of the community, all agents were randomly distributed in their corresponding community grid.

In addition, the impacts of the number, distribution, and capacity of evacuation shelter were worth to study, and the results can be useful in the evacuation plan or shelter plan. However, it is difficult to analyze all the factors in one study. Therefore, in this study, only one evacuation shelter was built and was assumed to be able to accommodate all agents.

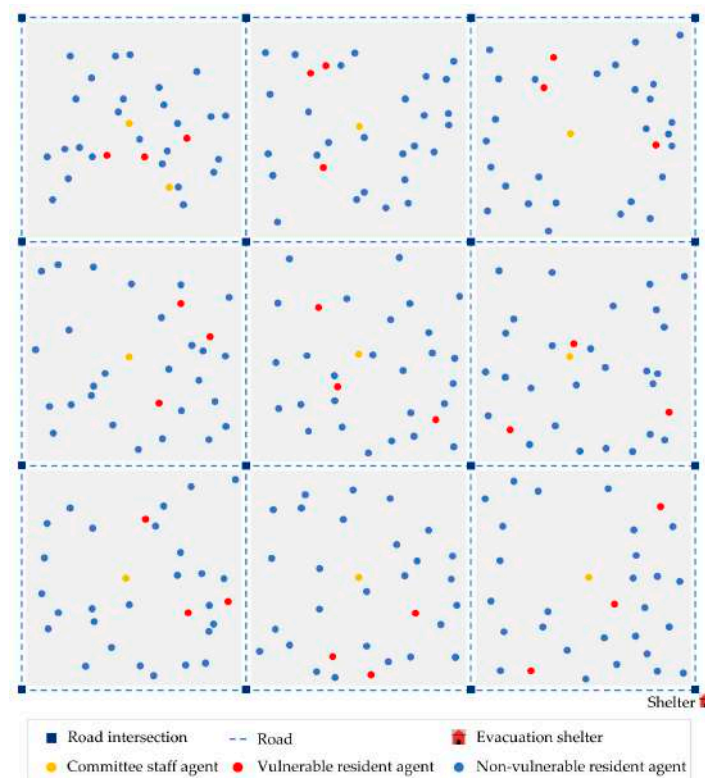


Figure 4. Illustration of the synthetic community. The community consisted of a road network, nine community grids, one shelter and a number of community residents committee staff agents and resident agents.

2.3.2. Scenario Design

Table 3 showed the values of model parameters. Those model parameters were important to build the agent-based model and necessary to format the agents' status and behaviors. As mentioned in Section 2.2.2, the resident agents obtained information from multiple separate sources and each agent can decide how much it adheres to its past risk perception when new information was available. However, the impact of different weights of information sources and learning rate were not the focus of this study. Therefore, with reference to previous studies, the weight of government information α_j and the weight of neighbor behavior β_j were set to 0.5 and 0.5, respectively, and the learning rate ω_j was sampled from a normal distribution with a mean of 0.5 and standard-deviation of 0.1. In addition, the value of the government flood risk warning *FRW* was set to 1, which means the red warning of flood risk. Moreover, the agents only received one flood risk warning at the beginning of the model execution, and would not receive any other flood risk warning in the following simulation.

Table 3. The Values of Model Parameters.

Parameters	<i>FRW</i>	α_j	β_j	ω_j
Values	1	0.5	0.5	0.5(0.1) ^a

^a $x_1(x_2)$ indicates the value of the parameter is sampled from a normal distribution with a mean of x_1 and standard-deviation of x_2 .

With the synthetic community as a case study area, the aims of this study were to explore how residents' heterogeneous behaviors (i.e., flood risk tolerance threshold), community properties, and mutual aid mechanism affect the emergency evacuation process. Four different scenarios were designed based on five important parameters (as shown in Table 4). The five parameters were respectively the flood risk tolerance threshold of the resident agents, the community density, the percentage of vulnerable resident agents, the mutual aid mechanism status, and the proportion of the non-vulnerable resident agents who willing to aid.

The first scenario aimed to investigate the impact of the community properties on the evacuation process. There are many variables can be used to measure the community characteristics, such as community size, community density, community layout, education level, etc. In this study, only community density was concerned, as it may significantly affect traffic during an emergency evacuation process. The second scenario investigated how the flood risk tolerance threshold of resident agents affects the evacuation process. The different threshold of flood risk tolerance represents the different residents' response to flood risk. Appropriate flood risk tolerance threshold could enable more efficient evacuation. The third scenario explored the effects of the community vulnerability (expressed by the percentage of the vulnerable resident agents) on the evacuation process under different community density. In the fourth scenario, the potential influence of mutual aid mechanism on emergency evacuation was investigated which combined with other three influencing factors.

Table 4. Parameters Design for Four Scenarios.

Scenario	<i>density</i>	<i>risk_tolerance</i>	<i>vulnerable_pct</i>	<i>aid_stat</i>	<i>help_pct</i>
Scenario 1	10:10:200 ^a	0.7(0.05) ^b	0.1	false	0.0
Scenario 2	10:20:200	0.5:0.1:0.9	0.1	false	0.0
Scenario 3	10:20:200	0.7(0.05)	0.1:0.1:0.5	false	0.0
Scenario 4	10:20:200	0.7(0.05)	0.1:0.1:0.5	true	0.1:0.1:1

^a $x_1 : d : x_2$ denotes a numeric vector from x_1 to x_2 with increment of d . For example, in scenario 2, the mean value of flood risk tolerance threshold 0.5:0.1:0.9 means vector [0.5 0.6 0.7 0.8 0.9]. ^b $x_1(x_2)$ indicates the value of the parameter is sampled from a normal distribution with a mean of x_1 and standard-deviation of x_2 .

3. Results and Discussion

3.1. Impacts of Community Density on the Evacuation Process

The first scenario was mainly to investigate the impact of community density on the emergency evacuation process. To be specific, this scenario addressed two questions: (1) Does the community density affect the evacuation process? (2) To what extent does the community density affect the evacuation efficiency? The first question was to demonstrate that the community density can affect the evacuation process and the second question was to attempt to evaluate the importance and the impact of community density in evacuation process.

Figure 5 showed the simulation results for the first scenario in which the mean value of flood risk tolerance threshold was 0.7, the percent of vulnerable resident agents was 10% and no mutual aid behavior between resident agents. The results indicated that the higher the community density, the longer the evacuation time required. In other words, the community density had a negative correlation with the evacuation efficiency. Moreover, when the community density was less than 120 agents/grid, the total evacuation time and average evacuation time gradually increased with the increase of community density. However, when the community density was greater than 120 agents/grid, the total evacuation time and average evacuation time increased rapidly. These results were similar to the findings in most published studies [26,28,41].

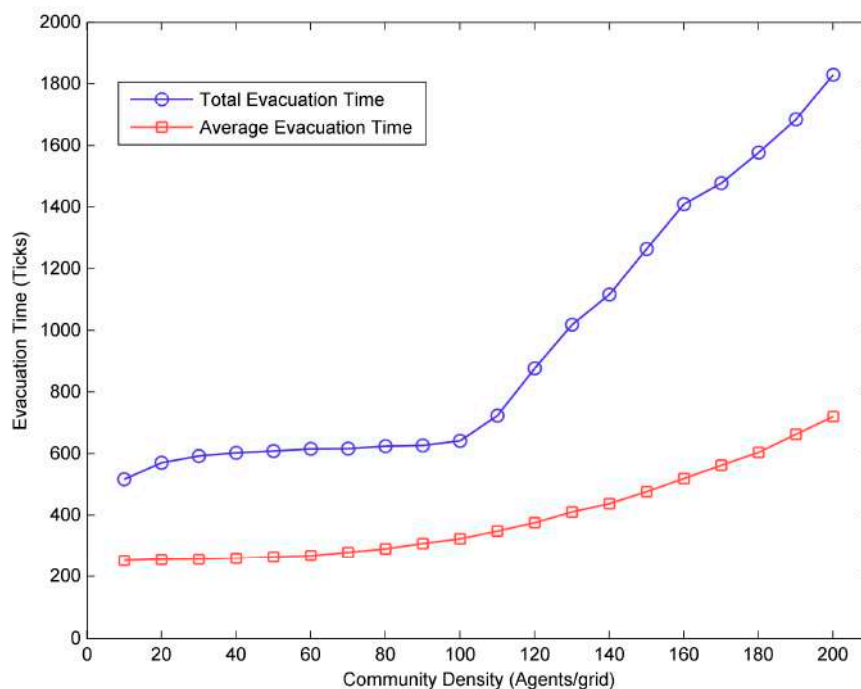


Figure 5. The impacts of community density on the total evacuation time.

In order to explore how community density affected the evacuation process, the changes in the percent of evacuated agents with time in communities with different densities were investigated (as shown in Figure 6). It was clear that the lower the community density, the faster the percent of the evacuated agents reached 100%. Furthermore, for every increase in community density, more and more evacuation time was needed to reach the same evacuation ratio, especially in the case of high evacuation ratio situation. In other words, when achieving a high level in the evacuation ratio, the increase in evacuation time was much larger than the increase in community density [28]. For example, considering the time needed for 90% of the resident agents evacuated to the shelter, when the community density increased from 40 to 80 agents/grid, the evacuation time increased by 20.65%, while when the community density increased from 160 to 200 agents/grid, the evacuation time

needed increased by 57.06%. In both cases, the community density increased by 40, but the increase of the total evacuation time of the latter (high-density community) was far higher than the former (low-density community). These results indicated that achieving high level of evacuation ratio was much more difficult in high-density community than in low-density community due to the marginal evacuation time needed rapidly increasing.

In addition, it was also worth noting that when the community density was greater than 120 agents/grid, the percentage of evacuees increased slowly or even stopped growing for a period of time (as shown in Figure 6). For example, when the community density was 160 agents/grid, the evacuation ratio slowly increased after reaching 80%. Besides, the percentage of evacuated agents did not increase for a period time. The reason for this phenomenon may be that a number of resident agents farther away from the shelter gather on the road intersections, which made the road intersections crowded and the moving speed of resident agents decreased. These results implied that traffic was a very important factor need to be considered in the emergency evacuation of high-density communities.

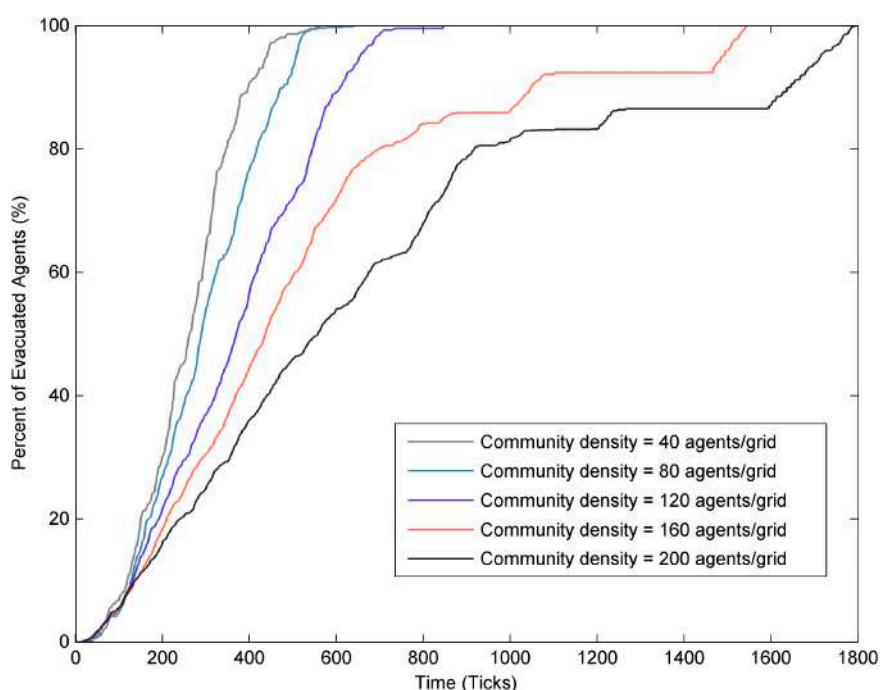


Figure 6. The percent of evacuated agents with time under different community density.

3.2. Impacts of Flood Risk Tolerance Threshold of Resident Agents on the Evacuation Process

The resident agents' behavioral heterogeneity (i.e., agents' flood risk tolerance threshold) indicated the different response behavior to the same flood risk condition. As mentioned in Section 2.2.2, the difference of the mean value of the flood risk tolerance threshold mainly influenced the evacuation decision-making timing of resident agents. Therefore, the second scenario was to find out how the mean value of the flood risk tolerance threshold of resident agents affects the evacuation process in communities with different densities. In this section, the difference of the total evacuation times in communities with different densities were compared to investigate this effect.

As shown in Figure 7, with regard to the flood risk tolerance threshold, its effects on the evacuation process varied in communities with different densities. In low-density community, such as communities with density less than 120 agents/grid, the difference in the flood risk tolerance threshold had slight impact on the evacuation process. To be specific, at a given community density range from 20 to 100 agents/grid, the total evacuation time fluctuated little no matter how the mean value of the flood risk tolerance threshold of resident agents changed. However, in the high-density communities (i.e., greater than 120 agents/grid), the impact of the flood risk tolerance threshold on the evacuation process can be

easily captured. It was clear that as the mean value of the flood risk tolerance threshold increased, more time was needed to evacuate all the resident agents to the shelter, especially in higher density communities, the total evacuation time can be reduced more by reducing the mean value of resident agents' flood risk tolerance threshold. For example, for two communities with different densities (such as 140 and 200 agents/grid), when the mean value of the flood risk tolerance threshold of resident agents was reduced from 0.9 to 0.5, the total evacuation time of the whole community was respectively reduced by 94 ticks and 166 ticks. These results implied that it was effective to reduce the residents' flood risk tolerance threshold in high-density communities because it reduced the total evacuation time and improve evacuation efficiency, while it was not effective in low-density communities.

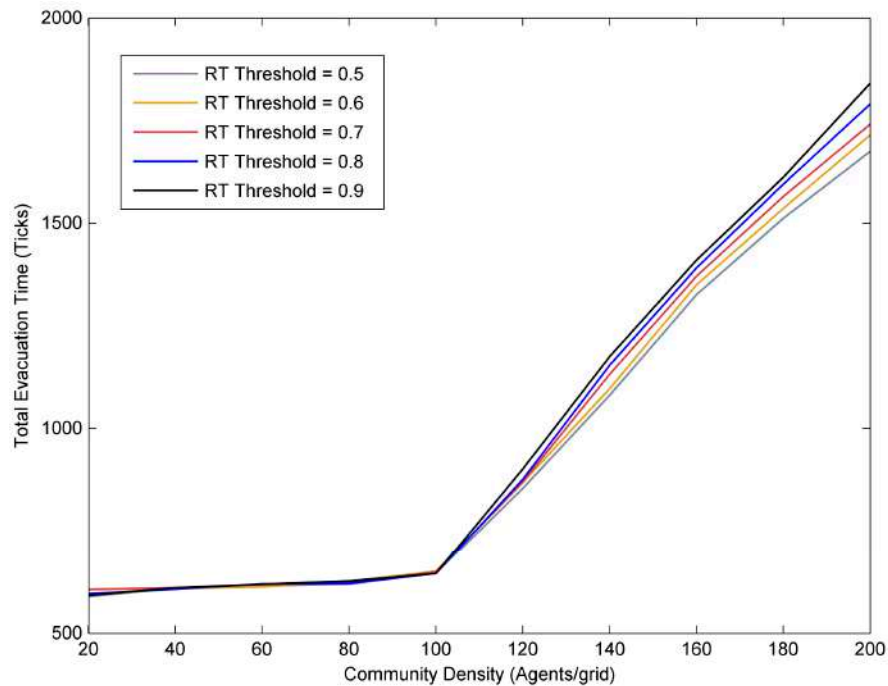


Figure 7. The impacts of residents' flood risk tolerance threshold on the total evacuation time.

3.3. Impacts of Vulnerable Residents on the Evacuation Process

The vulnerability of communities is an important issue that should be considered in the flood risk management of urban communities. As mentioned in Section 2.2.2, the vulnerable residents only evacuate when the community staff or other non-vulnerable residents inform them to leave and move to the shelter together. In general, the movement speed of the vulnerable residents is slower than the non-vulnerable residents. Thus, the number of vulnerable residents in the community would affect the entire community emergency evacuation process because the later evacuation behaviors and the slower movement speed of the vulnerable resident agents.

In this section, the relationship between the proportion of the vulnerable resident agents and the total evacuation time was studied to investigate how the vulnerable residents affects the evacuation process in communities with different densities. Communities were divided into three types, namely, low-density, medium-density and high-density communities. There were less than 120 agents/grid in low-density communities and more than 120 agents/grid in high-density communities. As shown in Figure 8, with the increase of the proportion of vulnerable resident agents, the total evacuation time showed different trends in the three types of communities. To be specific, (1) in low-density communities, the time required to evacuate all agents increased significantly as the proportion of vulnerable resident agents increased, and the result was similar to the previous study [26]; (2) in the medium-density communities, the total evacuation time firstly showed a slight trend of decline when the proportion of vulnerable resident agents increased from 5% to 30%, and then gradually increased

when the proportion of vulnerable resident agents continued to increase; (3) in the high-density communities, the increase in the percentage of vulnerable resident agents resulted in a slight decrease in total evacuation time, which was significantly different from the other two types of communities. These results demonstrated that the proportion of vulnerable resident agents is an important factor in community evacuation.

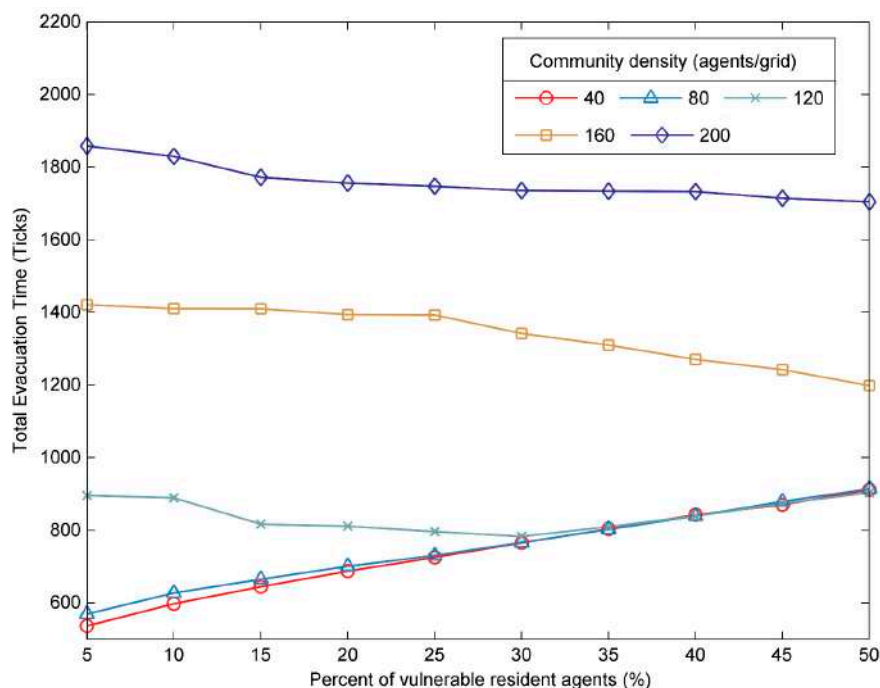


Figure 8. The impacts of the percent of vulnerable resident agents on the total evacuation time.

Then, the road congestion index was used to explore why the proportion of vulnerable resident agents had different effects on the evacuation process in three types of communities. As shown in Figure 9a, it can be found that in low-density communities, the congestion degree and the duration of congestion were relatively short (e.g., RCI less than 40%), and the increase in the proportion of vulnerable resident agents did not significantly affect the degree of road congestion. This was because a low number of resident agents did not significantly contribute to road congestion. Although the road congestion index in low-density communities was low, the increase in density can also lead to an increase in total evacuation time (as shown in Figure 8). This was mainly due to the slower movement speed of vulnerable resident agents, which required more time to evacuate. In addition, it can also be seen from Figure 9b that in high-density communities, the degree of road congestion remained at a high level, with RCI greater than 50% most of the time. However, an appropriate increase in the proportion of vulnerable resident agents could reduce the degree of road congestion, thus accelerating the evacuation of residents and reducing the evacuation time. For example, from 0 to 650 ticks, the higher the proportion of vulnerable resident agents, the lower the road congestion index. This was because vulnerable residents were evacuated later than non-vulnerable residents, so the evacuation process could be carried out in batches. Especially when the proportion of vulnerable resident agents was large, it can avoid a large number of resident agents pouring into the road at the same time, thus reducing the total evacuation time.

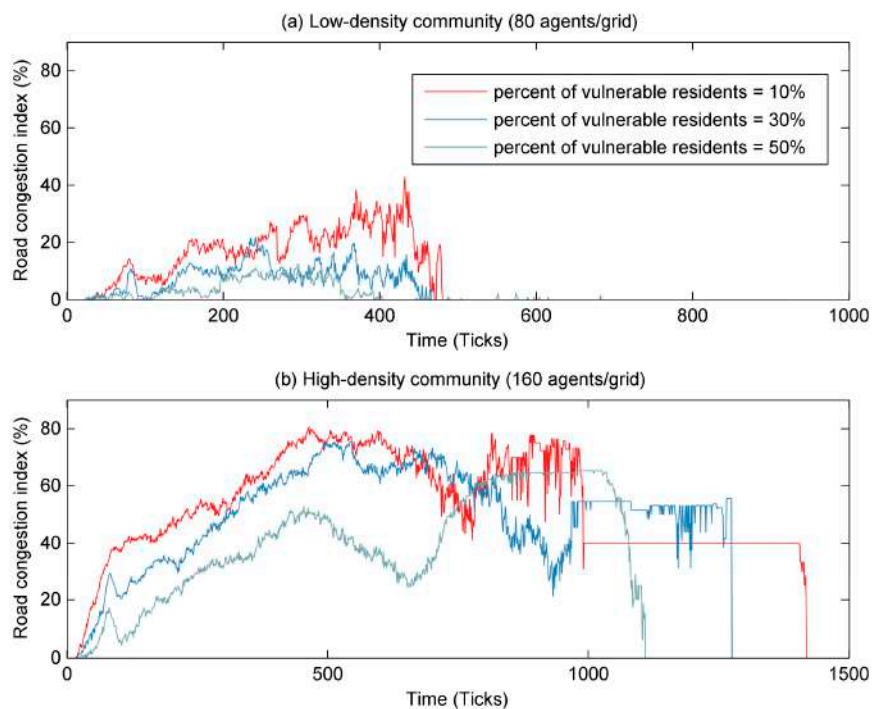


Figure 9. The changes in road congestion index with time in different communities. The percent of vulnerable resident agents was set as 10%, 30% and 50%. (a) The road congestion index in a low-density community (80 agents/grid); (b) The road congestion index in a high-density community (160 agents/grid).

These results implied that in low-density communities, the total evacuation time was mainly affected by the movement speed of vulnerable residents, while in high-density communities, the road congestion caused by a large number of residents was the main factor. With regard to the medium-density communities, as the proportion of vulnerable resident agents increased, total evacuation time was first mainly affected by the movement speed of vulnerable resident agents and then affected by the road congestion. Therefore, in vulnerable communities with different densities, government decision-makers need to formulate different evacuation policies according to the evacuation characteristics of the communities.

3.4. Impacts of Community Mutual Aid Mechanism on the Evacuation Process

Mutual aid behavior between neighbors is a common way to respond to the flood disaster events. However, whether this kind of behavior can significantly reduce evacuation time and improve evacuation efficiency has not been widely concerned and is worth studying. In order to investigate how the mutual aid mechanism affects the evacuation process of different communities, in this study, the percent of non-vulnerable resident agents willing to aid was used to indicate the mutual aid mechanism between neighbors. Besides, the community density and the percent of vulnerable resident agents were considered together to represent different types of communities. Similar to the Section 3.3, communities were divided into three categories: low-density, medium-density, and high-density. The results of the total evacuation time in different types of communities under the influence of mutual aid mechanism were shown in Figure 10.

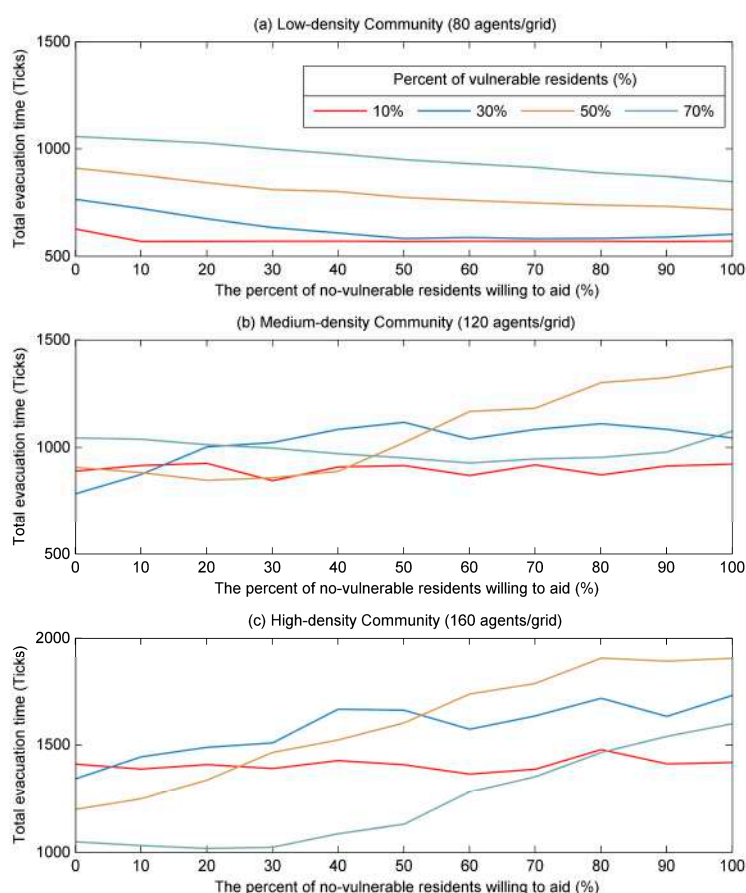


Figure 10. The impacts of the percent of non-vulnerable residents willing to aid on the total evacuation time. (a–c) The community density is 80, 120, and 160 agents/grid, respectively representing low-density, medium-density and high-density community. The percent of vulnerable residents (v) was set as 10%, 30%, 50%, and 70%.

In the low-density community, as shown in Figure 10a, it can be found that the mutual aid behavior between neighbors was effective and can reduce the total evacuation time significantly. When the problem of community vulnerability was serious (e.g., the proportion of vulnerable resident agents was 50% and 70%), more aid from non-vulnerable residents can significantly reduce the total evacuation time. To be specific, the total evacuation time decreased by 20% when the proportion of non-vulnerable residents willing to aid increased from 0% to 100%. However, when the proportion of vulnerable residents was 10% and 30%, the total evacuation time firstly decreased and then remained almost unchanged after the percent of non-vulnerable residents willing to aid increased to a certain proportion. This was because when the number of non-vulnerable residents willing to aid was equal to the number of vulnerable resident agents, all the non-vulnerable residents had been aided to go to the shelter. Therefore, continuing to increase the number of non-vulnerable residents willing to aid would no longer affect the total evacuation time.

With regard to the evacuation in the medium-density community, as shown in Figure 10b, the results indicated that the mutual aid mechanism between neighbors had little effect on the total evacuation time. For example, for a medium-density community with 10% or 70% vulnerable residents, the total evacuation time barely changed regardless of how many non-vulnerable residents were willing to aid. As for the community with 50% vulnerable residents, the time needed to evacuate all residents began to increase significantly after the percent of non-vulnerable residents willing to help reached to 40%. These results implied that the mutual aid mechanism between neighbors slightly affect the evacuation process in medium-density community, especially when the percent of the vulnerable residents was low or high (e.g., 10% and 70%). In other words, managers of medium-density communities should not promote a high percent of mutual aid behaviors.

In the emergency evacuation of high-density communities, especially those with a high proportion of vulnerable residents, the mutual aid mechanism was ineffective and actually increased the total evacuation time (as shown in Figure 10c). This result was completely contrary to the result of low-density communities. Specifically, for communities with 30% or more vulnerable residents, the total evacuation time increased significantly as more non-vulnerable residents were willing to aid. For example, in communities with 50% vulnerable residents, when the percentage of non-vulnerable residents willing to aid increased from 0 to 50%, the total evacuation time increased by 33.6%, and when the aid ratio increased to 100%, the evacuation time significantly increased by up to 58.7% percent. This may be because in high-density communities, the greater number of non-vulnerable residents help vulnerable residents to go to the shelter together, the more likely that a large number of residents would pour into the road at a certain moment, which would cause traffic congestion and increase evacuation time. The results suggested that the more non-vulnerable residents offered aid in high-density community, the less efficient evacuation because the total evacuation time increased significantly.

4. Conclusions

In this study, an agent-based modelling framework that incorporated the resident psychological model and transportation network model was conducted to explore the influence of community properties, resident's psychological attributes and mutual aid mechanism on the flood evacuation processes. Specifically, four main factors: community density, flood risk tolerance threshold of residents, percent of vulnerable residents and mutual aid mechanism were considered together to investigate how they interplay with each other to affect agents' flood evacuation process. Indicators such as total evacuation time, mean evacuation time, percent of evacuated agents and road congestion index were used to evaluate the evacuation efficiency of the whole community. The advantages of this study were mainly in three aspects. Firstly, this study considered residents' self-rescue and community staff's assistance at the same time which is more in line with the reality of community evacuation. Secondly, different from previous evacuation studies, this study focused on vulnerable communities, and the results can identify the main difficulties in evacuation in different types of vulnerable communities. Thirdly, this study highlighted the mutual aid mechanism among residents in the evacuation process, which were usually neglected in previous evacuation studies. The influence of mutual aid mechanism in different communities were identified and the results can provide community managers with information on how to deal with mutual aid behaviors in different types of communities.

The key findings from the simulation results under different scenarios were: (1) The community density was found to be negatively correlated with flood evacuation efficiency. Achieving a high level of evacuation ratio was much more difficult in high-density community than in low-density community due to the marginal time needed rapidly increasing. That was because evacuations from high-density communities can easily cause road congestion. (2) Lower flood risk tolerance threshold can help residents respond to flood disasters timely, but this effect was different in communities with different densities. In high-density communities, appropriately reducing the value of flood risk tolerance threshold of residents can obviously reduce the total evacuation time and improve evacuation efficiency, however, it was not effective in low-density communities. (3) The proportion of vulnerable resident agents had opposite effects in different types of communities. With the increase of the proportion of vulnerable resident agents, the total evacuation time increased significantly in low-density communities, decreased first and then increased in medium-density communities, and decreased in high-density communities. (4) Mutual aid mechanism can reduce evacuation time in low-density communities, and the effect was more pronounced with a higher proportion of vulnerable resident agents in the community. However, in high-density communities, the mutual aid mechanism would actually increase the evacuation time. Besides, the higher the proportion of vulnerable resident agents, the more the evacuation time would increase. In the medium-density community, the percent of non-vulnerable resident willing to aid had a negative relationship with total evacuation time, but it was not obvious.

Such information can help urban community managers and decision-makers increase disaster evacuation efficiency by developing different evacuation strategies according to the specific characteristics of different communities. For example, managers must pay special attention to the impact of community density, especially evacuation in high-density communities. Appropriately lowering the residents' flood risk tolerance threshold could prompt residents to make evacuation decisions earlier. The change of the proportion of vulnerable residents in low and medium-density communities can easily affect the evacuation efficiency. Community managers can adopt various means of transportation to improve the evacuation speed and encourage mutual aid behaviors between residents to reduce the evacuation time. While evacuation in the high-density community, the traffic congestion is the main challenge. Community managers should avoid road congestion caused by the mutual aid behaviors among a large number of people, and should arrange for evacuations in batches when road capacity is inadequate.

But, the limitation of the study should also be taken into consideration. Firstly, in order to make the agent-based model uncomplicated, feasible and operable, not all the factors affecting the residents' evacuation process were considered in this study. For example, the families or friends were assumed to evacuate at the same time in this study, but in reality, residents' behaviors of seeking relatives and friends during the evacuation are common. These searching behaviors are more complex and can affect the simulation results, which will be considered in future studies. Secondly, the agent-based model was conducted in a synthetic community and the usability of the model was verified by comparing the simulation results with previous studies and empirical data. However, due to the difficulty in obtaining more detailed evacuation data, it is difficult to further verify the simulation results of the entire evacuation process. Thirdly, the more parameters in ABM model, the more likely random results will appear. In this study, the model was running 500 times and calculated the truncated mean value to avoid randomness. However, it would be more time-consuming and labor consuming to increase the number of runs in order to get more stable model results. Even so, some interesting results were found and can be used to optimize flood risk management in urban community.

Future work will use the empirical data to measure the various behavioral parameters, modify and improve the mutual aid mechanism based on community interviews and survey results, use realistic communities and transportation networks as the research areas, consider the dynamic impact of flood events, and combine the spatial-temporal uncertainty of multi-stage flood warnings.

Author Contributions: Z.W. was responsible for literature search, survey design, data analysis, conceived the idea for the study and wrote the initial draft of the manuscript. J.K. was responsible for field interviews, data collection. J.H. contributed to the revision of English and style. H.W. principally provided comments of the manuscript and offered financial support. W.C. was responsible for investigation and data curation. All authors have read and agreed to the published version of the manuscript.

Funding: This research was funded by National Natural Science Foundation of China (Grant number 91846203, 71601070 and 41877526), National Key R & D Program of China (Grant number 2017YFC1502603) and the Fundamental Research Funds for the Central Universities (Grant number 2017B728X14).

Acknowledgments: The authors would like to express our gratitude to the Huimin Wang for her support to carry out the study. And the authors are grateful for the thoughtful suggestions and comments from the editor and reviewers.

Conflicts of Interest: The authors declare no conflicts of interest.

References

1. Wang, Z.Q.; Wang, H.M.; Huang, J.; Kang, J.L.; Han, D.W. Analysis of the public flood risk perception in a flood-prone city: The case of jingdezhen city in china. *Water* **2018**, *10*, 1577. [[CrossRef](#)]
2. Yu, J.; Zhang, C.R.; Wen, J.H.; Li, W.D.; Liu, R.; Xu, H. Integrating multi-agent evacuation simulation and multi-criteria evaluation for spatial allocation of urban emergency shelters. *Int. J. Geogr. Inf. Sci.* **2018**, *32*, 1884–1910. [[CrossRef](#)]
3. Cutter, S.L. The vulnerability of science and the science of vulnerability. *Ann. Assoc. Am. Geogr.* **2003**, *93*, 1–12. [[CrossRef](#)]

4. Turner, B.L., II; Kasperson, R.E.; Matson, P.A.; McCarthy, J.J.; Corell, R.W.; Christensen, L.; Eckley, N.; Kasperson, J.X.; Luers, A.; Martello, M.L.; et al. A framework for vulnerability analysis in sustainability science. *Proc. Natl. Acad. Sci. USA* **2003**, *100*, 8074–8079. [[CrossRef](#)]
5. Nasiri, H.; Mohd Yusof, M.J.; Mohammad Ali, T.A. An overview to flood vulnerability assessment methods. *Sustain. Water Resour. Manag.* **2016**, *2*, 331–336. [[CrossRef](#)]
6. Chu, H.; Yu, J.; Wen, J.H.; Yi, M.; Chen, Y. Emergency evacuation simulation and management optimization in urban residential communities. *Sustainability* **2019**, *11*, 795. [[CrossRef](#)]
7. Adelson-Velsky, G.M.; Levner, E. Project scheduling in and-or graphs: A generalization of dijkstra’s algorithm. *Math. Oper. Res.* **2002**, *27*, 504–517. [[CrossRef](#)]
8. Mehmood, S.; Ahmed, S.; Kristensen, A.S. Application of integrated model of evacuation psychology in an agent-based simulation. In Proceedings of the 11th International Conference on Computer Modeling and Simulation (ICCMS 2019) and 8th International Conference on Intelligent Computing and Applications (ICICA 2019), Melbourne, Australia, 16–19 January 2019; pp. 70–74. [[CrossRef](#)]
9. Toledo, T.; Marom, I.; Grimberg, E.; Bekhor, S. Analysis of evacuation behavior in a wildfire event. *Int. J. Disaster Risk Reduct.* **2018**, *31*, 1366–1373. [[CrossRef](#)]
10. Li, Y.; Liu, H.; Liu, G.P.; Li, L.; Moore, P.; Hu, B. A grouping method based on grid density and relationship for crowd evacuation simulation. *Physica A* **2017**, *473*, 319–336. [[CrossRef](#)]
11. Morss, R.E.; Demuth, J.L.; Lazo, J.K.; Dickinson, K.; Lazrus, H.; Morrow, B.H. Understanding public hurricane evacuation decisions and responses to forecast and warning messages. *Weather Forecast.* **2016**, *31*, 395–417. [[CrossRef](#)]
12. Chen, Y.; Zhou, H.; Zhang, H.; Du, G.; Zhou, J. Urban flood risk warning under rapid urbanization. *Environ. Res.* **2015**, *139*, 3–10. [[CrossRef](#)] [[PubMed](#)]
13. Isobe, M.; Adachi, T.; Nagatani, T. Experiment and simulation of pedestrian counter flow. *Physica A* **2004**, *336*, 638–650. [[CrossRef](#)]
14. Liu, X.F.; Lim, S.S. Integration of spatial analysis and an agent-based model into evacuation management for shelter assignment and routing. *J. Spat. Sci.* **2016**, *61*, 283–298. [[CrossRef](#)]
15. Zhu, J.X.; Dai, Q.; Deng, Y.H.; Zhang, A.R.; Zhang, Y.Z.; Zhang, S.L. Indirect damage of urban flooding: Investigation of flood-induced traffic congestion using dynamic modeling. *Water* **2018**, *10*, 622. [[CrossRef](#)]
16. Macal, C.M. Everything you need to know about agent-based modelling and simulation. *J. Simul.* **2016**, *10*, 144–156. [[CrossRef](#)]
17. Zou, Q.; Fernandes, D.S.; Chen, S. Agent-based evacuation simulation from subway train and platform. *J. Trans. Saf. Secur.* **2019**, 1–22. [[CrossRef](#)]
18. D’Orazio, M.; Spalazzi, L.; Quagliarini, E.; Bernardini, G. Agent-based model for earthquake pedestrians’ evacuation in urban outdoor scenarios: Behavioural patterns definition and evacuation paths choice. *Saf. Sci.* **2014**, *62*, 450–465. [[CrossRef](#)]
19. Liang, W.; Lam, N.S.N.; Qin, X.J.; Ju, W.X. A two-level agent-based model for hurricane evacuation in new orleans. *J. Homel. Secur. Emerg.* **2015**, *12*, 407–435. [[CrossRef](#)]
20. Mostafizi, A.; Wang, H.Z.; Cox, D.; Dong, S.J. An agent-based vertical evacuation model for a near-field tsunami: Choice behavior, logical shelter locations, and life safety. *Int. J. Disaster Risk Reduct.* **2019**, *34*, 467–479. [[CrossRef](#)]
21. Wijerathne, L.; Petprakob, W.; Aguilar, L.; Hori, M.; Ichimura, T. Scalable hpc enhanced agent based system for simulating mixed mode evacuation of large urban areas. *Transp. Res. Proc.* **2018**, *34*, 275–282. [[CrossRef](#)]
22. Liu, X.F.; Lim, S. An agent-based evacuation model for the 2011 brisbane city-scale riverine flood. *Nat. Hazards* **2018**, *94*, 53–70. [[CrossRef](#)]
23. Poulos, A.; Tocornal, F.; de la Llera, J.C.; Mitrani-Reiser, J. Validation of an agent-based building evacuation model with a school drill. *Transp. Res. C Emerg. Technol.* **2018**, *97*, 82–95. [[CrossRef](#)]
24. Marzouk, M.; Mohamed, B. Integrated agent-based simulation and multi-criteria decision making approach for buildings evacuation evaluation. *Saf. Sci.* **2019**, *112*, 57–65. [[CrossRef](#)]
25. Karbovskii, V.; Voloshin, D.; Karsakov, A.; Bezgodov, A.; Zagarskikh, A. Multiscale agent-based simulation in large city areas: Emergency evacuation use case. *Procedia Comput. Sci.* **2015**, *51*, 2367–2376. [[CrossRef](#)]
26. Du, E.; Cai, X.; Sun, Z.; Minsker, B. Exploring the role of social media and individual behaviors in flood evacuation processes: An agent-based modeling approach. *Water Resour. Res.* **2017**, *53*, 9164–9180. [[CrossRef](#)]

27. Cimellaro, G.P.; Mahin, S.; Domaneschi, M. Integrating a human behavior model within an agent-based approach for blasting evacuation. *Comput. Aided Civ. Infrastruct. Eng.* **2019**, *34*, 3–20. [[CrossRef](#)]
28. Du, E.; Rivera, S.; Cai, X.; Myers, L.; Ernest, A.; Minsker, B. Impacts of human behavioral heterogeneity on the benefits of probabilistic flood warnings: An agent-based modeling framework. *J. Am. Water Resour. Assoc.* **2017**, *53*, 316–332. [[CrossRef](#)]
29. Tonn, G.L.; Guikema, S.D. An agent-based model of evolving community flood risk. *Risk Anal.* **2018**, *38*, 1258–1278. [[CrossRef](#)]
30. Reynaud, A.; Aubert, C.; Nguyen, M.-H. Living with floods: Protective behaviours and risk perception of vietnamese households. *Geneva Pap. Risk Insur. Issues Pract.* **2013**, *38*, 547–579. [[CrossRef](#)]
31. Ghaderi, J.; Srikant, R. Opinion dynamics in social networks with stubborn agents: Equilibrium and convergence rate. *Automatica* **2014**, *50*, 3209–3215. [[CrossRef](#)]
32. Boeing, G. Osmnx: New methods for acquiring, constructing, analyzing, and visualizing complex street networks. *Comput. Environ. Urban Syst.* **2017**, *65*, 126–139. [[CrossRef](#)]
33. Cova, T.J.; Johnson, J.P. A network flow model for lane-based evacuation routing. *Transp. Res. Part A Policy Pract.* **2003**, *37*, 579–604. [[CrossRef](#)]
34. Zhang, B.; Ukkusuri, S.V.; Chan, W.K. Agent-based modeling for household level hurricane evacuation. In Proceedings of the 2009 Winter Simulation Conference (WSC), Austin, TX, USA, 13–16 December 2009; pp. 2778–2784.
35. Dijkstra, E.W. A note on two problems in connexion with graphs. *Numer. Math.* **1959**, *1*, 269–271. [[CrossRef](#)]
36. Nagel, K.; Schreckenberg, M. A cellular automaton model for freeway traffic. *J. Phys. I* **1992**, *2*, 2221–2229. [[CrossRef](#)]
37. Liu, S.B.; Yang, L.Z.; Fang, T.Y.; Li, J. Evacuation from a classroom considering the occupant density around exits. *Physica A* **2009**, *388*, 1921–1928. [[CrossRef](#)]
38. Stepanov, A.; Smith, J.M. Multi-objective evacuation routing in transportation networks. *Eur. J. Oper. Res.* **2009**, *198*, 435–446. [[CrossRef](#)]
39. Ji, J.W.; Lu, L.G.; Jin, Z.H.; Wei, S.P.; Ni, L. A cellular automata model for high-density crowd evacuation using triangle grids. *Physica A* **2018**, *509*, 1034–1045. [[CrossRef](#)]
40. Lo, S.; Fang, Z.; Lin, P.; Zhi, G. An evacuation model: The sgem package. *Fire Saf. J.* **2004**, *39*, 169–190. [[CrossRef](#)]
41. Bassett, D.S.; Alderson, D.L.; Carlson, J.M. Collective decision dynamics in the presence of external drivers. *Phys. Rev. E* **2012**, *86*, 036105. [[CrossRef](#)]
42. McCullen, N.J.; Rucklidge, A.M.; Bale, C.S.E.; Foxon, T.J.; Gale, W.F. Multiparameter models of innovation diffusion on complex networks. *SIAM J. Appl. Dyn. Syst.* **2013**, *12*, 515–532. [[CrossRef](#)]
43. Martins, A.C.; Galam, S. Building up of individual inflexibility in opinion dynamics. *Phys Rev E* **2013**, *87*, 042807. [[CrossRef](#)] [[PubMed](#)]
44. Kroese, D.P.; Brereton, T.; Taimre, T.; Botev, Z.I. Why the monte carlo method is so important today. *Wiley Interdiscip. Rev. Comput. Stat.* **2014**, *6*, 386–392. [[CrossRef](#)]
45. Rothenberg, T.J.; Fisher, F.M.; Tilanus, C.B. A note on estimation from a cauchy sample. *J. Am. Stat. Assoc.* **1964**, *59*, 460–463. [[CrossRef](#)]
46. Railsback, S.; Ayllón, D.; Berger, U.; Grimm, V.; Lytinen, S.; Sheppard, C.; Thiele, J. Improving execution speed of models implemented in netlogo. *J. Artif. Soc. Soc. Simul.* **2017**, *20*. [[CrossRef](#)]



ARTICLES FOR FACULTY MEMBERS

RESCUE VESSEL OPERATION FOR FLOOD EVACUATION PROTOCOL

Title/Author	Autonomous surface vessel for search and rescue operation / Mansor, H., Norhisam, M. H., Abidin, Z. Z., & Gunawan, T. S.
Source	<i>Bulletin of Electrical Engineering and Informatics</i> Volume 10 Issue 3 (2021) Pages 1701–1708 https://doi.org/10.11591/EEI.V10I3.2599 (Database: IAES)

Autonomous surface vessel for search and rescue operation

Hasmah Mansor¹, Muhammad Haziq Norhisam², Zulkifli Zainal Abidin³, Teddy Surya Gunawan⁴

^{1,2,4}Department of Electrical and Computer Engineering, Kulliyah of Engineering, International Islamic University Malaysia (IIUM), Jalan Gombak, 53100 Kuala Lumpur, Malaysia

³Department of Mechatronics Engineering, Kulliyah of Engineering, International Islamic University Malaysia (IIUM), Jalan Gombak, 53100 Kuala Lumpur, Malaysia

Article Info

Article history:

Received May 5, 2020

Revised Dec 5, 2020

Accepted May 3, 2021

Keywords:

Arduino
Autonomous surface vessel
GPS
Search and rescue
Sonar sensor

ABSTRACT

Search and rescue operation is performed to save human life, for example during natural disasters, unfortunate incidents on the land, in the deepwater, or lakes. There were incidents happened to the search and rescue crew during the operation although they were well trained. A new method using robotic technology is important to reduce the crew's risk during operations. This research proposed a development of an autonomous surface vessel for search and rescue operations for deepwater applications. The proposed autonomous surface vessel is equipped with a global positioning system (GPS) and underwater sensor to search for the victims, black box, debris, or other evidence on the surface and underwater. The vessel was designed with monitoring and control via radio frequency wireless communication. The autonomous surface vessel prototype was developed and tested successfully with the telemetry at the ground station. The ground station acts as the control centre of the overall system. Results showed the vessel successfully operated autonomously. The operator at the ground station was able to monitor the sensor data and control the vessel's manoeuvre according to the created path. The telemetry coverage to monitor the water surroundings and control the vessel's manoeuvre was around 100 meters.

This is an open access article under the [CC BY-SA](https://creativecommons.org/licenses/by-sa/4.0/) license.



Corresponding Author:

Hasmah Mansor
Department of Electrical and Computer Engineering
International Islamic University Malaysia (IIUM)
Jalan Gombak, 53100 Kuala Lumpur, Malaysia
Email: hasmahm@iium.edu.my

1. INTRODUCTION

Search and rescue, SAR is an operation to search for the living victims that are in danger. However, many cases have happened where SAR crew to be in danger and involved in fatal accidents during the operation. For example, six firemen in Malaysia drown during rescuing a drowning teenager at a mine [1]. In Indonesia, during the search and rescue mission for the Lion Air aeroplane crashed, one of the divers died during the operation due to the decompression of the human body in the deep sea [2].

Nowadays, robotic technologies offer many innovative solutions to assist and reduce the risk of humans at work. Autonomous surface vessel (ASV) has been used in many areas that are considered to be dangerous and risky. Biologists have used ASV to monitor the quality of the water, the military operation has been using ASV for monitoring coastal area and detecting sea mines, drones and robots have been using in handling chemicals and other dangerous tasks those could cause health problems [3]-[5] and many more. It has been proven that the utilisation of ASV and robots have increased productivity, improved time efficiency with more flexibility.

Recent research on ASV mainly focuses on general control objectives such as asymptotic tracking, guaranteed transient tracking performance, the stability of the vessel, robustness towards disturbances, adaptation to environmental change, and collision avoidance. Y. Hu *et al.* [6] has developed an avoidance system using real-time fuzzy logic, considering the steering dynamic of the ASV. Based on experience, an algorithm called fuzzy case base reasoning has been proposed. The proposed system was able to avoid a collision when similar cases happened in ASV heading control system. Z. I. Bell *et al.* [7] and C. Dong *et al.* [8] have developed adaptive controllers for ASV subject to parametric uncertainties and time-varying disturbances. The Lyapunov theory has been used as the adaptive algorithm. The vessel was successfully operated subject to parametric uncertainties and time-varying disturbances. Another challenge, ASV, when operated on the sea yaw angle, is exposed to disturbances. Therefore robust control is suggested by W. Guan *et al.* [9]. The technique used was closed-loop shaping, which incorporates with recursive least squares method. Astrov *et al.* [10] has proposed neural predictive control for ASV. The work conducted focused on modelling and simulation of a nonlinear system of ASV via Simulink/Matlab. The research conducted on ASV has successfully achieved its objectives. However, the complete design of ASV for safety and rescue mission is still not available. Therefore the design and implementation of ASV for search and rescue are proposed.

The SAR team has used a sonar sensor from Germany to find two drowned victims in the lake [11]. The mission used a side-scan sonar sensor, and it was successful. The victim was found in just several hours instead of several days for manual diver search. There were research about sidescan imaging sonar for SAR in improving the quality of sonar image. For example author in [12] proposed quantitative model for by predicting the shadow contrast ratio. With this motivation, the proposed ASV will use a sonar sensor to identify the depth of water or shape/object underwater.

SAR missions usually involved a wide coverage area. The most critical features of the ASV system's wireless communication are reliability, real-time data transfer (position and sensor status). In the HydroNet ASV water quality project, the data has been transferred using a WiFi module and 433Mhz channel module [3]. The system was able to communicate approximately 10km apart between the rover and ground station and locate three rovers simultaneously during the execution of the mission. Jafaar Fahad A. Rida [13] has proposed improving mobile wireless communication based on non-line of sight; however, for this SAR application, the ASV is operated at the water surface where there are no high rise buildings and trees at the searching area. Other wireless communications that have been used in ASV are radio frequency (RF) and global system for mobile (GSM), as discussed in [14-17]. Shadman Sakib Arnob *et al.* [17], GSM was used to notify the control room if the passenger boat is overloaded and in danger. The author used the global positioning system (GPS) and proportional integral controller (PID) to track and avoid the autonomous boat. The proof of concept was tested on a miniature boat where the communication range of the ultrasonic sensor achieved during the experiment was between 30cm to 200cm. Similar to SAR missions, [18] developed eCall for Malaysia's automotive industries when accidents occurred. The system automatically transmits a call to the public service answering point and certain vehicle-related information using a microcomputer, GSM, and GPS technologies when a collision was detected; to inform the emergency response unit for their immediate action.

Some examples of the application used at the ground station for ASV monitoring are XRradioLS D4 and quantum first-person view (FPV). XRLS D4 was successfully deployed with first-person view video footage and can control the rover [19]. It is costly, compared to quantum FPV. Quantum FPV ground station was built for video streaming purposes only, without control features of UAV [20]. FPV camera in a rover has also been used as visual monitoring in SAR application. From the FPV camera, information from surrounding was collected and work lifting to collect/remove load was also performed [21]. In the proposed research, the monitoring and control of ASV will be conducted by the SAR crew at the ground station where GPS data is used to determine the real-time position of ASV. All data from the ASV and sensors would be acquired.

In a more complex autonomous system such as light-detection-and-ranging (LiDAR) where various parameters are to be configured simultaneously, [22] developed genetic algorithm for robot navigation system for the robot to be navigated from one point to another in a fast and safe environment; without hitting static or dynamic obstacles. LiDAR can collect more than 1 million points per second of high-quality 3D data, make the simultaneous localisation and mapping (SLAM) algorithm for mapping and localisation using robotic operating system (ROS) important [23]. LiDAR is usually used to measure the ground's shape and contour from the air, but not suitable for underwater scanning.

In summary, ASV for search and rescue operation has been proposed in this research. The ASV is equipped with a side-scan sensor that could help in the searching operation, suitable for underwater scanning. The data collected from the sensor could be access from the ground station where the SAR team could access

the area's current situation. The SAR team would monitor and control the ASV with the help of video footage at the ground station via RF wireless communication.

2. RESEARCH METHOD

The overall design of ASV for SAR proposed in this research is shown in Figure 1. It involved three components: surface vessel, ground station, and communication system. The ground station controls the ASV and monitors the monitoring aid system's data via a communication line (wireless RF). The surface vessel can be controlled by the operator remotely either in autonomous or manual mode.



Figure 1. Overall system design of ASV for SAR

2.1. Surface vessel

The ASV is designed with three main components that are hull design, communication system, and manoeuvring system. The selection of hull design is essential as it affects the stability and performance of the vessel. In the hull prototype design, a single planning hull design with deep-V style has been proposed due to easy manoeuvring a higher speed and smooth ride through the rough water surface. The vessel/hull has been installed with several sensors and actuators, as shown in Table 1. All of the sensors and actuators are powered up using an 18.0V LiPo battery. Two 18V LiPo battery with a capacity of 5200 mAh is connected in parallel to double output capacity to deliver to the system, thus double up the working hours.

Table 1. Electronic component specification

Sensor/Actuator	Voltage (V)	Current (A)	Supply Voltage (V)
Motor (Thruster)	18	-	18
Motor Driver (120A Max)	-	120	-
Servo (HS=805BB)	4.5-6	8m	5
APM (ArduPilot Mega)	5	-	5
GPS (Garmin 19X HVS)	8-33	40m	18
Side Scan Sonar (CruzPro DSP Active Depth and Temperature Transducers)	9.5-16	3.5m	12

2.2. Portable ground station

A portable ground system is used to monitor and control the ASV using RF telemetry. It consists of an industrial computer, wireless module connection for sensor data transfer, and remote control for manual control of the vessel manoeuvring system. LiPo battery has been chosen due to its small size and portable.

2.3. Communication system

In the proposed design of ASV for SAR, there are two parts of communications required. The first part is RF wireless communication used to transmit data from the side-scan sonar sensor to the ground station for underwater image analysis and perform manual control of USV. The second part is to receive data from the GPS to keep track of the ASV location and control the ASV with the desired location.

2.3.1. Data transmission

In the proposed system, RF wireless telemetry has been used for the communication system on data transmission due to its capability to transmit the data at long range. RF connection allows the data packet to

be transferred between vessels and the ground station. At the ASV, the sensor data are transferred using the National Marine Electronics Association (NMEA) 0183 standard protocol. NMEA 0183 is a standard marine data protocol that provides multiple data in one input string. NMEA protocol enables one talker to provide multiple data in a single string for a listener at one time. Besides that, the NMEA 0183 standard data protocol provides extra reliability on data transmission [24]. In this system, the sensors that are using NMEA protocol are GPS and single beam side scan sonar. Since more than one sensor is used in this system, the data from the sensors are combined using the NMEA data combiner to make the data transfer across one telemetry connection. The architecture of the communication system is shown in Figure 2.



Figure 2. The architecture of the ASV communication system

2.3.2. Autonomous system

In Figure 3, the ASV has been set with the desired location in the autonomous system design. A microcontroller, ArduPilot Mega (APM), has been used and installed at the vessel. The APM has been programmed to operate the vessel autonomously from the ground station.

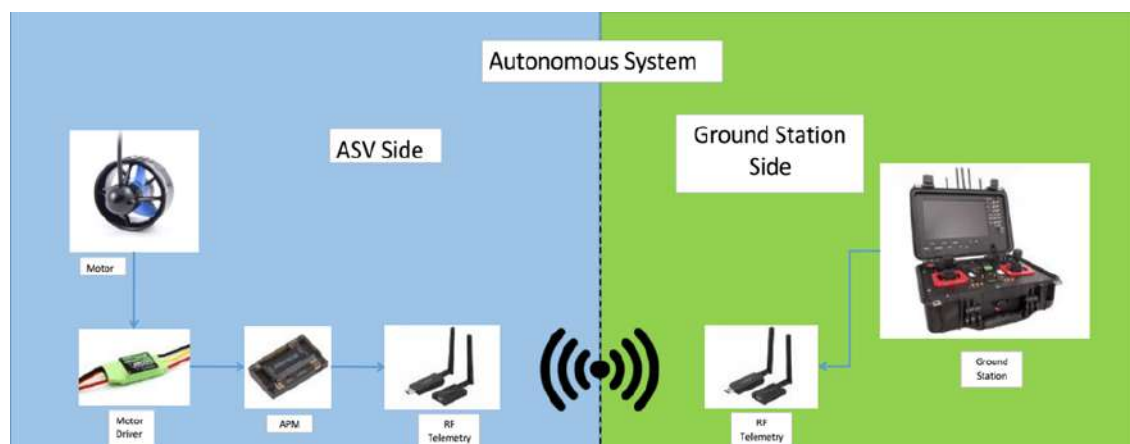


Figure 3. Autonomous system diagram

The ASV could be monitored and controlled from the ground station wirelessly. The connection has been established using RF telemetry communication between the ground stations with the vessel. Data of the specific setting and desired location have been sent from the ground station to the microcontroller. The microcontroller has processed all the data by comparing it with the GPS and inertial measurement unit (IMU) data. Based on the comparison between these data, the APM control the vessel autonomously.

2.3.3. Search and rescue monitoring system

Search and rescue monitoring system has been set at the ground station. Data from side-scan sonar and global positioning system, GPS are received. Side-scan sonar provides surrounding data on the water surface and underwater and draws the underwater image that made underwater searching possible. GPS sensor is used to provide location data of the vessel.

3. RESULTS AND DISCUSSION

The integration of the overall system, as shown in Figure 4, has been done to evaluate the ASV system's performance. GPS and single beam echo sounder (sonar sensor) have been installed at the vessel, the communication system and the ground station have been integrated. The system was tested at Tasek Selayang, Malaysia.



Figure 4. Experimental setup of ASV

3.1. Experiment on global positioning sensor data

In this project, GPS has been used to provide real-time positioning of the vessel. The sensor used an RS232 serial communication interface connected to the computer or sensor. In order to read the data of the sensor, the GPS was connected to the computer. Data was read at the computer, using raw data reader software called Teraterm. Figure 5(a) shows the data of the GPS using the NMEA 0183 standard protocol. This data can be used in mapping software to visualise the real-time position of the vessel. The definition of each NMEA sentence identifier can be found in [25].

3.2. Experiment on single beam echo sounder data

In this research, a sonar sensor was used to help in underwater search operations by scanning an underwater image. Figure 5(b) shows single beam echo sounder NMEA 0183 data sentences obtained from the experimental work at Tasek Selayang. The data contained information on the depth and temperature of the water.

3.3. Experiment on wireless serial communication

All the sensors' data from the surface vessel was sent wirelessly to the ground station for monitoring purposes. The Arduino read the data and then sent to the ground station through the HC-12 wireless module. Figure 6(a) shows the developed wireless communication prototype of the overall autonomous system diagram (ASV side) of Figure 4. The sensor used RS232 physical protocol, which used 12V signal logic. Due to the ArduPilot Mega (APM) microcontroller signal requirement of $\pm 5V$, RS232 to TTL converter was used to convert 12V signal logic to 5V signal logic. APM then sent the sensor data via the HC-12 transceiver wireless module to the ground station. The data was received at the ground station through the HC-12 transceiver module, which was connected to another Arduino microcontroller. The Arduino was connected to the ground station's computer via a USB port. In order to check the connection, the Teraterm software was used to display all the data received from the vessel to the ground station.

3.4. Experiment on real-time positioning

Using google earth pro software, the real-time GPS data were plotted during the experimental test at Tasek Selayang. The result showed that the location of the vessel was plotted and display at the ground station. As the vessel moved across the lake, its route was mapped on the Google Earth Pro as a red line. The result is shown in Figure 6(b). The data of the GPS were sent by APM using the HC-12 wireless module. At the ground station, the receiver was connected to the computer and displayed the vessel movement's position using google earth pro software.

\$GPRMC,053645.3,A,0315.17402,N,10143.82493,E,000.17,356.5,171018,000.2,W,A*	\$SDMTW,033.8,C*3C
\$GPGGA,053645.3,0315.17402,N,10143.82493,E,1,08,1.0,80.6,M,-3.6,M,,*75	\$SDDPT,002.6,*7D
\$GPVTG,356.5,T,356.6,M,000.17,N,0000.31,K,A*14	\$SDDBT,008.5,f,002.6,M,001.4,F*0A
\$GPRMC,053645.4,A,0315.17402,N,10143.82493,E,000.19,356.5,171018,000.2,W,A*	\$SDMTW,033.8,C*3C
\$GPGGA,053645.4,0315.17402,N,10143.82493,E,1,08,1.0,80.6,M,-3.6,M,,*72	\$SDDPT,002.6,*7D
\$GPVTG,356.5,T,356.6,M,000.19,N,0000.35,K,A*1E	\$SDDBT,008.5,f,002.6,M,001.4,F*0A
\$GPRMC,053645.5,A,0315.17402,N,10143.82493,E,000.19,356.5,171018,000.2,W,A*	\$SDMTW,033.8,C*3C
\$GPGGA,053645.5,0315.17402,N,10143.82493,E,1,08,1.0,80.6,M,-3.6,M,,*73	\$SDDPT,002.6,*7D
\$GPVTG,356.5,T,356.6,M,000.19,N,0000.35,K,A*1E	\$SDDBT,008.5,f,002.6,M,001.4,F*0A
\$GPRMC,053645.6,A,0315.17402,N,10143.82493,E,000.19,356.5,171018,000.2,W,A*	\$SDMTW,033.8,C*3C
\$GPGGA,053645.6,0315.17402,N,10143.82493,E,1,08,1.0,80.6,M,-3.6,M,,*70	\$SDDPT,002.6,*7D
\$GPVTG,356.5,T,356.6,M,000.19,N,0000.35,K,A*1E	\$SDDBT,008.5,f,002.6,M,001.4,F*0A
\$GPRMC,053645.7,A,0315.17402,N,10143.82493,E,000.21,356.5,171018,000.2,W,A*	\$SDMTW,033.8,C*3C
\$GPGGA,053645.7,0315.17402,N,10143.82493,E,1,08,1.0,80.6,M,-3.6,M,,*71	\$SDDPT,002.6,*7D
\$GPVTG,356.5,T,356.6,M,000.21,N,0000.38,K,A*18	\$SDDBT,008.5,f,002.6,M,001.4,F*0A
\$GPRMC,053645.8,A,0315.17402,N,10143.82493,E,000.21,356.5,171018,000.2,W,A*	\$SDMTW,033.8,C*3C
\$GPGGA,053645.8,0315.17402,N,10143.82493,E,1,08,1.0,80.6,M,-3.6,M,,*7E	\$SDDPT,002.6,*7D
\$GPVTG,356.5,T,356.6,M,000.21,N,0000.38,K,A*18	\$SDDBT,008.5,f,002.6,M,001.4,F*0A
\$GPRMC,053645.9,A,0315.17396,N,10143.82493,E,000.24,356.5,171018,000.2,W,A*	\$SDMTW,033.8,C*3C
\$GPGGA,053645.9,0315.17396,N,10143.82493,E,1,08,1.0,80.6,M,-3.6,M,,*75	\$SDDPT,002.6,*7D
\$GPVTG,356.5,T,356.6,M,000.24,N,0000.44,K,A*16	

Figure 5. These figures are, (a) Example of GPS, (b) Single beam echo sound raw data

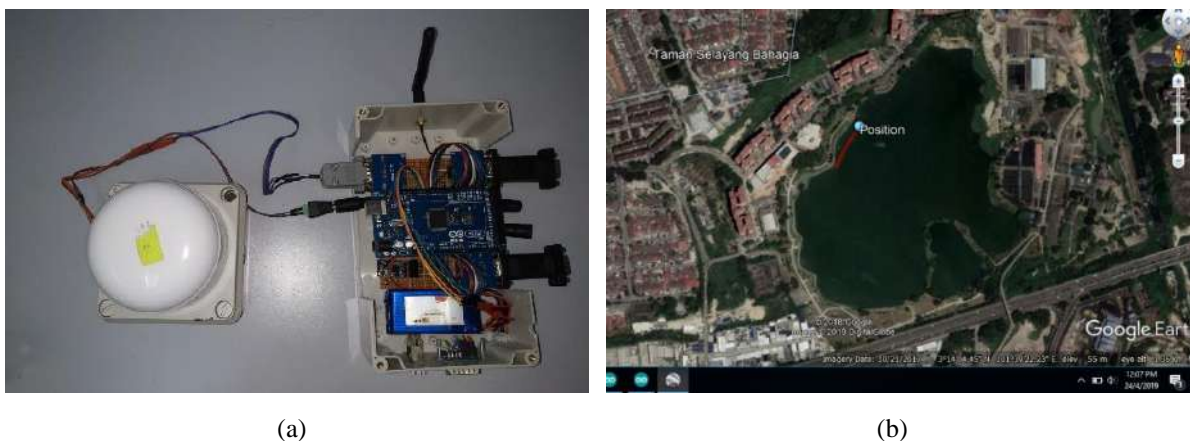


Figure 6. Wireless module and path movement, (a) Wireless communication module, (b) Vessel path movement on google earth pro

3.5. Experiment on single beam echo sounder underwater mapping

A single beam echo sounder was used to scan the 2D image of the underwater cross-section where the depth and shape underwater surface could be identified. The sensor data was sent through the wireless module and received by the Arduino at the ground station in real-time. Since there is no available open-source software to sketch the 2D underwater image, NMEA data was used by the microcontroller to obtain the depth of water. The data was visualised using a serial plotter function in Arduino IDE, as shown in Figure 7. From the graph, the depth of the lake water is around 5 meters.

3.6. Experiment on the autonomous system

In the autonomous system, the Ardupilot board or APM was used to control the vessel's movement using open-source software, Mission Planner. The board was placed on the vessel and controlled from the ground station using a telemetry receiver that receives the flight data from the telemetry transmitter at the ground station. The vessel was controlled using the path planning function, which guides the vessel's movement according to the path created.

The autonomous system was tested on the lake. First, the path was created using the Mission Planner. Then, the path was uploaded to the vessel via telemetry (transmitter). Once the telemetry (receiver) received the signal, the vessel started the mission by following the path created. As shown in Figure 8, the path created is shown in the yellow line. The purple line shows the actual direction of the vessel. Due to some factors from the climate change during the experiment, the telemetry coverage to monitor the underwater image and control the vessel's manoeuvre was around 100 meters.

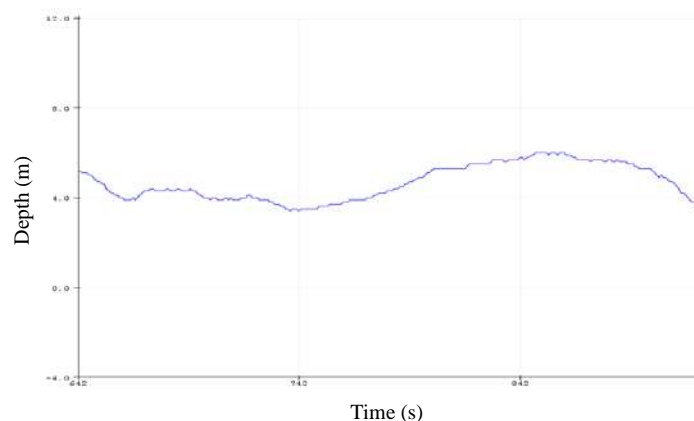


Figure 7. Graph showing the depth of the water



Figure 8. Experiment on path planning of the autonomous system

4. CONCLUSION

In conclusion, the objective of this research has been achieved. An autonomous surface vessel for search and rescue for a deepwater operation has been designed and developed. The developed prototype includes a portable ground station where RF wireless communication has used the communication between the vessel and the ground station. Experiment results showed that the proposed system could scan the 2D image of the underwater cross-section, which were the depth and temperature of the water; shown at the ground station. When the SAR crew created a path at the telemetry, the vessel moved successfully to the created path. Future research includes integration with more sensors for intelligence, surveillance, command and control for the possibility to be implemented for military purposes.

ACKNOWLEDGMENTS

The authors would like to thank Centre of Unmanned Technology (CUTe) and International Islamic University Malaysia (IIUM) for providing the research and development facility and the full support towards the completion of this project.

REFERENCES

- [1] The chronology of tragedy 6 members of Bomba Limp in Bahasa. [Online]. Available: <https://www.bharian.com.my/berita/kes/2018/10/481651/kronologi-tragedi-6-anggota-bomba-lemas>. [Access: April 1, 2020]
- [2] Lion JT610: A diver died during the evacuation process in Bahasa. [Online]. Available: <https://www.bbc.com/indonesia/indonesia-46081626>. [Access: April 15, 2020]
- [3] G. Ferri, A. Manzi, F. Fornai, F. Ciuchi and C. Laschi, "The HydroNet ASV, a Small-Sized Autonomous Catamaran for Real-Time Monitoring of Water Quality: From Design to Missions at Sea," in *IEEE Journal of Oceanic Engineering*, vol. 40, no. 3, pp. 710-726, July 2015, doi: 10.1109/JOE.2014.2359361.

- [4] M. A. M. Basri and A. Nordin, "Optimal Backstepping Control of Quadrotor UAV using Gravitational Search Optimization Algorithm," in *Bulletin of Electrical Engineering and Informatics*, vol. 9, no. 5, pp. 1819-1826, 2020.
- [5] A. Benedetto, P. Luca, M. Marco, A. Corrieri, D. Masti and L. Vanni, "Development of an innovative and sustainable sail-drone," *2017 IEEE International Conference on Environment and Electrical Engineering and 2017 IEEE Industrial and Commercial Power Systems Europe (EEEIC / I&CPS Europe)*, pp. 1-6, 2017.
- [6] Y. Hu, X. Meng, Q. Zhang and G. Park, "A Real-Time Collision Avoidance System for Autonomous Surface Vessel Using Fuzzy Logic," in *IEEE Access*, vol. 8, pp. 108835-108846, 2020, doi: 10.1109/ACCESS.2020.3001626.
- [7] Z. I. Bell, J. Nezvadovitz, A. Parikh, E. M. Schwartz and W. E. Dixon, "Global Exponential Tracking Control for an Autonomous Surface Vessel: An Integral Concurrent Learning Approach," in *IEEE Journal of Oceanic Engineering*, vol. 45, no. 2, pp. 362-370, April 2020, doi: 10.1109/JOE.2018.2880622.
- [8] C. Dong, S. He and S. -L. Dai, "Performance-Guaranteed Tracking Control of an Autonomous Surface Vessel With Parametric Uncertainties and Time-Varying Disturbances," in *IEEE Access*, vol. 7, pp. 101905-101914, 2019, doi: 10.1109/ACCESS.2019.2931337.
- [9] W. Guan, W. Cao, J. Sun and Z. Su, "Steering Controller Design for Smart Autonomous Surface Vessel Based on CSF L2 Gain Robust Strategy," in *IEEE Access*, vol. 7, pp. 109982-109989, 2019, doi: 10.1109/ACCESS.2019.2931887.
- [10] I. Astrov, A. Udál, I. Roasto and H. Mölder, "Target Tracking by Neural Predictive Control of Autonomous Surface Vessel for Environment Monitoring and Cargo Transportation Applications," *2020 17th Biennial Baltic Electronics Conference (BEC)*, 2020, pp. 1-4, doi: 10.1109/BEC49624.2020.9277115.
- [11] Side-scan sonar for first responders & search and rescue (SAR). [Online]. Available: <https://blacklaserlearning.com/sonar-for-first-responders-marine-rescue/>. [Access: April 3, 2020]
- [12] D. A. Cook and D. C. Brown, "Synthetic Aperture Sonar Image Contrast Prediction," in *IEEE Journal of Oceanic Engineering*, vol. 43, no. 2, pp. 523-535, 2018.
- [13] Jafaar Fahad A. Rida, "Improvement for performance radio frequency in wireless communication based on impulse signal," *Indonesian Journal of Electrical Engineering & Computer Science (IJECS)*, vol 18, no 2, pp. 903-916 May 2020, doi: 10.11591/ijeecs.v18.i2.pp903-916.
- [14] A. Denker and M. C. İşeri, "Design and implementation of a semi-autonomous mobile search and rescue robot: SALVOR," *2017 International Artificial Intelligence and Data Processing Symposium (IDAP)*, 2017, pp. 1-6, doi: 10.1109/IDAP.2017.8090184.
- [15] Hui Liu, Shuaiqi Gan, Jialei Zhang and Xianbo Xiang, "Control system of a mini-ASV prototype: Design and implementation," *2016 IEEE International Conference on Underwater System Technology: Theory and Applications (USYS)*, Penang, 2016, pp. 110-114.
- [16] Z. Z. Abidin, M. R. Arshad and U. K. Ngah, "Waypoint control of Drosobots: Swarms of mini ASVs," *2010 IEEE Symposium on Industrial Electronics and Applications (ISIEA)*, Penang, Malaysia, 2010, pp. 556-561, doi: 10.1109/ISIEA.2010.5679401.
- [17] Shadman Sakib Arnob, Adiba Sumaiya Khan, Rashed Shelim, Mahmood Chowdhury, "Safe sailing: GSM and GPS controlled autonomous boat with overweight detection and obstacle avoidance," *Indonesian Journal of Electrical Engineering & Computer Science (IJECS)*, vol. 14, no. 2, pp. 715-724, May 2019, doi: 10.11591/ijeecs.v14.i2.pp715-724.
- [18] M. A. Mushthalib, H. Mansor and Z. Z. Abidin, "Development of eCall for Malaysia's Automotive Industries," *2019 7th International Conference on Mechatronics Engineering (ICOM)*, Putrajaya, Malaysia, 2019, pp. 1-5, doi: 10.1109/ICOM47790.2019.8952044.
- [19] XLRs D4: Ground Control Station PFV & UAV. [Online]. Available: https://d3.xlrs.eu/en/xlrs_d4/. [Access: Jun 12, 2020].
- [20] Quantum FPV Ground Station Review. [Online]. Available: <http://www.droneuplift.com/quantum-fpv-ground-station-review/>. [Access: Jun 12, 2020]
- [21] R. M. Ramli, N. A. Herman, M. R. Mazlan, A. S. Nazaruddin, M. A. Tuah, A. N. E. Abd S, K. Othman, Y. M. Esmail "Development of Robotic Rover with Controller & Vision System," *Indonesian Journal of Electrical Engineering & Computer Science (IJECS)*, vol. 18, no. 2, pp. 766-773, May 2020 doi: 10.11591/ijeecs.v18.i2.pp766-773.
- [22] S. N. Anual, M. F. Ibrahim, N. Ibrahim, A. Hussain, M. M. Mustafa, A. Baseri Huddin, F. H. Hashim, "GA-based Optimisation of a LiDAR Feedback Autonomous Mobile Robot Navigation System," *Bulletin of Electrical and Informatics (BEEI)*, vol. 7, no 3, pp. 433-441, September 2018, doi: 10.11591/eei.v7i3.1275.
- [23] S. Abdul-Rahman, M. S. Abd Razak, A. H. Mohd Mushin, R. Hamzah, N. Abu Bakar, and Z. Abd Aziz. "Simulation of simultaneous localisation and mapping using point cloud data," *Indonesian Journal of Electrical Engineering and Computer Science (IJECS)*, vol. 16, no 2, pp. 941-949, 2019, doi: 10.11591/ijeecs.v16.i2.pp941-949.
- [24] R. Coleman, "A Self-Healing Plug-in Parser for NMEA Streams," *Fifth International Conference on Information Technology: New Generations (itng 2008)*, 2008, pp. 1023-1027, doi: 10.1109/ITNG.2008.238.
- [25] M. Shoab, K. Jain, M. Anulhaq and M. Shashi, "Development and implementation of NMEA interpreter for real time GPS data logging," *2013 3rd IEEE International Advance Computing Conference (IACC)*, Ghaziabad, India, pp. 143-146, 2013.





ARTICLES FOR FACULTY MEMBERS

RESCUE VESSEL OPERATION FOR FLOOD EVACUATION PROTOCOL

Title/Author	Estimation of the Evacuation Time According to Different Flood Depths / Suwanno, P., Yaibok, C., Tsumita, N., Fukuda, A., Theerathitichaipa, K., Seefong, M., Jomnonkwao, S., & Kasemsri, R.
Source	<i>Sustainability (Switzerland)</i> Volume 15 Issue 7 (2023) Pages 1-23 https://doi.org/10.3390/su15076305 (Database: MDPI)

Article

Estimation of the Evacuation Time According to Different Flood Depths

Piyapong Suwanno ^{1,†}, Chaiwat Yaibok ^{1,†}, Noriyasu Tsumita ², Atsushi Fukuda ²,
Kestsirin Theerathitichaipa ³, Manlika Seefong ³, Sajjakaj Jomnonkwao ³ and Rattanaporn Kasemsri ^{4,*}

¹ Research Unit of Technology and Innovation on Civil Engineering, Rajamangala University of Technology Srivijaya University, Nakhon Si Thammarat 80210, Thailand

² Department of Transportation Systems Engineering, Nihon University, Chiba 274-8501, Japan

³ School of Transportation Engineering, Suranaree University of Technology, Nakhon Ratchasima 30000, Thailand

⁴ School of Civil Engineering, Suranaree University of Technology, Nakhon Ratchasima 30000, Thailand

* Correspondence: kasemsri@sut.ac.th; Tel.: +66-65953-1565

† These authors contributed equally to this work.

Abstract: This study focused on pre-flood measures to estimate evacuation times impacted by flood depths and identify alternate routes to reduce loss of life and manage evacuation measures during flood disasters. Evacuation measures, including traffic characteristics, were reviewed according to different flood depths. Several scenarios were constructed for different flooding situations and traffic volumes. Evacuation times in the study area were evaluated and compared for all scenarios with reference to dry conditions. Results of network performance indicators compared to the dry situation showed that average speed dropped to 2 km/h, VHT rose above 200%, and VKT rose above 30%. Cumulative evacuee arrival percentage increased when flood levels were higher than 5 cm. Flood levels of 10–15, 15–20, 20–25, and 25–30 cm represented percentages of remaining evacuees at 9%, 19%, 49%, and 83%, respectively. Time taken to evacuate increased according to flood level. For flood depths of 5–30 cm, travel time increased by 40, 90, 260, and 670 min, respectively, suggesting the need for early evacuation before the flood situation becomes serious.

Keywords: traffic behavior; evacuation time; flood water evacuation; road network



Citation: Suwanno, P.; Yaibok, C.; Tsumita, N.; Fukuda, A.; Theerathitichaipa, K.; Seefong, M.; Jomnonkwao, S.; Kasemsri, R. Estimation of the Evacuation Time According to Different Flood Depths. *Sustainability* **2023**, *15*, 6305. <https://doi.org/10.3390/su15076305>

Academic Editors: Aoife Ahern and Matjaž Šraml

Received: 13 January 2023

Revised: 20 March 2023

Accepted: 28 March 2023

Published: 6 April 2023



Copyright: © 2023 by the authors. Licensee MDPI, Basel, Switzerland. This article is an open access article distributed under the terms and conditions of the Creative Commons Attribution (CC BY) license (<https://creativecommons.org/licenses/by/4.0/>).

1. Introduction

In cities in Southeast Asia, due to squalls and typhoons during the rainy season, floods occur frequently, causing great damage to people's lives. Especially in urban areas, most of the ground is covered with concrete, which has low rainwater infiltration capacity and insufficient drainage. Therefore, once a flood occurs, the inundation progresses rapidly, and it is not uncommon for many residents to be unable to evacuate and suffer damage. In order to deal with this problem, it is necessary to predict the occurrence of floods, secure evacuation routes in advance in response to ever-changing flood conditions, and reduce loss of life.

The city of Hat Yai, which was the subject of this study, is the economic and transportation center of Songkhla Province and southern Thailand and is the gateway for car, train, and air travel to Malaysia and Singapore. Hat Yai city is located on a large plain as a pan basin surrounded by mountains to the west, south, and east. The area slopes to the south and west toward Songkhla Lake. The climate in Hat Yai city consists of northeast monsoon winds from October to January and southwest monsoon winds from May to October, resulting in heavy rainfall and runoff from the mountains into the U-Tapao Canal. This was designed to support only 500 cubic meters per second of water flow.

As shown in Figure 1, between 2010 and 2019, low- and medium-density residential areas and rural agricultural areas in Hat Yai City experienced urbanization with the construction of infrastructure such as roads and houses. The construction of this infrastructure

proceeded without strict enforcement of urban planning laws, which reduced the water intake area due to land reclamation and surface concrete, which had a significant impact on water runoff during the rainy season [1].

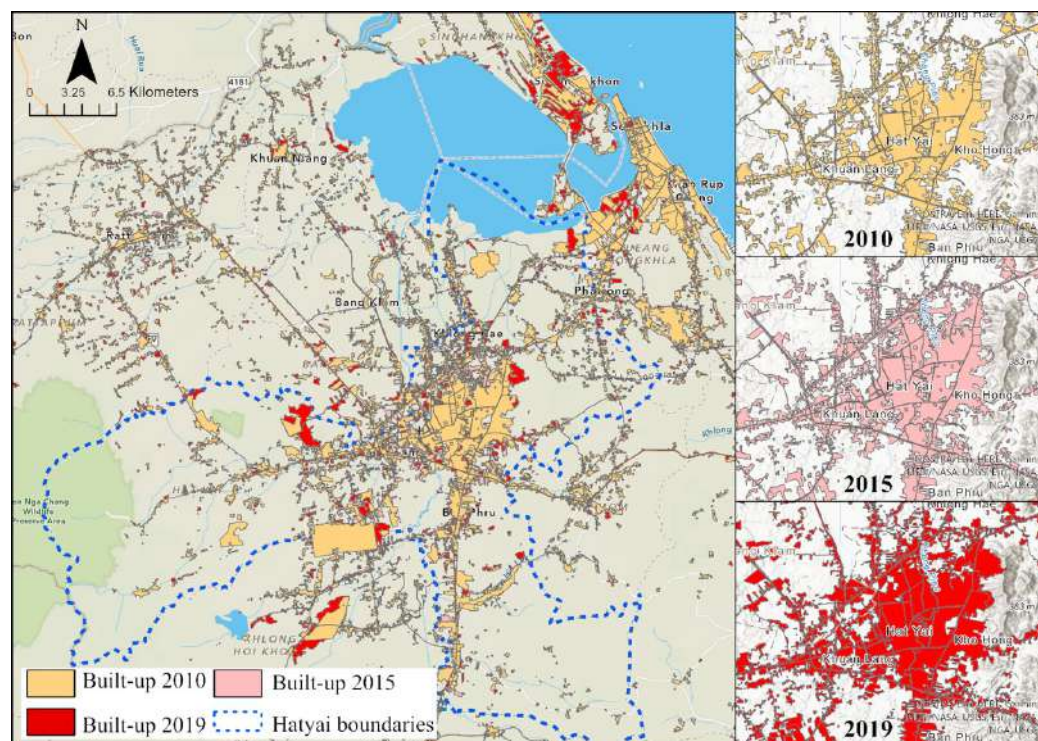


Figure 1. The expansion of Hat Yai city, a major city in southern Thailand, from 2010–2019.

The reduction in natural water intake areas has resulted in frequent flooding problems. Frequent flooding areas (red pins) are recorded by the Hat Yai municipality and identified from the analysis of satellite imagery. Figure 2a shows the pattern of flooding in Hat Yai. The Khlong U-Tapao Basin (black arrow) in Sadao District flows through Hat Yai City and drains into the Songkhla Lake within 10–30 h, causing the U-Tapao Canal to overflow. Rainfall of more than 100 mm in 6 h causes runoff from Khohong Hill (brown arrow) into the Khlongrien Basin [2]. Repeatedly flooded areas are also shown in Figure 2a. Damage caused by flood has been huge. For example, the flood event in 1988 caused damage of more than THB 2000 million, while 12 years later in 2000, flooding caused damages of THB 10 billion and the deaths of 30 people.

After this flood, the government upgraded the U-Tapao Canal by constructing natural branch drainage canals [3]. However, the fact that a major flood in 2010 impacted 80% of the area shows that these structural improvements to the drainage of the area did not reduce economic losses and social risks. Data analysis from field surveys [4], showed that many roads were cut off by the flood, as shown in Figure 2b. A maximum flood level of 4 m was recorded, with damage estimated at more than THB 16 billion. Therefore, in addition to upgrading the canal, flood countermeasures such as ensuring of evacuation routes need to be adequately carried out by meeting about the situation before, during, and after flood events.

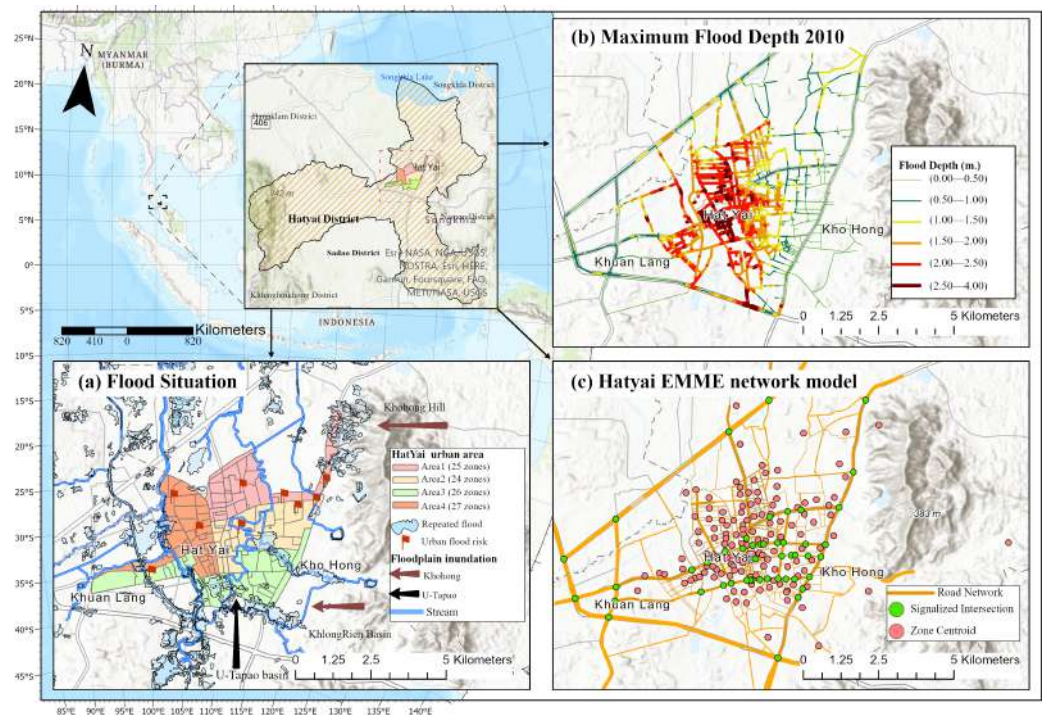


Figure 2. Location, maximum flood depth, frequency flood, and network model of Hat Yai city.

The objective is to evaluate the road network and suggest alternate routes during flood disasters using a dynamic traffic assignment (DTA) model to reduce loss of life and manage evacuation measures. Subsequently, the secondary objective of this study is to estimate evacuation time and identify measures to control flooding based on past evaluations.

This paper is organized as follows. First, the background and objectives of the study are explained in the introduction. Second, the literature on the identification of flooding evacuation procedures and dynamic traffic assignment (DTA) is reviewed. Third, the summary of background information, such as flooding impact on road transportation and actual evacuation behavior in Hat Yai, is described. Fourth, the DTA model network by Dynameq is explained. Fifth, the result of the scenario analysis is analyzed and evaluated based on the travel speed, VHT, and VKT. Finally, conclusions and possibilities for future work are summarized.

2. Literature Review

Planning an evacuation is the best way to avoid or mitigate the effects of disasters such as hurricanes [5–8], nuclear power plant accidents [9–11], and earthquakes [12–14]. Several previous studies have also been conducted to identify flooding evacuation procedures and instigate optimal preventive measures [15–20]. Evacuation success depends on adequate warning time, public preparedness, clear instructions, evacuation routes, traffic conditions, and dynamic traffic management measures [19,20]. In particular, findings showed that the key elements influencing the efficiency of evacuation services included controlling road conditions at the outgoing motorway connections in the given network during the evacuation period and access capacity from the downtown area to outbound freeway links. A thorough analysis of the traffic impacts of a mass evacuation of the Halifax Peninsula under several flooding scenarios was also conducted [21]. However, variables such as human behavior and the type of disaster that triggers the evacuation are uncertainties [22].

In an evacuation scenario, extremely concentrated time-varying origin–destination (O-D) demands result in highly unstable and disorderly link flows, with oversaturated queues. In practice, the methodology generally followed by evacuation studies is to assume the percentage of the population that is going to evacuate and then use behavioral response curves to estimate the timing of the evacuation under random population

distributions [23,24] with demand based on linearized S-curves at half-hour intervals related to a clearance time lower in magnitude than the average travel time. The clearance time may be insufficient to provide adequate planning measures unless comprehensively analyzed. Evacuation response problems can also be solved using census demographic data and travel survey data to calculate the proportion of the population commuting into, out of, or across an at-risk area to generate the percentage of the population that is going to evacuate and make predictions on the behavioral capabilities of the different social groups [25]. To prevent traffic congestion, staggered departure times could be assigned to different groups of evacuees in endangered areas [26,27]. Evacuation overcrowding on the roadways will result in a partial or full loss of capacity at certain network links [24,28–31] because it affects reliable evacuation times under realistic transportation network conditions.

An evacuation planning model aims to achieve different network optimal states that mirror real-world evacuation events. The network might lose capacity as a result of both human and disaster-related factors, while variations in the size and timing of evacuation demand generated by the dynamic traffic assignment (DTA) model will provide more realistic outcomes. DTA has been used to determine evacuation scenarios in macroscopic [32–34], mesoscopic [35–38], and microscopic models [39–44].

The viability of using the Dynasart-P DTA model was assessed for alternate traffic evacuation tactics in downtown Minneapolis, Minnesota in the event of an emergency requiring the evacuation of a sold-out crowd from the Metrodome [45].

Several previous studies were conducted to identify flooding evacuation procedures and instigate optimal preventive measures. Land surface modeling connecting the Halifax Stream and transportation networks was used to determine the magnitude of the flood and associated network disruption. An examination of network performance showed persistent congestion of 4 to 7 h during the evacuation. An analysis of transportation systems in emergency conditions due to disaster scenarios was also presented in Di Gangi (2009) [46]. Piyapong et al. (2021) used mesoscopic (DTA) as a tool to improve road network traffic flow performance under different flood conditions by applying the concept of the Macro Fundamental Diagram (MFD) and take appropriate traffic control measures. A mesoscopic (DTA) model was developed to determine quantitative indicators for estimating the exposure component of total risk incurred by road networks [47]. Appropriate quantitative methodologies based on a dynamic approach (DA) are a useful tool to support evacuation strategic planning at different regional scales. A DA concept to simulate the supply of transportation and the interplay between supply and demand for travel in an urban road transportation system under emergency circumstances was presented [48]. Traffic data were collected during a practical evacuation experiment carried out at Melito di Porto Salvo, Italy and used to calibrate and validate transport supply models. A calibrated DA model can be a helpful tool when planning and managing road networks and transportation in emergency situations. A modeling approach was conducted on the Boston, Massachusetts road network and a range of practical challenges related to evacuation modeling was examined in Balakrishna et al. (2008) [49].

There is a case study used DynaMIT, a cutting-edge DTA model, to demonstrate the advantages of network management methods. A Cellular Automata-based Dynamic Route Optimization (CADRO) method was also considered for hydrodynamics, terrain, and human response time to determine dynamic flood evacuation routes (FERs) [50]. The CADRO method was employed in a suburb of Yangzhou City, China. Findings showed that compared to the conventional method used for evacuation route optimization, average and max lengths of FERs were reduced by roughly 32.70%, 34.04%, and 7.90%, respectively. Mathematical model formulations underlying traffic simulation models used in evacuation studies and behavioral assumptions were assessed by Pel, Bliemer, and Hoogendoorn (2012) [51].

Evacuation travel behavior, which is based on the viewpoint from the social sciences, as well as empirical investigations have also been discussed in detail. Traveler decisions, such as whether to evacuate, what time to leave, where to go, and how to get there,

can be forecasted using simulations. Facets of transportation systems under emergency circumstances brought on by dangerous events were examined by Di Gangi (2011) [52] using a mesoscopic (DTA) model to produce objective measurements and assess the exposure attributes of overall risk suffered by regional road networks. Impacts on the transport network were examined to demonstrate how effective quantitative approaches built on a DA concept were a helpful tool to aid evacuation strategic planning. A macroscopic traffic flow model utilizing a DYNEV II large-scale evacuating planning system was presented by Lieberman and Xin (2012) [34]. This concept was represented as a single processing unit for generalized networks with connection lengths ranging from 100 feet to several miles. The model allowed simulation time steps of one minute or longer, significantly greater than utilized for other models, and supported up to four turn motions from each link with a wide variety of traffic controls at junctions to accurately reflect congested areas and their spill back processes.

Therefore, this study creates a novel model to determine the effect on flood evacuation time estimation of varying water depth with evacuation behaviors. Generally practical, the methodology followed by evacuation studies is to assume the percentage of the population that is going to evacuate. Then, it uses behavioral response curves to estimate the timing of the evacuation under random population distributions [23,24] with demand based on linearized S-curves at half-hour intervals related to a clearance time lower in magnitude than the average travel time. The clearance time may be insufficient to provide adequate planning measures unless comprehensively analyzed. However, this study fills the gap by using the data from the questionnaire survey on flood evacuation behavior in Hat Yai Municipality to analyze evacuation behavior during the flood. Moreover, this study considers the efficiency of the road network, which decreases with rising water levels, leading to the ability to estimate evacuation time. This can be determined from the inundation model characterizing the inundation in the study area. The model used in this study brings the advantage from both macroscopic and microscopic levels, called the mesoscopic level, which is a novel application for solving the road traffic network that increases the modeling accuracy compared to the macroscopic without the need to prepare the same in-depth details as on the microscopic level. The expectation is to obtain the preparation plan, which is a solution helping government officials to avoid evacuation delays and loss of life and property.

3. Background Information

Travel models can analyze evacuation processes and estimate evacuation times. However, simulation is a time-consuming process that includes model development, validation of data collection, model testing, and data interpretation. In this study, the authors updated the existing traffic demand by using a static origin–destination (OD) matrix to describe the trip distribution. The estimation was based on current traffic counts using matrix algorithms, which have been available for many years for static assignment models and can be used to pre-process demand matrices for dynamic traffic assignment (DTA) models. Trips were assigned to the city’s traffic analysis zones and existing roadway networks extracted from the model. Reference trip tables were constructed for areas outside the city to form background vehicle traffic as trips traveling to or from evacuation zones. Data were taken directly from the travel model for a typical day and then distributed over each hour of the day. The DTA model only reflected personal vehicle traffic, with travel modes such as public transit or walking not considered. The overall vehicle travel demand was based on hourly typical travel daily activity until the evacuation notice was given. The travel demand for evacuation zones was separated from background traffic not associated with evacuation zones. Departure times for leaving the evacuation zones varied according to the time and type of the event. To conduct this study, the existing traffic demand was updated as a static origin–destination (OD) matrix. Flood evacuation behavior in each area was reviewed including percentages of evacuation timing (do not evacuate immediately after warning or based on flood level), evacuation destination (out zone, evacuation center), and

travel patterns used for evacuation (walking, passenger car, motorcycle). These variables are important to estimate the OD matrix of each flood scenario in a particular area.

3.1. Network Configuration and Parameter Setting

Estimating the spatial and temporal distribution of travel demand is important for DTA models. One common approach is to use the calibrated OD matrix of macroscopic travel demand models as Static Traffic Assignment (STA). This study used the OD matrix from the regional demand model of Hat Yai District developed by Luathep et al. (2013) [53] using the EMME program. The road network of Hat Yai City consists of 2507 links and 923 nodes including 142 zone centroids. Among the nodes, 41 are intersections with a traffic signal, as shown in Figure 2c. Connectors were used to link the zone centroids to the network. These were carefully placed to be as reflective of the actual situation as possible while avoiding false network congestion.

The regional demand model data were then imported into the Dynameq program, and a DTA road network was set up. Signalized intersections and signal plans and timings were imported from the real world. The following settings correspond to Dynameq settings required to run the assignment. This was implemented in order to get reasonable paths while still respecting the observed free-flow times on locals and collectors. Dynameq allows for signal offsets as inputs and provides improved computational efficiency compared to a microscopic model in a regional network. This is particularly important for simulation-based DTA. All movement capacities were calculated based on their types and parameters, such as gap acceptance and property relationships. At intersections, movements and rules were based on the signal plans. Links in the modeled network, characteristics of network geometry including position, shape, and length, and functional characteristics such as free-flow speed correspond to the real-world existing road network. Link capacity was calculated using three factors: link free-flow speed, effective vehicle length, and vehicle reaction time.

There is the possibility to clear the traffic during the flood by controlling the traffic signals using a detecting system, which gives an input to the current system, with the goal that it can adjust the changing traffic density patterns and provides a vital sign to the controller in a continuous activity. Using this method, improvement of the traffic signal switching expands the street limit, saves time for traveling, and prevents traffic congestion.

As mentioned above, model parameters such as drivers' response time and vehicle relative length can vary. Here, 6.25 m and 1.25 s were chosen as the worldwide effective vehicle length and response time parameters, respectively. In Dynameq there are default values for passenger car average effective length (6.25 m) and average response time (1.25 s). The default and user-specified effective length and response time values can also be altered for entire scenarios or for individual links through the use of multiplier factors for Effective Length and Response Time. Any modifications to these two parameters resulted in a change in jam density and maximum flow rate at each link. The free-flow speed is also an important component that defines link capacity.

3.2. Origin–Destination Matrix

Data to produce the DTA model were obtained from the Hat Yai regional demand model. This static assignment model could be reused for long periods and was also used as a pre-processed travel demand matrix for the DTA model. Static traffic demand was designed using a conventional 4-step model. Trip distribution was divided into two groups as aggregate (secondary data) and disaggregate (survey) methods. Both models were also combined as mixed distribution models [54]. A trip distribution model can be estimated using a Poisson regression using variables extracted from a trip generation model [55], with no constraints on the spatial relationships between origins or destinations, thereby guaranteeing good reliability of the estimated parameters [56]. The cost objective, referred to as an entropy function, plays a key role in terms of potential, exponential, and combined trip distribution and is most commonly used to describe the empirical relationships between

economic and behavioral variables [57]. For this study, with extracted trip production and trip attraction from the Hat Yai regional model for every zone in the network, we then used the growth rate of the population [58] to calculate the production and attraction trip of 2022. The calculation of the entropy function between each OD pair d , E_d in the network is defined as

$$E_d = \exp\left(-\frac{u_{od}}{\bar{u}}\right) \quad (1)$$

where

u_{od} is the free-flow speed travel time between OD pair d ;

\bar{u} is the mean of free-flow travel time between all OD pairs.

The process of trip distribution to find the prior OD matrix, the matrix balancing method [59], was used, which balances the matrix of trip production data and attraction data by entropy as weight for distribution. The prior matrix from the previous one will be calibrated based on the observed hourly link volume. Using this method, the travel demand matrix was automatically adjusted to existing peak-hour traffic volume. This model was also used as a gradient method [60] to minimize the objective function as a measure of the distance between observed flows (v'_a) and assigned flows $v(g)$. This distance was weighted by the constant α , ($0 \leq \alpha \leq 1$), which was used to weigh deviations from the counts, the sum of squares between the new matrix, and also the difference between the adjusted matrix g and the original matrix to be adjusted g' , as a constant used to weigh deviations from the adjusted and the original matrices [61].

The mathematical formulation is shown in Equation (2).

$$\text{Minimize: } z(v, g) = \alpha \sum_{a \in A} (v_a(g) - v'_a)^2 + (1 - \alpha) \sum_{i \in I} (g_i - g'_i)^2 \quad (2)$$

where

$a \in A$ are the links that have counts;

$v(g)$ is the assigned flow using the adjusted matrix;

$(1 - \alpha)$ is used to weigh the deviations from the adjusted and the original matrices, and OD pairs are denoted by the index $i, i \in I$;

I is the OD cells that are included in the demand term of the objective function.

The best value choice as parameter α is dependent on the data when a particular adjustment is carried out, such as the number of links with counts. The higher the value of α , the more weight is given to fitting the counts. To preserve the structure of the adjusted matrix, a judicial value of α would give weight to the demand matrix deviations. The model was calibrated using a set of 1-morning peak hour of traffic counts and included data from annual average daily traffic (AADT) converted to peak hour by comparing the percentage of 1 peak hour with daily traffic. Peak-hour morning traffic was used for calibration because the distribution of traffic was more uniform than in the afternoon, as seen from the Peak Hour Factor (PHF). The 110 traffic links were compared with the model and results were assessed using Bland–Altman plots, as shown in Figure 3.

Figure 3 is the plot of differences between model flow and observed flow vs. the average of the two measurements, which help to investigate any possible relationship between measurement error and the true value. Results show a bias of 19 units, represented by the gap between the X-axis, corresponding to zero differences, and the parallel line to the X-axis at 19 units. After ensuring that our differences are normally distributed, we can use the standard deviation (SD = 144) to define the limits of agreement at a 95% confidence interval. So, results measured by model flow are approximately 305 units below or 264 above observed flow (red line).

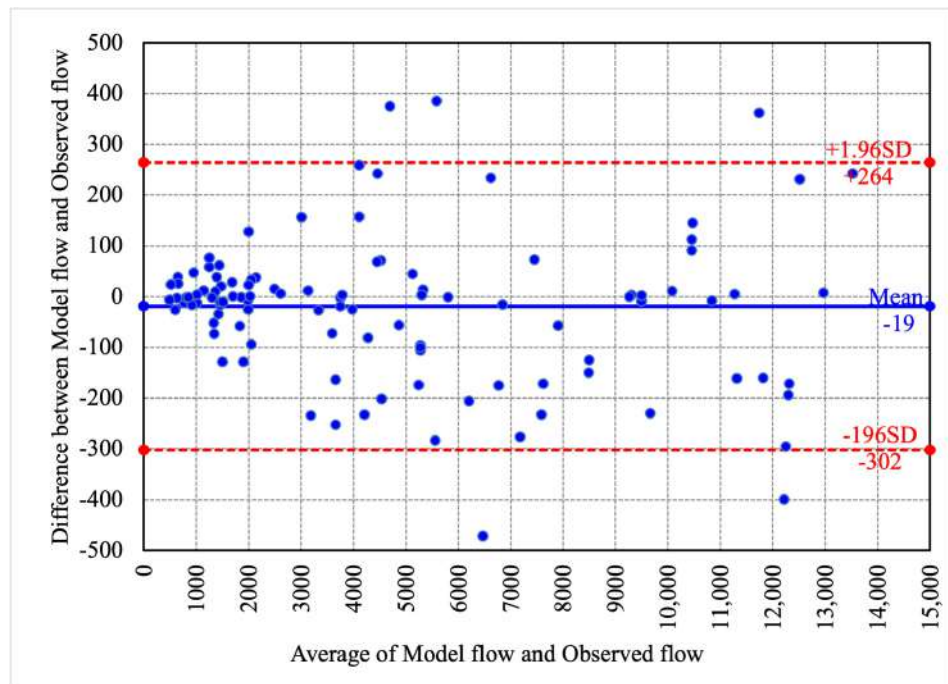


Figure 3. Bland–Altman plots between model flow and observed flow.

Then, considering the statistical values by using a two-sample *t*-test between model flow and observed flow, the results are as follows. The mean in the model flow group was 4896.945 (SD = 3804.629), whereas the mean in the observed flow was 4878.239 (SD = 3793.905). A two-sample *t*-test showed that the difference was not statistically significant at the *t*-test statistic value, where *p*-value = 0.971 > 0.05 (95 percent confidence). The degree of correlation was determined after traffic demand was adjusted by the iteration process. The degree of correlation was calculated between the manually counted traffic volume and the developed model traffic volume. Results showed that the developed model was calibrated at 0.986, as shown in Figure 4.

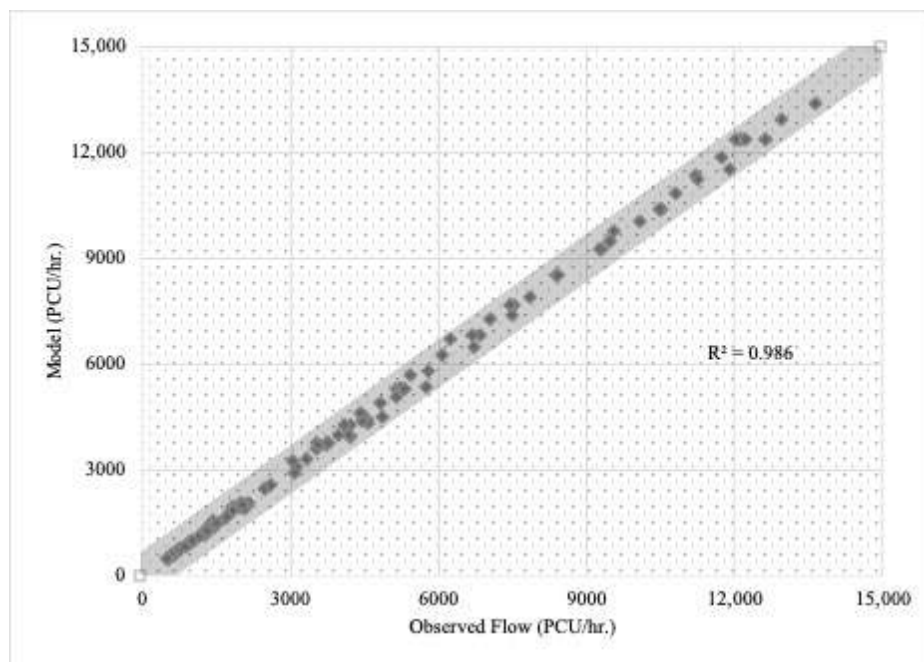


Figure 4. Relationship between modeled and observed link volumes.

3.3. Evacuation Behavior during the Flood

Travel and evacuation behavior data collected from a questionnaire were used to investigate people’s behavior before, during, and after a flood incident from past experiences. A total of 102 affected communities (zones) were integrated into four main areas (zone groups) according to the Hat Yai flood response [62] to determine the proportions of different evacuation decisions during flooding, as shown in Figure 5. More people in all four areas of Hat Yai decided to evacuate than decided not to evacuate. Evacuation scenarios were evaluated immediately after the warning: water level less than 50 cm, water level of 50–100 cm, and water level of 100–150 cm.

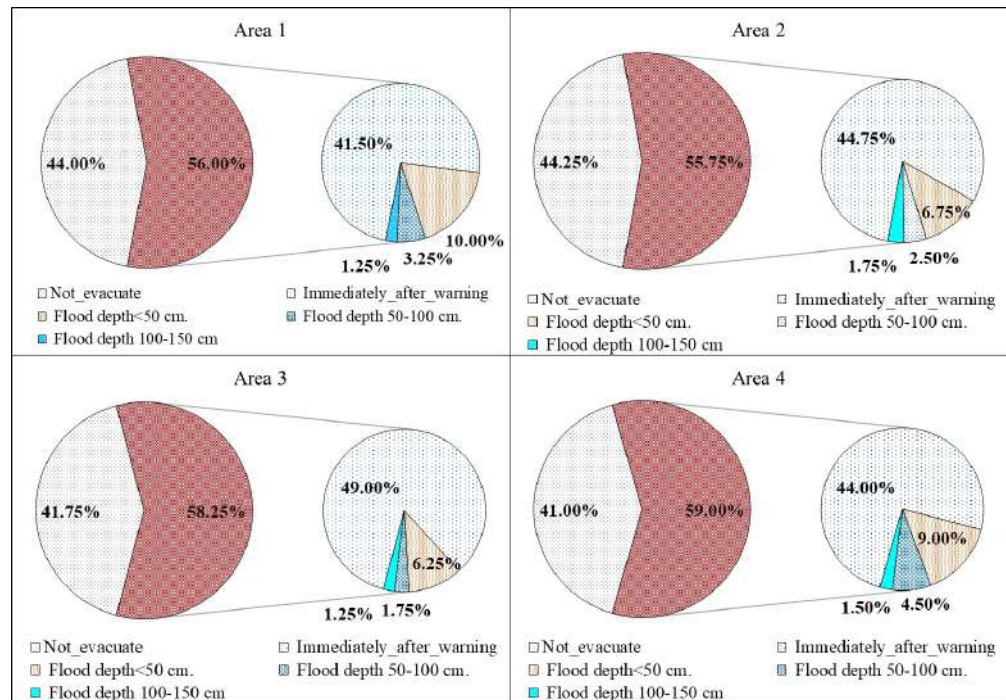


Figure 5. Percentages of evacuation timing.

The secondary data in Table 1 were examined to determine the evacuation behavior of people in Hat Yai municipality. Results showed that, on average, 71% of people chose to go to evacuation centers provided by the local government within each flooded area, with 29% going to centers outside the flooded areas. For evacuation, 88.75% of people chose private cars as the primary mode of transport.

Table 1. Data from the questionnaire on flood evacuation behavior in Hat Yai Municipality.

Area	Destination(%)		Transport Mode Choice (%)		
	Evacuation Center	Outzone	Walking	Passenger Care	Public Transport
1	74.60	25.40	11.11	87.98	0.91
2	67.00	33.00	9.00	90.00	1.00
3	71.60	28.40	8.20	90.40	1.40
4	70.74	29.26	11.80	86.60	1.60
Average	71.00	29.00	10.02	88.75	1.23

Source: kb.psu.ac.th/psukb/handle/2016/11582 (accessed on 29 May 2022).

For sudden flood situations, this study applied the calibrated static OD matrix as a 1 h peak to evaluate an evacuation plan. This plan was then analyzed to determine the proportion of evacuation decisions during flooding with water levels less than 50 cm and then consider the trip production of zones distributed to trip attractions as evacuation

zones designated by the local government. Private cars were selected as the main mode of transport for evacuation, as shown in Table 1. Cars could drive through flooded roads with water levels less than 50 cm and were assigned based on reduced road efficiency according to flood depth.

3.4. Flooding Impact on Road Transport

Flood levels have different effects on the safety and reliability of the road network. Several studies examined flooding effects on vehicle speed [63–78]. Pregolato, Ford et al. [79] combined data from experimental studies, observations, and modeling to develop a function that described speed limits of different vehicle types based on their dimensions (small vehicles, large vehicles, and heavy vehicles). Interviews with taxi drivers and pickup truck drivers also showed a relationship between flood depth and vehicle speed as a curve trend (orange line) and combined data from experimental studies, observations, and modeling to develop a function that described speed limits of different vehicle types based on their dimensions (small vehicles, large vehicles, and heavy vehicles). Interviews with taxi drivers and pickup truck drivers also showed a relationship between flood depth and vehicle speed [80] as a curve trend (estimated function), as shown in Figure 6. For this study, we change the the free-flow speed parameter on the link to the set value according to the results obtained by the flood function at different levels. However, we consider a flood depth not exceeding 30 cm, in which the vehicles' speed is reduced to 0 km/h as the ultimate level for safe driving of most vehicles. At a flood depth of 30 cm, vehicle speed is reduced to 0 km/h. When driving through flood water of less than 30 cm depth, drivers should consider safety as their main priority. Driving in a water level of 5–10 cm is considered safe because the water can easily be seen on the road surface. A water level of 10–20 cm is also considered safe for cars to pass normally, but it may impact the movement of smaller cars with lower ground clearance. Most passenger cars have a height clearance of 150–170 cm, and water at a 20–30 cm depth will cover the exhaust pipe outlet. Short distances are manageable, but traveling long distances is not recommended for safe driving. Water levels above 30 cm are considered dangerous for all types of vehicles, and driving is not recommended.

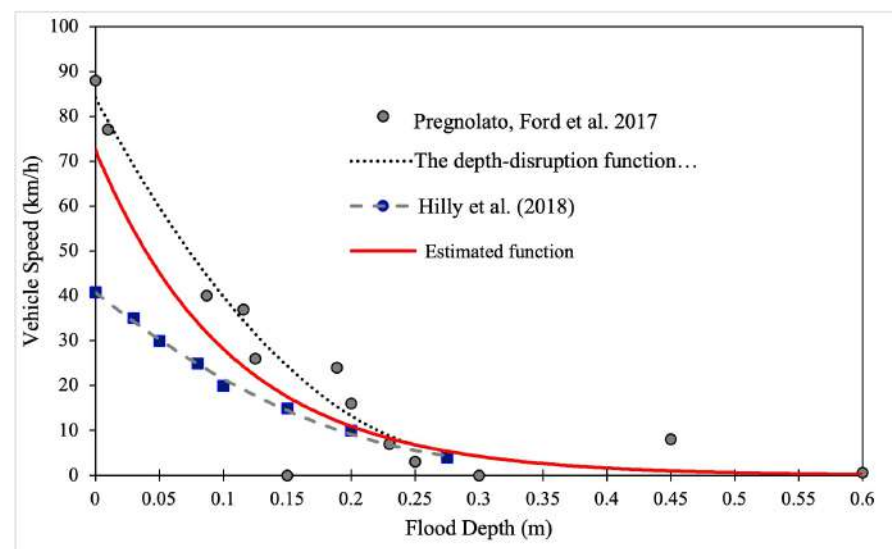


Figure 6. Relationships between flood depth and vehicle speed [65–75,80].

4. DTA Model Network

This study presented the DTA at the mesoscopic scale using Dynameq 4 to efficiently model traffic lane usage. Traffic flow is described with three components: car following, gap acceptance, and lane changing [81]. Following the above, the application of the relationships between flood depth and vehicle speed, which define vehicle motion on the roadway through time of the car-following model, is shown in Equation (3).

$$x(t) = \text{MIN}[(x_f(t - RT) + FFS \times RT), (x_l(t - R) - EL)] \quad (3)$$

where

x_f is the location of the following vehicle at time t ;

x_l is the location of the primary vehicle at time t ;

FFS is the free speed of the roadway (km/h).

Equation (3) describes the trajectory of a vehicle based on a triangular diagram, as shown in Figure 7, defined by the three parameters of free-flow speed (FFS), maximum flow (q_m), and jam density (k_j), which represent flow as a function of density in each link. This is similar to how Newell's kinematic wave theory [82] was used for the propagation of traffic delay. A positive slope in the first segment (increase, $k < k_c$) indicates a vehicle moving at FFS , where the absolute value of the negative slope in the second segment (decrease, $k > k_c$) is equal to the backward wave speed (BWS).

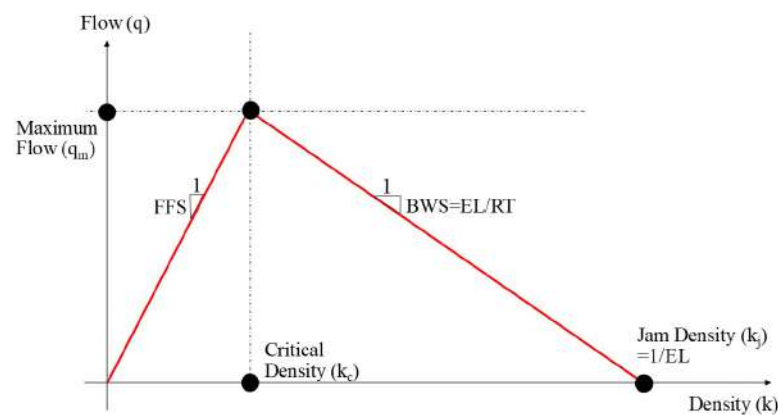


Figure 7. The triangular fundamental diagram.

This fundamental diagram shape changes if the average vehicle speed is reduced as a result of any condition, such as bad weather affecting the maximum flow that can traverse a road segment. The Dynameq program used a triangular shape diagram to describe only three macroscopic traffic flow parameters (maximum flow, jam density, and wave speed), thereby reducing the required input data. Values of the three macro traffic flow parameters for a specific vehicle type and a specific road were determined from the free speed of the link, the effective length, and the response time of the vehicle type, as shown in Equation (4) below.

$$q_m = \frac{1}{(RL + \frac{EL}{FFS})}, k_j = \frac{1}{EL}, v_{wave} = \frac{EL}{RL} \quad (4)$$

where

q_m is the maximal possible flow rate (veh/h/lane);

k_j is the stationary state when traffic flow stops completely, or jam density (veh/km/lane);

v_{wave} is the speed at which shock waves move through a platoon of traffic against the direction of flow for a specific vehicle type (km/h);

EL is the average space that the vehicle occupies on the road;

RL is the driver response time to change speed when the traffic flow state ahead changes and the backward wave speed (BWS) is the rate of propagation of the change in traffic flow state upstream as a result of changes in the downstream traffic flow.

At DTA equilibrium, vehicles starting their trips in the same zone and ending their trips at the same destination will have the same travel time. To reduce travel time, the dynamic user equilibrium (DUE) model was used [83]. This is a time-dependent path flow that uses the method of successive averages (MSA). Corresponding path travel times were determined following the method of Mahut et al. (2004) [84] using the Dynameq 4 program. The overall structure of the study is presented as a schematic algorithm in Figure 8.

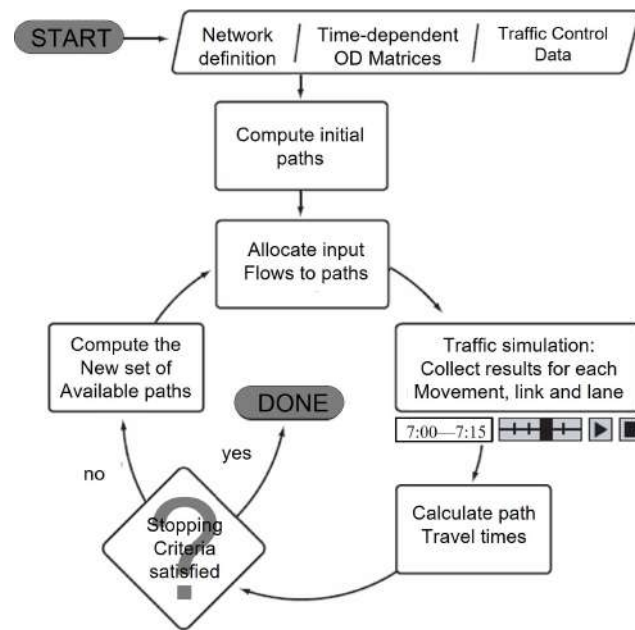


Figure 8. Structure of the solution algorithm.

This study used two major components. The first determined the latest set of time-dependent paths using the last cycle time-dependent paths, while the second defined the actual travel time after completion of a given set of path flow rates. Large numbers of vehicles in each particular zone caused network loading problems. To solve this, a route-based dynamic traffic model was adopted. The initial paths must be provided to start the algorithm; to satisfy this, the shortest paths are used based on the free-flow circumstances. The mathematical equation representing dynamic equilibrium, consisting of demand for the OD pair $I(g_i^a)$, path flow for path $k(h_k^{(a,n)})$, travel time for path $k(s_k^{(a,n)})$, and the shortest travel time for the OD pair $I(u_i^{(a,n)})$, was calculated for every time interval during the assignment (a) for all iterations made during the simulation (n). The procedure is shown below (Algorithm 1).

Algorithm 1 Dynamic MSA Equilibration Algorithm [85–88]

- Step 0 Initialization (iteration $n = 1$); compute dynamic shortest paths based on free-flow travel times and load the demands to obtain an initial solution; $n = n + 1$
- Step 1 If $n \leq N$, compute a new dynamic shortest path and input path flow $(h_k^{(a,n)})$ to each path $k \in K$

$$h_k^{a,n} = \frac{g_i^a}{n}, i = 1, 2, \dots, |i|$$

If $n > N$, identify the shortest among used paths and redistribute the flows as follows:

$$h_k^{a,n} = \begin{cases} h_k^{a,n-1} \left(\frac{n-1}{n} \right) + \frac{g_i^a}{n} & \text{if } s_k^{a,n}; k \in K, i \in I, \text{ all } a \\ h_k^{a,n-1} \left(\frac{n-1}{n} \right) & \text{otherwise} \end{cases}$$

- Step 2 If $N \leq L$ as the maximum number of iterations or $RGap \leq \varepsilon$ as maximum average relative gap, STOP; otherwise, return to step 1
-

Figure 8 illustrates the two main components of the Dynameq system, namely the route choice model and the dynamic road traffic network loading. The system uses an iterative approach to achieve dynamic user balance for dynamic traffic assignment (DTA) based on mesoscopic traffic simulation. In each iteration, the route choice model and the dynamic network loading model are run. The route choice model first allocates the OD traffic volume of each point in the road traffic demand OD matrix at each departure time to the effective road network based on the existing road traffic conditions. Subsequently, the traffic flow of the road section that changes with time is transferred to the traffic simulation model. This calculates the dynamic travel time of the road section, which is then sent to the route choice model to correct the next route choice. This iterative process continues until a predetermined critical value is reached, indicating equilibrium in the system. Overall, the Dynameq system provides a robust and efficient approach for simulating and analyzing dynamic traffic patterns under various scenarios [81].

A comparative gap is used in DTA to signify a perfect DUE flow. The stopping criterion of the MSA was defined using the gap function, as shown by Equation (5) [88].

$$RGap^{a,n} = \frac{\sum_{i \in I} \sum_{k \in K} h_k^{a,n} s_k^{a,n} - \sum_{i \in I} g_i^{a,n} u_i^{a,n}}{\sum_{i \in I} g_i^{a,n} u_i^{a,n}} \quad (5)$$

where

I is the set of all OD pairs;

K_i^a is the set of paths for the OD pair i and assignment interval a ;

$h_k^{a,n}$ is the path flow for path k in interval a in iteration n ;

g_i^a is the OD demand for OD pair i in interval a ;

$s_k^{a,n}$ is the travel time for path k in interval a in iteration n ;

$u_i^{a,n}$ is the shortest travel time for OD pair i in interval a in iteration n .

5. Results

This study was performed by adjusting the free-flow speed factors of the model. Alternative scenarios were developed based on evacuation demand (Flood ≤ 50) in Figure 6 and FFS according to flood depth and vehicle speed in Figure 7. In the first baseline scenario, the calibrated model identified potential congestion locations throughout the network. This situation was utilized as the baseline to compare other situations including flood depths of 0–5, 5–10, 10–15, 15–20, and 20–30 cm. The mesoscopic traffic network model for Hat Yai developed by the Dynameq 4 platform is shown in Figure 9.

There were 142 zones including 133 communities and 9 evacuation centers, 923 nodes, 2507 links, and 41 signals. The appropriate OD matrix of personal vehicles, estimated using the EMME subarea tool, was included in the imported demand matrices from the Hat Yai regional model. A simulation was conducted, without a traffic volume warm-up interval, to load the network at the beginning of the analysis period and cool down for network clearance. The authors selected a ten-minute assignment period. This was identical to 6 cycles for a 1 h allocated OD matrix. Up to 20 routes were searched for one assignment interval. Stop conditions were set at 200 cycles with a comparative difference of 1%.

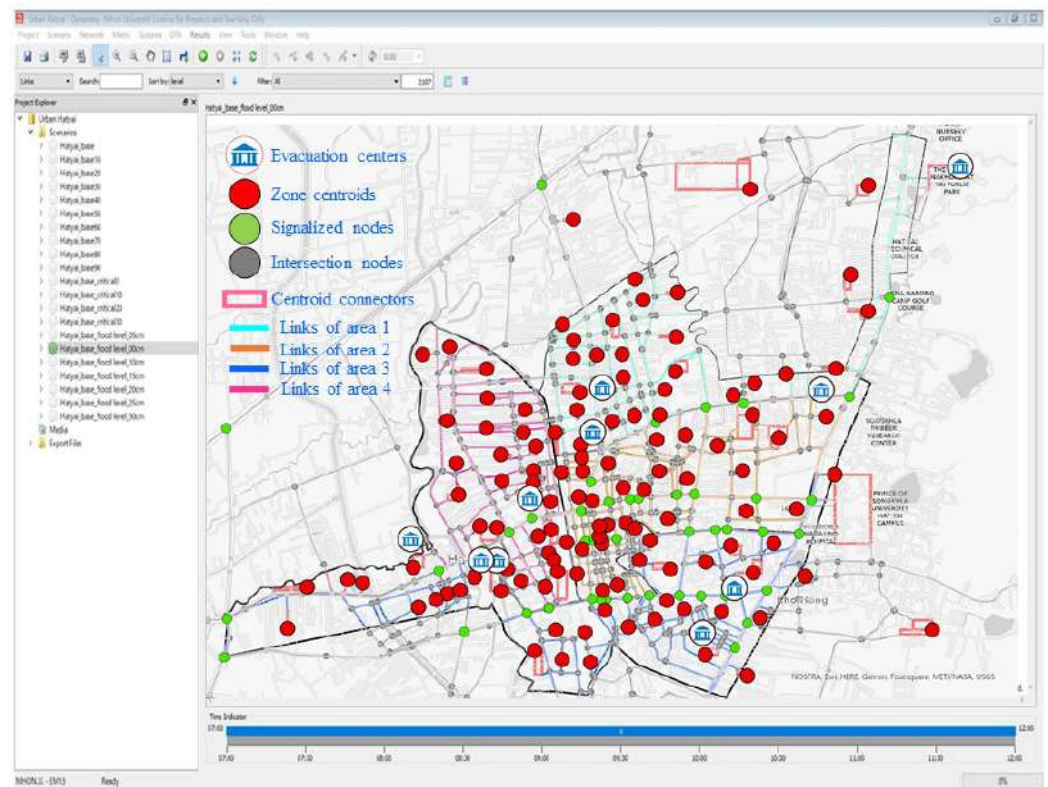


Figure 9. Road network in Hat Yai city with Dynameq platform.

5.1. Result of Model Convergence

There is consistency with previous research on short-notice evacuation events, as documented in the Approach to Modeling Demand and Supply for a Short-Notice Evacuation [89]. Departure time from the evacuation zones varies according to the flood levels, with residents in the greatest danger evacuated first followed by those closer to the highway. For events where ample notice is given, less time is required to prepare for the evacuation. The time required to prepare for an evacuation is typically longer, as residents need to pack their belongings and collect their animals. Using different evacuation starting times will lessen the impact of the evacuation on roadway conditions. The evacuation curve can be shifted or compressed toward the end of the assumed evacuation event. When considering evacuation orders, public officials must allow the residents ample preparation time for departure balanced against the dangers of delaying the evacuation. Integrating travel demand modeling and flood hazard risk analysis for evacuation and sheltering should ensure the redundancy of critical transportation routes and allow continued access and movement in the event of an emergency. This may also include addressing vulnerabilities of bridges, major roadways and highways, railways, traffic signals/traffic control centers, and other transportation facilities and infrastructure components to ensure the availability of multiple viable evacuation routes [90,91].

Considering the implemented transportation operational strategies for evacuation events, in the assessment above, capacities are based on typical limiting signal green time allocations. The development of an evacuation coordination plan would achieve additional capacity. Traffic signals in vulnerable areas could be prioritized, with improvements connected online to the Traffic Management Center together with contingency plans for loss of power and communications grids [92].

Before investigating the impact of floods on the road network, this study first assessed the sensitivity of the network's performance to degradation in free-flow speed under dry conditions. This was carried out by considering scenarios in which the free-flow speed was reduced by 10%, 20%, 30%, 40%, 50%, 60%, 70%, 80%, and 90% and then evaluating the resulting changes in average speed and vehicle hours traveled (VHT), as shown in

Figure 10. The aim was to understand how much the road network performance could be affected by changes in free-flow speed.

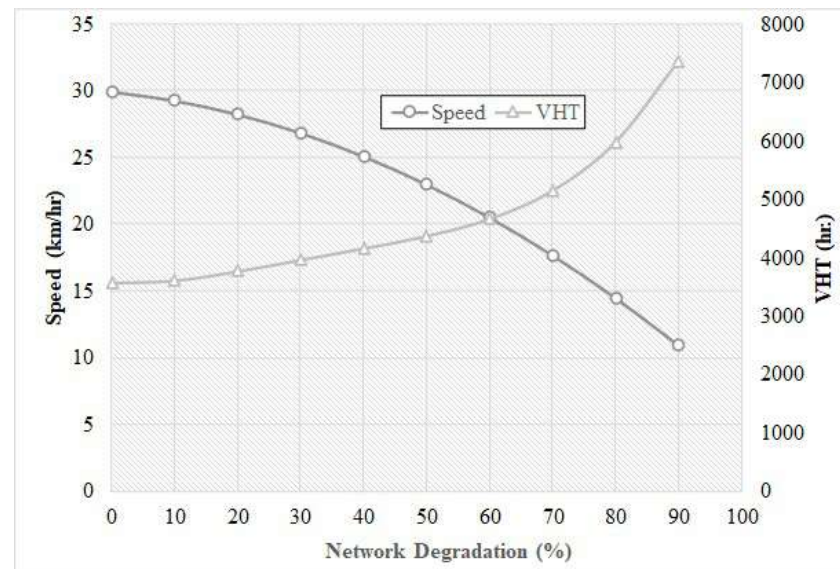


Figure 10. Free-flow speed network degradation.

The analysis revealed that the average speed on the network decreased linearly with a relatively stable slope as the free-flow speed was reduced. This indicates that the reduction in speed has a consistent impact on the network's performance, regardless of the severity of the speed reduction. However, the decrease in average speed was not the only factor affecting the network's performance. The study also found that the VHT gradually increased as the speed reduction became more severe, until the network degradation reached 60%, at which point the increase in VHT became more rapid. This suggests that the network was starting to experience congestion and delays as a result of the reduced speed, particularly when the speed reduction was more severe.

Overall, these findings highlight the importance of maintaining high levels of free-flow speed on road networks, as even relatively small reductions in speed can have significant impacts on travel times and congestion. The study also underscores the need to consider the sensitivity of road networks to different types of disruptions, such as floods, in order to better prepare for and mitigate the impacts of such events.

After running the DTA, it generated an output of model convergence to verify the path flow corresponding to each driver's assumed behavior mechanism in trying to reduce their own travel time. Figure 11 shows that the convergence output, as the value of the relative gap in the initial assignment interval, increased with an increase in departure time as network congestion increased. Percentage variation in travel times increased for the used pathways, according to the same starting time period, then steadily decreased, while relative gap values increased to the 100th iteration. Beyond a set number of cycles, the designed assignment resolved effectively, with an overall average difference of 5%. After 200 iterations, the relative gap for any given departure time interval became constant.

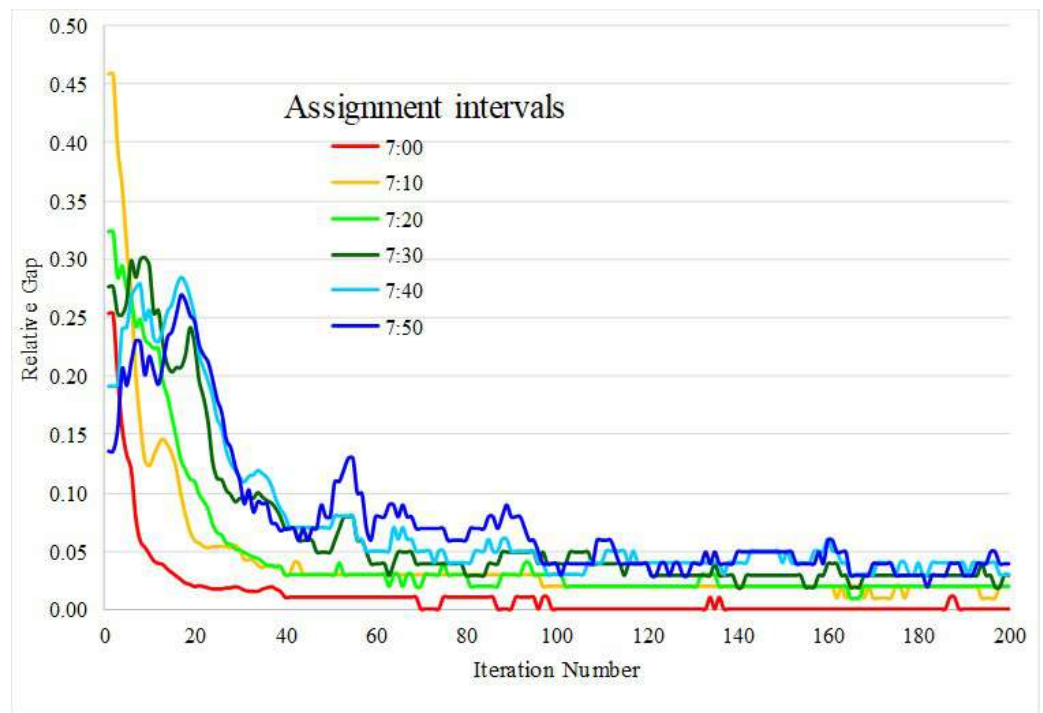


Figure 11. Model average convergence of baseline scenario.

At every time interval, trip assignments were completed, indicating that almost all vehicles arrived at their destinations and exited the road network within the time period following the final demand loads. Figure 12 compares the total number of cars waiting to access the network (on virtual connections) at the conclusion of the interval, measured by the waiting time (red line). The total number of cars in the network at the conclusion of the period was assessed by traveling time. Demand of departures during the first time interval to the last demand loads used 11 time intervals (100 min) for network clearance. All vehicles arrived at their destinations and exited the road network within a time interval after the last demand loads.

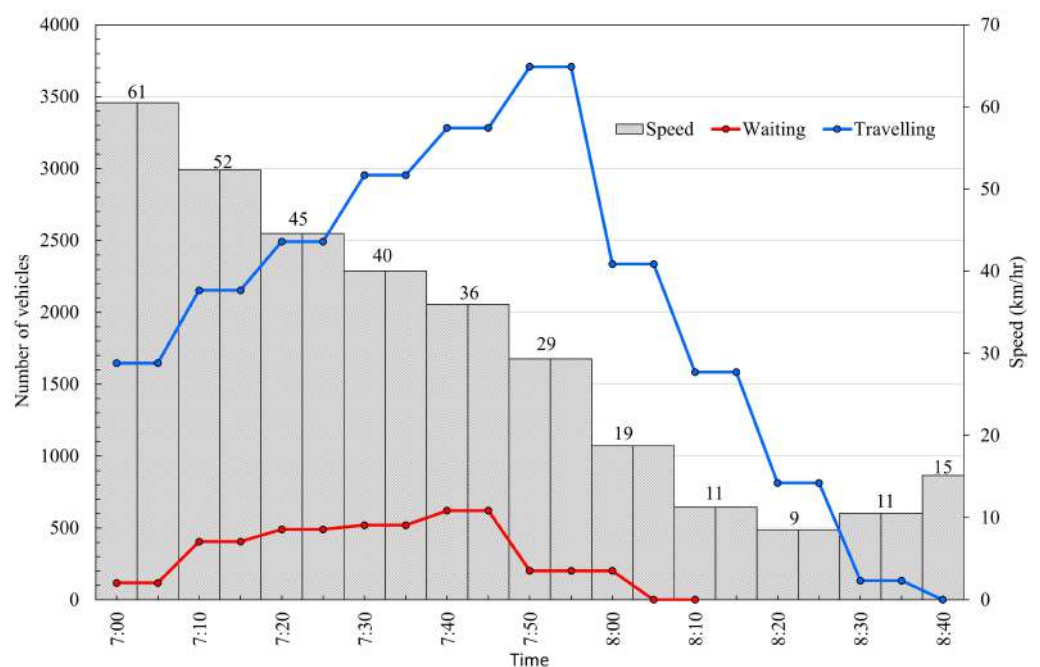


Figure 12. Total number of vehicles waiting and traveling in the network of baseline scenario.

The first time interval showed a non-congested situation and then traveling time increased and the network began to fill up. Congestion then occurred as well as cars waiting to enter the road network. Average speed continued to decrease, resulting in delay in the network until the sixth time interval. Then, no waiting caused the trend of traveling to decrease and speed increased.

5.2. Result of Scenario Evaluation

Urban floods affect transportation by increasing travel times, route changes, and congestion due to low speed. Roads with a flood depth of more than 50 cm are considered completely unusable by private vehicles. Therefore, evacuation timing demand in flood levels lower than 50 cm was assigned to evacuation centers and out areas to compare the efficiency of the road network under different flood conditions. Vehicles take the shortest path to reach their destinations but change to longer paths with longer travel time under flood conditions. For this model, variables of road function were degraded by flooding. Vehicles changed routes to reduce their travel time based on user equilibrium principles.

Table 2 shows network performance indicators during the seven scenarios. Vehicle speed during the flooding scenarios changed. The average speed during dry conditions was 29.72 km/h. During the 0–5 cm flooding situation, speed decreased to 27.70 km/h, a 6.79% speed decrease. Similarly, 5–10, 10–15, 15–20, 20–25, and 25–30 cm flooding scenarios decreased vehicle speed to 21.29, 14.43, 8.57, 4.08, and 2.03 km/h, with percentage changes in speed of –28.38, –51.45, –71.15, –86.26, and –93.16 from the dry scenario.

Table 2. Network performance indicators comparison.

Scenario	Performance Measure					
	Speed (km/h)		VHT (veh-h)		VKT (veh-h)	
	Value	Change (%)	Value	Change (%)	Value	Change (%)
Dry	29.72	-	3542.68	-	109,276.68	-
0–5 cm	27.70	–6.79	3794.14	7.10	109,220.79	–0.04
5–10 cm	21.29	–28.38	4835.76	34.08	109,634.47	0.33
10–15 cm	14.43	–51.45	7034.85	72.40	113,030.73	3.42
15–20 cm	8.57	–71.15	11,000.06	120.05	120,578.22	10.00
20–25 cm	4.08	–86.26	25,961.01	186.83	136,639.76	22.69
25–30 cm	2.03	–93.16	56,626.33	204.47	152,914.00	31.94

Vehicle hours traveled (VHT) increased as vehicle speed decreased by 204.47% of travel time from the dry condition to the 25–30 cm flooding scenario. Vehicle kilometers traveled (VKT) also increased because, due to flooding, drivers choose alternate routes to reach their destinations. The VKT value in a flood of 0–5 cm was negative. Drivers may choose the fastest route by time but there may be a shorter distance because the overall performance of the whole network at the flood level was not different from the dry condition. Kilometers traveled increased by 31.94% compared to the dry condition for the 25–30 cm flooding condition. Results showed that flooding scenarios had a negative impact on network performance.

Figure 13 represents the seven scenarios plotted as a percentage of evacuation against time. Evacuation time for the baseline was “0” as dry. The evacuees took 110 min to arrive at evacuation centers, while none remained in the road network. The dry condition was compared to the seven scenarios. Evacuation time increased with deeper flood levels. For the 0–10 cm depth, evacuation time was not different to the dry condition. When flood levels increased to 10–15, 15–20, 20–25, and 25–30 cm, evacuation times increased to 40, 90, 260, and 670 min, respectively. The remaining evacuees increased with increasing flood levels. For flood levels of 10–15, 15–20, 20–25, and 25–30 cm, the percentages of evacuees remaining were 9%, 19%, 49%, and 83%, respectively.

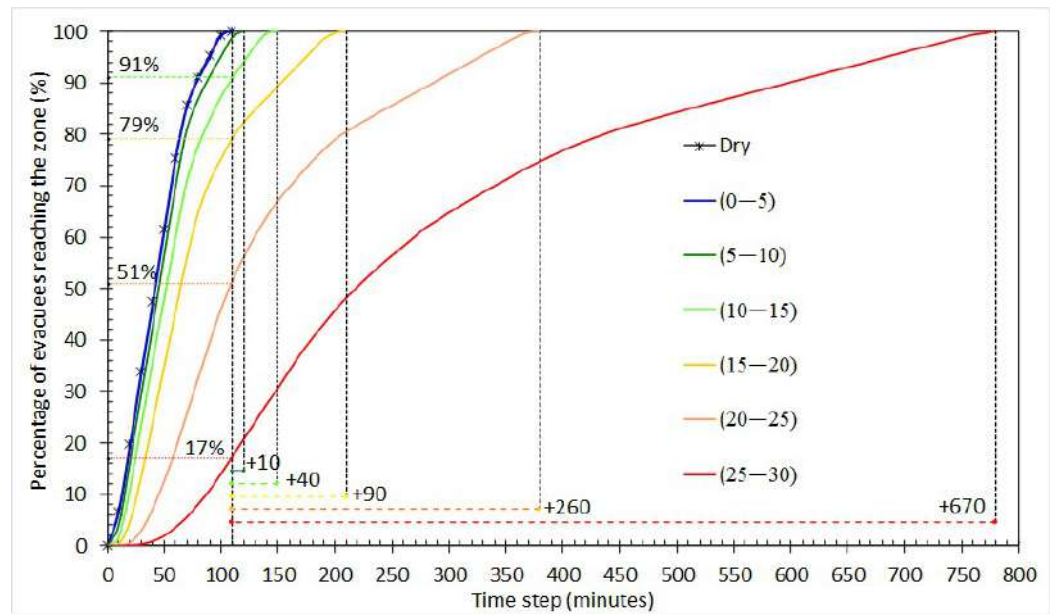


Figure 13. Cumulative evacuee arrival percentage.

6. Discussion and Conclusions

Hat Yai city, the economic and transportation hub of Songkhla province and southern Thailand, experiences heavy rainfall and flooding throughout the year due to northeast monsoon winds from October to January and southwest monsoon winds from May to October. Sudden flooding, in particular, makes it impossible for people to move and increases the risk of disaster. Therefore, people need to be evacuated quickly before flooding occurs to avoid injuries and deaths. Several scenarios were constructed by changing flooding situations and traffic volumes. Evacuation times in the study area were evaluated and compared for all scenarios with reference to dry conditions.

In this study, evacuation time was estimated and measures were identified for coming floods using past evaluation by providing dynamic alternate routes using DTA with a positive impact on network performance. Six flood level scenarios were used—0–5, 5–10, 5–10, 10–15, 15–20, and 25–30 cm—and compared with the dry situation. During flooding, the average speed dropped to 2 km/h, VHT rose above 200%, and VKT rose above 30%.

Cumulative evacuee arrival percentage showed that evacuees remaining in the road network increased when flood levels were higher than 5 cm. Flood levels of 10–15, 15–20, 20–25, and 25–30 cm represented percentages of remaining evacuees at 9%, 19%, 49%, and 83%, respectively. Time taken to evacuate increased according to flood level. For flood depths of 5–30 cm, travel time increased by 40, 90, 260, and 670 min, respectively. This suggests that it is necessary to start evacuation as soon as possible before the flood situation becomes serious.

This work was able to fully analyze the road network in depth to plan for route choice planning. The outcome of this study can be extended for actual operation, which can be identified to evaluate the road link that can be traveled the fastest in terms of travel time; the shortest available road network map will be provide this to the evacuation traffic planner. The avoidance route can be followed according to the historical data. The more necessary data to be included is the Flood Model for analyzing the road network flooding possibility. We conclude with some additional ideas to further expand on the topic of flood evacuation traffic management.

Integration of Emergency Response Plans: This study could explore the integration of emergency response plans into traffic management strategies during a flood evacuation. The study could analyze how different emergency response agencies can work together to coordinate traffic management efforts and ensure effective evacuation of affected areas. The

study could also consider the role of public information campaigns in promoting awareness and preparedness among the public.

Evaluation of Evacuation Routes: This study could evaluate the effectiveness of different evacuation routes in reducing traffic congestion during a flood event. The study could analyze how different factors, such as road capacity, network connectivity, and population density, affect the efficiency of evacuation routes. The study could also consider the impact of natural features, such as rivers or mountains, on the availability of evacuation routes.

Assessment of Driver Behavior: This study could assess how driver behavior affects traffic flow during a flood evacuation. The study could analyze how different factors, such as age, gender, and experience, influence driver decision making during a flood event. The study could also consider the impact of driver emotions, such as fear and anxiety, on traffic flow and evacuation efficiency.

Use of Intelligent Transportation Systems: This study could explore the use of intelligent transportation systems (ITSs) to improve flood evacuation traffic management. The study could analyze how different ITS technologies, such as connected vehicles, traffic signal prioritization, and dynamic message signs, can be integrated into traffic management strategies. The study could also consider the impact of ITSs on reducing traffic congestion and improving evacuation efficiency during a flood event.

Consideration of Vulnerable Populations: This study could consider the needs of vulnerable populations, such as elderly people or people with disabilities, during a flood evacuation. The study could analyze how different factors, such as accessibility of evacuation routes and availability of transportation options, affect the ability of vulnerable populations to evacuate. The study could also consider the impact of community outreach and support programs on improving evacuation outcomes for vulnerable populations.

Author Contributions: Conceptualization, P.S. and R.K.; Methodology, P.S., K.T., M.S. and R.K.; Software, N.T.; Formal analysis, P.S.; Investigation, C.Y.; Data curation, P.S. and C.Y.; Writing—original draft, P.S. and R.K.; Writing—review & editing, P.S. and R.K.; Supervision, A.F. and S.J.; Project administration, K.T. and M.S.; Funding acquisition, R.K. All authors have read and agreed to the published version of the manuscript.

Funding: This research was funded by SUT Research and Development Fund (Grant No. BRO7-712-65-12-05).

Institutional Review Board Statement: Not applicable.

Informed Consent Statement: Not applicable.

Data Availability Statement: Not applicable.

Acknowledgments: This work support by SUT Research and Development Fund .

Conflicts of Interest: The authors declare no conflict of interest.

References

1. Land Development Department (Ministry of Agriculture and Cooperatives) Land Use. 2022. Available online: <http://dinonline.ddd.go.th/Landuse.aspx>. (accessed on 29 May 2022).
2. Hatyai, (ASEAN Climate Change and Disaster Resilience Network Accredited Agency) Training for Creating Local Courses on Flood Response Hat Yai Municipality. 2014. Available online: <https://www.hatyaicityclimate.org/upload/forum/doc53d365c01b60f.pdf> (accessed on 29 May 2022).
3. GISTDA. Thailand Flood Monitoring System 2020. Available online: www.gistda.or.th/news_view.php?n_id=1586&lang=EN. (accessed on 29 November 2022).
4. Southern Regional Geo-Informatics and Space Technology Center. The Development of A Flood Model for Hatyai Municipality Using HEC-RAS 2D. Available online: https://www.gispsu.net/files/com_news_download/2018-01_3a4592ad2e3c59e.pdf. (accessed on 11 August 2022).
5. Baker, E.J. Hurricane evacuation behavior. *Int. J. Mass Emergencies Disasters* **1991**, *9*, 287–310. [CrossRef]
6. Chiu, Y.C.; Zheng, H.; Villalobos, J.A.; Peacock, W.; Henk, R. Evaluating regional contra-flow and phased evacuation strategies for Texas using a large-scale dynamic traffic simulation and assignment approach. *J. Homel. Secur. Emerg. Manag.* **2008**, *5*. [CrossRef]

7. Yazici, M.A.; Ozbay, K. Evacuation modelling in the United States: Does the demand model choice matter? *Transp. Rev.* **2008**, *28*, 757–779. [[CrossRef](#)]
8. Zou, N.; Yeh, S.T.; Chang, G.L.; Marquess, A.; Zezeski, M. Simulation-based emergency evacuation system for Ocean City, Maryland, during hurricanes. *Transp. Res. Rec.* **2005**, *1922*, 138–148. [[CrossRef](#)]
9. Gerber, B.J.; Ducatman, A.; Fischer, M.; Althouse, R.; Scotti, J.R. *The Potential for an Uncontrolled Mass Evacuation of the DC Metro Area Following a Terrorist Attack: A Report of Survey Findings*; West Virginia University: Morgantown, WV, USA, 2006; Volume 81.
10. Meit, M.; Briggs, T.; Kennedy, A. *Urban to Rural Evacuation: Planning for Rural Population Surge*; NORC Walsh Center for Rural Health Analysis: Chicago, IL, USA, 2008.
11. Zeigler, D.J.; Johnson, J.H. Evacuation behavior in response to nuclear power plant accidents. *Prof. Geogr.* **1984**, *36*, 207–215. [[CrossRef](#)]
12. Fraser, S.A.; Wood, N.J.; Johnston, D.; Leonard, G.S.; Greening, P.D.; Rossetto, T. Variable population exposure and distributed travel speeds in least-cost tsunami evacuation modelling. *Nat. Hazards Earth Syst. Sci.* **2014**, *14*, 2975–2991. [[CrossRef](#)]
13. León, J.; March, A. An urban form response to disaster vulnerability: Improving tsunami evacuation in Iquique, Chile. *Environ. Plan. Plan. Des.* **2016**, *43*, 826–847. [[CrossRef](#)]
14. Mas, E.; Koshimura, S.; Imamura, F.; Suppasri, A.; Muhari, A.; Adriano, B. Recent advances in agent-based tsunami evacuation simulations: Case studies in Indonesia, Thailand, Japan and Peru. *Pure Appl. Geophys.* **2015**, *172*, 3409–3424. [[CrossRef](#)]
15. Dawson, R.J.; Peppe, R.; Wang, M. An agent-based model for risk-based flood incident management. *Nat. Hazards* **2011**, *59*, 167–189. [[CrossRef](#)]
16. Dressler, G.; Müller, B.; Frank, K.; Kuhlicke, C. Towards thresholds of disaster management performance under demographic change: Exploring functional relationships using agent-based modeling. *Nat. Hazards Earth Syst. Sci.* **2016**, *16*, 2287–2301. [[CrossRef](#)]
17. Fujita, I.; Ito, T.; Sayama, T. Inundation analysis of the 2009 C hikusa R iver flood and comparison of evacuation criteria. *J. Flood Risk Manag.* **2014**, *7*, 54–64. [[CrossRef](#)]
18. Lim, H.R.; Lim, M.; Bernadeth, B.; Piantanakulchai, M. Determinants of household flood evacuation mode choice in a developing country. *Nat. Hazards* **2016**, *84*, 507–532. [[CrossRef](#)]
19. Masuya, A.; Dewan, A.; Corner, R.J. Population evacuation: Evaluating spatial distribution of flood shelters and vulnerable residential units in Dhaka with geographic information systems. *Nat. Hazards* **2015**, *78*, 1859–1882. [[CrossRef](#)]
20. Mordvintsev, A.; Krzhizhanovskaya, V.; Lees, M.; Slood, P. Simulation of city evacuation coupled to flood dynamics. In *Pedestrian and Evacuation Dynamics 2012*; Springer: Berlin/Heidelberg, Germany, 2014; pp. 485–499.
21. Alam, M.J.; Habib, M.A.; Quigley, K.; Webster, T.L. Evaluation of the traffic impacts of mass evacuation of Halifax: Flood risk and dynamic traffic microsimulation modeling. *Transp. Res. Rec.* **2018**, *2672*, 148–160. [[CrossRef](#)]
22. Lim, H., Jr.; Lim, M.B.; Piantanakulchai, M. A review of recent studies on flood evacuation planning. *J. East. Asia Soc. Transp. Stud.* **2013**, *10*, 147–162.
23. Mas, E.; Imamura, F.; Koshimura, S. An agent based model for the tsunami evacuation simulation. A case study of the 2011 great east Japan tsunami in Arahama town. In *Proceedings of the Joint Conference Proceeding. 9th International Conference on Urban Earthquake Engineering & 4th Asia Conference on Earthquake Engineering*; Tokyo Institute of Technology: Tokyo, Japan, 2012.
24. Yazici, A.; Ozbay, K. Evacuation network modeling via dynamic traffic assignment with probabilistic demand and capacity constraints. *Transp. Res. Rec.* **2010**, *2196*, 11–20. [[CrossRef](#)]
25. Setiadi, N.; Taubenböck, H.; Raupp, S.; Birkmann, J. Integrating socio-economic data in spatial analysis: An exposure analysis method for planning urban risk mitigation. In *Proceedings of the Corp Konferenz, Vienna, Austria, 18–20 May 2010*; pp. 1–8.
26. Post, J.; Wegscheider, S.; Mück, M.; Zosseder, K.; Kiefl, R.; Steinmetz, T.; Strunz, G. Assessment of human immediate response capability related to tsunami threats in Indonesia at a sub-national scale. *Nat. Hazards Earth Syst. Sci.* **2009**, *9*, 1075–1086. [[CrossRef](#)]
27. Saito, T.; Kagami, H. Simulation of evacuation behavior from tsunami utilizing multi agent system. In *Proceedings of the 13th World Conference on Earthquake Engineering, Vancouver, BC, Canada, 1–6 August 2004*; pp. 1–10.
28. Yazici, M.A.; Ozbay, K. Impact of probabilistic road capacity constraints on the spatial distribution of hurricane evacuation shelter capacities. *Transp. Res. Rec.* **2007**, *2022*, 55–62. [[CrossRef](#)]
29. Kalafatas, G.; Peeta, S. Planning for evacuation: Insights from an efficient network design model. *J. Infrastruct. Syst.* **2009**, *15*, 21–30. [[CrossRef](#)]
30. Ng, M.; Waller, S.T. Reliable evacuation planning via demand inflation and supply deflation. *Transp. Res. Part E Logist. Transp. Rev.* **2010**, *46*, 1086–1094. [[CrossRef](#)]
31. Li, J.; Ozbay, K. Evacuation planning with endogenous transportation network degradations: A stochastic cell-based model and solution procedure. *Netw. Spat. Econ.* **2015**, *15*, 677–696. [[CrossRef](#)]
32. Pel, A.J.; Bliemer, M.C.; Hoogendoorn, S.P. Analytical macroscopic modeling of voluntary and mandatory emergency evacuation strategies. In *Proceedings of the 10th International TRAIL Congress Netherlands TRAIL Research School, Rotterdam, The Netherlands, 14–15 October 2008*.
33. Yusoff, M.; Ariffin, J.; Mohamed, A. Optimization approaches for macroscopic emergency evacuation planning: A survey. In *Proceedings of the 2008 International Symposium on Information Technology, Kuala Lumpur, Malaysia, 26–29 August 2008* ; Volume 3, pp. 1–7.

34. Lieberman, E.; Xin, W. Macroscopic traffic modeling for large-scale evacuation planning. In Proceedings of the Transportation Research Board 91st Annual Meeting, Washington, DC, USA, 22–26 January 2012.
35. Naser, M.; Birst, S.C. *Mesoscopic Evacuation Modeling for Small-to Medium-Sized Metropolitan Areas*; Technical Report, Mountain-Plains Consortium; University of Wyoming: Laramie, WY, USA, 2010. Available online: <https://www.ugpti.org/resources/reports/downloads/mpc10-222.pdf> (accessed on 3 December 2022).
36. Marinov, M.; Viegas, J. A mesoscopic simulation modelling methodology for analyzing and evaluating freight train operations in a rail network. *Simul. Model. Pract. Theory* **2011**, *19*, 516–539. [\[CrossRef\]](#)
37. Di Gangi, M.; Polimeni, A. A mesoscopic approach to model route choice in emergency conditions. In *Proceedings of the International Conference on Optimization and Decision Science*; Springer: Berlin/Heidelberg, Germany, 2017; pp. 547–555.
38. Di Gangi, M.; Watling, D.; Di Salvo, R. Modeling evacuation risk using a stochastic process formulation of mesoscopic dynamic network loading. *IEEE Trans. Intell. Transp. Syst.* **2020**, *23*, 3613–3625. [\[CrossRef\]](#)
39. Stern, E.; Sinuany-Stern, Z. A behavioural-based simulation model for urban evacuation. In *Proceedings of the Papers of the Regional Science Association*; Springer: Berlin/Heidelberg, Germany, 1989; Volume 66, pp. 87–103.
40. Franzese, O.; Han, L. Using traffic simulation for emergency and disaster evacuation planning. In Proceedings of the 81st Annual Meeting of the Transportation Research Board, Washington, DC, USA, 13–17 January 2002.
41. Jha, M.; Moore, K.; Pashaie, B. Emergency evacuation planning with microscopic traffic simulation. *Transp. Res. Rec.* **2004**, *1886*, 40–48. [\[CrossRef\]](#)
42. Liu, M.; Kajita, Y.; Hirai, T.; Sumi, T. A Microscopic Simulation of Evacuation Model Considering Car-Following Behavior under Flood. *J. East. Asia Soc. Transp. Stud.* **2010**, *8*, 1–15.
43. Chen, X.; Zhan, F.B. Agent-based modeling and simulation of urban evacuation: Relative effectiveness of simultaneous and staged evacuation strategies. In *Agent-Based Modeling and Simulation*; Springer: Berlin/Heidelberg, Germany, 2014; pp. 78–96.
44. Lämmel, G.; Rieser, M.; Nagel, K.; Taubenböck, H.; Strunz, G.; Goseberg, N.; Schlurmann, T.; Klüpfel, H.; Setiadi, N.; Birkmann, J. Emergency preparedness in the case of a tsunami—Evacuation analysis and traffic optimization for the Indonesian city of Padang. In *Pedestrian and Evacuation Dynamics 2008*; Springer: Berlin/Heidelberg, Germany, 2010; pp. 171–182.
45. Kwon, E.; Pitt, S. Evaluation of emergency evacuation strategies for downtown event traffic using a dynamic network model. *Transp. Res. Rec.* **2005**, *1922*, 149–155. [\[CrossRef\]](#)
46. Gangi, M.D. Planning evacuation by means of a multi-modal mesoscopic dynamic traffic simulation model. In *Geocomputation and Urban Planning*; Springer: Berlin/Heidelberg, Germany, 2009; pp. 99–115.
47. Suwanno, P.; Kasemsri, R.; Duan, K.; Fukuda, A. Application of macroscopic fundamental diagram under flooding situation to traffic management measures. *Sustainability* **2021**, *13*, 11227. [\[CrossRef\]](#)
48. Musolino, G.; Vitetta, A. Calibration and validation of a dynamic assignment model in emergency conditions from real-world experimentation. *Procedia-Soc. Behav. Sci.* **2014**, *111*, 498–507. [\[CrossRef\]](#)
49. Balakrishna, R.; Wen, Y.; Ben-Akiva, M.; Antoniou, C. Simulation-based framework for transportation network management in emergencies. *Transp. Res. Rec.* **2008**, *2041*, 80–88. [\[CrossRef\]](#)
50. He, M.; Chen, C.; Zheng, F.; Chen, Q.; Zhang, J.; Yan, H.; Lin, Y. An efficient dynamic route optimization for urban flooding evacuation based on Cellular Automata. *Comput. Environ. Urban Syst.* **2021**, *87*, 101622. [\[CrossRef\]](#)
51. Pel, A.J.; Bliemer, M.C.; Hoogendoorn, S.P. A review on travel behaviour modelling in dynamic traffic simulation models for evacuations. *Transportation* **2012**, *39*, 97–123. [\[CrossRef\]](#)
52. Di Gangi, M. Modeling evacuation of a transport system: Application of a multimodal mesoscopic dynamic traffic assignment model. *IEEE Trans. Intell. Transp. Syst.* **2011**, *12*, 1157–1166. [\[CrossRef\]](#)
53. Luathep, P.; Suwanno, P.; Taneerananon, P. Identification of critical locations in road networks due to disasters. *East. Asia Soc. Transp. Stud.* **2013**, *9*, 206.
54. Cascetta, E.; Pagliara, F.; Papola, A. Alternative approaches to trip distribution modelling: A retrospective review and suggestions for combining different approaches. *Pap. Reg. Sci.* **2007**, *86*, 597–620. [\[CrossRef\]](#)
55. Hall, R. *Handbook of Transportation Science*; Springer Science & Business Media: Berlin/Heidelberg, Germany, 2012; Volume 23.
56. Griffith, D.A. Spatial structure and spatial interaction: 25 years later. *Rev. Reg. Stud.* **2007**, *37*, 28–38. [\[CrossRef\]](#)
57. Cascetta, E. *Transportation Systems Analysis: Models and Applications*; Springer Science & Business Media: Berlin/Heidelberg, Germany, 2009; Volume 29.
58. Hat Yai City Municipality. Basic Information: Demographics. 2022. Available online: <https://www.hatyaicity.go.th/content/general> (accessed on 23 June 2022).
59. Furness, K.P. Time function iteration. *Traffic Eng. Control* **1965**, *7*, 458–460.
60. Spiess, H. A gradient approach for the OD matrix adjustment problem. *Transp. Sci.* **1990**, *24*, 1–16. [\[CrossRef\]](#)
61. Florian, M.; Noriega, Y. OD Matrix Adjustment: Using a Reference Matrix and Multiclass Adjustments. In Proceedings of the Transportation Research Board 89th Annual Meeting, Washington, DC, USA, 10–14 January 2010.
62. Luathep, P.; Suwansunthon, A.; Sutthiphon, S.; Taneerananon, P. Flood evacuation behavior analysis in urban areas. *J. East. Asia Soc. Transp. Stud.* **2013**, *10*, 178–195.
63. Gallaway, B.; Ivey, D.; Hayes, G.; Ledbetter, W.; Olson, R.; Woods, D.; Schiller, R., Jr. *Pavement and Geometric Design Criteria for Minimizing Hydroplaning*; Texas Transportation Institute: Arlington, TX, USA, 1979.

64. Ong, G.P.; Fwa, T.F. Hydroplaning risk management for grooved pavements. In Proceedings of the 7th International Conference on Managing Pavement Assets, Alexandria, VA, USA, 2–4 June 2008; pp. 23–28.
65. Morris, B.; Notley, S.; Boddington, K.; Rees, T. External factors affecting motorway capacity. *Procedia-Soc. Behav. Sci.* **2011**, *16*, 69–75. [CrossRef]
66. Chung, Y. Assessment of non-recurrent congestion caused by precipitation using archived weather and traffic flow data. *Transp. Policy* **2012**, *19*, 167–173. [CrossRef]
67. Galatioto, F.; Glenis, V.; Roberts, R.; Kilsby, C. Exploring and modelling the impacts of rainfall and flooding on transport network. The case study of Newcastle upon Tyne. In *Proceedings of the 2nd International Conference on Urban Sustainability and Resilience*; Newcastle University: Newcastle upon Tyne, UK, 2014.
68. Pearson, M.; Hamilton, K. Investigating driver willingness to drive through flooded waterways. *Accid. Anal. Prev.* **2014**, *72*, 382–390. [CrossRef]
69. United States Comments to Proposed Requirements for EVS GTR on “Protection against Water”. Available online: <https://globalautoregs.com/documents/11234> (accessed on 10 August 2021).
70. Expert Advice: Driving Through Flood Water. Available online: <http://blog.greenflag.com/2015/expert-advice-driving-through-flood-water/> (accessed on 10 August 2021).
71. Boyce, L. As the Rain Keeps Falling, Will Driving through Puddles Damage Your Car Engine and Prove an Expensive Mistake? Available online: <http://www.thisismoney.co.uk/money/experts/article-2141778/Does-driving-puddles-cause-car-engine-damage.html#ixzz4Ky9gmDOq> (accessed on 22 January 2012).
72. Gissing, A.; Haynes, K.; Coates, L. Motorist behaviour during the 2015 Shoalhaven floods. *Aust. J. Emerg. Manag.* **2016**, *31*, 25–30.
73. Kramer, M.; Terheiden, K.; Wieprecht, S. Safety criteria for the trafficability of inundated roads in urban floodings. *Int. J. Disaster Risk Reduct.* **2016**, *17*, 77–84. [CrossRef]
74. Yin, J.; Yu, D.; Yin, Z.; Liu, M.; He, Q. Evaluating the impact and risk of pluvial flash flood on intra-urban road network: A case study in the city center of Shanghai, China. *J. Hydrol.* **2016**, *537*, 138–145. [CrossRef]
75. Pyatkova, K.; Chen, A.S.; Djordjević, S.; Butler, D.; Vojinović, Z.; Abebe, Y.A.; Hammond, M. Flood impacts on road transportation using microscopic traffic modelling techniques. In *Simulating Urban Traffic Scenarios*; Springer: Berlin/Heidelberg, Germany, 2019; pp. 115–126.
76. Choo, K.S.; Kang, D.H.; Kim, B.S. Impact assessment of urban flood on traffic disruption using rainfall–depth–vehicle speed relationship. *Water* **2020**, *12*, 926. [CrossRef]
77. How to Drive Through Floods. Available online: <http://www.telegraph.co.uk/cars/advice/how-to-drive-through-floods/> (accessed on 10 August 2021).
78. Tsumita, N.; Miyamura, K.; Jaensirisak, S.; Fukuda, A. Analysis of Travel Behavior Under Flooding Condition Based on Probe Data in Ubon Ratchathani City, Thailand. In *Proceedings of the Second International Conference of Construction, Infrastructure, and Materials*; Springer: Berlin/Heidelberg, Germany, 2022; pp. 303–316.
79. Pregolato, M.; Ford, A.; Wilkinson, S.M.; Dawson, R.J. The impact of flooding on road transport: A depth-disruption function. *Transp. Res. Part D Transp. Environ.* **2017**, *55*, 67–81. [CrossRef]
80. Hilly, G.; Vojinovic, Z.; Weesakul, S.; Sanchez, A.; Hoang, D.N.; Djordjevic, S.; Chen, A.S.; Evans, B. Methodological Framework for Analysing Cascading Effects from Flood Events: The Case of Sukhumvit Area, Bangkok, Thailand. *Water* **2018**, *10*, 81. [CrossRef]
81. Mahut, M.; Florian, M. Traffic simulation with dynameq. In *Fundamentals of Traffic Simulation*; Springer: Berlin/Heidelberg, Germany, 2010; pp. 323–361.
82. Newell, G.F. A simplified car-following theory: A lower order model. *Transp. Res. Part Methodol.* **2002**, *36*, 195–205. [CrossRef]
83. Ran, B.; Boyce, D.E. A link-based variational inequality formulation of ideal dynamic user-optimal route choice problem. *Transp. Res. Part C Emerg. Technol.* **1996**, *4*, 1–12. [CrossRef]
84. Mahut, M.; Florian, M.; Tremblay, N.; Campbell, M.; Patman, D.; McDaniel, Z.K. Calibration and application of a simulation-based dynamic traffic assignment model. *Transp. Res. Rec.* **2004**, *1876*, 101–111. [CrossRef]
85. Friesz, T.L.; Bernstein, D.; Smith, T.E.; Tobin, R.L.; Wie, B.W. A variational inequality formulation of the dynamic network user equilibrium problem. *Oper. Res.* **1993**, *41*, 179–191. [CrossRef]
86. Mahut, M.; Florian, M.; Tremblay, N. Space-time queues and dynamic traffic assignment: A model, algorithm and applications. In Proceedings of the Transportation Research Board 82nd Annual Meeting Transportation Research Board, Washington, DC, USA, 12–16 January 2003.
87. Mahut, M.; Florian, M.; Tremblay, N. Traffic simulation and dynamic assignment for off-line applications. In Proceedings of the 10th World Congress on Intelligent Transportation Systems, Madrid, Spain, 16–20 November 2003.
88. Florian, M.; Mahut, M.; Tremblay, N. Application of a simulation-based dynamic traffic assignment model. *Eur. J. Oper. Res.* **2008**, *189*, 1381–1392. [CrossRef]
89. Noh, H.; Chiu, Y.C.; Zheng, H.; Hickman, M.; Mirchandani, P. Approach to modeling demand and supply for a short-notice evacuation. *Transp. Res. Rec.* **2009**, *2091*, 91–99. [CrossRef]

90. Kim, K.; Pant, P.; Yamashita, E. Integrating travel demand modeling and flood hazard risk analysis for evacuation and sheltering. *Int. J. Disaster Risk Reduct.* **2018**, *31*, 1177–1186. [[CrossRef](#)]
91. Russo, F.; Chilà, G. Safety of users in road evacuation: RP vs. SP surveys in demand analysis. *WIT Trans. Built Environ.* **2008**, *101*, 703–713.
92. Reis, L. Evacuation Assessment—Date: 10.07.2021, Rancho Cucamonga, California. United States of America. 2021. Available online: <https://policycommons.net/artifacts/2459538/evacuation-assessment-date/3481335/> (accessed on 3 April 2023).

Disclaimer/Publisher’s Note: The statements, opinions and data contained in all publications are solely those of the individual author(s) and contributor(s) and not of MDPI and/or the editor(s). MDPI and/or the editor(s) disclaim responsibility for any injury to people or property resulting from any ideas, methods, instructions or products referred to in the content.

ARTICLES FOR FACULTY MEMBERS

RESCUE VESSEL OPERATION FOR FLOOD EVACUATION PROTOCOL

Title/Author	Flood evacuation mapping using a time-distance cartogram / Park, S., Lee, G., & Kim, J. O.
Source	<i>ISPRS International Journal of Geo-Information</i> Volume 9 Issue 4 (2020) Pages 1-15 https://doi.org/10.3390/ijgi9040207 (Database: MDPI)

Article

Flood Evacuation Mapping Using a Time–Distance cartogram

Seula Park ¹, Gunhak Lee ^{2,*} and Jung Ok Kim ³

¹ Department of Civil and Environmental Engineering, Seoul National University, Seoul 08826, Korea; seula90@snu.ac.kr

² Department of Geography and Institute for Korean Regional Studies, Seoul National University, Seoul 08826, Korea

³ Advanced Institute of Convergence Technology, Suwon 16229, Korea; geostar1@snu.ac.kr

* Correspondence: gunhlee@snu.ac.kr; Tel.: +82-2-880-4019

Received: 17 February 2020; Accepted: 27 March 2020; Published: 29 March 2020



Abstract: When flooding occurs, people should be evacuated safely to designated shelters along the optimal routes to minimize serious damages on lives and properties. However, in general, only limited information related to evacuation procedures and using a directional arrow to indicate existing shelters is provided on the evacuation map. Moreover, the evacuation routes leading to nearby shelters are not presented effectively to people in an emergency situation. This paper aimed to provide an approach to generate a flood evacuation cartogram based on an actual evacuation. The proposed time–distance cartogram preserves the topological characteristics by minimizing distortion in transforming the evacuation routes. To empirically evaluate its application, we applied the proposed method to Siheung city in Korea. As a result, optimal shelter and evacuation routes were derived by considering significant factors influencing the actual access to the facilities. Moreover, the flood evacuation cartogram provides a more intuitive visualization than classic topographic maps, by relocating shelters and reshaping the routes intended for evacuation. The suggested method is significant as it provides practical flood evacuation information effectively and intuitively, and the generated cartograms as empirical results also provide helpful insights for more efficient evacuation plans.

Keywords: flood evacuation map; flood evacuation cartogram; time–distance cartogram; optimal shelter location; optimal evacuation route

1. Introduction

As the development of coastal areas continues through land reclamation, the risk of flooding is increasing and the risks related to huge losses of both life and property caused by inundation are increasing as well [1,2]. Natural disasters, such as hurricanes and tsunamis, can cause serious damage in coastal cities. In the case of such a disaster, it is critical to evacuate people as quickly as possible to minimize fatalities. When an evacuation order is issued by the government, people should move to the closest shelter as quickly as possible. However, the current evacuation system does not prescribe how evacuees should choose a route [3]. Therefore, people generally lack information on which shelter is the closest and easiest for them to access. Especially for circumstances in which inundation is occurring, accurate forecasts and prevention measures using various physical and statistical models are challenging due to the complexity of the hydrological process [4].

Moreover, the actual evacuation distance and time could change due to the dynamic situations created by a natural disaster event. Therefore, it is obviously necessary to deploy an actual evacuation time to extract the optimal route to the most accessible shelter to facilitate an evacuation during a flood.

Moreover, the visual provision of evacuation information related to shelter locations and corresponding routes is essential for the effective evacuation of people in real time. As shown in Figure 1, disaster information maps in Korea show only the locations of shelters in a particular area or provide simple directions to the shelters outside of the flooded area. It is difficult to identify the exact shelter location to which people in a particular place should move [5]. Specifically, if only location information of shelters is provided as shown in Figure 1a, there is a dearth of reliable information to select which evacuation path is the safest and fastest. Figure 1b shows the direction of evacuation route with arrows, but it is not explicit to know the time it takes to evacuate or the shelters that can be reached at the shortest time. In other words, if several adjacent shelters exist, it is impossible to determine which shelter is most accessible in the shortest amount of time based on the information represented in the disaster map in Figure 1. This lack of information may result in the loss of valuable time needed for evacuation and increase damages [6].

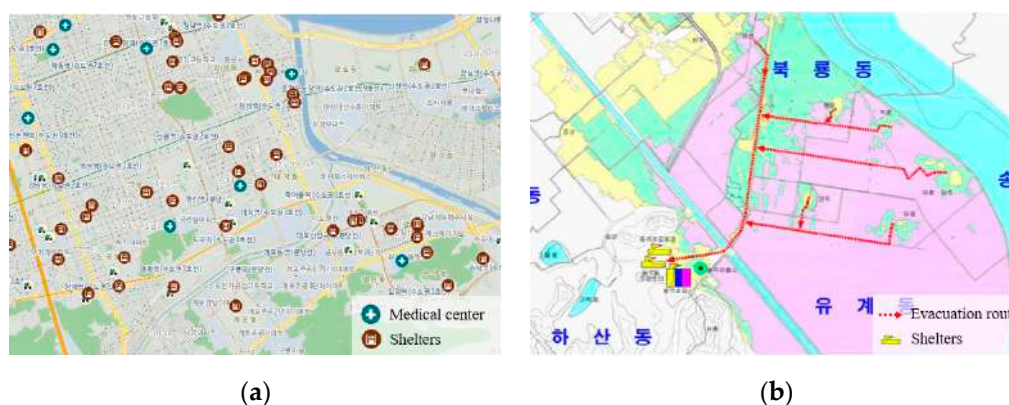


Figure 1. Disaster information maps in Korea; (a) Disaster information map for Gangnam-gu, Seoul (<http://safecity.seoul.go.kr>) (b) Disaster information map for Gwangsan-gu, Gwangju (<https://www.gwangsan.go.kr/>).

In this context, this paper suggests an alternative method for constructing a flood evacuation map by incorporating the actual travel time for a given distance during a flood situation, and a more effective visualization method for a time–distance cartogram. We provide an effective flood evacuation map for Siheung city in South Korea as an empirical example; in this location, spatially concentrated heavy rain often occurs on a seasonal basis. For the flood evacuation map, we first extracted the optimal inundation shelters and routes specifically based on the evacuation time derived from the pedestrian network in residential areas. The evacuation time cartogram, which was created by replacing the geographical distance between the residential areas and the flood evacuation shelters with the evacuation time attribute, was generated to visualize evacuation routes and optimal shelters effectively. The suggested flood evacuation cartogram would provide very intuitive and effective visual information about optimal shelters and evacuation routes for those who do not know the optimal shelter and even for those who have received limited evacuation information. Moreover, it provides significant insights for policy makers wishing to construct their own flood evacuation plans.

This paper is organized as follows. In Section 2, previous studies related to flood evacuation and the concept of a time cartogram are discussed. Then, an alternative method for creating a flood evacuation map is proposed in Section 3. In Section 4, the empirical application of this approach to flood evacuation mapping is shown using Siheung city in Korea as an example. Finally, the conclusions and future work are discussed in Section 5.

2. Related Works

Various studies have been carried out on evacuation situations in flooded areas for decades, including an analysis of the service area and the accessibility of shelters, as well as the derivation of

optimal evacuation routes. For example, Masuya et al. [7] analyzed the areas vulnerable to flooding and computed their accessibility to shelters. Moreover, Zhang et al. [8] investigated a methodology of feasible evacuation planning for dike-break flood with flooded roads extraction and flood simulation. Coles et al. [9] integrated flood inundation modelling with service area analysis of emergency services and analyzed the accessibility of districts during flood through a network analysis. Kulkarni [10] used elevation data to assess the safety of routes, considering the depth of the inundation. The system used for route selection in flooding situations was designed to extract the optimal evacuation route through the path and randomized segment penalty algorithms. However, it is difficult to recognize which route is more suitable based on the evacuation time because all routes are equally represented on the topographic map without considering the temporal weights for evacuation.

Moreover, no studies have been conducted thus far that effectively provide results from the flood evacuation analysis for those individuals who are actually endeavoring to escape. Although it is noteworthy that Uno and Kashiyama [11] proposed an evacuation simulation system for disasters by visualizing an evacuation situation using 3D animation, there is still a lack of intuitive information about the optimal shelters to which people can escape. To visualize results from a flood evacuation analysis, Leskens et al. [12] developed an interactive simulation and visualization tool for flood analysis. The arrival time of a simulated flood and the accessibility of the roads were visualized, while the evacuation route information was not included in the results. Similarly, although Zhang et al. [8] provided information on heavily congested roads and vulnerable villages and Masuya et al. [7] analyzed vulnerable residential houses, the evacuation time was not intuitively expressed visually in both studies.

Among the wide range of visualization techniques, in the context of flood evacuation, one useful method is a cartogram that highlights information related to the actual evacuation time instead of precise spatial information for shelters. Cartograms have become popular in various fields of application to supplement existing maps [13,14]. They take an advantage of visualizing geographical information with statistical information simultaneously [15]. Although a cartogram might distort the actual geometry of the map, it is more helpful in understanding the intended attribute of the phenomena. Especially for time information, mapping time information spatially would lead to have better understanding in travel perceptions and patterns [16]. Regarding the flood evacuation map, a distance cartogram is appropriate because it visualizes the relative time and distance and is therefore useful for identifying the actual movement of the routes and the nearest shelters within a pedestrian network during a flood. Many studies have been introduced that create distance cartograms representing various spatial relationships by replacing the geographical distance with other attributes. The methods previously introduced have mostly been limited by their unrecognizable levels of distortion or the uncertainty of the information [17]. In addition, various visualization techniques emphasize the phenomena represented by the data, but they are not suitable for expressing temporal information [18,19]. A time cartogram is a map that replaces the geographic distance between locations with a time-related property; therefore, the geography is transformed in response to that property [20].

Many studies have been carried out regarding the creation of time cartograms using information from various attributes. Shimizu and Inoue [17] proposed a process for creating intuitive and easy-to-use distance cartograms, in which the bearing was applied to the initial value to modify the Levenberg-Marquardt method. However, this method only describes how a network can be transformed over travel time. Buchin et al. [21] proposed a model suitable for visualizing travel times using road networks. The travel time was expressed through the length of the segments using sinusoid curves, but it was difficult to intuitively recognize the travel time because the position was fixed and there was no deformation for straight distances. Kaiser et al. [22] proposed a modified time–distance deformation algorithm for multi-scale road networks. The technique can be used for a visualization that can improve spatial perception, but the complexity of the operation when applied to a large range of networks is limited. Kraak et al. [23] introduced a kind of line cartogram by combining time and distance cartograms to identify the primitive characteristics of movement behavior, allowing users to

explore these characteristics directly through a Web-based visualization of the movements. However, the network for the movement was not preserved.

Ullah and Kraak [20] proposed a technique to generate the centered time cartogram using scheduled movement data. By applying this method, the station, railway, and boundary of the Dutch railway network are deformed to create a cartogram. The locations of the stations are displaced in proportion to the travel time from the departure point to each station, and the travel time is represented using concentric circles. For railway networks and the map's boundary, the homeomorphism and topology were maintained by a visually continuous and smooth. Since the deformation criterion of railway links and station nodes in the same railway network is different, the resultant cartogram may be severely distorted. Moreover, the computation is complicated because the deformation must be performed separately. Conversely, Lee et al. [24] analyzed and visualized time–distance-based accessibility using traffic data. The movement graph was constructed to search for the shortest path and calculated accessibility based on the travel time of the path. However, there was a limit to the effective provision of the linear path information, since the results were visualized using an areal shape.

3. Methods: Flood Evacuation Mapping and Cartogram Visualization

When a flood disaster happens, an immediate evacuation is necessary, but it is difficult to use vehicles and other forms of public transportation for evacuation. Therefore, it is necessary to find the path of the shortest distance that is available on the pedestrian level as an optimal escape route [5]. In this study, we assumed a situation in which pedestrian evacuation is possible such as slow rising floods. This study calculated the evacuation time and extracts the escape route based on pedestrian networks, which are characterized by more detailed walkways, to create a more suitable evacuation map for an actual situation (Figure 2).

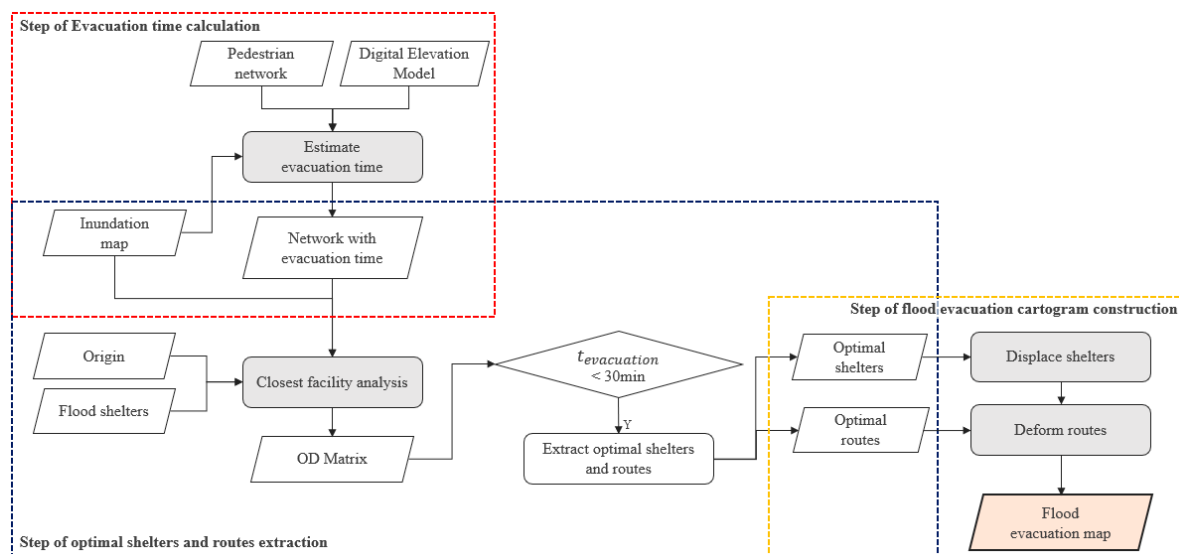


Figure 2. The process of flood evacuation mapping and visualization.

Kim and Lee [5] extracted the service area of the shelter after estimating the pedestrian evacuation time in accordance with the influence of the inundation depth and the slope. Similarly, as our first step in generating the flood evacuation map, the pedestrian network and Digital Elevation Model (DEM) data were used to calculate the actual escape time reflecting the slope of the pathway, as shown in Figure 2. When calculating the evacuation time, a decrease in walking speed due to flooding is considered for those in the expected inundation area which is represented in inundation map. Moreover, for the area with deeper depth than critical inundation depth, an extremely high time cost was assigned as the evacuation time to avoid passing through those areas. After designating the flood shelters and origins, and establishing the expected flooded area as the restricted area, the Origin and

Destination (OD) matrix between each individual residence and shelter can be created using the closest facility analysis. The Central Disaster and Safety Countermeasures Headquarters and the National Emergency Management Agency of Korea have recommended a 30-minute emergency evacuation. Therefore, to extract the most feasible evacuation route, the routes with a total travel time of 30 min or less were selected as the optimal routes with optimal shelters. Thereafter, the optimal shelter was displaced based on the evacuation time, and the evacuation route was deformed according to the relocated shelter to create the flood evacuation map.

3.1. Calculation of the Evacuation Time

Since walking time increases with an upward slope, the modified Langmuir's law [25] was applied to each link to calculate the travel time according to the slope. Table 1 shows the equations for walking time according to a given slope by the modified Naismith–Langmuir law. According to the law in Table 1, elevation difference should be calculated and stored in the pedestrian network to reflect the increase and decrease of evacuation time by the slope. Increased evacuation time can be calculated by overlaying the pedestrian network and DEM, assigning elevation values to each node, and calculating the difference in elevation between both end nodes of each link. [5]

Table 1. Modified Naismith–Langmuir law [25].

Slope(°)	Equation for Walking Time (t)
Flat (0° ~ -5°)	$t(min) = \frac{L(m)}{v(m/min)}$
Ascents (over 0°)	$t'(min) = t(min) + 0.1 \times \Delta E(m)$
Moderate descents (-5° ~ -12°)	$t'(min) = t(min) - 0.03 \times \Delta E(m)$
Steep descents (under -12°)	$t'(min) = t(min) + 0.03 \times \Delta E(m)$

t : walking time, t' : changed walking time considering slope, L : length of travel link, v : walking speed, ΔE : elevation difference.

Moreover, the evacuation time increases as evacuees pass through the flooded area. In this study, the equation in [26] is modified to calculate walking speed v during immersion which decreases linearly by the flood depth as follow:

$$v \text{ (m/s)} = 2 - 0.011d \text{ (cm)} \quad (1)$$

where v is the walking speed by the flood depth; d is the depth of water; 0.011 is the decreasing rate by the inundation depth in the equation in [26]; 2 is the average walking speed in a normal state. In previous studies [27–29], the average speed of fast walking for adults is in the range of 1.32–2.53 m/s. To estimate travel time that increases with slope and immersion depth, the standard for fast walking is set as 2 m/s in this study. In addition, it is possible to walk only by relying on a fixed object in a waterway when its immersion depth reaches 0.55 m [30]. Therefore, the critical water depth for evacuation is set to 0.55 m, so evacuation routes can be calculated using a detour route for areas in which flooding is expected to occur above the critical depth.

3.2. Extraction of the Optimal Shelters and Routes

In this study, residential clusters in the area where inundation has occurred in the past or is expected in the future are used to define the evacuation points for the analysis of the closest facility. Residential clusters are formed based on densely distributed housing areas. Since densely distributed housing areas are regions with a large population, they can be considered as areas in which evacuation is generally urgent. To create residential clusters, dwelling types, such as single-family houses, multi-family houses, or apartment buildings are extracted from the building layers of the Korean Road Name Address Map database provided by the Ministry of the Interior and Safety of Korea. Houses with a high possibility of flooding are selected by overlapping the buildings, the inundation

trace map [31], and the inundation map, and are assigned to the nearest shelter based on the shortest evacuation time. An inundation map represents expected flooded areas, expected damage range, and the depth of inundation, considering the traces of flooding in the past, including factors such as earthquake-induced tsunamis, extreme rainfall, and the collapse and overflow of dams; meanwhile, inundation trace maps are created to show previous inundation areas, and the attributes of flooding depth and time are depicted on continuous cadastral and digital topographic maps. Because the adjacent buildings are assigned to the same shelter and therefore have a very similar escape route, residential clusters are created for adjacent building groups and the centroid of each cluster is set as the origin for evacuation.

In this study, only flood shelters which are particularly subject to altitude conditions were extracted and entered as a facility layer to perform the closest facility analysis. In the case of an actual evacuation, it is necessary to analyze the evacuation route by establishing the inundation area as the restricted area, since access to the flooded area may be prohibited. Therefore, the expected flooded areas are entered as restricted for the closest facility analysis to derive a detour route for those flooded areas above the critical water depth. The expected flooded areas are derived from the previously established inundation map (Areas comprising the inundation map are classified into inland-flooded and outwater-flooded areas and detailed expected flooded areas by frequency of occurrence and rainfall are constructed in a polygon) [32]. Using evacuation origins and the restricted area for facilities and pedestrians, the closest facility analysis can be performed by defining the travel time of each link as the cost, and the OD matrix is then established. Consequently, optimal shelters and routes are selected with an evacuation time of less than 30 min based on the OD matrix.

3.3. Construction of the Flood Evacuation Time–Distance Cartogram

To provide intuitive and effective information on the optimal shelter and its path as people are being evacuated, it is essential to transform the evacuation map based on travel time to the shelter. For each evacuation origin, the route to the optimal shelter is deformed using the time of the evacuation, and the shelter is relocated to create time–distance cartograms for use during a flood evacuation. The process for constructing the time–distance cartogram is shown in Algorithm 1. If many optimal shelters are available for a single origin, all corresponding routes can be combined into one layer and processed at one time.

Algorithm 1 Algorithm for flood evacuation cartogram

- (1) Split the route links into segments at the point at which the direction changes and create nodes at the segmented locations
 - (2) Assign nodes of route links and shelters to a set of points P
 - (3) Calculate the evacuation time distance d_{t_i} and the time–distance coefficient r_t based on the following equation: $d_{t_i} = r_t \times d_i$, where $r_t = \sum_{n=1}^k l_n / \sum_{m=1}^k t_m$ where,
 - a. location of the origin = $[X_0, Y_0]$
 - b. location of point $i = [X_i, Y_i] \forall i = 1, \dots, k$
 - c. straight distance from origin to each point $i = l_i$
 - d. travel time from origin to point $i = t_i$
 - e. evacuation time distance = d_{t_i}
 - f. time–distance coefficient = r_t
 - (4) Adjust the locations of P based on the following equation: $X'_t = \frac{(X_i - X_0) \cdot d_{t_i}}{l_i} + X_0$ $Y'_t = \frac{(Y_i - Y_0) \cdot d_{t_i}}{l_i} + Y_0$ where adjusted location of point $i' = [X'_t, Y'_t]$
 - (5) Construct the displaced shelter layer by extracting the last point of adjusted P
 - (6) Deform the evacuation routes by reconnecting the adjusted nodes of route links
-

First, the route links for each evacuation origin are split into segments based on the point at which the direction of the link is switched, and nodes are created at the segmented locations and combined with the optimal shelter layer. Through the combination of the corresponding layers, the shelter can constitute the last node of each route. According to the station relocation principle from [20], every point can be displaced by converting the geographical distances into evacuation time distances while maintaining the directional information of the shelters and the nodes from the origin. The geographical distance utilizes the straight-line distance from the origin to the corresponding point. The evacuation time distance d_{t_i} can be calculated to reflect the ratio of the time that is required to reach each segment node along the pedestrian network to the total evacuation time required to travel from one origin to an optimal shelter. While maintaining the direction of each point from the origin, the straight-line distance from the origin to each point is replaced by d_{t_i} to adjust the position of the point. The layer with relocated shelters can be created by extracting the last node from a point layer, whose location has been adjusted. It is also possible to reconfigure nodes that have been relocated to deform the evacuation routes. Even in cases in which there are multiple evacuation routes to different shelters, if the directions of the shelters are similar, some sections are moved through the same links, and information on such redundant paths must be preserved after the link is deformed. If the link is modified by the proposed method, it is possible to preserve the redundant path since it is modified by applying the same time distance coefficient r_t . Although the post-transformed link shape is distorted for the existing path, it is easy to recognize the evacuation route because the direction information from the origin is preserved for all changing direction points of the link, that is, all the nodes comprising the route link.

After the time–distance–based cartogram has been created through the relocation of shelters and link deformation, five-minute intervals of concentric circles can be added to provide direct information on the evacuation time to optimal shelters.

4. Empirical Applications

4.1. Results of Empirical Applications

In this section, we present an empirical application for the proposed approach to flood evacuation mapping using the case of Siheung, a coastal city in South Korea. Siheung is suitable as a study area from which flood evacuation maps are created, as it is considered to be at high risk of flooding due to its small number of mountainous areas and large number of coastal reclamation sites [32]. According to the guidelines for disaster maps provided by the Ministry of the Public Administration and Security [33], a disaster map should be generated for severe instances of inundation. In addition, Siheung is affected by river flooding. Therefore, the expected inundation area is established using an inundation map, where 500 mm is the maximum rainfall and 10 years is the maximum frequency. Figure 3a shows Siheung in South Korea and Figure 3b represents the pedestrian network with the expected outwater inundation area based on a 500 mm/10 year-frequency for Siheung.

A total of 38 flood evacuation shelters were designated in Siheung (Figure 4a). Existing flood shelters in Figure 4a are distributed throughout Siheung, including the expected inundation areas. Flood shelters are designated with sufficient altitude due to the nature of the flood, and more shelters are concentrated near dense residential clusters and the expected inundation area which has a high probability of damage. The shelter layer was used as the facility data for the closest facility analysis. To establish the evacuation origin points based on the residential clusters, a group of buildings classified as 'housing' were first extracted from the building layer of the Korean New Address Map database. The centroid of the clustered buildings was then extracted and the optimal shelter and corresponding evacuation route from the residential cluster centroid are derived by conducting the closest facility analysis. Since the analysis shows that adjacent buildings are allocated to the same shelter and their evacuation routes are also equivalent, it is reasonable to combine buildings into one group to create a cluster. The centroid of each residential cluster was used as the evacuation origin point, as shown in (Figure 4b), which shows 20 points of evacuation origins for Siheung. Even areas that are less likely to

be flooded because they are far from the expected inundation area may be additionally selected as origins since they are dense residential clusters which require prearranged evacuation plans.

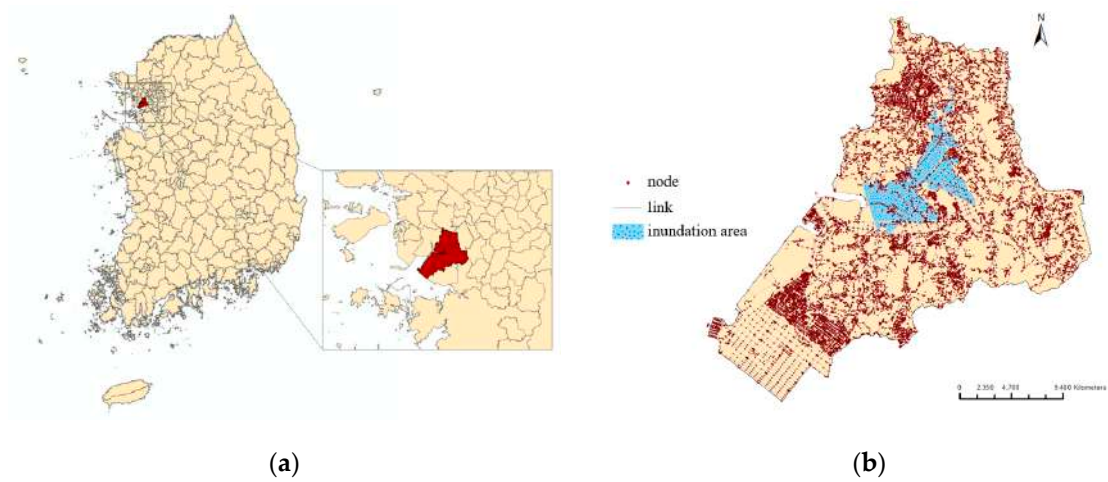


Figure 3. (a) Siheung city in South Korea (b) Pedestrian network with inundation areas in Siheung.

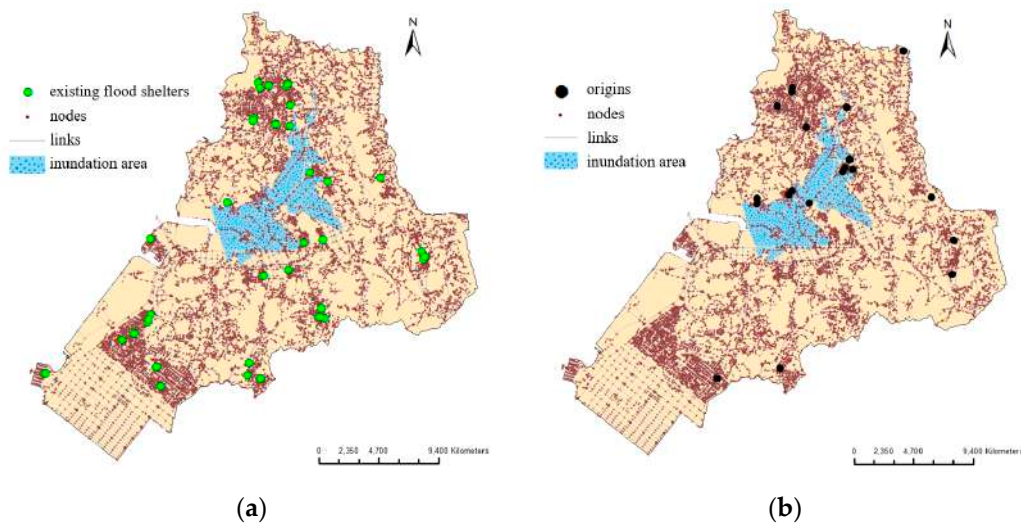


Figure 4. Facility and origin layer for Siheung: (a) Flood shelters (b) Extracted origins.

Using the pedestrian network and DEM with a $90\text{m} \times 90\text{m}$ resolution [34], the altitude value was assigned to each node on the network, such that the varying elevation is stored in the pedestrian routes. Then, the evacuation time per link was calculated based on the slope by applying the formula in Table 1. Using the inundation map, the evacuation time for the links that were included in the expected inundation areas could be calculated to consider a reduction in walking speed in the flooded area. Moreover, a portion of the expected flooded area was defined as a restricted area, which was classified as such once it exceeded the critical water depth. Based on the pedestrian network, which includes evacuation time and restriction attributes, a closest facility analysis between the shelter and the evacuation origin is performed. ‘Origin 16’ is located near the inundation area, and the route to the nearby shelters is often through the inundation area. Figure 5 shows the change in the optimal evacuation route both with and without the inundation area restriction for ‘origin 16’. To intuitively show that the optimal shelter and evacuation route is altered by the inundation area, the route to 20 nearby shelters was derived for two cases without limiting the maximum evacuation time for ‘origin 16’: (1) No reflection of the inundation area (Figure 5a), and (2) Reflection of the decrease in walking speed according to the water depth of the inundation area (Figure 5b). As shown in Figure 5b, when

the flooded area is introduced, it can be confirmed that a new route bypassing that area is then derived as a new optimal evacuation route.

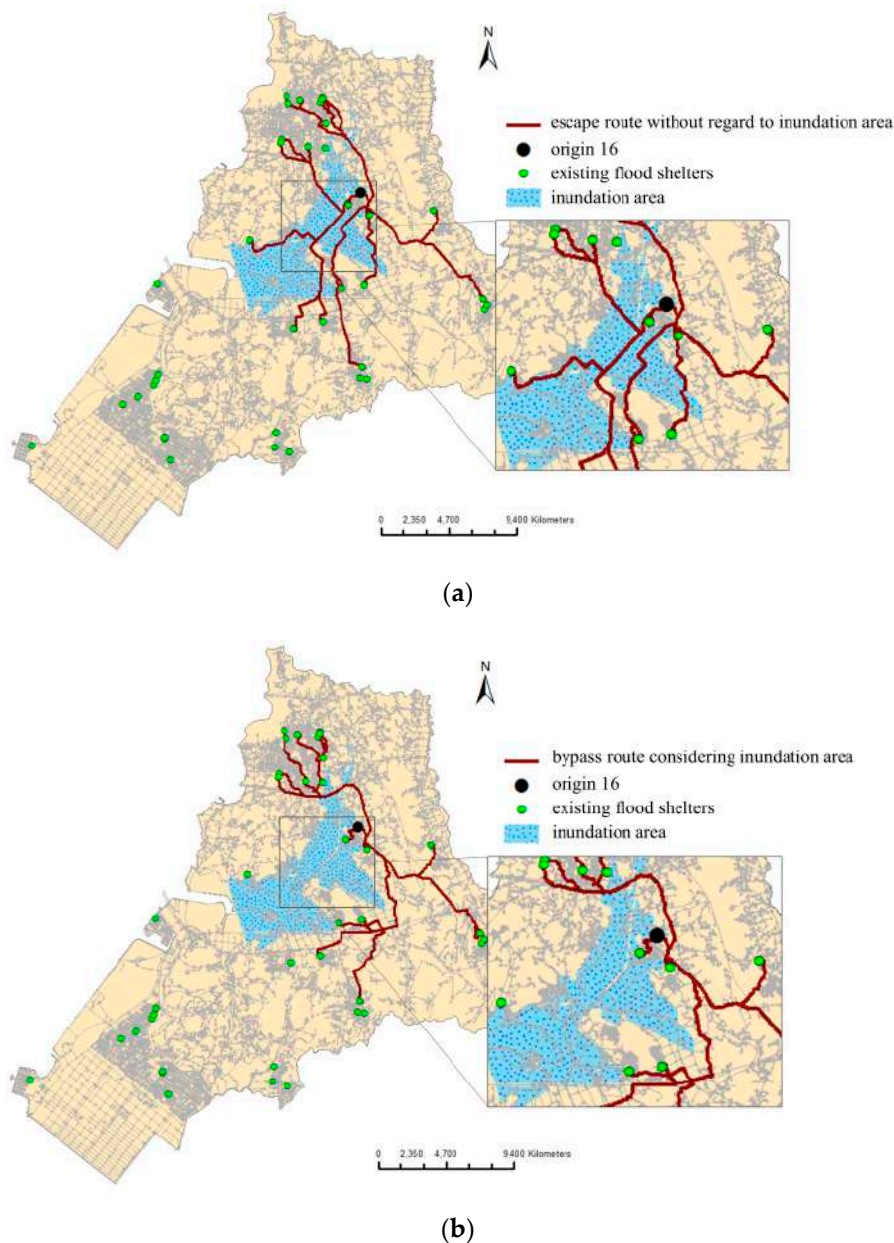
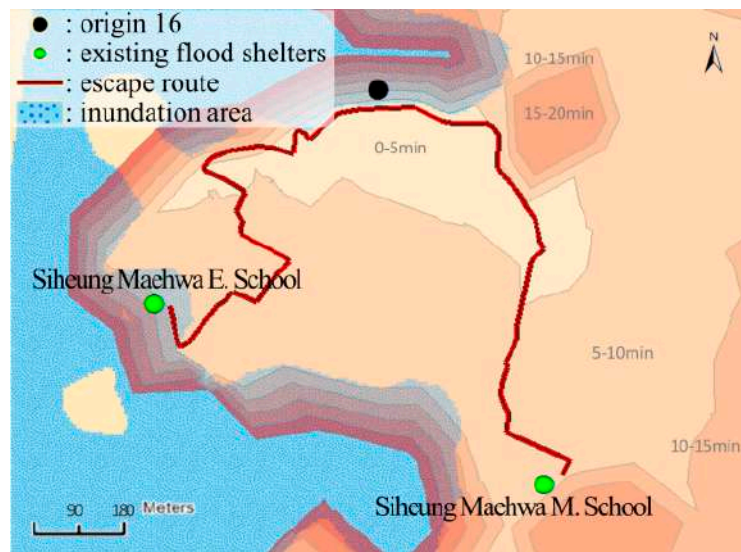
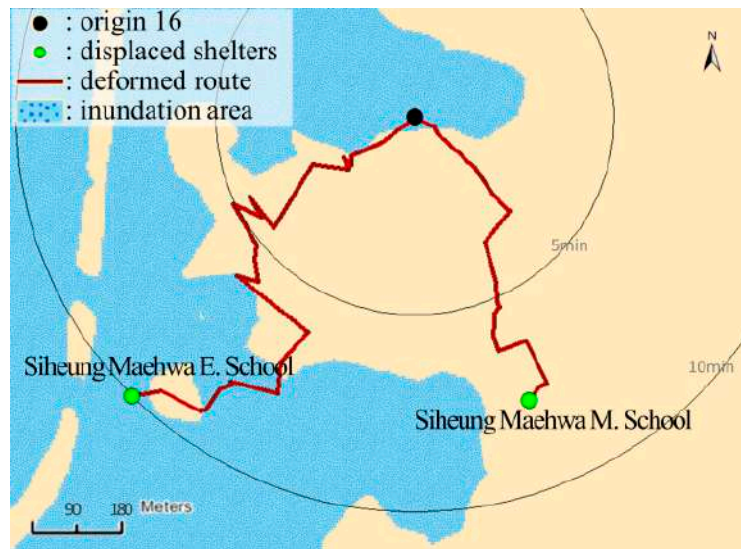


Figure 5. Optimal evacuation routes of 'origin 16': (a) without expected inundation area (b) with expected inundation area.

Next, the flood evacuation cartogram was generated to achieve a better understanding of the actual shortest evacuation paths in terms of walking mode and to quickly identify the nearest shelter in a flood emergency. An evacuation time of half an hour was defined as the threshold for extracting the optimal shelters and their routes. Then, shelter displacement and route deformation were efficiently performed using the suggested distance cartogram algorithm shown in Algorithm 1. Figure 6 shows the result of relocating the shelter and transforming the escape route by substituting the geographical distance with that of time while maintaining the original direction for 'origin 16'.



(a)



(b)

Figure 6. Shelter relocations: (a) routes based on the geographical distance (b) routes based on the evacuation time cartogram.

Figure 6 shows the time required to reach each shelter from ‘origin 16’ by adding isochrones to the result, which was derived from the optimal shelter and its route based on the geographical distance. ‘Siheung Maehwa Elementary School’ which is closer in terms of geographical distance seems to be the optimal shelter. However, in an actual situation, considering the restricted area and varying time distances for evacuation, the escape route to ‘Siheung Maehwa Elementary School’ would actually take longer because the route passes through the expected flooded area. Therefore, it can be concluded that ‘Siheung Maehwa Middle School’ is more suitable as an optimal shelter, as shown in the evacuation time cartogram (Figure 6b).

Figure 7 shows the original escape routes leading from ‘origin 10’ to the existing shelters and deformed routes based on actual evacuation time. For the deformed escape routes, the locations of the existing shelters were relocated if more time is required to reach them, in reality. This is because the lengths of the route links have been modified based on the actual escape time. Moreover, since the same time–distance coefficients were applied for all nodes of the route, it is possible to preserve the

redundant routes passing through the same links toward ‘Siheung Social Welfare Center for Disabled’ and ‘Chongwang Social Welfare Center’. Therefore, the cartogram algorithm minimizes the distortion created by the transformation of the paths and preserves the topological characteristics.

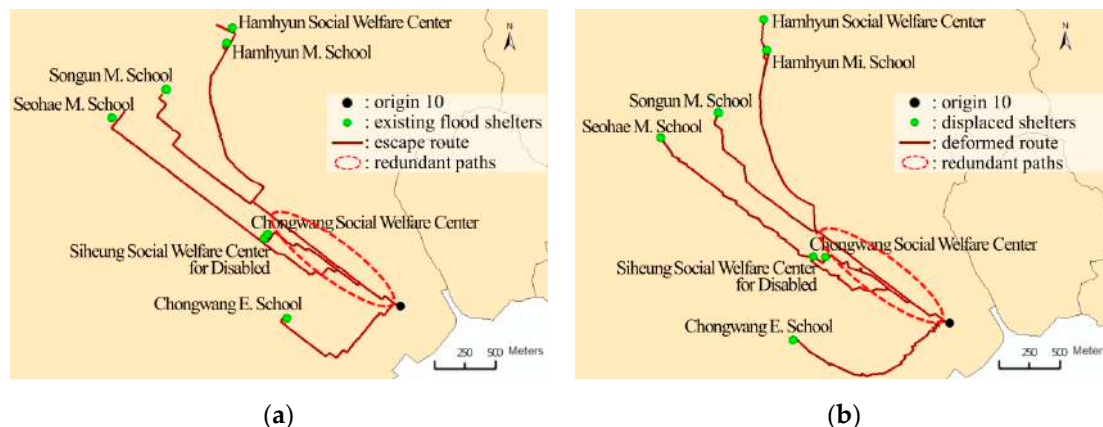


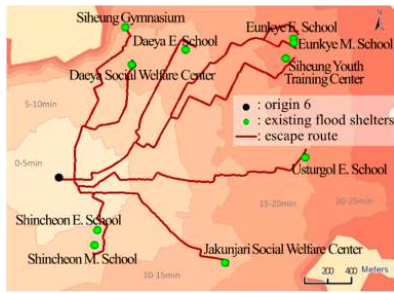

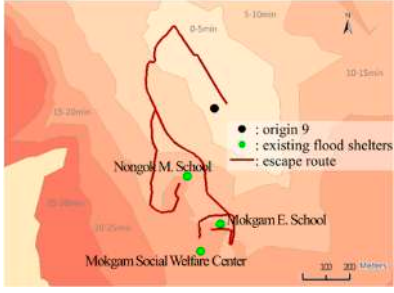
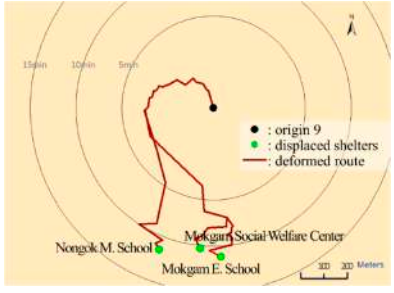


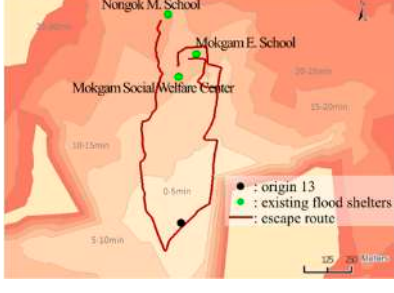

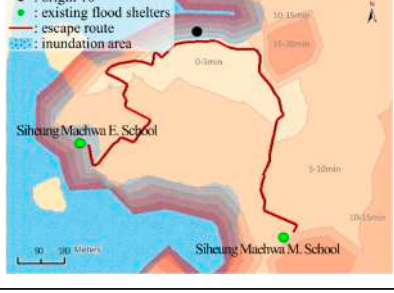

Figure 7. Preservation of redundant paths; (a) original escape route (b) deformed escape route.

4.2. Discussion of Flood Evacuation Cartograms

Table 2 illustrates the flood evacuation maps created for five different origins using the suggested algorithm for the flood evacuation cartogram. Nine of the total twenty origins were still assigned to the same shelter locations and optimal routes because only one shelter could be reached within 30 min. In addition, six origins were excluded from the cartogram because the geographical and evacuation time distances are not significantly different. For five origins (6, 9, 10, 13, 16), which reveal a significant difference between geographical and evacuation time distances, the optimal shelters were relocated and the route links were deformed to create an evacuation time cartogram to provide an intuitive and effective representation of escape route information.

For ‘origin 6’, it is noted that the geographical distance-based optimal shelters and the evacuation time distance-based optimal shelters are slightly different because the origin and the optimal shelter are not affected by the expected flooded areas. However, the reversal of the shelters still occurs. Interestingly, for ‘origin 9’, if the evacuation plan is devised by referencing a geographical distance-based evacuation map, it is highly likely that the evacuees will be guided to the nearest ‘Nongok Middle School’, thus over the capacity of that shelter. As shown in the cartogram of ‘origin 9’, it is easy to realize that the distances to shelters are different, but the evacuation times to those shelters are similar. Specifically, it can be visually observed that three viable evacuation shelters are all located within 30 min’ travel time and thus, guidance for the distributed evacuation routes to any of the shelters can be provided. ‘Origin 10’ is also likely to attract evacuees to ‘Chongwang Elementary School’, which is geographically closer than other shelters, but in reality, ‘Siheung Social Welfare Center for Disabled’ or ‘Chongwang Social Welfare Center’ are more appropriate options in terms of evacuation time. Based on the evacuation time for ‘origin 13’, the optimal shelter is ‘Mokgam Elementary School’ which is located in ‘Nongok-dong’, rather than the ‘Mokgam Social Welfare Center’ which is geographically closer and located in ‘Chonam-dong’ the same administrative district. Although the relocated optimal shelter, ‘Siheung Maehwa Middle School’, is located within a different administrative district than the residential areas in which ‘origin 16’ is situated, it is selected as the optimal shelter with shorter evacuation time. This implies the cartogram can deliver the information about an optimal shelter and its actual route more intuitively than a classic topographic map, even if shelters are not within a same administrative district than the residential areas in which origins are located.

Table 2. Flood evacuation maps (E.School and M.School mean Elementary school and Middle school, respectively).

Origin ID	Flood Evacuation Map Based on Geographical Distance	Flood Evacuation Cartogram Based on Escape Time
6		
9		
10		
13		
16		

Not all of geographic features, including the road network and administrative boundaries, were transformed as deformed solutions based on the actual evacuation time. Therefore, there might be a visual difference between the deformed routes and displaced shelters and the reality with which people are familiar. This is very common regarding the intended distortion of reality, which occurs

in a distance cartogram. Alternatively, it is generally recommended to use additional information to counteract the lack of visual familiarity so people can move along the deformed route on the evacuation map without delay. For instance, adding some important POI (Point of Interest) information on the escape routes could be helpful to mediate the effect of shelter and link deformation.

In this study, the evacuation time per link according to slope was calculated using DEM as reference data for altitude value. It is assumed that the resolution of DEM which is similar to the mean length of segments is not too low for assigning altitude value to end nodes of segments. However, by using a high-resolution DEM, new nodes can be created at the point of change in altitude value, and the link is split with those nodes. With these newly processed nodes and links as input data, it is expected that changes in travel speed and evacuation time according to the slope can be measured in detail. In addition, although this study assumes a pedestrian evacuation situation for ordinary adults, various alternatives may exist in addition to vehicles and pedestrians. For the further study, through applying behavior information according to travel mode such as speed, or using different type of network, the study can be extended to cartogram construction considering evacuation situation by other travel modes in detail.

5. Conclusions

This paper addressed an alternative method for generating flood evacuation maps to effectively visualize the optimal shelters and routes for residents in emergencies caused by flooding. To extract the optimal shelters and escape routes, information regarding the elevation and the pedestrian network were combined to derive the actual evacuation time. Moreover, expected inundation areas are also considered restricted when identifying an escape route. Therefore, the actual escape time, which considers the variance in walking speed based on flood depth, was successfully modeled to create the flood evacuation map. Further, the optimal routes to accessible shelters within the standard maximum time were presented for use in an actual evacuation based on evacuation origins. Moreover, the algorithm used to create the flood evacuation cartogram was developed for a more effective visualization of the optimal evacuation shelters and routes. Optimal shelters in the suggested cartogram are much more clearly and easily recognized than the closest option based on geographical distance because they can preserve the directional information related to the origins. Since the same time–distance coefficients have been applied to all nodes along the route, the topological characteristics between the origin and the shelter are well maintained.

For an example of its empirical application, five flood evacuation maps were constructed for Siheung city of Seoul. As a result, there is a position reversal in which the shelter perceived as significantly closer and located the shortest distance from the origin but with a relatively longer evacuation time is further away than other shelters in the flood evacuation cartogram. In other words, the flood evacuation cartogram is able to convey more effective and intuitive information regarding the optimal shelter, which is actually closer based on actual evacuation time, although the geographic distance from the origin is longer. In addition, because the routes are deformed using the same time–distance coefficients as the displaced shelters for all nodes on the route links, the distortion of the escape route could be minimized and information regarding redundant routes could be preserved.

Although the proposed cartogram can effectively identify the evacuation shelters and routes that are optimally determined, there is the visual gap of evacuation routes and the reality. However, this can be complemented by representing auxiliary information such as POI on the flood evacuation cartogram. In addition, further consideration of more dynamic factors, such as immersion speed, may improve the accuracy of evacuation time calculations. We believe that the suggested flood evacuation cartogram is significant, in that it provides practical flood evacuation information very effectively and intuitively for people in a real flooding situation. Our empirical results also provide helpful insights for disaster authorities or policy makers to facilitate the creation of more efficient evacuation plans. Nevertheless, additional investigation will be necessary if we wish to evaluate the actual effect of the information delivery for such a cartogram approach on users.

Author Contributions: Conceptualization, S.P. and G.L.; Investigation, S.P. and J.O.K.; Methodology, S.P., G.L. and J.O.K.; Software, S.P. and J.O.K.; Supervision, G.L.; Validation, S.P. and G.L.; Visualization, S.P.; Writing—original draft, S.P.; Writing—review and editing, S.P. and G.L.. All authors have read and agreed to the published version of the manuscript.

Funding: This research was supported by the Ministry of Education of the Republic of Korea and the National Research Foundation of Korea (NRF-2017S1A5A2A01023539).

Conflicts of Interest: The authors declare no conflict of interest.

References

1. Douben, K.J. Characteristics of river floods and flooding: a global overview, 1985–2003. *Irrig. Drain.* **2006**, *55*, S9–S21. [[CrossRef](#)]
2. Raposeiro, P.D.; Fortes, C.J.E.M.; Reis, M.T.; Ferreira, J.C. Development of a methodology to evaluate the flood risk at the coastal zone. In *Geographic Technologies Applied to Marine Spatial Planning and Integrated Coastal Zone Management*; Calado, H., Gil, A., Eds.; CIGPT: Ponta Delgada, Portugal, 2010; pp. 129–237.
3. Sadri, A.M.; Ukkusuri, S.V.; Murray-Tuite, P.; Gladwin, H. How to evacuate: model for understanding the routing strategies during hurricane evacuation. *J. transp. Eng.* **2013**, *140*, 61–69. [[CrossRef](#)]
4. Chen, S.H.; Lin, Y.H.; Chang, L.C.; Chang, F.J. The strategy of building a flood forecast model by neuro-fuzzy network. *Hydrol. Process.* **2006**, *20*, 1525–1540. [[CrossRef](#)]
5. Kim, J.O.; Lee, J.K. Safety Analysis of Pedestrian-centered Flood Evacuation Facility. *J. Korean Soc. Hazard Mitig.* **2018**, *18*, 449–456. [[CrossRef](#)]
6. Simonovic, S.; Ahmad, S. Computer-based model for flood evacuation emergency planning. *Nat. Hazards.* **2005**, *34*, 25–51. [[CrossRef](#)]
7. Masuya, A.; Dewan, A.; Corner, R.J. Population evacuation: evaluating spatial distribution of flood shelters and vulnerable residential units in Dhaka with geographic information systems. *Nat. Hazards.* **2015**, *78*, 1859–1882. [[CrossRef](#)]
8. Zhang, W.; Zhou, J.; Liu, Y.; Chen, X.; Wang, C. Emergency evacuation planning against dike-break flood: a GIS-based DSS for flood detention basin of Jingjiang in central China. *Nat. Hazards.* **2016**, *81*, 1283–1301. [[CrossRef](#)]
9. Coles, D.; Yu, D.; Wilby, R.L.; Green, D.; Herring, Z. Beyond ‘flood hotspots’: Modelling emergency service accessibility during flooding in York, UK. *J. Hydrol.* **2017**, *546*, 419–436. [[CrossRef](#)]
10. Kulkarni, P.P. Design of a System for Multiple Route Selection in the Presence of Flooding. Master’s Thesis, University of Houston, Houston, TX, USA, 2018.
11. Uno, K.; Kashiyama, K. Development of simulation system for the disaster evacuation based on multi-agent model using GIS. *Tsinghua Sci. Technol.* **2008**, *13*, 348–353. [[CrossRef](#)]
12. Leskens, J.G.; Kehl, C.; Tutenel, T.; Kol, T.; De Haan, G.; Stelling, G.; Eisemann, E. An interactive simulation and visualization tool for flood analysis usable for practitioners. *Mitig. Adapt. Strateg. Glob. Chang.* **2017**, *22*, 307–324. [[CrossRef](#)]
13. Pappenberger, F.; Cloke, H.L.; Baugh, C.A. Cartograms for Use in Forecasting Weather-Driven Natural Hazards. *Cartogr. J.* **2019**, *56*, 1–12. [[CrossRef](#)]
14. Nusrat, S.; Alam, M.J.; Kobourov, S. Evaluating cartogram effectiveness. *IEEE Trans. Vis. Comput. Graph.* **2018**, *24*, 1077–1090. [[CrossRef](#)] [[PubMed](#)]
15. Nusrat, S.; Alam, M.J.; Scheidegger, C.; Kobourov, S. Cartogram visualization for bivariate geo-statistical data. *IEEE Trans. Vis. Comput. Graph.* **2018**, *24*, 2675–2688. [[CrossRef](#)] [[PubMed](#)]
16. Todd, S.W.; Yettsko, A.; Hay, C. Time-space Visualization of Automobile and Airplane Travel Time from Chicago to Various Destination Cities. In Proceedings of the International Cartographic Association, Tokyo, Japan, 15–20 July 2019.
17. Shimizu, E.; Inoue, R. A new algorithm for distance cartogram construction. *Int. J. Geogr. Inf. Sci.* **2009**, *23*, 1453–1470. [[CrossRef](#)]
18. Li, X.; Kraak, M. The time wave. A new method of visual exploration of geo-data in time–space. *Cartogr. J.* **2008**, *45*, 193–200. [[CrossRef](#)]
19. Andrienko, G.; Andrienko, N.; Dykes, J.; Kraak, M.J.; Schumann, H. GeoVA (t)—Geospatial visual analytics: focus on time. *J. Locat. Based Serv.* **2010**, *4*, 141–146. [[CrossRef](#)]

20. Ullah, R.; Kraak, M. An alternative method to constructing time cartograms for the visual representation of scheduled movement data. *J. Maps*. **2015**, *11*, 674–687. [[CrossRef](#)]
21. Buchin, K.; van Goethem, A.; Hoffmann, M.; van Kreveld, M.; Speckmann, B. Travel-time maps: Linear cartograms with fixed vertex locations. In Proceedings of the International Conference on Geographic Information Science, Vienna, Austria, 24–26 September 2014.
22. Kaiser, C.; Walsh, F.; Farmer, C.J.; Pozdnoukhov, A. User-centric time-distance representation of road networks. In Proceedings of the International Conference on Geographic Information Science, Heidelberg, Berlin, 14–17 September 2010.
23. Kraak, M.; Köbben, B.; Tong, Y. Integrated time and distance line cartogram: a schematic approach to understand the narrative of movements. *Cartogr. Perspect.* **2014**, *77*, 7–16. [[CrossRef](#)]
24. Lee, K.; Park, J.; Goh, S.; Choi, M. Accessibility Measurement in Transportation Networks and Application to the Seoul Bus System. *Geogr. Anal.* **2018**, *51*, 339–353. [[CrossRef](#)]
25. Langmuir, E. *Mountaincraft and Leadership: A Handbook for Mountaineers and Hillwalking Leaders in the British Isles*; The Scottish Sport Council: Glasgow, Scotland, 1984.
26. Lee, H.; Hong, W.; Lee, Y. Experimental study on the influence of water depth on the evacuation speed of elderly people in flood conditions. *Int. J. Disaster Risk Reduct.* **2019**, *39*, 101–198. [[CrossRef](#)]
27. Bohannon, R.W. Comfortable and maximum walking speed of adults aged 20–79 years: reference values and determinants. *Age Ageing.* **1997**, *26*, 15–19. [[CrossRef](#)] [[PubMed](#)]
28. Muhdi, R.; Davis, J.; Blackburn, T. Improving occupant characteristics in performance-based evacuation modeling. In *Proceedings of the Human Factors and Ergonomics Society Annual Meeting*; SAGE Publications: Los Angeles, CA, USA, 2006; pp. 1199–1203.
29. Sun, J.; Guo, Y.; Li, C.; Lo, S.; Lu, S. An experimental study on individual walking speed during ship evacuation with the combined effect of heeling and trim. *Ocean Eng.* **2018**, *166*, 396–403. [[CrossRef](#)]
30. Kang, S. Study on refuge behavior and its critical inundation depth in low area. *J. Korean Soc. Civ. Eng.* **2003**, *23*, 561–565.
31. The Open Data Portal. Available online: <https://www.data.go.kr/> (accessed on 16 February 2020).
32. *Development of the Evaluation Technology for Complex Causes of Inundation Vulnerability and the Response Plans in Coastal Urban Areas for Adaptation to Climate Change*; (in Korean with English abstract); Ministry of the Interior and Safety: Sejong, Seoul, 2018.
33. *Disaster Map Guidelines, Republic of Korea (in Korean)*; Ministry of the Interior and Safety: Sejong, Seoul, 2017.
34. National Spatial Data Infrastructure Portal. Available online: <http://www.nsd.go.kr/> (accessed on 16 February 2020).



© 2020 by the authors. Licensee MDPI, Basel, Switzerland. This article is an open access article distributed under the terms and conditions of the Creative Commons Attribution (CC BY) license (<http://creativecommons.org/licenses/by/4.0/>).


ARTICLES FOR FACULTY MEMBERS

RESCUE VESSEL OPERATION FOR FLOOD EVACUATION PROTOCOL

Title/Author	Flood evacuation routes based on spatiotemporal inundation risk assessment / Lee, Y. H., Kim, H. Il, Han, K. Y., & Hong, W. H.
Source	<i>Water (Switzerland)</i> Volume 12 Issue 8 (2020) Pages 1-18 https://doi.org/10.3390/w12082271 (Database: MDPI)

Article

Flood Evacuation Routes Based on Spatiotemporal Inundation Risk Assessment

Yoon Ha Lee ¹, Hyun Il Kim ² , Kun Yeun Han ² and Won Hwa Hong ^{3,*}

¹ Sustainable Building Material and Construction Laboratory, Hanyang University,ERICA Campus, 55 Hanyangdaehak-ro, Sangnok-gu, Ansan, Gyeonggi-do 15588, Korea; dldbsgk123@naver.com

² Department of Civil Engineering, Kyungpook National University, 80 Daehak-ro, Buk-gu Daegu 41566, Korea; hyuun228@gmail.com (H.I.K.); kshanj@knu.ac.kr (K.Y.H.)

³ School of Architectural, Civil, Environmental and Energy Engineering, Kyungpook National University, 80 Daehak-ro, Buk-gu Daegu 41566, Korea

* Correspondence: hongwonhwa@gmail.com; Tel.: +82-53-950-5597

Received: 23 July 2020; Accepted: 11 August 2020; Published: 13 August 2020



Abstract: For flood risk assessment, it is necessary to quantify the uncertainty of spatiotemporal changes in floods by analyzing space and time simultaneously. This study designed and tested a methodology for the designation of evacuation routes that takes into account spatial and temporal inundation and tested the methodology by applying it to a flood-prone area of Seoul, Korea. For flood prediction, the non-linear auto-regressive with exogenous inputs neural network was utilized, and the geographic information system was utilized to classify evacuations by walking hazard level as well as to designate evacuation routes. The results of this study show that the artificial neural network can be used to shorten the flood prediction process. The results demonstrate that adaptability and safety have to be ensured in a flood by planning the evacuation route in a flexible manner based on the occurrence of, and change in, evacuation possibilities according to walking hazard regions.

Keywords: spatiotemporal flood fluctuations; inundation risk assessment; evacuation route; artificial neural network; geographic information system

1. Introduction

Natural disasters threaten the lives and valuable assets of thousands of people every year [1], and widespread destruction, economic loss, and loss of life are global phenomena. Korea is historically vulnerable to flooding due to high precipitation (annual precipitation in Seoul is 1200–1600 mm) compared to other regions of the same latitude [2]. Generally, flooding is caused by a complex combination of meteorological and hydrological phenomena such as extreme rainfall and flowing water [3]. Moreover, an impermeable layer such as a road or paved surface in an urban development assigns much more vulnerability to any given rainfall runoff phenomenon. Losses due to flooding can be reduced by better land-use planning, regulations, law enforcement, and non-physical mitigation management such as the establishment of shelters and evacuation routes [4]. Disaster managers are attempting to predict floods and flood management and establish action plans by utilizing prediction materials. The main purpose of flood prediction is to eliminate or lessen the causal factors that trigger flood disasters [5]. For example, successful prediction of rainfall and flood progress is utilized in flood management by such means as the preparation of flood hazard maps, contributing significantly to the reduction of casualties [6]. Representative models for predicting urban flooding include deterministic models based on numerical analysis and data-driven models using artificial neural networks that have learned the rainfall runoff relation. In the case of urban flooding prediction based on a numerical analysis model, this provides accurate and precise results, but the problem is that

pre- and post-processing takes quite some time. In the case of data-driven models, one possibility is to employ a stochastic model that is based on data established in advance, including target values and real-time simulation or prediction using an artificial neural network (ANN). In particular, if the database used in a data-driven model is based on the result of deterministic model results, it carries the advantage of enhancing the accuracy of the target value's representation while simultaneously securing sufficient time for evacuation [7].

To date, studies using artificial neural networks, genetic algorithms, and deep learning models have been carried out variously with the purpose of predicting or controlling floods. According to Mosavi et al. [8], the application of machine learning to hydraulic and hydrology has increased. According to the same study, there is no absolutely predominant machine learning model, and it seems that useful machine learning techniques differ depending on the purpose, data, and results of the study. Jhong et al. [9] established an inundation prediction model by combining support vector machine (SVM) and multi-objective genetic algorithm (MOGA) based on effective materials concerning typhoons, and this made it possible to reduce the prediction time and to optimize input data. Granata et al. [10] conducted post-rainfall overflow analysis through support vector regression (SVR) and compared it with the results of the US Environmental Protection Agency's Storm Water Management Model (EAP-SWMM) to demonstrate that overflow had been overestimated in comparison to the SVR results. Tehrany et al. [11] used the SVR to analyze flood susceptibility with different kinds of kernel function. This research indicated that SVR could yield reliable assessment results for a flood susceptibility map. Chang et al. [12] predicted flood depth, enabling sufficient time for evacuation by using rainfall and stream runoff data and comparison with simulation results that indicated outstanding prediction capability. A prediction of stream runoff was carried out by Zhou et al. [13], using the radial basis function network (RBFN), extreme learning machine (ELM), and Elman network's ensemble technique. Empirical wavelet transform (EWT) was employed for data pre-processing, and the average monthly runoff of the stream subject to study was predicted. Deep learning techniques have been adopted in the water resource field to enhance floodgate predictions and to include more concepts in the model. Hu et al. [14] used long short-term memory (LSTM) for rainfall runoff simulation with 86 items of rainfall runoff pattern data. These results were compared with the ANN model to validate the superiority of the LSTM neural network. Rahman et al. [15] developed a method by integrating artificial neural network (ANN), logistic regression (LR), frequency ratio (FR), and analytical hierarchy process (AHP) for flood susceptibility assessment. The integrated LR-FR model showed high predictive power. This series of studies opens up new opportunities for planning and designing flood control measures.

Meanwhile, evacuation is an effective measure for minimizing damage and loss of life caused by flooding [16,17]. However, according to studies on the lessons that can be learned from disasters, it is apparent that, sometimes, evacuation to designated evacuation centers is not carried out [18–20]. The reasons for this were diverse and included problems in forecast and warning systems, in the location of evacuation centers and evacuation routes, and in evacuation center functions. Such studies throw doubt on the practicality of flood management policies, such as the preparation of evacuation maps based on maximum inundation scope and flood depth. Meanwhile, the problem of assigning location can be defined according to two factors—space and time—and, fundamentally, these two factors must be analyzed simultaneously [21]. In addition, the impacts of spatial and temporal changes in flooding can have significant consequences for the assessment of urban flood risks [22]. From this perspective, a few studies have recently conducted spatial and temporal analyses of urban flooding. Huang et al. [23] analyzed the spatial–temporal patterns of urban floods during the period of 2009–2015 in the central area of Guangzhou, China. Ahmad and Simonovic [22] mentioned that although it is necessary to quantify the uncertainty of spatial and temporal changes in flood inundation, this was hardly considered. Furthermore, they developed a map demonstrating the spatial and temporal variation in reliability vulnerability, robustness, and resiliency indices through fuzzy analysis. Chen et al. [24] integrated the flood risk factors for coastal lowland regions in 1970, 2004, and 2013 using a geographic information system (GIS) and analyzed flood hazard assessment maps for each of

those years based on multi-criteria decision analysis. Results demonstrated that flood occurrence was extremely variable in terms of time and space, depending on the associated flood risk factors. Therefore, considering such circumstances in general, the appropriate solution to the problem of evacuation route assignment should consist of real-time evacuation guidance following temporal and spatial inundation progress. This study aimed to propose a methodology for designating such real-time evacuation route guidance by analyzing spatial inundation progress following temporal inundation progress. We aimed to predict flood overflow using a dynamic artificial neural network and to analyze expected flood regions in advance through a two-dimensional submergence analysis of city regions. A methodology then was proposed for designating an evacuation route based on inundation progress and evacuation by walking hazard, and this was applied to the study area.

2. Materials and Methods

This study aimed to propose and apply a method for designating evacuation routes following temporal and spatial inundation progress due to doubt in the practicality and utilization of the method of preparing evacuation maps based on maximum inundation scope and flood depth.

The study comprised two stages, and the study flow can be seen in Figure 1 below.

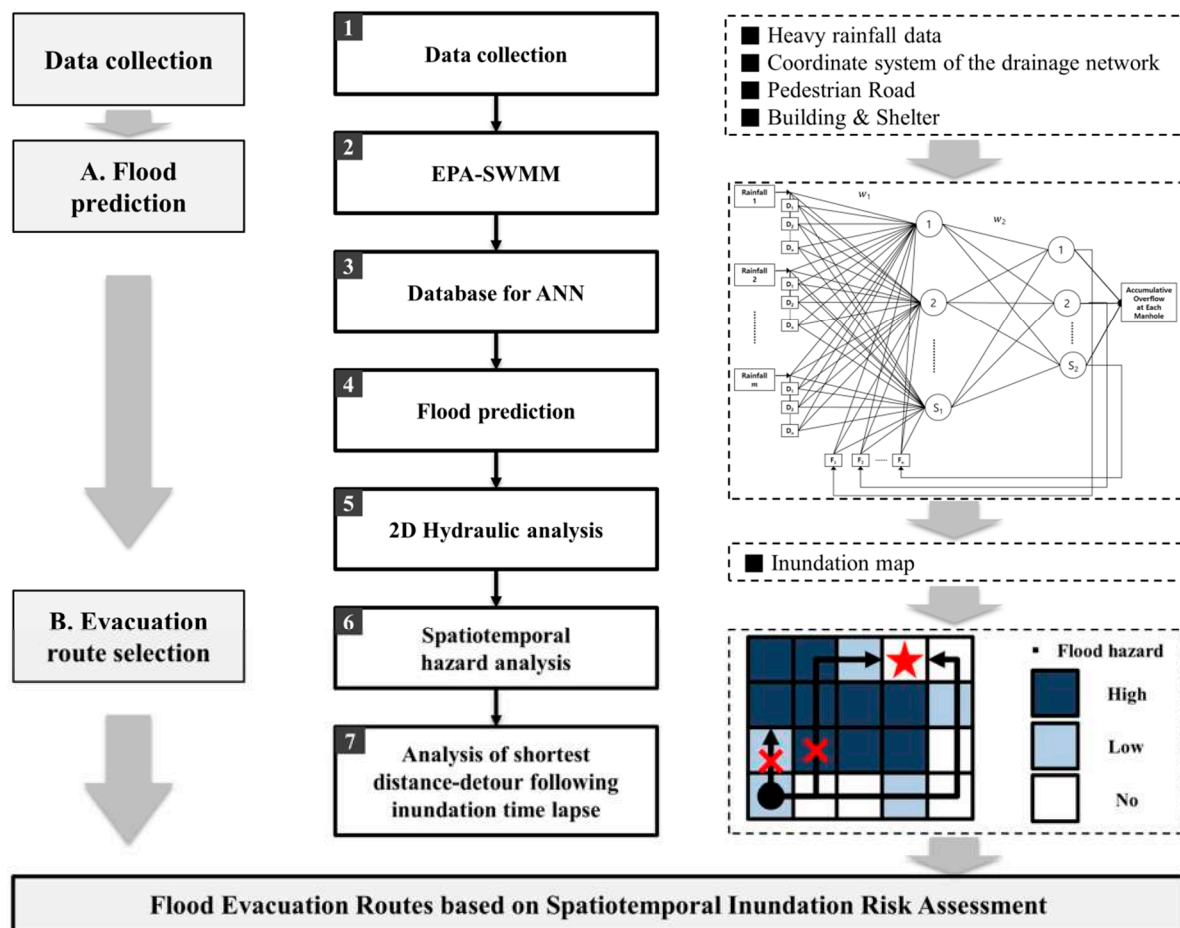


Figure 1. Flowchart of study methodology.

The first stage consisted of executing an inundation prediction for the study area. For this purpose, various rainfall scenarios were analyzed and a one-dimensional runoff interpretation was carried out with the SWMM provided by the EPA. SWMM is a one-dimensional urban runoff model based on hydraulic calculation with consideration of the drainage network system. In this study, SWMM was used to calculate the overflows in the urban basin, which were used as target data of the NARX

(Nonlinear Auto Regressive with eXogenous inputs) neural network. Accordingly, dynamic neural network input and learning were executed based on the accumulative rainfall–accumulative outflow and established so as to enable the prediction of accumulative overflow in real-time for specific rainfall instances. In this study, data concerning rainfall in the Gangnam region (Seoul city, Korea) which lasted for 6 h on 21 September 2010 were used and the accumulative overflow was predicted. A two-dimensional flood analysis was conducted based on predicted accumulative overflow and, in turn, the flood depth and velocity of flow were calculated for every 10 min period during this 2010 occurrence of heavy rain in the study area.

The second stage involved the prediction of a safe evacuation route in consideration of spatial and temporal demand change. Inundation scope by duration, flood depth, and flow velocity were utilized to assign a flood hazard grade for inundation scope, using the risk calculation method proposed by the UK Department for Environment, Food and Rural Affairs (DEFRA) and the Environment Agency [25]. The flood hazard grade classified the evacuation by walking possibility per duration by overlapping with the pedestrian road network within the study area. In addition, a methodology for identifying the shortest route from buildings within the expected flood region to the designated evacuation center, or a detour route, was proposed.

The materials utilized for the methodology for the evacuation route prediction proposed in this study are shown in Table 1 below.

Table 1. Required data.

Objective	Data	Properties	Data Collection Source
A. Flood prediction	Rainfall scenario	Rainfall data in 10 min units, duration	Calculation of probable rainfall and Meteorological Administration Agency data
	Overflow per manhole point	Overflow, duration of velocity of flow	SWMM interpretation result
	Predicted accumulative overflow	Accumulative overflow, duration of velocity of flow	Prediction result of NARX neural network
	Digital elevation map (DEM)	Grid coordinates and elevation	LiDAR detailed topographic map
B. Evacuation route selection	Building	Coordinates, purpose	www.juso.go.kr
	Evacuation shelter	Coordinates, area	https://safecity.seoul.go.kr
	Pedestrian road data	Coordinates	www.juso.go.kr
	Predicted flood data	Maximum and hourly flood depth per grid	Comprehensive analysis results of NARX and 2D immersion analysis program

3. Results

3.1. Study Area

In this study, the drainage sectors of Nonhyeon, Yeoksam, Seocho-3, Seocho-4, and Seocho-5, including the Gangnam station region, were selected as the study area. The total area of the study area was 7.4 km² and the areas of each drainage sector were 1.8 km² for Nonhyeon, 1.9 km² for Yeoksam, 1.8 km² for Seocho-3, 1.1 km² for Seocho-4, and 0.8 km² for Seocho-5 (Figure 2).

The study area, that is, the Gangnam station area, is relatively low in comparison with the other regions, and with its complex sewer network, it can be considered a place with a high inundation risk [26]. Moreover, it has a history of inundation in excess of 1.4 km² as evidenced by an inundation trace tap caused by heavy rainfall on 21 September 2010. The major manhole points selected in this study, taking account of the SWMM, overflow, and frequency, are depicted in Figure 3.

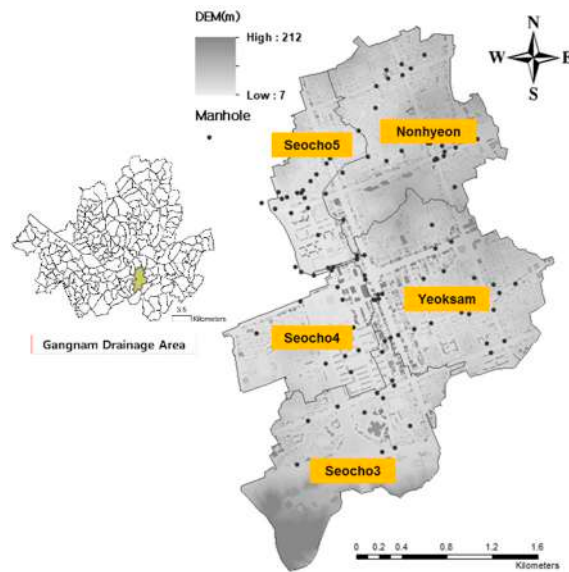


Figure 2. Study area: Gangnam drainage area, Seoul metropolitan city, Korea.



Figure 3. Establishment of Storm Water Management Model (SWMM) and major manhole points.

3.2. Artificial Neural Network-Based Inundation Forecasting

In this study, the flood overflow prediction model was established for the subject regions with sufficient lead time in order to provide two-dimensional inundation mapping for calculating the evacuation center location and evacuation route by hour. The NARX was used as the neural network. NARX is a circulation-type dynamic neural network with a feedback connection surrounding multiple neural network layers and has high learning ability for times series-based input data [27]. In this study, the NARX neural network consisted of an input layer, one hidden layer, and a layer for output. A single hidden layer neural network was used because there was insufficient data to use more than two hidden layers. The input layer contains rainfall input data and feedback target data.

The input rainfall data for NARX used 24 probability rainfalls with a duration of 1 h, 80 probability rainfalls with a duration of 2 and 3 h, and 18 observed rainfalls. The 24 sets of probability rainfall data correspond to durations of 1 h in 10 mm increments of rainfall, ranging from 50 mm to 100 mm in total. In addition, for rainfall, a rainfall duration of 2 or 3 h and a total of 80 rainfall events were used with Huff's temporal distribution data on rainfall frequencies of 2, 3, 5, 10, 20, 30, 50, 70, 80, and 100

year periods. Each accumulated rainfall event was made from a single sequence of data (Figure 4a). The target value data was used by accumulating SWMM simulation results for each rainfall event and making them into a single sequence of data (Figure 4b). Following this, the input value and target value of the neural network can be seen in Figure 4. The exogenous input for NARX training is accumulative overflow in this study. A total of 103 manholes were considered and over 122 scenarios, actual rainfall event data, and accumulative overflow data for each manhole were used for learning. Data for training, validation, and testing were used by randomly extracting 70%, 15%, and 15% from all data. To avoid overfitting, all of the aforementioned 122 rainfall runoff data sets were applied to NARX, and the datasets for training, validation, and testing were chosen randomly. The prediction of accumulative overflow for each manhole point was conducted for the 21 September 2010 rainfall.

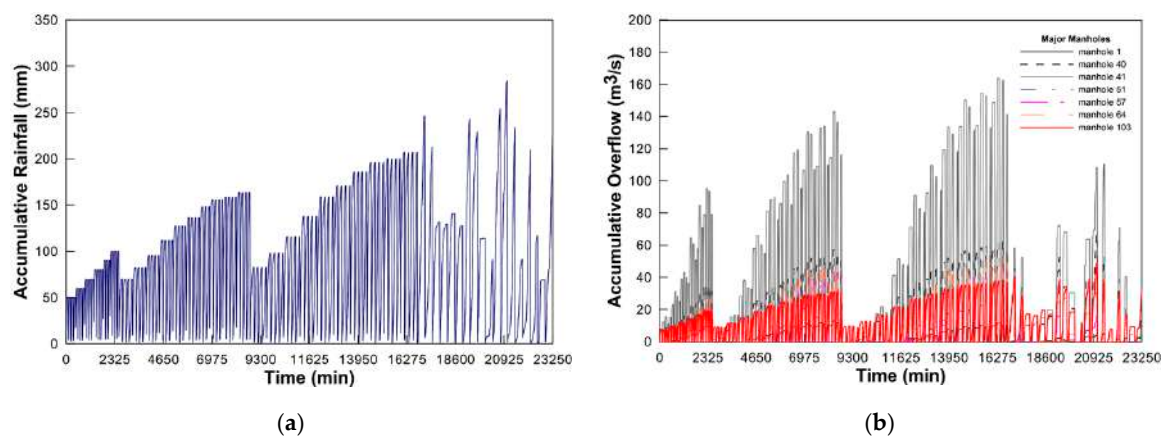


Figure 4. Flood prediction training data: (a) input data; (b) target data.

The NARX neural network has two main parameters; one is the delay time of input data (p) and the other is the delay time of target (feedback) data (q). In this study, the values of 1, 3, and 6 were applied to q parameter, and the value of 0 was used for p parameter. As the time delay of target data increased, the number of feedback input data was more plentiful. The accumulative overflow prediction by manhole point for the study region was conducted with prediction time delays of $T + 1$ (10 min), $T + 3$ (30 min), and $T + 6$ (60 min). The prediction time delay could be selected by the user. It was performed to confirm the prediction result of NARX according to the time delay. When using the $T + 1$ delay time, two target value data were fed back to the input layer, and when using the $T + 3$ delay time, four target value data were fed back to the input layer. When using $T + 6$ delay time, six target value data were fed back to the input layer. As the number of feedback data increased, the learning time increased. With regard to the 2010 rainfall event subject to prediction, the SMWW result was calculated at seven manhole points, and the NARX prediction was also made for seven manhole points (Figure 5).

The results from the NARX neural network were evaluated together with statistical analysis of the previously constructed input data. The performance was evaluated using the root mean square error (RMSE) to compare the SWMM results with prediction model results as a basic index, as defined in Equation (1). The RMSE is an index that quantifies the error between the simulation value and prediction result. The RMSE at each manhole is shown in Table 2.

$$\text{RMSE} = \sqrt{\frac{\sum (Q_{\text{simulated}} - Q_{\text{predicted}})^2}{n}} \quad (1)$$

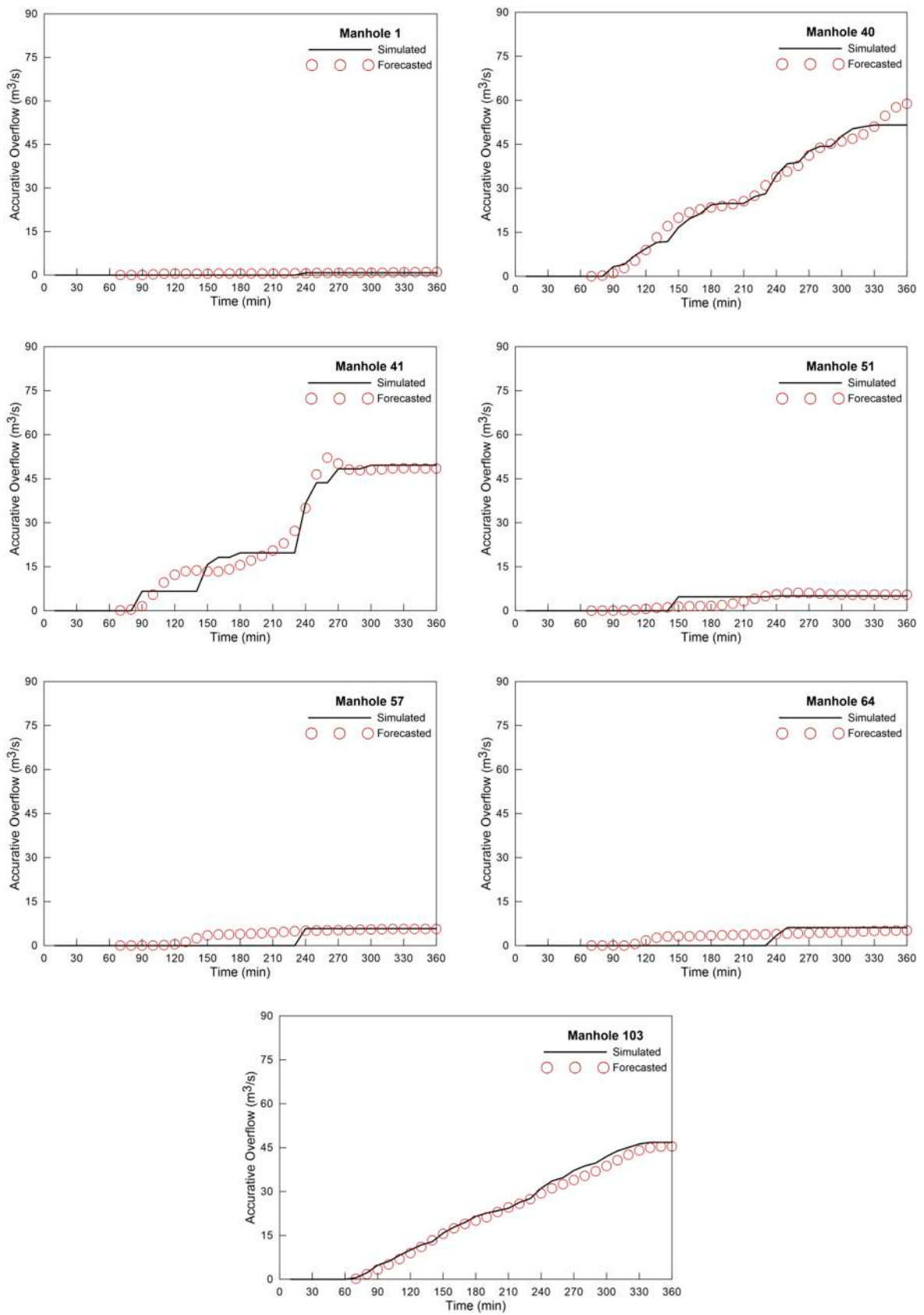


Figure 5. Accumulative overflow prediction results.

Table 2. Root mean square error (RMSE) at each manhole (21 September 2010 event).

Classification		Root Mean Square Error (m ³ /s) at Each Manhole						
		Manhole 1	Manhole 40	Manhole 41	Manhole 51	Manhole 57	Manhole 64	Manhole 103
Time delay	T + 1	0.606	2.44	4.702	1.008	2.992	4.626	1.134
	T + 3	0.270	3.491	4.131	0.628	1.677	2.471	1.013
	T + 6	0.285	3.918	3.157	1.375	1.945	2.059	1.532

RMSE observations standard deviation ratio (RSR) was also considered for more statistical error analysis. RSR standardizes RMSE using the standard deviation in the observations, and it combines both an error index and some additional information. RSR was calculated as the ratio of the RMSE to the standard deviation of the measured data, as shown in Equation (2).

$$RSR = \frac{\sqrt{\sum (Q_{\text{simulated}} - Q_{\text{predicted}})^2}}{\sqrt{\sum (Q_{\text{simulated}} - Q_{\text{simulated.mean}})^2}} \tag{2}$$

The coefficient of determination (R²) was analyzed in addition to quantitative error analysis. The coefficient of determination is a square value of the correlation coefficient (R) and ranges from 0 ≤ R² ≤ 1. This indicates that the simulated and predicted values have some constant tendencies, but the two values are not identical.

The Nash–Sutcliffe efficiency coefficient (NSEC) was used to evaluate the prediction performance of the model presented in this paper. The NSEC is a standardized value of residual relative degree that ranges from −∞ < NSEC ≤ 1. The closer the NSEC value is to 1, the more it indicates an accurate result of the prediction model. In Equations (1)–(3), Q_{simulated} refers to the simulated flow result, Q_{predicted} refers to the predicted flow result, and Q̄_{predicted} refers to the mean of the predicted flow result. The values of RSR, NSEC, and R-square are represented in Table 3.

$$NSEC = 1 - \frac{\sum (Q_{\text{simulated}} - Q_{\text{predicted}})^2}{\sum (Q_{\text{simulated}} - \bar{Q}_{\text{predicted}})^2} \tag{3}$$

Table 3. Total overflow error analysis.

Classification	RSR			Nash–Sutcliffe			R-Square		
	T + 1	T + 3	T + 6	T + 1	T + 3	T + 6	T + 1	T + 3	T + 6
Time delay	0.199	0.129	0.151	0.963	0.985	0.979	0.969	0.985	0.982

Accumulative overflow prediction results confirmed that, when compared to the results of error by delay time analysis, the longer the predicted delay time, the better the prediction ability. In the case of two-dimensional interpretation through predicted accumulative overflow, a 60 min prediction result delay time was used as well as LiDAR’s detailed topographical data and composite roughness coefficient. Two-dimensional interpretation was conducted using the established topographical data and predicted overflow data, and a 10 min simulation of the 21 September 2010 rainfall event with 6 h duration was conducted. The process involved is shown in Figure 6.

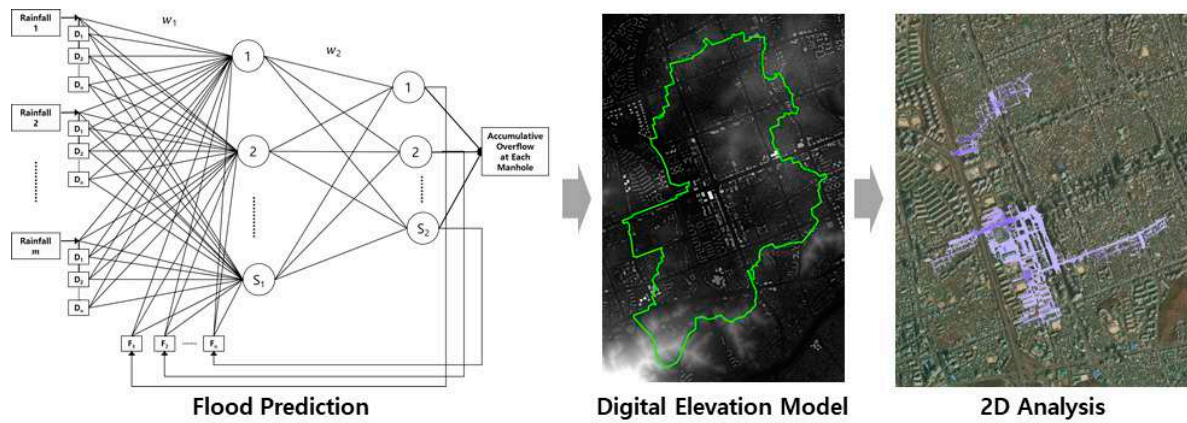


Figure 6. Flood prediction-based inundation map.

The results of conducting two-dimensional interpretation based on accumulative overflow prediction results are given in Figure 7, and the prediction result appropriateness was validated through the National Disaster Management System (NDMS) and inundation trace map. The suitability of the simulation results and the flooding trace was found to be 81%. Therefore, the inundation simulation results applied in this study were deemed to be feasible for application as baseline data for selecting evacuation routes by recurrence hour and evacuation center.

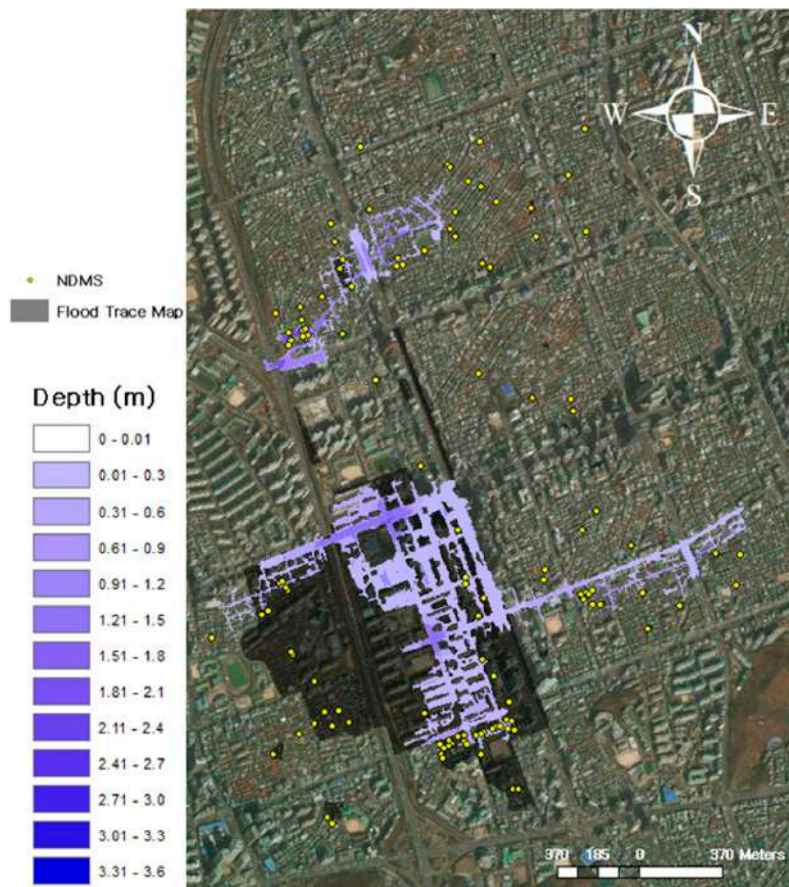


Figure 7. Inundation map results.

3.3. Spatial and Temporal Flood Hazard Analysis

Studies aiming to estimate the scale of damage loss arising from flooding have been carried out comprehensively, including such approaches as the development of the mortality rate function (e.g., [28,29]). However, studies of evacuation under life-threatening circumstances caused by floods are rare [30–33]. Studies of the direct and indirect effect of flooding on people have focused primarily on the inundation depth and velocity for evacuation by walking [25] (Table 4).

Table 4. Hazards as a function of inundation depth and velocity [25].

$d \times (v + 0.5)$	Flood Hazard Degree	Description
<0.75	Low	Caution “Flood zone with shallow flowing water or deep standing water”
0.75–1.25	Moderate	Dangerous for some (i.e., children) “Danger: flood zone with deep or fast flowing water”
1.25–2.5	Significant	Dangerous for most people “Danger: flood zone with deep fast flowing water”
>2.5	Extreme	Dangerous for all “Extreme danger: flood zone with deep fast flowing water”

DEFRA and the Environment Agency [25] mentioned the need for the classification of flood hazards and proposed a classification of inundation hazards that can be seen in Table 4. Otherwise, research into evacuation speed during inundation or risk classification have been carried out in preceding studies such as Kang [20], OFAT et al. [30], Ishigaki [31], Ishigaki et al. [32], and Lee et al. [34]. In this study, DEFRA and the Environment Agency’s [25] risk classification method was applied based on inundation depth per hourly progress and velocity of flow via artificial neural network, and the flood hazard result obtained is shown in Figure 8 below. This method makes it easy to evaluate flood hazards based on the depth and flow velocity of the two-dimensional flood analysis and NARX results. Other previous research results mentioned above can provide data for categorizing flood hazards, but it is difficult to generalize because there are few test subjects, and experiments are conducted at characteristic places.

After 1 h, only a small district was flooded and there were no regions that exceeded 0.75 in terms of risk classification. However, after 2 h, there were some regions that exceeded a risk classification of 0.75. As can be seen in Table 5, regions with inundation risk increased rapidly between 1~2 h and 2~3 h.

Table 5. Time-dependent changes in flood hazard area.

Classification	1 h	2 h	3 h	4 h	5 h	6 h	7 h	8 h
Area (m ²)	0	71,625	150,600	150,825	150,925	151,475	151,575	151,750
Increment (m ²)	-	71,625	78,975	225	100	550	100	175

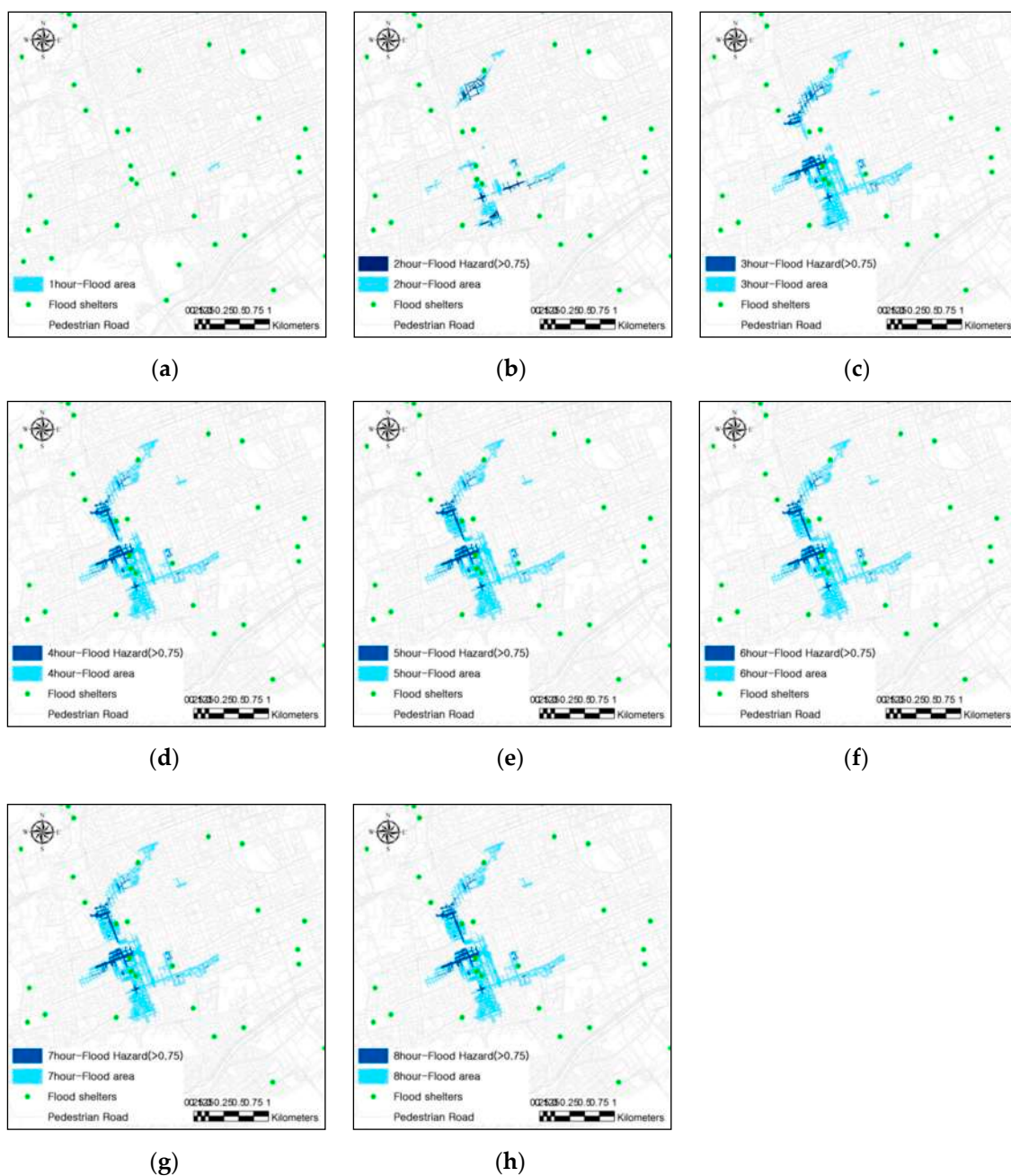


Figure 8. Flood hazard spatial and temporal variation analysis results (1~8 h). (a) 1 h elapsed; (b) 2 h elapsed; (c) 3 h elapsed; (d) 4 h elapsed; (e) 5 h elapsed; (f) 6 h elapsed; (g) 7 h elapsed; (h) 8 h elapsed.

3.4. Evacuation Route Analysis

In order to designate an evacuation route, there must be a point of departure and a destination. In this study, a building within the maximum expected flood scope was set as the demand point. The destination was the flood evacuation facility designated within the subject site. The area of maximum expected flood scope in the study area, Gangnam station region, is 772,425 m², and 1153 buildings are distributed within the expected scope. Location-allocation analyses have been utilized to establish evacuation plans, including evacuation routes in multiple preceding studies, but this study excluded quantitative analysis of evacuation demand and evacuation facility capacity.

Furthermore, as the assumption was made that evacuees would evacuate to the closest evacuation facility, the closest facility analysis was utilized to assign the evacuation route. In addition, prohibited pedestrian sector by hourly progress was set by overlapping flood risk regions identified in Section 3.3

with road data, and was utilized as a barrier of network analysis. The results of the evacuation route temporal and spatial variable analysis are given in Figure 9.

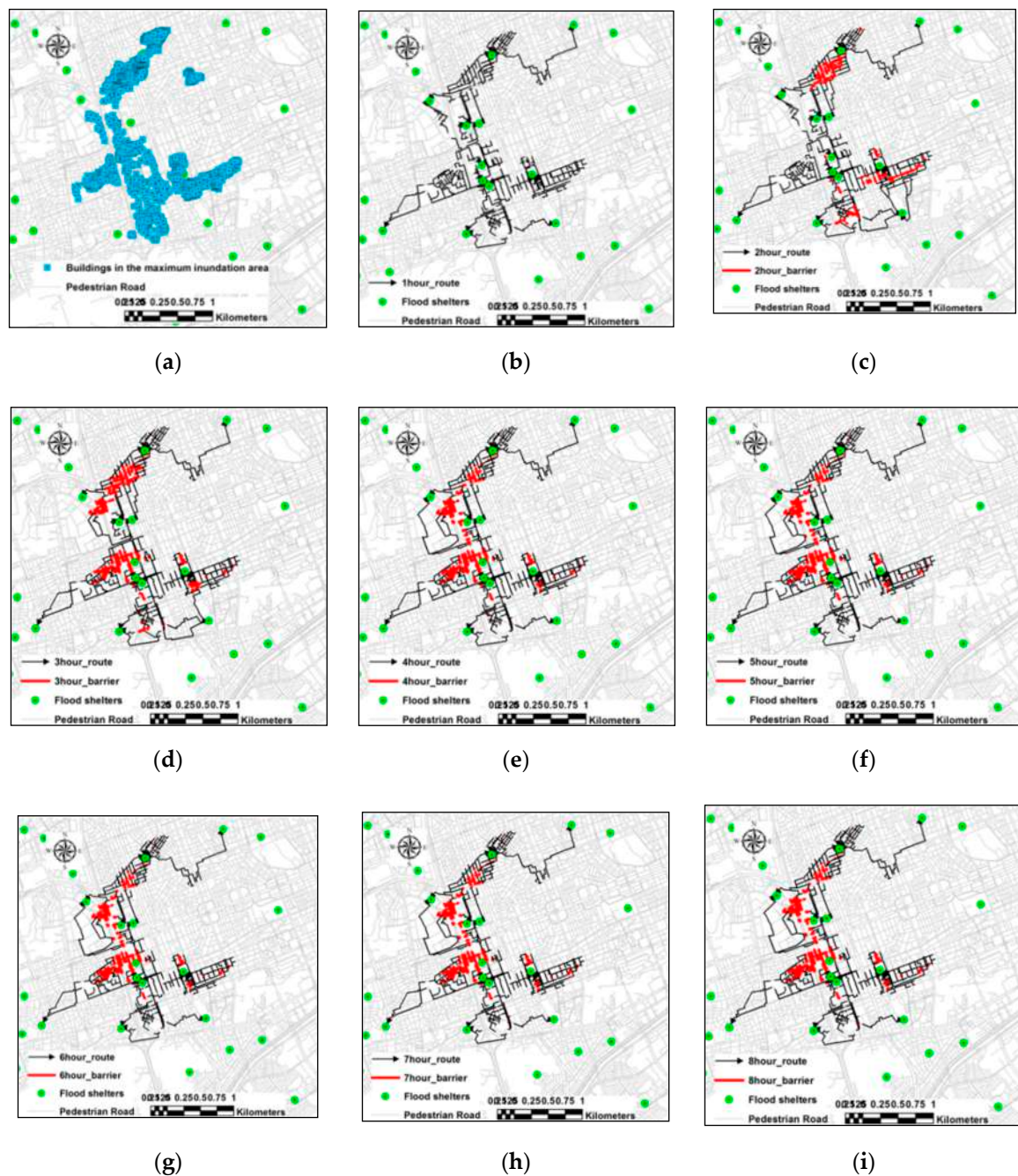


Figure 9. Evacuation route spatial and temporal variation analysis results (1~8 h). (a) Buildings in areas where flooding is expected; (b) 1 h elapsed; (c) 2 h elapsed; (d) 3 h elapsed; (e) 4 h elapsed; (f) 5 h elapsed; (g) 6 h elapsed; (h) 7 h elapsed; (i) 8 h elapsed.

In the event that evacuation is not carried out prior to flooding, the pedestrian evacuation hazard region increases with the inundation progress, and the number of buildings from which evacuation by walking was deemed impossible (dangerous) is shown in Table 6 below. After 2 h, 200 of the 1153 buildings distributed within the maximum inundation scope were deemed dangerous for evacuation by walking. The time when buildings would be predicted to have the highest ratio of evacuation by

walking danger would be after 3 h (22.12%). Results further indicated that an average of 15.51% of buildings would be expected to face difficulty in terms of evacuation by walking.

Table 6. Analysis results for buildings with possibility of evacuation by walking by hourly progress.

Classification	Number of Buildings in Flooded Areas		
	Buildings Where Evacuation by Walking is Possible (a)	Buildings Where Evacuation by Walking not Possible (b)	Percentage of Buildings Where Evacuation by Walking not Possible (b/a + b)
1 h	1153	0	0.00%
2 h	953	200	17.35%
3 h	898	255	22.12%
4 h	957	196	17.00%
5 h	958	195	16.91%
6 h	958	195	16.91%
7 h	958	195	16.91%
8 h	958	195	16.91%

Analyzing the evacuation route under the assumption that evacuation by walking would cause a detour into dangerous regions, leading to the closest evacuation facility, the evacuation by walking distance by hourly progress results are shown in Figure 10 below. Buildings where evacuation by walking is impossible have been excluded from the evacuation by walking distance analysis in Table 6. Prior to flooding, the average evacuation distance from 1153 buildings to the closest evacuation facility was 478.85 m, and the longest evacuation distance was 1183.30 m. In the event of evacuation by avoiding regions where evacuation by walking is impossible (dangerous) as flooding progresses, it was determined that there would not be a significant change in the average walking distance by hourly progress.

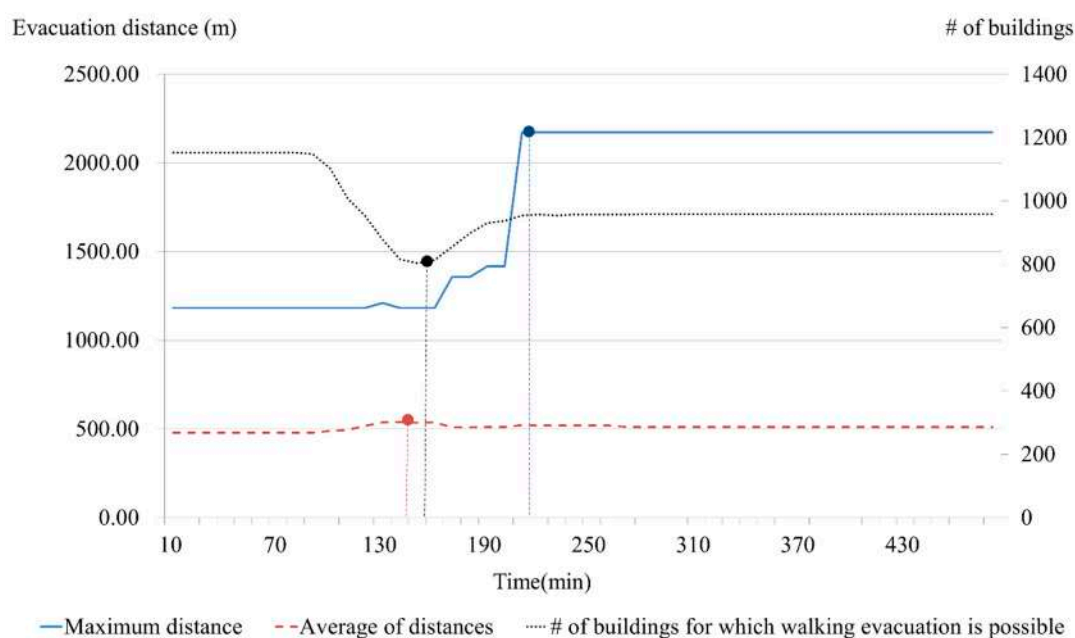


Figure 10. Time-dependent changes in pedestrian evacuation distance and number of buildings in the flooded area for which evacuation by walking is possible.

However, analysis indicated that the longest evacuation distance would increase significantly after 2 ~ 4 h, and that the occurrence of evacuation by walking hazard region (inundated buildings) following inundation progress increased rapidly between 90 ~ 160 min, and then dropped slightly.

Accordingly, the average evacuation by walking distance reached its maximum value at 140 min, but the maximum evacuation by walking distance occurred at 210 min. The number of buildings where evacuation by walking was impossible following evacuation by walking hazard region reached a maximum at 150 min.

4. Discussion

4.1. Inundation Forecasting

The purpose of this study was to identify an evacuation route with consideration of spatial inundation progress following the time lapse related to flooding after heavy rainfall. Moreover, inundation progress was predicted by using a dynamic artificial neural network because, ultimately, the aim was to provide a real-time evacuation route. This is because urban flood predictions based on numerical analysis models provide accurate and precise results, but the necessary pre- and post-processing takes quite some time. The accumulative overflow for manhole points was predicted through use of the NARX neural network, and after conducting two-dimensional inundation interpretation with the predicted value, an inundation map by hour was created. Comparing the inundation trace map and the NDMS resident report point concerning the two-dimensional interpretation results, appropriateness was judged to be 81%. By predicting the two-dimensional model input data with the NARX neural network, it was possible to save time following one-dimensional urban runoff interpretation. In this study, the inundation prediction via NARX neural network was completed within 3 s, and in the same computer environment, an inundation prediction via SWMM takes approximately 10 min. It can be applied to other river basins or stream floods if rainfall, flood data, and a spatial distribution technique of flood depth are provided. The rainfall, flood volume, and flood depth data can be calculated through a numerical analysis model or can be obtained from observed values. In this study, the flood depth was predicted through a flood volume prediction system using NARX and by linking a two-dimensional flood analysis model. It can be applied to other water basins or flood types if the data can be pre-processed sufficiently.

In this study, the total flood volume of the rainfall input data was predicted in real-time using the NARX neural network. This was then inputted into a two-dimensional flood analysis program to calculate the flood map. It is different from other studies that predict the flood volume only for rainfall events. Also, it has an advantage in that the predicted total flood volume is the sum of the flood volumes predicted for each of the manhole points and so the flood risk for each point can be identified quickly. Since the time may be depicted in the two-dimensional flood analysis simulation, if the spatial distribution of the flood depth can be predicted in real-time, it could be a very practical method. However, for the preparation of a two-dimensional inundation map in this study, the real-time provision of evacuation route information via numerical analysis was still poor.

4.2. Flood Hazard and Walking Evacuation

An evacuation route was selected under the assumption that buildings distributed within the maximum inundation scope were set as representing evacuation demand, and that people would evacuate to the closest evacuation facility. In the case of the study area, it was observed that buildings where evacuation by walking became impossible following inundation progress increased significantly after 2 ~ 3 h. Regarding the detour evacuation route distance, it was observed that this increased significantly after 2 ~ 4 h. Such analysis results show that adaptability and safety have to be ensured in inundated situations by planning in a flexible manner following the occurrence and change of evacuation by walking hazard regions in the process of selecting an evacuation route. Considering such results, the methodology of this study has been deemed usable for the purposes of establishing an evacuation plan that takes into account the situation after a disaster occurs. Although it can serve to contribute to the achievement of substantiation when establishing evacuation plans in the future, integrated analysis of occurrence and change in the evacuation by walking hazard region, distribution

of buildings within the expected inundation region (evacuation demander), and the road network is required for this. Moreover, as 10 min and 1 h inundation prediction data were utilized to assign evacuation routes by hour in this study, the inundation progress of each point was not analyzed in detail. Therefore, it is recommended that studies such as the development of a methodology for evaluating the flood risk of pedestrian evacuation in a road network by analyzing the flooding progress in detail (e.g., trend analysis and space–time cluster analysis) be conducted. Such a methodology could lead to the development of an evacuation decision model for buildings in the expected flooding area according to the progress of flooding.

The flood hazard classification method applied in this study [25] can be applied to various flood types such as flash floods, coastal floods, and urban floods because it uses the relationship between flood depth and flow velocity. However, studies based on experiments [20,31,32,34] suggest that the inundation depth of a specific location (e.g., underground or stairs) or water level that an adult can walk in is 30 ~ 50 cm. Therefore, careful notice must be taken when applying the flood hazard risk classification of DEFRA and the Environment Agency [25]. Also, it is necessary to modify the standards related to flood hazard to people through the collection of experimental data related to the safety of people during a flood according to the specific location or their gender, age, and disability.

Evacuees often choose the wrong direction (due to personal wrong choice or leader follow effect) due to panic or lack of evacuation information. To prevent this, it is important to provide real-time evacuation information to evacuees. In this respect, real-time evacuation guidance using mobile applications is drawing attention from researchers (e.g., [35–37]). By applying the methodology proposed in this study, it is possible to minimize the casualties caused during the evacuation process by selecting the evacuation route when flooding occurs. However, for real-time evacuation guidance, the role of IoT (Internet of Things) technologies is important because it is necessary to provide the evacuee's location-based evacuation routes. Evacuation guidance and information related to IoT technologies have recently attracted the attention of researchers and have been studied by Krytska et al. [38], Zualkernan et al. [39], and Yin et al. [40], for example.

Meanwhile, “in rapid-onset disasters the time needed for evacuation is crucial” [41]. However, in large-scale evacuation situations, time delays occur due to congestion (e.g., bottleneck effect). Phased evacuation was suggested in a simulation-based previous study [42–44] as a method to reduce the time delay due to congestion in an evacuation situation. Since this study focuses on the prediction of the changing pattern of urban flooding according to the progress of flooding, it can be used to establish a phased evacuation strategy.

5. Conclusions

This study aimed to perform inundation map forecasting with artificial neural network-based methodology. In addition, it proposed a methodology for selecting an evacuation route by considering temporal and spatial evacuation by walking hazard. Previous studies have not focused on the necessity of temporal and spatial changes in the flood evacuation route, but this study once again demonstrates that need. In addition, the evacuation route is determined according to the hazard of walking evacuation, thus minimizing the hazard for evacuees during the evacuation process. The proposed methodology is not a field test-based or practical application method for establishing a flood evacuation plan, but it shows great potential in terms of efficiency. For example, if a further study can predict not only urban runoff but also inundation map, the evacuation route can be calculated more quickly. In addition, the proposed methodology can be extended to a model for calculating the spatial and temporal changes in evacuation demand according to the flooding progress. It is envisaged that this research will provide a basis for future comprehensive and cohesive research on flood evacuation strategies according to the progress of flooding. In turn, research will lead to better preparedness and response to flood evacuation problems.

Author Contributions: All authors contributed extensively to the work. Y.H.L. and W.H.H. conceptualized and designed the study. Y.H.L. and H.I.K. produced the data required to apply the methodology to the study area and

conducted the model simulation, validation, and writing—original draft preparation. Y.H.L. and H.I.K. analyzed the results, completed the manuscript, wrote the review, and conducted editing. K.Y.H. and W.H.H. supervised the project and acquired the funding. All authors have read and agreed to the published version of the manuscript.

Funding: This research was funded by the Korea Ministry of Environment (MOE).

Acknowledgments: This work was supported by the Korea Environment Industry & Technology Institute (KEITI) through the Water Management Research Program, funded by the Korea Ministry of Environment (MOE) (79609).

Conflicts of Interest: The authors declare no conflict of interest.

References

1. Liu, X.; Lim, S. A Spatial Analysis Approach to Evacuation Management: Shelter Assignment and Routing; Research@Locate'15, Brisbane, Australia. 10–12 March 2015. Available online: <http://ceur-ws.org> (accessed on 23 July 2020).
2. Hwang, K.; Schuetze, T.; Amoruso, F.M. Flood Resilient and Sustainable Urban Regeneration Using the Example of an Industrial Compound Conversion in Seoul, South Korea. *Sustainability* **2020**, *12*, 918. [[CrossRef](#)]
3. Jha, A.K.; Bloch, R.; Lamond, J. *Cities and Flooding: A Guide to Integrated Urban Flood Risk Management for the 21st Century*; The World Bank: Washington, DC, USA, 2012.
4. Atmojo, P.S.; Sachro, S.S. Disaster management: Selections of evacuation routes due to flood disaster. *Procedia Eng.* **2017**, *171*, 1478–1485. [[CrossRef](#)]
5. Lee, B. A study on the characteristics and composition direction of urban flood control system. *Water Future* **2006**, *39*, 50–54.
6. Kim, J.; Kuwahara, Y.; Kumar, M. A DEM-based evaluation of potential flood risk to enhance decision support system for safe evacuation. *Nat. Hazards* **2011**, *59*, 1561–1572. [[CrossRef](#)]
7. Kim, H.I.; Keum, H.J.; Han, K.Y. Real-Time Urban Inundation Prediction Combining Hydraulic and Probabilistic Methods. *Water* **2019**, *11*, 293. [[CrossRef](#)]
8. Mosavi, A.; Ozturk, P.; Chau, K.W. Flood Prediction Using Machine Learning Models: Literature Review. *Water* **2018**, *10*, 11. [[CrossRef](#)]
9. Jhong, B.; Wang, J.; Lin, G. Improving the long lead-time inundation forecasts using effective typhoon characteristics. *Water Resour. Manag.* **2016**, *30*, 4247–4271. [[CrossRef](#)]
10. Granata, F.; Gargano, R.; De Marinis, G. Support vector regression for rainfall-runoff modeling in urban drainage: A comparison with the EPA's storm water management model. *Water* **2016**, *8*, 69. [[CrossRef](#)]
11. Tehrany, M.S.; Pradhan, B.; Mansor, S.; Ahmad, N. Flood Susceptibility Assessment Using GIS-based Support Vector Machine Model with Different Kernel Types. *Catena* **2015**, *125*, 91–101. [[CrossRef](#)]
12. Chang, L.; Amin, M.Z.M.; Yang, S.; Chang, F. Building ANN-based regional multi-step-ahead flood inundation forecast models. *Water* **2018**, *10*, 1283. [[CrossRef](#)]
13. Zhou, J.; Peng, T.; Zhang, C.; Sun, N. Data pre-analysis and ensemble of various artificial neural networks for monthly streamflow forecasting. *Water* **2018**, *10*, 628. [[CrossRef](#)]
14. Hu, C.; Wu, Q.; Li, H.; Jian, S.; Li, N.; Lou, Z. Deep learning with a long short-term memory networks approach for rainfall-runoff simulation. *Water* **2018**, *10*, 1543. [[CrossRef](#)]
15. Rahman, M.; Ningsheng, C.; Islam, M.M.; Dewan, A.; Iqbal, J.; Washakh, R.M.A.; Shufeng, T. Flood Susceptibility Assessment in Bangladesh Using Machine Learning and Multi-criteria Decision Analysis. *Earth Syst. Environ.* **2019**, *3*, 585–601. [[CrossRef](#)]
16. Na, L.; Xueyan, S.; Mingliang, Q. A bi-objective evacuation routing engineering model with secondary evacuation expected costs. *Syst. Eng. Procedia* **2012**, *5*, 1–7. [[CrossRef](#)]
17. Lim, H., Jr.; Lim, M.B.; Piantanakulchai, M. A review of recent studies on flood evacuation planning. *J. East. Asia Soc. Transp. Stud.* **2013**, *10*, 147–162.
18. Shekhar, S.; Yang, K.; Gunturi, V.M.; Manikonda, L.; Oliver, D.; Zhou, X.; George, B.; Kim, S.; Wolff, J.M.; Lu, Q. Experiences with evacuation route planning algorithms. *Int. J. Geogr. Inf. Sci.* **2012**, *26*, 2253–2265. [[CrossRef](#)]
19. Mayunga, J.S. Assessment of public shelter user's satisfaction: Lessons learned from south-central Texas flood. *Nat. Hazards Rev.* **2012**, *13*, 82–87. [[CrossRef](#)]
20. Kang, S. Study on refuge behavior and its critical inundation depth in low area. *J. Korean Soc. Civ. Eng.* **2003**, *23*, 561–565.

21. Arabani, A.B.; Farahani, R.Z. Facility location dynamics: An overview of classifications and applications. *Comput. Ind. Eng.* **2012**, *62*, 408–420. [[CrossRef](#)]
22. Ahmad, S.S.; Simonovic, S.P. Spatial and temporal analysis of urban flood risk assessment. *Urban Water J.* **2013**, *10*, 26–49. [[CrossRef](#)]
23. Huang, H.; Chen, X.; Zhu, Z.; Xie, Y.; Liu, L.; Wang, X.; Wang, X.; Liu, K. The changing pattern of urban flooding in Guangzhou, China. *Sci. Total Environ.* **2018**, *622*, 394–401. [[CrossRef](#)] [[PubMed](#)]
24. Chen, H.; Ito, Y.; Sawamukai, M.; Su, T.; Tokunaga, T. Spatial and temporal changes in flood hazard potential at coastal lowland area: A case study in the Kujukuri Plain, Japan. *Nat. Hazards* **2016**, *84*, 1513–1527. [[CrossRef](#)]
25. DEFRA and the Environment Agency. *R&D Outputs: Flood Risks to People. Phase 2. FD2321/TR1 The Flood Risks to People Methodology*; Department for Environment Food and Rural Affairs and the Environment Agency: London, UK, 2006.
26. Choi, S.; Yoon, S.; Lee, B.; Choi, Y. Evaluation of high-resolution QPE data for urban runoff analysis. *J. Korea Water Resour. Assoc.* **2015**, *48*, 719–728. [[CrossRef](#)]
27. Shen, H.; Chang, L. Online multistep-ahead inundation depth forecasts by recurrent NARX networks. *Hydrol. Earth Syst. Sci.* **2013**, *17*, 935. [[CrossRef](#)]
28. Penning-Rowsell, E.; Floyd, P.; Ramsbottom, D.; Surendran, S. Estimating injury and loss of life in floods: A deterministic framework. *Nat. Hazards* **2005**, *36*, 43–64. [[CrossRef](#)]
29. Jonkman, S.; Vrijling, J.; Vrouwenvelder, A. Methods for the estimation of loss of life due to floods: A literature review and a proposal for a new method. *Nat. Hazards* **2008**, *46*, 353–389. [[CrossRef](#)]
30. OFEE, OFAT, OFEFP, 1997: *Prise en Compte des Dangers dus aux Crues dans le Cadre des Activités de l'Aménagement du Territoire. Recommandations*, Office Fédéral de l'Économie des Eaux (OFEE), Office Fédéral de l'Aménagement du Territoire (OFAT), Office fédéral de l'Environnement, des Forêts et du Paysage (OFEFP). Available online: http://www.planat.ch/fileadmin/PLANAT/planat_pdf/alle_2012/1996-2000/Lateltin_1997_-_Prise_en_compte_des_dangers.pdf (accessed on 23 March 2020).
31. Ishigaki, T. Evacuation criteria during urban flooding in underground space. In Proceedings of the 11th ICUD, Edinburgh, UK, 31 August–5 September 2008.
32. Ishigaki, T.; Baba, Y.; Toda, K.; Inoue, K. Experimental study on evacuation from underground space in urban flood. In Proceedings of the Korea Water Resources Association Conference, Iksan, Korea, 20–21 May 2005; pp. 261–262.
33. Jonkman, S.; Penning-Rowsell, E. Human Instability in Flood Flows 1. *JAWRA J. Am. Water Resour. Assoc.* **2008**, *44*, 1208–1218. [[CrossRef](#)]
34. Lee, H.; Hong, W.; Lee, Y. Experimental study on the influence of water depth on the evacuation speed of elderly people in flood conditions. *Int. J. Disaster Risk Reduct.* **2019**, *39*, 101198. [[CrossRef](#)]
35. Zhang, P.; Liu, Y.; Yang, R.; Zhang, H.; Gong, Z. Improving urban traffic evacuation capability in emergency response by using smart phones. In Proceedings of the Asia-Pacific Web Conference, Suzhou, China, 23–25 September 2016; Springer: Cham, Switzerland, 2016; pp. 241–252.
36. Kairupan, I.; Huang, Z.Y.; Chang, H.C.; Chang, C.W. Emergency navigation and alarm with flooding models—A real case study of Manado City. In Proceedings of the 2016 International Conference on Communication Problem-Solving (ICCP), Taipei, Taiwan, 7–9 September 2016; pp. 1–2.
37. Krajewski, W.F.; Ceynar, D.; Demir, I.; Goska, R.; Kruger, A.; Langel, C.; Mantilla, R.; Niemeier, J.; Quintero, F.; Seo, B.C.; et al. Real-time flood forecasting and information system for the state of Iowa. *Bull. Am. Meteorol. Soc.* **2017**, *98*, 539–554. [[CrossRef](#)]
38. Krytska, Y.; Skarga-Bandurova, I.; Velykzhanin, A. IoT-based situation awareness support system for real-time emergency management. In Proceedings of the 9th IEEE International Conference on Intelligent Data Acquisition and Advanced Computing Systems: Technology and Applications (IDAACS), Bucharest, Romania, 21–23 September 2017; Volume 2, pp. 955–960.
39. Zualkernan, I.A.; Aloul, F.A.; Sakkia, V.; Al Noman, H.; Sowdagar, S.; Al Hammadi, O. An IoT-based Emergency Evacuation System. In Proceedings of the IEEE International Conference on Internet of Things and Intelligence System (IoTIS), Bali, Indonesia, 5–7 November 2019; pp. 62–66.
40. Yin, L.; Chen, J.; Zhang, H.; Yang, Z.; Wan, Q.; Ning, L.; Hu, J.; Yu, Q. Improving emergency evacuation planning with mobile phone location data. *Environ. Plan. B Urban. Anal. City Sci.* **2020**, *47*, 964–980. [[CrossRef](#)]

41. Kubisch, S.; Stötzer, J.; Keller, S.; Bull, M.T.; Braun, A. Combining a social science approach and GIS-based simulation to analyse evacuation in natural disasters: A case study in the Chilean community of Talcahuano. In Proceedings of the 16th International Conference on Information Systems for Crisis Response and Management (ISCRAM 2019), Valencia, Spain, 19–22 May 2019.
42. Li, M.; Xu, J.; Li, J.; Liu, X.; Ru, H.; Sun, C. A model for phased evacuations for disasters with spatio-temporal randomness. *Int. J. Geogr. Inf. Sci.* **2019**, *33*, 922–944. [[CrossRef](#)]
43. Zhang, Z.; Spansel, K.; Wolshon, B. Effect of phased evacuations in megaregion highway networks. *Transp. Res. Rec. J. Transp. Res. Board* **2014**, *2459*, 101–109. [[CrossRef](#)]
44. O’Shea, T.; Bates, P.; Neal, J. An agent-based model for flood risk warning. *Nat. Hazards Earth Syst. Sci. Discuss.* **2019**, 1–32. [[CrossRef](#)]



© 2020 by the authors. Licensee MDPI, Basel, Switzerland. This article is an open access article distributed under the terms and conditions of the Creative Commons Attribution (CC BY) license (<http://creativecommons.org/licenses/by/4.0/>).

ARTICLES FOR FACULTY MEMBERS

RESCUE VESSEL OPERATION FOR FLOOD EVACUATION PROTOCOL

Title/Author	Research on Optimal Model of Maritime Search and Rescue Route for Rescue of Multiple Distress Targets / Ho, W. C., Shen, J. H., Liu, C. P., & Chen, Y. W.
Source	<i>Journal of Marine Science and Engineering</i> Volume 10 Issue 4 (2022) Pages 1-16 https://doi.org/10.3390/jmse10040460 (Database: MDPI)

Article

Research on Optimal Model of Maritime Search and Rescue Route for Rescue of Multiple Distress Targets

Wen-Chih Ho ¹, Jian-Hung Shen ¹, Chung-Ping Liu ^{2,*} and Yung-Wei Chen ¹

¹ Department of Marine Engineering, National Taiwan Ocean University, Keelung City 202301, Taiwan; 20766003@email.ntou.edu.tw (W.-C.H.); 20666006@email.ntou.edu.tw (J.-H.S.); cyw0710@ntou.edu.tw (Y.-W.C.)

² Department of Merchant Marine, National Taiwan Ocean University, Keelung City 202301, Taiwan

* Correspondence: ntouimt@email.ntou.edu.tw; Tel.: +886-2-24622192

Abstract: Coastal countries began to develop green energy, and offshore wind power equipment in coastal areas was gradually built. Since coastal wind power generation often requires carrying out maintenance between wind turbines with the assistance of service operation vessels, this situation may cause coastal areas to be prone to people falling into the water. However, traditional maritime search and rescue plans take a long time to gather information from man overboard incidents. In order to minimize injuries to people in distress, the maritime search and rescue process must be as short as possible. Despite that all the search and rescue plans are based on the concept of the shortest path, the efficient plans must not only consider the distance but also consider the cost of search and rescue. Therefore, this study established a set of practices applicable to the on-site commander (OSC) to dispatch rescue ships, as well as the planning of maritime search and rescue route models. Based on the easy-to-observe state of the target in distress, the model is analyzed and calculated by Floyd–Warshall algorithm and Grey relational analysis so as to sort the rescue plan and optimize the effect of the search and rescue route at sea. According to the simulation analysis, when the man overboard incident occurs in the coastal area, the OSC can immediately use this model to plan the best search and rescue route and dispatch a reasonable number of rescue ships.

Keywords: maritime search and rescue; coastal countries; rescue ships; distress targets



Citation: Ho, W.-C.; Shen, J.-H.; Liu, C.-P.; Chen, Y.-W. Research on Optimal Model of Maritime Search and Rescue Route for Rescue of Multiple Distress Targets. *J. Mar. Sci. Eng.* **2022**, *10*, 460. <https://doi.org/10.3390/jmse10040460>

Academic Editor: Sergei Chernyi

Received: 22 February 2022

Accepted: 22 March 2022

Published: 24 March 2022

Publisher's Note: MDPI stays neutral with regard to jurisdictional claims in published maps and institutional affiliations.



Copyright: © 2022 by the authors. Licensee MDPI, Basel, Switzerland. This article is an open access article distributed under the terms and conditions of the Creative Commons Attribution (CC BY) license (<https://creativecommons.org/licenses/by/4.0/>).

1. Introduction

Offshore wind power is an energy that does not emit pollutants. Some coastal countries have begun to build a large number of offshore wind power plants to develop green energy [1,2]. With related wind power facilities being widely constructed, the importance of maritime search and rescue operations is more emphasized by coastal countries. Still, research in respect of applicable search and rescue routes for wind farm personnel falling water incidents has not been proposed. A personnel falling water incident is an emergency in which a person (crew or passenger) of a vessel at sea falls into the sea. This incident is one of the most common main causes of endangering the lives and safety of ship personnel at sea, particularly in large ships with slow sailing speeds, or in small ships with few personnel [3]. Under such circumstances, the vessel is built with a high risk and less protection of life and the property and environment regarding the personnel.

A maritime search and rescue operation provides reliable assistance to people in danger or at a potential risk at sea. Traditional maritime search and rescue uses factors, such as time gap, leeway, tide or currents, and swell of the distress target, to set the search datum point. The on-scene commander (OSC) uses these data to evaluate and subsequently plan a maritime search and rescue; meanwhile, it is in accordance with the international maritime organization search and rescue (IMOSAR Manual) specifications [4,5]. However, traditional search and rescue route plans require to go through the steps of spending and collecting a large amount of time and data, and then move on to the next discussion. The

“golden window” for victims is closing. The crux in the search and rescue mission is how to quickly and effectively buy time to increase the possibility of survival. From these points, maritime search and rescue plans and operations are executed on the basis of limited information. Without a complete search and rescue route planning, maritime search and rescue will be a time-consuming and resource-consuming task.

In the situation that there are multiple targets in distress at sea at the same time, if the rescue mission is still conducted as the previous search and rescue mode, the rescue time will be inevitably delayed. Hence, if the current search and rescue mode can be optimized by converting factors of the traditional maritime search and rescue mode into the rescue costs and calculating the shortest path, coastal countries will achieve search and rescue missions more objectively and quickly. This study intends to propose an optimal rescue maritime search model for persons in distress, considering the location, situation and distance so that it could assist the OSC in planning the execution and to improve the efficiency of maritime search and rescue. This model makes it easy to obtain and observe the status of the marine distress target, immediately sorts the rescue plan by the existing rescue resources, and optimizes the search and rescue route of the rescue fleet to quickly arrive at the location of the marine distress target.

In this study, the shortest path algorithm of Floyd–Warshall was adopted. By setting target 1 as the place of departure of the search and rescue fleet, the remaining nodes are designed as targets of distress at sea (e.g., people who have fallen into the water at sea). Furthermore, it is known from previous research that the path planning research can be calculated in combination with Grey theory to obtain appropriate path planning results [6–8]. The study adopted the Floyd–GRA algorithm as the analysis method. The reason for adopting this algorithm in this study is the Floyd–Warshall algorithm is faster than other path algorithms when performing calculations. Furthermore, after quantifying the information, such as the fall into the sea, wearing life-saving equipment, and the person’s situation of injury, through Grey relational analysis (GRA), this can be combined with the distance matrix of the shortest path Floyd–Warshall algorithm. Through the information, such as the scenario of the person falling into the water, wearing a rescue suit, and the person’s injury, the model combines with the navigation distance between the rescue ship and the person in distress (targets) and whether there is a barrier during the rescue voyage. As a result, the search and rescue route at sea can be more efficient and suitable. This is the innovation of this research.

The research goal of this paper is to establish a model of optimized maritime rescue routes for the search and rescue of maritime personnel of coastal countries, and this model can assist on-site commanders in planning search and rescue routes and dispatching rescue ships. However, considering the priority of rescuing human lives at sea, the model is not involved in oil spill monitoring. This model makes it easy to obtain and observe the status of the marine distress target, immediately sorts the rescue plan by the existing rescue resources, and optimizes the search and rescue route of the rescue fleet to quickly arrive at the location of the marine distress target. Although the emergency decision-making path plan for rescuing people who have fallen into the water considered weather and sea conditions, it does not extend the aspects of early warning of oil spills at sea and pollution prevention and control. The principle of the above functions is that, in all the decisions concerning marine distress, saving human lives should be the primary consideration rather than monitoring oil spills at sea; thus, the environmental impacts caused by oil spills are not discussed in depth in this study.

The remainder of this paper comprises four sections. Section 2 reviews the literature on maritime search and rescue routes and defines the research problem as well. Section 3 outlines the detailed steps of the proposed method. Section 4 discusses the analysis results that arise from the proposed method. Section 5 presents conclusions and future applications.

2. Maritime Rescue Route and Shortest Path Algorithm Literature Review

In addition to search and rescue ships, present maritime search and rescue missions are generally operated by helicopters as a supporter [9,10]. In recent years, many scholars' studies have shown that search and rescue work can be combined with drones to assist a person in distress [10–12]. In the part of the academic research about planning maritime search and rescue operations, Barciu [13] used risk assessment to determine the search area to enhance the effectiveness of maritime search and rescue operations. Ai et al. [14] proposed the intelligent decision-making algorithm to solve the problems of resource allocation and situation scheduling in the maritime search and rescue mission. Agbissoh OTOTE et al. [15] adopted a decision-making algorithm that is based on the optimal search theory to optimize the calculation process of the probability of containment and the probability of detection for improving the success rate of the maritime search and rescue.

Wu et al. [16] proposed the light-weight prediction-based opportunistic routing algorithm to select and prioritize the forwarding nodes. According to the research results, the trading of a 2% additional energy consumption per node for a 30% better delivery success rate was desirable. Zhang et al. [17], according to the actual situation of maritime search and rescue, improved an ant colony algorithm that is proposed for the route design. The simulation results show that the improved algorithm can be used for route design and obtain the optimal route suitable for sea search and rescue. Benz et al. [18] used semi-structured interviews with 24 experts, which provides the framework based on a literature review of the dimensions of search and rescue in the Arctic.

Cho et al. [19] proposed two phase methods for solving the coverage path planning problem of multiple heterogeneous unmanned aerial vehicles. The experimental results show that the randomized search heuristic yields are a better solution since, approximately, the optimality gap has a shorter computation time than a commercial solver. Zou et al. [20] adapted the extension cloud theory to the situation safety of two collisions, which was evaluated, and the evaluation results reflect the effectiveness of the model. Furthermore, many scholars and experts have researched and discussed the issue of the search area of maritime search and rescue [11,14,21].

The route planning of maritime search and rescue is like the vehicle routing problem (VRP) on the shore. By meeting the needs of customers (distress targets), at the same time, under certain constraints, the goals of the shortest distance, the least cost, or the least time are achieved [22,23]. Nowadays, the shortest path algorithm theories are well developed, including the Bellman–Ford algorithm, Dijkstra's algorithm, Floyd–Warshall algorithm, Johnson algorithm, and other algorithms. However, various algorithmic theories have their advantages and disadvantages. For example: the Johnson algorithm is known for its best rescue effect, but its complex computational process is not suitable for emergencies [24]. The Dijkstra algorithm has lower computational complexity, but the analysis process cannot effectively handle cases with negative edge weights [25]. The Bellman–Ford algorithm can handle situations with negative edge weights efficiently, but its complex computational process is not suitable for emergencies [26]. Floyd–Warshall algorithms can deal with cases with negative edge weights, but the computational process is somewhat more complicated than the Dijkstra algorithm [27].

Based on the above theory of summarizing the shortest path algorithms, this study adopted the Floyd–Warshall algorithm to plan the optimal maritime search and rescue route. The Floyd–Warshall algorithm can be used to find the shortest path to either of two points under multiple targets [28,29]. In addition, the Floyd–Warshall algorithm is a dynamically programmed algorithm that can effectively process the case of positive and negative edge weights [27,30]. The Floyd–Warshall algorithm quoted in this study is no longer limited to the sea distance of the traditional Floyd–Warshall algorithm but can be measured by factors such as the fall into the sea, if the person wore life-saving equipment, and the person's situation of injury. By setting target 1 as the place of departure of the search and rescue fleet, the remaining nodes are designed as targets of distress at sea (e.g., people who have fallen into the sea). The algorithm has a distance cost matrix on the left

and a node matrix on the right. In the distance cost matrix, it is not limited to the sea distance but can be measured in terms of personnel, ships, weather and sea conditions, and other factors. The practice is to first normalize the values of the factors to be measured individually into a de-united value between 0 and 1, and, after the standardized values of each measurement factor are summed and then multiplied by the large circle navigation distance between each node, it is brought into the distance matrix intermediate courtyard of the Floyd–Warshall algorithm.

As for the restricted areas where search and rescue units cannot enter, or if the direct route results in being indirect due to random dynamic drifting objects at sea (such as islands, sea drifts, offshore working platforms, etc.), the Floyd–Warshall algorithm can find the location of the transit point of the sea search and rescue route by setting the distance cost between the nodes to ∞ . The search and rescue fleet transit point may be more than one, but it can make the total search and rescue route shorter and save more time regarding the total search and rescue sea voyage.

3. Research Method

The concept of method in this paper is to convert the factors in the maritime search and rescue into the search and rescue cost and calculate the shortest path in order to accelerate the completion of the search and rescue mission. From the very beginning, the shortest path situation is calculated according to the Floyd–Warshall algorithm. Afterwards, by Grey relational analysis (GRA), the weight value of search and rescue factor is calculated and converted into distance weight. Finally, based on the above analysis results, an optimized path model is constructed; on the other hand, optimized solutions of search and rescue are obtained.

3.1. Floyd–Warshall Algorithm

The main issue of the shortest path is to explore the shortest path between two target points. This problem was first developed by military strategy, whose purpose is to consider the transportation of strategic materials and tactical interception [28,31].

Robert Floyd proposed the Floyd–Warshall algorithm in 1962. It is one of the algorithms to solve the problem of shortest path besides the Dijkstra algorithm [27]. Floyd–Warshall algorithm is a type of algorithm of all pair shortest path, which finds the shortest route for all pairs of nodes that exist on a graph. This algorithm does not just explore the path between two particular nodes but creates the shortest path table between the nodes. This algorithm is not only weighted and directed graph but also calculates the negative cost [29,30]. Floyd–Warshall algorithm is one of the variants of dynamic programming, which solves the problem by searching for mutually bound solutions from inspecting other solutions. Thus, the solutions are formed by the front solutions, and more than one solution is found.

The Floyd–Warshall algorithm starts with the iteration from the first point. Then, the track or path is added by evaluating all points to the destination point. Briefly describe the calculation process of Floyd–Warshall algorithm as follows: Assuming that G is represented as an $n \times n$ matrix, the weight of its side is $W = [w_{ij}]$, as shown in Equation (1).

$$W_{ij} = \left\{ \begin{array}{ll} 0 & , i = j \\ w(i, j) & , i \neq j \text{ and } (i, j) \in E \\ \infty & , i \neq j \text{ and } (i, j) \notin E \end{array} \right\} \quad (1)$$

Let $d_{ij}^{(k)}$ be the distance of the shortest path from i to j , and all nodes on the path are set to $\{1, 2, \dots, k\}$. Further, let $d_{ij}^{(0)}$ be W_{ij} ; that is, there is no node; let $D^{(k)}$ be an $n \times n$ matrix $[d_{ij}^{(k)}]$. Therefore, if the shortest path d_{ij} includes node k , the shortest path of d_{ij} is composed of sub-paths d_{ik} and d_{kj} . Each sub-path can only contain nodes between $\{1, 2, \dots, k - 1\}$; that is, its distance is: $d_{ik}^{(k-1)}$ and $d_{kj}^{(k-1)}$. According to the aforementioned calculation

concept, $D^{(0)} = [W_{ij}]$ and the above verified $D^{(k)}$, the following Equations (2) and (3) can be obtained:

$$d_{ij}^{(0)} = \begin{cases} 0 & , i = j \\ W_{ij} & , i \neq j \end{cases} , i, j = \{1, 2, \dots, n\} \tag{2}$$

$$d_{ij}^{(k)} = \min \left\{ d_{ij}^{(k-1)} , d_{ik}^{(k-1)} + d_{kj}^{(k-1)} \right\} , \begin{cases} k = \{1, 2, \dots, n\} \\ k \neq i, j \end{cases} \tag{3}$$

3.2. Grey Relational Analysis

GRA is an analysis model proposed by Professor Deng in 1982. The features of GRA can perform data analysis and calculations for things such as uncertainty, multivariate input, discrete data, and data incompleteness [32–34]. GRA can project the sequence data on the geometric space by finding the correlation of one sequence to other sequences. Then, use the method of measuring the proximity of geometric shapes to solve the shortcomings of general traditional statistical regression. Briefly describe the calculation process of the GRA method as follows:

Let $X = \{x_0, x_1, x_2, \dots, x_i\}$ be a sequence (alternative) set; x_0 expresses the referential alternative and x_i refers to the compared alternative. Suppose x_{0i} and x_{ij} are the respective values at criterion k , while $k = 1, 2, \dots, n$ for x_0 and x_i . The Grey relation coefficient $\gamma(x_0(k), x_i(k))$ of the alternatives at criterion k can be obtained by Equation (4)

$$\gamma(x_0(k), x_i(k)) = \frac{\min_i \min_k \Delta_{0i}(k) + \zeta \max_i \max_k \Delta_{0i}(k)}{\Delta_{0i}(k) + \zeta \max_i \max_k \Delta_{0i}(k)} \tag{4}$$

where $\Delta_{ij} = |x_0(k) - x_i(k)|$, ζ is the distinguishing coefficient and $\zeta \in [0, 1]$. ζ is used to weaken the situation where the value of $\max_i \max_k \Delta_{0i}(k)$ is too large and distorted. ζ will change the relative value of $\gamma(x_0(k), x_i(k))$ but does not affect the ranking of the Grey correlation degree [32–34]. As shown in Equation (5):

$$\gamma(x_0(k), x_i(k)) = \sum_{j=1}^n \gamma(x_0(k), x_i(k)) \tag{5}$$

This paper comprehensively averages the Grey correlation degree obtained by each ζ value at first and calculates the weight value after obtaining the comprehensive Grey correlation sequence. As shown in Equation (6):

$$W(V)_n = \frac{G_n}{\sum G} \tag{6}$$

The $(W(V))$ obtained from GRA is used as the $(W'(V))$ of the Floyd–Warshall algorithm. According to the reference, also pointed out that the Floyd–Warshall algorithm can find all the distances of each node and calculate the minimum weight of all paths [27,29,30]. Before becoming $(W'(V))$, since the original point weight value is positive, the calculation method of the Floyd–Warshall algorithm is reversed, the evaluation index needs to be normalized, and this process can set all values to $[0, 1]$. The evaluation index in the article needs to be standardized through the *Min* index value and the *Max* index value, as shown in Equations (7) and (8):

$$Min : \frac{Min (W(V))}{W(V)_n} \tag{7}$$

$$Max : \frac{W(V)_n}{Max (W(V))} \tag{8}$$

After the calculation of $(W'(V))$ is completed, it is continued to convert $(W'(V))$ to $(W(E))$. In the conversion process, the ratio of the destination to all vertices other than the departure point needs to be considered, as Equation (9) shows:

$$W(E)_{ij} = \frac{W'(V)_j}{\sum_{k=1}^n W'(V)_k - W'(V)_i} \quad (9)$$

The final weighted distance is the value obtained by considering both $(W(E))$ and distance cost $(D_{ij} * W(E)_{ij})$. In this article, the solution process of optimizing the maritime search and rescue route is presented in the form of graphic method. This study considers the shortest search and rescue route and cost to achieve the effect of optimizing the maritime search and rescue route of coastal countries. When calculating the distance weight, $(W'(V))$ (the weight of the search and rescue target) needs to be converted to $(W(E))$ (the weight of the distance between the two targets) to generate a distance weight in accordance with the actual situation.

4. Experimental Results and Analysis

The Floyd–Warshall algorithm can find all the shortest paths in the multi-source shortest path problem, which indicates that this mode can effectively allocate and find the best search and rescue route and plan [29,30]. In order to optimize the formulation of maritime search and rescue routes, the research adopts the practice to convert the distress target information into weights by using GRA. The search and rescue cost is added as a consideration in the calculation process. The search and rescue cost and distance will be the following basis of evaluation of the shortest maritime search and rescue route. Through the information of these known distress targets, the optimized maritime search and rescue route is generated, so the OSC can use the evaluation results as the consideration of the overall search and rescue dispatch. It makes OSC dispatch search and rescue fleets more accurate and allows all the targets in distress to be rescued more safely within the effective time.

This research used a simulation case to illustrate the planning of maritime search and rescue routes. In the test case of this article, the shortest path will first be used to plan the maritime search and rescue route, and then the search and rescue cost is added based on the analysis results of the shortest path to obtain the optimized maritime search and rescue route.

The simulation case in the study is set as a ship in distress at sea, and the people falling into the water are waiting for rescue while they are in the water or in a lifeboat. The target in distress represents a person in distress, and the situation of each target in distress is as follows: rescue departure target 1 is the place of departure of the search and rescue fleet. In distress target 2, the person falling into the water is wearing life-saving equipment but is seriously injured. In distress target 3, the person who is falling into the water did not wear life-saving equipment and is slightly injured. In distress target 4, the person falling into the water is wearing life-saving equipment and suffered minor injuries. In distress target 5, the person falling into the water is wearing life-saving equipment and suffered minor injuries. In distress target 6, the person in distress is not injured and is waiting for rescue on the ship in distress. The distance between the distress targets is shown as Table 1.

The value of the distance table matrix in Table 1 is the direct sea navigation distance between rescue departure target 1 and the distress targets (distress target 2 to distress target 6), but the diagonal distance value is located in the position of each target itself and is fixed to 0 (ie., distress target 2 to distress target 2, distance = 0). In the study, the value of the direct sailing distance between the two targets is calculated by the great circle sailing. For example, the value of 14.78 in Table 1 is the direct sailing distance from rescue departure target 1 to distress target 2; the value of 0.16 in the table is the direct sailing distance from distress target 3 to distress target 5, and so on.

Table 1. Distress target distance situation.

	1	2	3	4	5	6
1	0.00	14.78	17.86	16.38	17.21	16.49
2	14.78	0.00	0.57	0.79	0.86	0.84
3	17.86	0.57	0.00	0.29	0.16	0.25
4	16.38	0.79	0.29	0.00	0.14	0.12
5	17.21	0.86	0.16	0.14	0.00	0.06
6	16.49	0.84	0.25	0.12	0.06	0.00

Note: the unit is nautical mile.

4.1. The Shortest Maritime Search and Rescue Route

This study adopted the Floyd–Warshall algorithm to calculate the shortest path. For the distance situation of each distress target, refer to Table 1. This research provides examples of data and how they are used, as shown in Appendix A. In Appendix A, this study explains the calculation process graphically, as shown in Tables A1–A6. The results after analysis and calculation are shown in Table 2.

Table 2. Floyd–Warshall algorithm calculation matrix.

Vertex	1	2	3	4	5	6		1	2	3	4	5	6
1	0.00	14.78	15.35	15.57	15.51	15.57	1	1	2	2	2	3	5
2	14.78	0.00	0.57	0.79	0.73	0.79	2	1	2	3	4	3	5
3	15.35	0.57	0.00	0.29	0.16	0.22	3	2	2	3	4	5	5
4	15.57	0.79	0.29	0.00	0.14	0.12	4	2	2	3	4	5	6
5	15.51	0.73	0.16	0.14	0.00	0.06	5	3	3	3	4	5	6
6	15.57	0.79	0.22	0.12	0.06	0.00	6	5	5	5	4	5	6

In the study, the two matrix values presented in Table 2 are brought into the initial matrix data of the Floyd–Warshall algorithm matrix calculus according to the values of Table 1, where the left matrix is the distance matrix (brought in by Table 1) and the right matrix is the node matrix (adopted to cooperate with the calculation of whether the node route of the optimal search and rescue route is directly sailing or it needs to be navigated around other targets).

According to the results of the Floyd–Warshall algorithm analysis, the shortest maritime search and rescue route and the navigation distance of search and rescue ships are shown in Table 3 below.

Table 3. Floyd–Warshall algorithm shortest search and rescue route results.

Shortest Search and Rescue Route	Search and Rescue Ship Sailing Distance
1→2→3	15.35
1→2→4	15.57
1→3→5	15.51
1→5→6	15.57
2→3→5	0.73
2→5→6	0.79
3→5→6	0.22

The results of finding the shortest search and rescue route by using the Floyd–Warshall algorithm show that, during the maritime search and rescue process, two ships need to be assigned to search and rescue. One ship departs from rescue departure target 1, passing by distress target 2, and finally reaches distress target 4. It sails 15.57 nautical miles. Another ship departs from rescue departure target 1, passing by distress target 2, distress target 3, and distress target 5, and finally reaches distress target 6, sailing 15.57 nautical miles. In the case of completing maritime search and rescue missions, the shortest rescue distance can be obtained.

4.2. Optimized Maritime Search and Rescue Route

In this study, three factors, including the situation of people in distress wearing life-saving equipment, the situation of injury, and whether they fell into the water, will be used for the evaluation indicators of search and rescue costs. The purpose is that, at the moment of a shipwreck, these three evaluation indicators are the information of persons in distress at sea that can be immediately known or directly observed.

To evaluate the weight value corresponding to the search and rescue, this study assumes several weight values. In the case of people in distress wearing life-saving equipment or not, the weight values are set to 3 for those not wearing it, 2 for one who is wearing, and 1 for one who is in the boat in distress. In the case of people falling into water or not, the weight values are set to 2 for one who is falling and 1 for one who is not falling. In the case of severity of people’s injury, the weight values are set to 3 for one who is seriously injured, 2 for one who is slightly injured, and 1 for one who is not injured. By quantifying and sorting, the result of the matrix is shown in Table 4. The GRA analyses calculated according to the results are shown in Table 5. In the study, the results in Table 5 were also drawn into Figure 1 for presentation. In this way, errors of the GRA calculation results can be checked.

Table 4. Arrangement of Grey correlation matrix of marine distress situation.

Distress Target	Evaluation Index	Life-Saving Equipment	Fell into the Sea	Situation of Injury
	2	2	2	3
	3	3	2	2
	4	2	2	2
	5	2	2	2
	6	1	1	1

Table 5. GRA analysis and calculation.

Distress Target	Distinguishing Coefficient (ζ)										Grey Correlation Degree	GREY Relational Ordinal	Weight
	0.1	0.2	0.3	0.4	0.5	0.6	0.7	0.8	0.9	1.0			
2	0.722	0.762	0.792	0.815	0.833	0.848	0.861	0.872	0.881	0.889	0.828	1	0.067
3	0.167	0.286	0.375	0.444	0.500	0.545	0.583	0.615	0.643	0.667	0.483	3	0.200
4	0.141	0.246	0.327	0.392	0.444	0.489	0.526	0.558	0.586	0.611	0.432	4	0.267
5	0.444	0.524	0.583	0.630	0.667	0.697	0.722	0.744	0.762	0.778	0.655	2	0.133
6	0.091	0.167	0.231	0.286	0.333	0.375	0.412	0.444	0.474	0.500	0.331	5	0.333

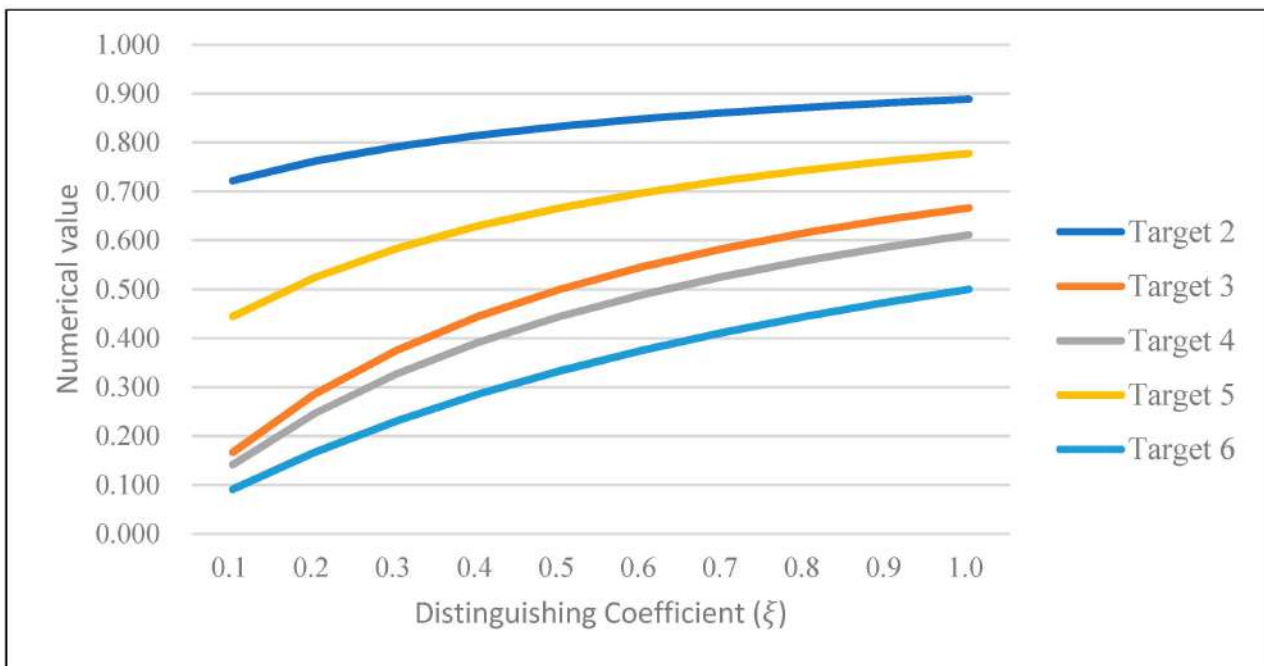


Figure 1. Line chart of GRA analysis results.

According to the results in Table 5 and Figure 1, the GRA calculation results are significant. The last step is to calculate the weighted distance of the distress target through Equations (7)–(9) in this article to obtain the GRA analysis results. Then, start calculating $(W'(V))$ and $(W(E))$. The results are shown in Table 6. This research provides examples of data and how they are used, as shown in Appendix B. In Appendix B, this study explains the calculation process, as shown in Tables A7–A9.

Table 6. Weighted distance sorting of distress targets.

	1	2	3	4	5	6
1	0.00	14.78	5.95	4.10	8.61	3.30
2	14.78	0.00	0.09	0.09	0.21	0.08
3	5.95	0.27	0.00	0.07	0.07	0.05
4	4.10	0.45	0.06	0.00	0.04	0.01
5	8.61	0.47	0.03	0.02	0.00	0.01
6	3.30	0.53	0.05	0.02	0.02	0.00

After obtaining the weighted distance, this study uses the Floyd–Warshall algorithm again to calculate. This research provides examples of data and how they are used, as shown in Appendix C. In Appendix C, this study explains the calculation presented graphically, as shown in Tables A10–A15. The results by analysis and calculation are shown in Table 7. The Example Calculation is attached in Table S1 in the Supplemental Material available online.

Regarding the results of the analysis, the optimized maritime search and rescue route and navigation distance are shown in Table 8 below.

Table 7. The best search and rescue route calculation matrix.

Vertex	1	2	3	4	5	6		1	2	3	4	5	6
1	0.00	3.62	3.35	3.32	3.32	3.30	1	1	6	6	6	6	6
2	3.38	0.00	0.09	0.09	0.10	0.08	2	6	2	3	4	6	6
3	3.35	0.27	0.00	0.07	0.07	0.05	3	6	2	3	4	5	6
4	3.31	0.33	0.06	0.00	0.03	0.01	4	6	3	3	4	6	6
5	3.31	0.30	0.03	0.02	0.00	0.01	5	6	3	3	4	5	6
6	3.30	0.32	0.05	0.02	0.02	0.00	6	1	3	3	4	5	6

Table 8. Optimized search and rescue route results collation.

The Best Maritime Search and Rescue Route	Weighted Distance for Search and Rescue Ships
1→6→2	3.62
1→6→3	3.35
1→6→4	3.32
1→6→5	3.32
2→6→1	3.38
2→6→5	0.10
3→6→1	3.35
3→4	0.07
4→6→1	3.31
4→3→2	0.33
4→3	0.06
4→6→5	0.03
5→6→1	3.31
5→3→2	0.30
6→3→2	0.32
6→3	0.05

According to the results compiled in Table 8, the best situation for maritime search and rescue is to assign two search and rescue ships. A ship departs from rescue departure target 1, passing by distress target 6, and finally reaches distress target 4. The weighted distance of the ship is 3.32, and the navigation distance of the search and rescue ship is 16.61 nautical miles. The other ship departs from rescue departure target 1, passing by distress target 6, distress target 5, and distress target 3, and finally reaches distress target 2. The navigation distance of this ship is 3.62, and the navigation distance of the search and rescue ship is 17.28 nautical miles.

5. Discussion and Conclusions

In conducting maritime search and rescue tasks, a traditional maritime search and rescue plan needs a great deal of time for collecting information regarding falling water events. However, in order to minimize the harm of people in distress, the process of search and rescue at sea must be as short as possible. The optimized maritime search and rescue route established in this study can balance both the criticality of the distress target and the distance cost. The simulation results show that the proposed modeling method is an effective plan for maritime search and rescue routes.

This paper has built a set of maritime search and rescue route models for coastal countries, which are suitable for the on-scene commander planning search and rescue routes and dispatching rescue ships. The model based on the observable state of the distress targets sequences the rescue plan and optimizes the marine search and rescue route. When the search and rescue center receives the status of the target in distress, including the location and distance of the person who fell into the sea, the optimized planning of the maritime search and rescue route developed by this research can provide suggestions for the search and rescue operations. If the search and rescue center obtained only the distance of the target in distress, it could still dispatch the fastest search and rescue ship in the task through this shortest path mode.

Not every maritime distress incident must immediately dispatch a great deal of manpower and equipment. Aside from the factor of limited search and rescue resources, it is important to avoid depleting all the rescue resources on a single case, with the result being that there are not enough to be transferred to other distressed areas when receiving word of other simultaneous incidents. In the distance matrix of the Floyd–Warshall algorithm, the optimization model of this study introduces a concept similar to the classification guidance of marine injury inspection. This can help the maritime search and rescue commander to dispatch a high-precision rescue fleet to participate in the falling water incident. At the same time, it can also reduce the waste of search and rescue resources and the situation of insufficient rescue energy.

In addition, the current maritime search and rescue system does not have a set of global universal maritime injury classification guidelines, which is not as complete as the emergency medical examination system of the land hospital. This study can assist in planning maritime search and rescue routes in time-critical situations. This route can reasonably allocate the fleet resources required by the search and rescue route. This avoids resource shortages and delays of search and rescue at sea. In terms of future research, the evaluation method of vital signs can be adopted. By introducing the concept of vital signs of casualties on land, the accuracy of the assessment of the injuries of those who have fallen into the sea would be improved. In this way, it can increase the chance of rescue of persons in distress at sea.

The research goal of this paper is to establish a model of optimized maritime rescue routes for the search and rescue of maritime personnel of coastal countries, and this model can assist on-site commanders in planning search and rescue routes and dispatching rescue ships. Although the emergency decision-making path plan for rescuing people who have fallen into the water considered weather and sea conditions, it does not extend to the aspects of early warning of oil spills at sea and pollution prevention and control. Some topics for future study include, for example, adjusting the search and rescue route by adding the oil spill monitoring model. In addition, it will be an interesting topic regarding comparing the efficiency between search and rescue ships and search and rescue helicopters.

Supplementary Materials: The following supporting information can be downloaded at: <https://www.mdpi.com/article/10.3390/jmse10040460/s1>, Table S1. Example Calculation.

Author Contributions: W.-C.H. contributed to the conception of the work (writing, data collection), analyzed the data, and interpreted the results. J.-H.S. contributed to the conception and design of the work (literature search, data collection). C.-P.L. designed, drafted, and revised the work. Y.-W.C. contributed to the conception and design of the work (study design, data interpretation). All authors have read and agreed to the published version of the manuscript.

Funding: The authors declare no funding information and funding sponsor.

Conflicts of Interest: The authors declare no conflict of interest.

Appendix A

The calculation processes presented graphically are shown in Tables A1–A6. These data sources come from Table 1.

Table A1. The step 1 graphical process of Floyd–Warshall algorithm.

Step 1													
Vertex	1	2	3	4	5	6		1	2	3	4	5	6
1	0.00	14.78	17.86	16.38	17.21	16.49	1	1	2	3	4	5	6
2	14.78	0.00	0.57	0.79	0.86	0.84	2	1	2	3	4	5	6
3	17.86	0.57	0.00	0.29	0.16	0.25	3	1	2	3	4	5	6
4	16.38	0.79	0.29	0.00	0.14	0.12	4	1	2	3	4	5	6
5	17.21	0.86	0.16	0.14	0.00	0.06	5	1	2	3	4	5	6
6	16.49	0.84	0.25	0.12	0.06	0.00	6	1	2	3	4	5	6

Table A2. The step 2 graphical process of Floyd–Warshall algorithm.

Step 2													
Vertex	1	2	3	4	5	6		1	2	3	4	5	6
1	0.00	14.78	15.35	15.57	15.64	15.62	1	1	2	2	2	2	2
2	14.78	0.00	0.57	0.79	0.86	0.84	2	1	2	3	4	5	6
3	15.35	0.57	0.00	0.29	0.16	0.25	3	2	2	3	4	5	6
4	15.57	0.79	0.29	0.00	0.14	0.12	4	2	2	3	4	5	6
5	15.64	0.86	0.16	0.14	0.00	0.06	5	2	2	3	4	5	6
6	15.62	0.84	0.25	0.12	0.06	0.00	6	2	2	3	4	5	6

Table A3. The step 3 graphical process of Floyd–Warshall algorithm.

Step 3													
Vertex	1	2	3	4	5	6		1	2	3	4	5	6
1	0.00	14.78	15.35	15.57	15.51	15.60	1	1	2	2	2	3	3
2	14.78	0.00	0.57	0.79	0.73	0.82	2	1	2	3	4	3	3
3	15.35	0.57	0.00	0.29	0.16	0.25	3	2	2	3	4	5	6
4	15.57	0.79	0.29	0.00	0.14	0.12	4	2	2	3	4	5	6
5	15.51	0.73	0.16	0.14	0.00	0.06	5	3	3	3	4	5	6
6	15.60	0.82	0.25	0.12	0.06	0.00	6	3	3	3	4	5	6

Table A4. The step 4 graphical process of Floyd–Warshall algorithm.

Step 4													
Vertex	1	2	3	4	5	6		1	2	3	4	5	6
1	0.00	14.78	15.35	15.57	15.51	15.60	1	1	2	2	2	3	3
2	14.78	0.00	0.57	0.79	0.73	0.82	2	1	2	3	4	3	3
3	15.35	0.57	0.00	0.29	0.16	0.25	3	2	2	3	4	5	6
4	15.57	0.79	0.29	0.00	0.14	0.12	4	2	2	3	4	5	6
5	15.51	0.73	0.16	0.14	0.00	0.06	5	3	3	3	4	5	6
6	15.60	0.82	0.25	0.12	0.06	0.00	6	3	3	3	4	5	6

Table A5. The step 5 graphical process of Floyd–Warshall algorithm.

Step 5													
Vertex	1	2	3	4	5	6		1	2	3	4	5	6
1	0.00	14.78	15.35	15.57	15.51	15.57	1	1	2	2	2	3	5
2	14.78	0.00	0.57	0.79	0.73	0.79	2	1	2	3	4	3	5
3	15.35	0.57	0.00	0.29	0.16	0.22	3	2	2	3	4	5	5
4	15.57	0.79	0.29	0.00	0.14	0.12	4	2	2	3	4	5	6
5	15.51	0.73	0.16	0.14	0.00	0.06	5	3	3	3	4	5	6
6	15.57	0.79	0.22	0.12	0.06	0.00	6	5	5	5	4	5	6

Table A6. The step 6 graphical process of Floyd–Warshall algorithm.

Step 6													
Vertex	1	2	3	4	5	6		1	2	3	4	5	6
1	0.00	14.78	15.35	15.57	15.51	15.57	1	1	2	2	2	3	5
2	14.78	0.00	0.57	0.79	0.73	0.79	2	1	2	3	4	3	5
3	15.35	0.57	0.00	0.29	0.16	0.22	3	2	2	3	4	5	5
4	15.57	0.79	0.29	0.00	0.14	0.12	4	2	2	3	4	5	6
5	15.51	0.73	0.16	0.14	0.00	0.06	5	3	3	3	4	5	6
6	15.57	0.79	0.22	0.12	0.06	0.00	6	5	5	5	4	5	6

Appendix B

The calculation processes of $(W'(V))$ and $(W(E))$ are shown in Tables A7–A9.

Table A7. Minimum revise table.

Distress Target	Grey Relational Ordinal	W	Revise W
1	NIL.	0.00	0.00
2	1	0.07	1.00
3	3	0.20	0.33
4	4	0.27	0.25
5	2	0.13	0.50
6	5	0.33	0.20

Table A8. $(W'(V))$ table.

	1	2	3	4	5	6
1	0.00	1.00	0.33	0.25	0.50	0.20
2	1.00	0.00	0.16	0.12	0.24	0.10
3	0.33	0.48	0.00	0.23	0.46	0.18
4	0.25	0.57	0.19	0.00	0.29	0.11
5	0.50	0.55	0.18	0.14	0.00	0.11
6	0.20	0.63	0.21	0.16	0.32	0.00

Table A9. $(W(E))$ table.

	1	2	3	4	5	6
1	0.00	14.78	5.95	4.10	8.61	3.30
2	14.78	0.00	0.57	0.79	0.86	0.84
3	17.86	0.57	0.00	0.29	0.16	0.25
4	16.38	0.79	0.29	0.00	0.14	0.12
5	17.21	0.86	0.16	0.14	0.00	0.06
6	16.49	0.84	0.25	0.12	0.06	0.00

Appendix C

The calculation processes presented graphically are shown in Tables A10–A15. These data sources come from Table 6.

Table A10. The step 1 graphical process of the best search and rescue route.

Step 1													
Vertex	1	2	3	4	5	6		1	2	3	4	5	6
1	0.00	14.78	5.95	4.10	8.61	3.30	1	1	2	3	4	5	6
2	14.78	0.00	0.09	0.09	0.21	0.08	2	1	2	3	4	5	6
3	5.95	0.27	0.00	0.07	0.07	0.05	3	1	2	3	4	5	6
4	4.10	0.45	0.06	0.00	0.04	0.01	4	1	2	3	4	5	6
5	8.61	0.47	0.03	0.02	0.00	0.01	5	1	2	3	4	5	6
6	3.30	0.53	0.05	0.02	0.02	0.00	6	1	2	3	4	5	6

Table A11. The step 2 graphical process of the best search and rescue route.

Step 2													
Vertex	1	2	3	4	5	6		1	2	3	4	5	6
1	0.00	14.78	5.95	4.10	8.61	3.30	1	1	2	3	4	5	6
2	14.78	0.00	0.09	0.09	0.21	0.08	2	1	2	3	4	5	6
3	5.95	0.27	0.00	0.07	0.07	0.05	3	1	2	3	4	5	6
4	4.10	0.45	0.06	0.00	0.04	0.01	4	1	2	3	4	5	6
5	8.61	0.47	0.03	0.02	0.00	0.01	5	1	2	3	4	5	6
6	3.30	0.53	0.05	0.02	0.02	0.00	6	1	2	3	4	5	6

Table A12. The step 3 graphical process of the best search and rescue route.

Step 3													
Vertex	1	2	3	4	5	6		1	2	3	4	5	6
1	0.00	6.23	5.95	4.10	6.02	3.30	1	1	3	3	4	3	6
2	6.04	0.00	0.09	0.09	0.16	0.08	2	3	2	3	4	3	6
3	5.95	0.27	0.00	0.07	0.07	0.05	3	1	2	3	4	5	6
4	4.10	0.33	0.06	0.00	0.04	0.01	4	1	3	3	4	5	6
5	5.98	0.30	0.03	0.02	0.00	0.01	5	3	3	3	4	5	6
6	3.30	0.33	0.05	0.02	0.02	0.00	6	1	3	3	4	5	6

Table A13. The step 4 graphical process of the best search and rescue route.

Step 4													
Vertex	1	2	3	4	5	6		1	2	3	4	5	6
1	0.00	4.43	4.16	4.10	4.14	3.30	1	1	4	4	4	4	6
2	4.19	0.00	0.09	0.09	0.13	0.08	2	4	2	3	4	4	6
3	4.17	0.27	0.00	0.07	0.07	0.05	3	4	2	3	4	5	6
4	4.10	0.33	0.06	0.00	0.04	0.01	4	1	3	3	4	5	6
5	4.12	0.30	0.03	0.02	0.00	0.01	5	4	3	3	4	5	6
6	3.30	0.33	0.05	0.02	0.02	0.00	6	1	3	3	4	5	6

Table A14. The step 5 graphical process of the best search and rescue route.

Step 5													
Vertex	1	2	3	4	5	6		1	2	3	4	5	6
1	0.00	4.43	4.16	4.10	4.14	3.30	1	1	4	4	4	4	6
2	4.19	0.00	0.09	0.09	0.13	0.08	2	4	2	3	4	4	6
3	4.17	0.27	0.00	0.07	0.07	0.05	3	4	2	3	4	5	6
4	4.10	0.33	0.06	0.00	0.04	0.01	4	1	3	3	4	5	6
5	4.12	0.30	0.03	0.02	0.00	0.01	5	4	3	3	4	5	6
6	3.30	0.33	0.05	0.02	0.02	0.00	6	1	3	3	4	5	6

Table A15. The step 6 graphical process of the best search and rescue route.

Step 6													
Vertex	1	2	3	4	5	6		1	2	3	4	5	6
1	0.00	3.62	3.35	3.32	3.32	3.30	1	1	6	6	6	6	6
2	3.38	0.00	0.09	0.09	0.10	0.08	2	6	2	3	4	6	6
3	3.25	0.27	0.00	0.07	0.07	0.05	3	6	2	3	4	5	6
4	3.31	0.33	0.06	0.00	0.03	0.01	4	6	3	3	4	6	6
5	3.31	0.30	0.03	0.02	0.00	0.01	5	6	3	3	4	5	6
6	3.30	0.32	0.05	0.02	0.02	0.00	6	1	3	3	4	5	6

References

1. Chipindula, J.; Botlaguduru, V.S.V.; Du, H.; Kommalapati, R.R.; Huque, Z. Life cycle environmental impact of onshore and offshore wind farms in Texas. *Sustainability* **2018**, *10*, 2022. [CrossRef]
2. Wu, Y.; Tao, Y.; Zhang, B.; Wang, S.; Xu, C.; Zhou, J. A decision framework of offshore wind power station site selection using a PROMETHEE method under intuitionistic fuzzy environment: A case in China. *Ocean Coast. Manag.* **2020**, *184*, 105016. [CrossRef]
3. Meinhard, E. *Drowning by Accident: Why So Many People Drown*; Troubador Publishing Ltd.: Market Harborough, UK, 2022; pp. 29–34.
4. Burciu, Z. Bayesian methods in reliability of search and rescue action. *Pol. Marit. Res.* **2010**, *17*, 72–78. [CrossRef]
5. Gözalan, A.; John, O.; Lübcke, T.; Maier, A.; Reimann, M.; Richter, J.G.; Zverev, I. Assisting Maritime Search and Rescue (SAR) Personnel with AI-Based Speech Recognition and Smart Direction Finding. *J. Mar. Sci. Eng.* **2020**, *8*, 818. [CrossRef]
6. You, D.M.; Han, B.; Li, L. Mountainous Highway Routing Decision-Making Model Based on Variable Weight Grey Theory. In *Applied Mechanics and Materials*; Trans Tech Publications Ltd.: Stafa-Zurich, Switzerland, 2012; pp. 1864–1869.
7. Zhao, F.; Lv, H.X.; Wang, B. Research on Comprehensive Evaluation Method of Regional Railway Network Scale. In Proceedings of the International Conference on Smart Vehicular Technology, Transportation, Communication and Applications, Cham, Switzerland, 1 December 2018.
8. Yao, H. Application of artificial intelligence algorithm in mathematical modelling and solving. *Appl. Math. Nonlinear Sci.* **2021**, *1*–7. [CrossRef]
9. Chen, Z.; Liu, H.; Tian, Y.; Wang, R.; Xiong, P.; Wu, G. A particle swarm optimization algorithm based on time-space weight for helicopter maritime search and rescue decision-making. *IEEE Access* **2020**, *8*, 81526–81541. [CrossRef]
10. Zheng, L.; Hu, J.; Xu, S. Marine search and rescue of uav in long-distance security modeling simulation. *Pol. Marit. Res.* **2017**, *24*, 192–199. [CrossRef]
11. Queralta, J.P.; Taipalmaa, J.; Pullinen, B.C.; Sarker, V.K.; Gia, T.-N.; Tenhunen, H.; Gabbouj, M.; Raitoharju, J.; Westerlund, T. Collaborative multi-robot search and rescue: Planning, coordination, perception, and active vision. *IEEE Access* **2020**, *8*, 191617–191643. [CrossRef]
12. Li, Q.; Taipalmaa, J.; Queralta, J.P.; Gia, T.-N.; Gabbouj, M.; Tenhunen, H.; Raitoharju, J.; Westerlund, T. Towards active vision with UAVs in marine search and rescue: Analyzing human detection at variable altitudes. In Proceedings of the 2020 IEEE International Symposium on Safety, Security, and Rescue Robotics, Abu Dhabi, United Arab Emirates, 4–6 November 2020; pp. 65–70. [CrossRef]
13. Burciu, Z. Reliability and uncertainty in determining search area during Search-and Rescue action. *Pol. Marit. Res.* **2012**, *19*, 21–30. [CrossRef]
14. Ai, B.; Li, B.; Gao, S.; Xu, J.; Shang, H. An intelligent decision algorithm for the generation of maritime search and rescue emergency response plans. *IEEE Access* **2019**, *7*, 155835–155850. [CrossRef]
15. Agbissoh OTOTE, D.; Li, B.; Ai, B.; Gao, S.; Xu, J.; Chen, X.; Lv, G. A decision-making algorithm for maritime search and rescue plan. *Sustainability* **2019**, *11*, 2084. [CrossRef]
16. Wu, H.; Wang, J.; Ananta, R.R.; Kommareddy, V.R.; Wang, R.; Mohapatra, P. Prediction based opportunistic routing for maritime search and rescue wireless sensor network. *J. Parallel Distrib. Comput.* **2018**, *111*, 56–64. [CrossRef]
17. Zhang, H.; Sun, J.; Yang, B.; Shi, Y.; Li, Z. Optimal Search and Rescue Route Design Using an Improved Ant Colony Optimization. *Inf. Technol. Control* **2020**, *49*, 438–447. [CrossRef]
18. Benz, L.; Münch, C.; Hartmann, E. Development of a search and rescue framework for maritime freight shipping in the Arctic. *Transp. Res. Part A Policy Pract.* **2021**, *152*, 54–69. [CrossRef]
19. Cho, S.-W.; Park, H.-J.; Lee, H.; Shim, D.-H.; Kim, S.-Y. Coverage path planning for multiple unmanned aerial vehicles in maritime search and rescue operations. *Comput. Ind. Eng.* **2021**, *161*, 107612. [CrossRef]
20. Zou, Y.; Zhang, Y.; Ma, Z. Emergency Situation Safety Evaluation of Marine Ship Collision Accident Based on Extension Cloud Model. *J. Mar. Sci. Eng.* **2021**, *9*, 1370. [CrossRef]
21. Liu, H.; Chen, Z.; Tian, Y.; Wang, B.; Yang, H.; Wu, G. Evaluation method for helicopter maritime search and rescue response plan with uncertainty. *Chin. J. Aeronaut.* **2021**, *34*, 493–507. [CrossRef]

22. Çam, Ö.N.; Sezen, H.K. The formulation of a linear programming model for the vehicle routing problem in order to minimize idle time. *Decis. Mak. Appl. Manag. Eng.* **2020**, *3*, 22–29. [[CrossRef](#)]
23. Das, M.; Roy, A.; Maity, S.; Kar, S.; Sengupta, S. Solving fuzzy dynamic ship routing and scheduling problem through new genetic algorithm. *Decis. Mak. Appl. Manag. Eng.* **2021**, 1–33. [[CrossRef](#)]
24. Yu, M.Y.; Vasudevan, R.; Johnson-Roberson, M. Occlusion-aware risk assessment for autonomous driving in urban environments. *IEEE Robot. Autom. Lett.* **2019**, *4*, 2235–2241. [[CrossRef](#)]
25. Chambers, A.; Eavis-O’Quinn, M.; Roberge, V.; Tarbouchi, M. Route planning for electric vehicle efficiency using the Bellman-Ford algorithm on an embedded GPU. In Proceedings of the 2018 4th International Conference on Optimization and Applications (ICOA), Mohammedia, Morocco, 26–27 April 2018. [[CrossRef](#)]
26. Prasetyo, B.I.A.; Maslan, A. Analisis Perbandingan Pada Algoritma Bellman Ford Dan Dijkstra Pada Google Map. *Khazanah Ilmu Berazam* **2020**, *3*, 337–349.
27. Solichudin, S.; Triwiyatno, A.; Riyadi, M.A. Conflict-free dynamic route multi-agv using dijkstra Floyd-warshall hybrid algorithm with time windows. *Int. J. Electr. Comput. Eng.* **2020**, *10*, 3596. [[CrossRef](#)]
28. Hussain, I.; Bingcai, C. Cluster formation and cluster head selection approach for vehicle ad-hoc network (VANETs) using K-means and Floyd-Warshall technique. *Int. J. Adv. Comput. Sci. Appl.* **2017**, *8*, 11–15.
29. Liu, L.; Luo, S.; Guo, F.; Tan, S. Multi-point shortest path planning based on an improved discrete bat algorithm. *Appl. Soft Comput.* **2020**, *95*, 106498. [[CrossRef](#)]
30. Sakharov, V.; Chernyi, S.; Saburov, S.; Chertkov, A. Automatization Search for the Shortest Routes in the Transport Network Using the Floyd-warshell Algorithm. *Transp. Res. Procedia* **2021**, *54*, 1–11. [[CrossRef](#)]
31. Mirino, A.E. Best routes selection using Dijkstra and Floyd-Warshall algorithm. In Proceedings of the 2017 11th International Conference on Information & Communication Technology and System, Surabaya, Indonesia, 31–31 October 2017; pp. 155–158. [[CrossRef](#)]
32. Liou, S.-T.; Liu, C.-P.; Chang, C.-C.; Yen, D.-C. Restructuring Taiwan’s port state control inspection authority. *Gov. Inf. Q.* **2011**, *28*, 36–46. [[CrossRef](#)]
33. Rapeti, P.; Pasam, V.K.; Gurram, K.M.R.; Revuru, R.S. Performance evaluation of vegetable oil based nano cutting fluids in machining using grey relational analysis-A step towards sustainable manufacturing. *J. Clean. Prod.* **2018**, *172*, 2862–2875. [[CrossRef](#)]
34. Yazdani, M.; Kahraman, C.; Zarate, P.; Onar, S.C. A fuzzy multi attribute decision framework with integration of QFD and grey relational analysis. *Expert Syst. Appl.* **2019**, *115*, 474–485. [[CrossRef](#)]

ARTICLES FOR FACULTY MEMBERS

RESCUE VESSEL OPERATION FOR FLOOD EVACUATION PROTOCOL

Title/Author	Time to rescue for different paths to survival following a marine incident / Solberg, K. E., Jensen, J. E., Barane, E., Hagen, S., Kjøl, A., Johansen, G., & Gudmestad, O. T.
Source	<i>Journal of Marine Science and Engineering</i> Volume 8 Issue 12 (2020) Pages 1-16 https://doi.org/10.3390/jmse8120997 (Database: MDPI)

Article

Time to Rescue for Different Paths to Survival Following a Marine Incident

Knut Espen Solberg ^{1,2}, Jan Erik Jensen ³, Endre Barane ⁴, Snorre Hagen ⁵, Andreas Kjøl ⁶, Gudmund Johansen ⁷ and Ove Tobias Gudmestad ^{2,7,*} 

¹ GMC Maritime, 4077 Hundvåg, Norway; knut.espen.solberg@gmc.no

² Department of Mechanical and Structural Engineering and Materials Science, University of Stavanger, 4021 Stavanger, Norway

³ Petroleum Safety Authority Norway, 4021 Stavanger, Norway; jan.erik.jensen@ptil.no

⁴ Norwegian Coast Guard, Haakonsværn, 5173 Laksevåg, Norway; endrebarane@gmail.com

⁵ Lufttransport AS, Svalbard Air Base, 9170 Longyearbyen, Norway; post@lufttransport.no

⁶ Norwegian Coastal Administration, 6002 Aalesund, Norway; andreas.kjol@kystverket.no

⁷ Department of Technology and Safety, University of Tromsø—The Arctic University of Norway, 9010 Tromsø, Norway; gudmund.johansen@uit.no

* Correspondence: ove.t.gudmestad@uis.no; Tel.: +47-48100259

Received: 30 October 2020; Accepted: 1 December 2020; Published: 7 December 2020



Abstract: The time required for rescue is a critical factor for surviving a marine incident. The regulatory framework, International Maritime Organization (IMO) Polar Code, utilizes a risk-based approach. It states that the vessel operators are to define the time required for rescue but never less than 5 days. Based on experience from the classification society DNV GL, utilization of the minimum requirement of five days is the current industry standard when conducting risk assessments. The dimensioning of search and rescue resources is a national issue. There are no international requirements defining the adequacy of the resources for different geographical areas. The remoteness and lack of resources present within the IMO Polar Code area imposes a significant challenge for mariners in distress. The time required for rescue is highly dependent on multiple variables. Based on this study, the number of persons to be rescued, the number and type of evacuation platforms and the distance each evacuation platform must travel significantly impacts the time required for rescue. In addition, the meteorological and oceanographical (metocean) conditions play a significant role when determining the efficiency of a search and rescue operation.

Keywords: time to rescue; IMO Polar Code; Arctic; search; rescue; passenger vessel

1. Introduction

Providing adequate SAR facilities dimensioned to handle the large passenger vessels in the Arctic is challenging from an economic, practical and logistical perspective. Large distances, lack of infrastructure and harsh metocean conditions represent risks that must be handled.

A substantial increase in the polar cruise tourism activity is expected, especially around Svalbard [1]. Several frameworks address the additional risks associated with this kind of activity [2,3]. However, few quantitative studies address one of the key elements essential for survival—the time to rescue (TTR). The time to rescue is mainly determined by the availability of SAR resources, which to a great extent is determined by geographical distances, political decisions and the financial strength of the business/governmental funding.

This paper assesses the time to rescue (TTR) for different scenarios, utilizing different paths to survival (PTS) and investigates the factors influencing the outcome.

2. Definitions

There is no international consensus with regards to the interpretation and definition of many of the commonly used expressions relevant for the topic. In this paper the following definitions are utilized:

- Evacuation platform—means to evacuate the crew/passengers from the water, survival craft or shore to a place of safety/temporary place of safety.
- FRC—fast rescue craft/mob-boat.
- JRCC—joint rescue coordination center, coordination of the resources to be utilized in the SAR operation.
- Place of safety—location where rescue operations are considered to terminate; where survivors' safety or life is no longer threatened; where their basic human needs (such as food, clothing, accommodation, and communications and medical needs) can be met; and from where transportation arrangements can be made for their next or final destination [4].
- PTS/Path to survival—the crew/passengers of a vessel of distress will have different options with regards to maintaining survival until being rescued. The chosen combination of options is defined as a path to survival. The preferred paths will depend on elements like:
 1. Condition of vessel
 2. Available equipment
 3. Metocean conditions
 4. Number of people involved
 5. Access to SAR resources
 6. Governing procedures
 7. Organization and competence, including systems for training
 8. Personnel judgment

An example of a path to survival (PTS) can be from a survival craft to FRC, further transportation by FRC to SAR-vessel.

- Rescue—the crew/passengers are considered to be rescued when they are placed in a place of safety or a temporary place of safety. The temporary place of safety will prohibit further escalation of the incident on an individual level, e.g., onboard a helicopter, at a temporary place of safety or onboard a SAR-vessel.
- SAR vessel—a purposely built vessel with competent crew, including FRCs and helicopter support facilities, coming to aid the vessel of distress.
- Survival Craft—lifeboat or life raft.
- Temporary place of safety—a location where persons are protected from hazards to life and health and provided with basic humanitarian services such as shelter from the elements, warmth, first aid medical treatment, food, water and sanitation, where communications with the JRCC and a means of accounting for and identifying surviving persons are provided and from which the survivors may be safely transferred to a place of safety [4]. Ideally this will be located close to a helicopter fuel depo to enable efficient refueling of the helicopter.
- Time to rescue (TTR)/time to recover—is the length of time beginning with the completion of the ship abandonment and ending when all persons have been recovered from survival crafts into a place of safety or a temporary place of safety [4].
- Vessel of distress—the vessel that is seeking help due to an unforeseen incident.

3. Model

The approach outlined in this paper is based on a case study approach. The research design is based on the “gaps and holes” methodology [5] with the aim of advancing theoretical explanations. The subjects of the case study have defined the input parameters required for a theoretical model.

They have been obtained based on earlier incidents/accidents. In addition, parameters have been gathered from full scale training/exercises involving the SAR providers. The objective of the study has been to utilize the model to assess the efficiency of different approaches to rescue.

Based on simple relationships between travel speed, distance, time, resources available and downtime (e.g., rest/maintenance), the TTR was calculated for different paths to survival. This required input parameters representing real life conditions. Each path to survival was broken down into subprocesses to provide an adequate model-resolution in the time domain. Most of the defined parameters are based on expert opinions, gathered from experienced SAR-operators. These values assume:

- (1) Adequate metocean conditions to conduct an efficient operation
- (2) Adequate number of competent personnel to conduct the operation in a safe manner
- (3) No technical breakdowns

Due to large sensitivity, many of the parameters have external and internal mechanism; the above assumptions were required to narrow down the process of time to rescue to comparable units. As a result, the model is deterministic and does not consider robustness or reliability. Due to the above assumptions, the model can be regarded as a “best case”. The model has been generated utilizing the computer program Python 3.7.

The model has further been validated by comparing the results to real incidents, e.g., the helicopter operation carried out on Viking Sky, the rescue of the crew of Northguider and the SAR-operation carried out during the Maxim Gorkiy incident [6].

3.1. Discrepancies between the Model and a Real Scenario

Modeling of TTR involves handling a substantial amount of uncertainty. Every vessel that comes to rescue will have its own specific resources, including level of training and number of personnel.

The following discrepancies are to be expected between the model and a real scenario:

- Number of available evacuation platforms—the available number of helicopters and FRCs might be reduced during the operation due to technical failures, maintenance intervals and grounding incidents.
- Level of crew training will greatly affect the efficiency and risk involved in the operation.
 - o The ability to get personnel from the survival crafts onboard the evacuation platform will be affected by the sea state.
 - o The model does not consider any time spent for searching. With a controlled evacuation and the IMO Polar Code requirement of equipment for communication between the survival crafts, this should not represent a large challenge. It is however, to be recognized that this will require functional communication equipment, which represents an uncertainty if comparing the model with a real scenario.
 - o For operations that have an extended duration, the survival crafts are expected to be scattered over an extensive area. Transportation and coordination of the effects caused by the scattering effect are not considered in the model.
 - o The model considers a controlled evacuation and rescue effort. It does not consider a melee situation, picking up individual survivors from the sea.
 - o In a real situation, a combination of survival paths is to be expected. The model only assesses each survival path individually.
 - o The resources mobilized to the scene of the accident will be a dynamic process. This will change throughout the operation and will be affected by mechanisms like availability, access to well rested crew, technical breakdowns, maintenance intervals and duration of the operation.
- The model does not consider the effects of bad weather delaying or stopping the operation.

3.2. Assigned Values

Based on best practice and practical experience from real-time operations, the following values have been assigned to the different variables and utilized in the model:

- Transit speed of the SAR-vessel = 15 (knots) (ice free waters)
 - o Distance from SAR-vessel to survival craft when commencing FRC operations = 1 (nautical mile) [7].
 - o Distance from survival craft to temporary place of safety (e.g., shore/vessel of opportunity) = 4 (nautical miles)
 - o Time used for preparations before departure for the helicopter = 60 (min). Requirement from the Governor of Svalbard [8]
 - o Time used for preparations before departure for the SAR-vessel = 60 (min)
- Number of FRC's utilized in the operation/carried onboard the SAR vessel = 2
- Average speed of the FRCs = 15 (knots) [9]
- Time utilized per person to embark from the survival craft to the FRC = 1.5 (min) [9]
- Time per person utilized to embark off the FRC = 0.3 (min) [9]
- Time utilized to lower and hoist the FRC = 3 (min) [9]
- Time utilized to refuel the FRC = 15 (min) [9]
- Refueling interval for the FRC = 60×4 (min) [9]
 - o Number of passengers carried onboard the FRC (excluding FRC crew) = 10 (persons) [9]. This is based on the capacity of the MOB boats utilized by the Norwegian Coast Guard. According to SOLAS requirements [10], the MOB boat is only required to carry 5 persons sitting, in addition to one person on a stretcher.
- Number of helicopters involved in the operation = 2
- Speed of helicopter (AS332L1 Super Puma) = 120 (knots) [11]
- Average time utilized to hoist 2 persons simultaneously = 2.5 (min) [11]
 - o Time utilized for each person to depart from the helicopter, including landing procedures = 0.5 (min)
- Time utilized for refueling of helicopter = 10 (min) [11]
- Refueling interval of helicopter = 4 (h) [11]
- Time utilized for helicopter critical maintenance/daily check = 30 (min) [11]
- Critical maintenance interval = 24 (h) [11]
- Number of passengers onboard the helicopter (excluding helicopter crew) = 15 persons
 - o Time for maintenance and refueling is executed when the FRC or helicopter is at the SAR-vessel, at the temporary place of safety or at the helicopter base.
- Additional helicopter crews are brought into the operation to ensure proper rest time.
 - o The time required from when a distress call is initiated until it is received by the JRCC is not considered as it is expected to be relatively short.
 - o All equipment has an up-to-date maintenance schedule and no major maintenance intervals (putting the helicopter out of service) are occurring during the rescue operation.
 - o The temporary place of safety has unlimited capacity to handle survivors.

Due to the elements mentioned above, it is to be expected that in a real scenario the time to rescue is to be significantly longer than the absolute values identified by the model. However, the model gives an indication of the sensitivity associated with the different paths to survival.

3.3. Paths to Survival

Surviving a marine incident is a result of a combination of measures. The combination of measures is defined as a path to survival (PTS). An example of a path to survival is PTS3. The survivors are initially located inside a survival craft. From the survival craft, they are evacuated on to an FRC and further onto a SAR-vessel. The model assesses the following paths to survival (Table 1).

Table 1. Paths to survival considered in this document.

Path to Survival	Evacuation From	Means Loading	Platform	Evacuated To	Means Unloading
PTS1	Vessel of distress/survival craft	Hoist	Helicopter	Shore/nearby vessel of opportunity	Walk
PTS2	Survival craft	Hoist	Helicopter	Helicopter base	Walk
PTS3	Survival craft	Hoist & crawl	Helicopter & FRC	SAR-vessel	Walk
PTS4	Survival craft	Crawl	FRC	SAR-vessel	Walk
PTS5	Shore	Walk	Helicopter & FRC	SAR-vessel	Walk
PTS6	Vessel of distress/shore	Walk	FRC	SAR-vessel	Walk

PTS3 and PTS5 assume that the helicopter immediately will start to transport survivors to the SAR vessel as it is transiting to the scene of the accident. In PTS3 and PTS4, the FRC operation (transporting survivors from the survival crafts to the SAR-vessel) is not commenced until the SAR-vessel is located less than 1 nautical mile from the scene of the accident.

Each path to survival has been broken down to individual subprocesses. The time required for conduction of each subprocess was calculated and accumulated. For the paths to survival, this includes the following subprocesses in chronological order, Table 2:

Table 2. The individual processes associated with the paths to survival.

Process Number	Processes
1	Mobilize and transport the SAR resources to the scene of the accident.
2	Lower the FRC on the SAR vessel (for scenarios where applicable).
3	Transport the survival crafts/shore with an evacuation platform (helicopter/FRC).
4	Load the survivors from the survival craft/shore to the evacuation platform (helicopter/FRC) within the capacity of the evacuation platform.
5	Transport the evacuation platform back to the SAR vessel/reception facility.
6	Hoist the FRC on the SAR vessel (for scenarios where applicable).
7	Unload the survivors from the evacuation platform.
8	Maintenance, if critical maintenance intervals were exceeded.

For incidents involving a large number of persons, the processes 2 to 9 were conducted continuously until all the survivors were rescued.

The time required to conduct each process has been accumulated. The time required for some of the processes is directly correlated with the number of persons involved, e.g., embarking from a survival craft to a FRC, while other processes are not correlated with the number of persons involved, e.g., hoisting/lowering of FRC.

4. Results

The model has been run to assess different paths to survival for three scenarios. To capture the effects different parameters had on the time to rescue, the scenarios were chosen to differ in both distance from infrastructure and number of persons to be rescued. Both the number of persons to be rescued and the distance from infrastructure were chosen based on realistic numbers associated with marine activities along the coast of Svalbard.

4.1. Scenario 1—Small Passenger Vessel (Carrying Up to 600 Passengers) Operating in a Region 200 Nautical Miles from Helicopter Base and Nearest SAR Vessel

The scenario assesses a relatively small passenger vessel carrying up to 600 passengers, at a distance of 200 nautical miles from the nearest helicopter base and 200 nautical miles from the nearest SAR-vessel. This can be representative for the expedition cruise vessels operating in remote regions.

PTS2 has been left out of the plot as it would have taken more than 80 h to complete the task. This path of survival proved however to be efficient for a lower number of passengers, involving only one or two flights.

The plot (Figure 1) reveals that it will take about 14 h until the first marine resource is available at the scene of the accident and can start the rescue by FRCs. However, for PTS3 and PTS5 the helicopters can start to move survivors from the scene of the accident to the approaching SAR-vessel/temporary place of safety immediately upon being deployed, and the FRCs will be involved in the operation as the SAR-vessel arrives at the scene on the incident.

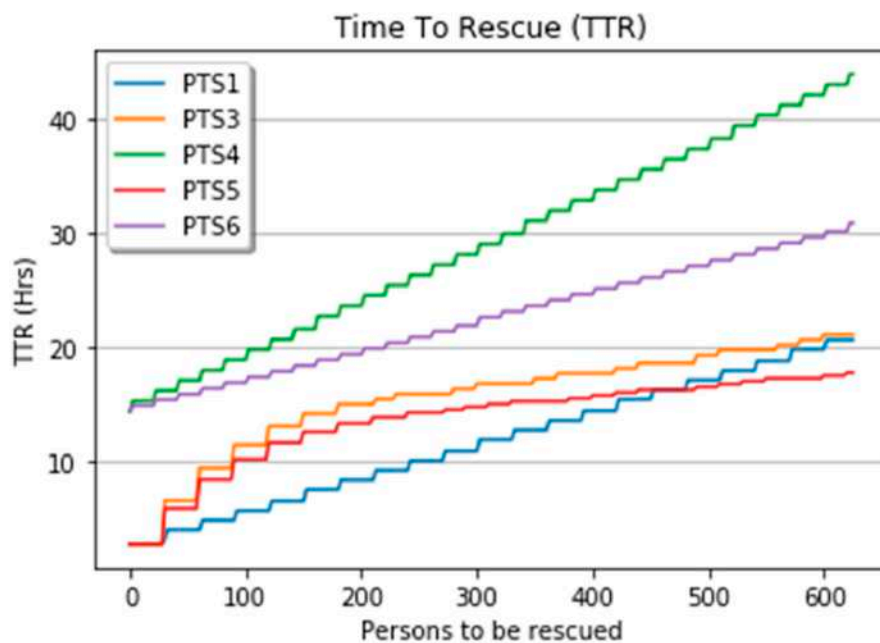


Figure 1. Time to rescue for small passenger vessel operating in a remote region.

For vessels in Scenario 1 involving 600 people, there is a relatively marginal difference between PTS1, PTS3 and PTS5. They all have in common that the helicopters are deployed to the scene of the incident and that one starts the evacuation by helicopter immediately upon arrival. In PTS1 the survivors are shipped to the shore/nearby vessel of opportunity while in PTS3 and PTS5 they are shipped back to the approaching SAR-vessel. The effect of FRCs contributing to the operation is not critical for vessels carrying less than 500 people due to the relatively long response time associated with the marine resources. The helicopter will be the critical asset and have completed most of the evacuation before the SAR-vessel arrives.

For vessels carrying less than about 500 persons, utilizing the helicopter for evacuation of personnel from the survival crafts to an onshore safe haven/vessel of opportunity (PTS1) is the preferred solution.

4.2. Scenario 2—A Larger Passenger Vessel Operating in Vicinity of Infrastructure and a SAR-Vessel

The second scenario is based on a passenger vessel carrying up to 3000 passengers, operating in closer vicinity to infrastructure, 50 nautical miles from a helicopter base and 50 nautical miles from a SAR vessel.

It is evident (Figure 2) that there is little time required to get the SAR resources in position. The effectiveness of the FRC operation compared with a helicopter hoisting operation outweighs the reduced travelling time of the helicopter. The most efficient means of rescue is the utilization of FRCs in combination with helicopters (PTS3 and PTS5). It is also evident that avoiding hoisting and enabling the personnel to “walk” onto the evacuation platforms increases efficiency substantially, reducing the TTR with about 33%, from 46 to 31 h. This would require the survivors to evacuate to land by themselves. In a real scenario, a temporary place of safety should be established at the same location.

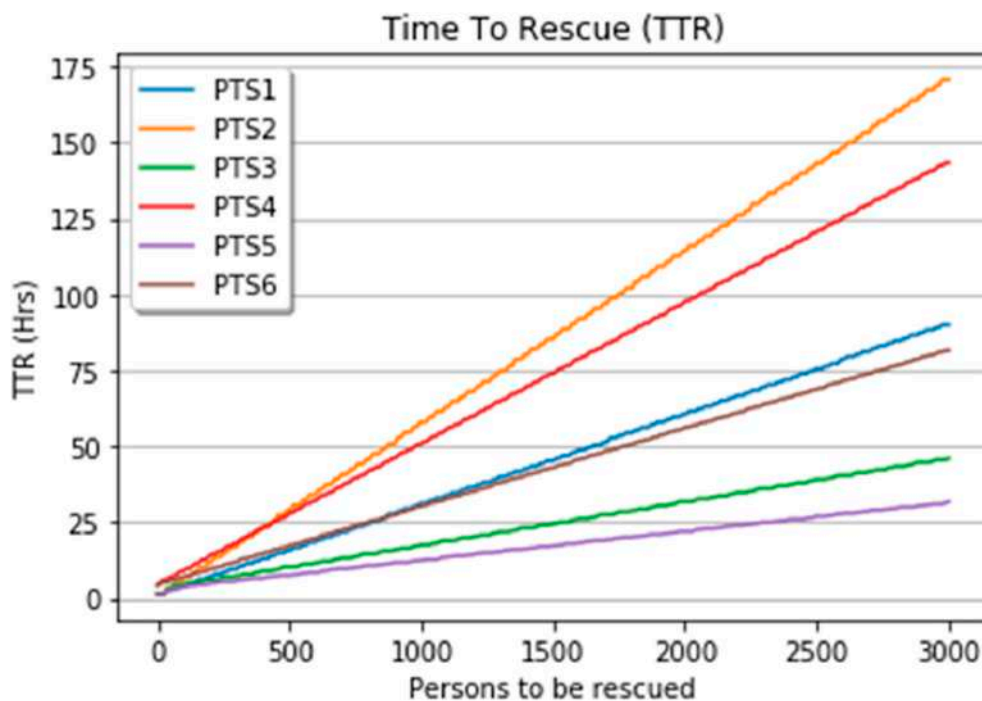


Figure 2. Time to rescue for a larger passenger vessel operating in vicinity of infrastructure and a SAR-vessel.

4.3. Scenario 3—A Larger Passenger Vessel Operating in a Remote Region

Scenario 3 is based on a relatively large cruise vessel (up to 3000 persons onboard) operating in a remote region, 200 nautical miles from a helicopter base and 200 nautical miles away from the nearest SAR-vessel.

The plot (Figure 3) for PTS2, flying the survivors directly back to the helicopter base is removed from the plot as it would take more than 400 h and is not regarded as a feasible option.

Due to the long response time for the SAR-vessel, it is evident that with the exception of PTS1, establishing and flying the survivors to a safe haven/vessel of opportunity near the scene of the incident, the operation will not reach its full effectiveness until about 14 h into the operation. The helicopter is an important asset, but the FRCs play an important role for the larger part of the operation.

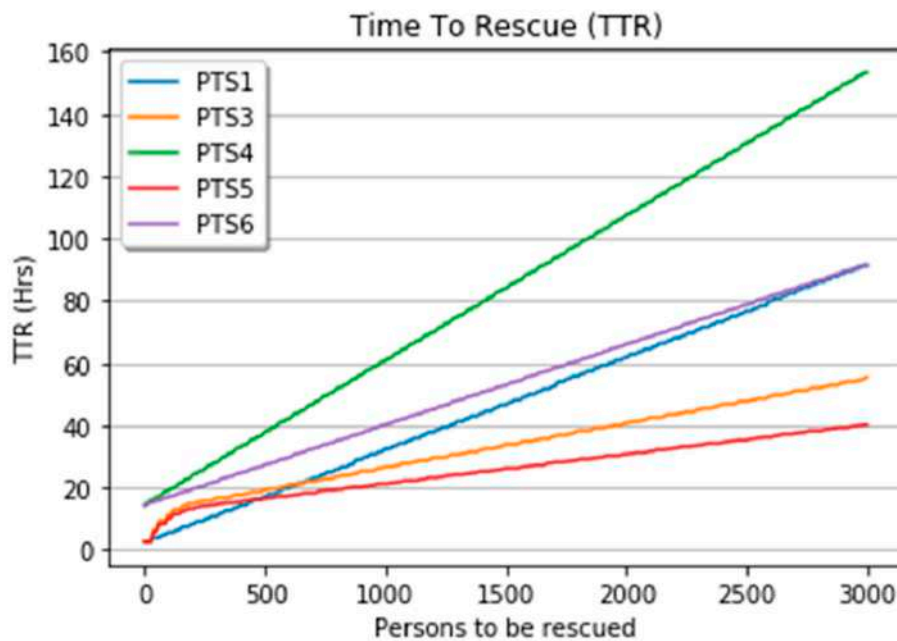


Figure 3. Time to rescue for a larger passenger vessel operating in a remote region.

4.4. Uncertainty Associated with the Results

The uncertainty associated with the model is defined as the model's ability to provide an accurate answer that represents the time to rescue associated with a real scenario. Due to the static nature of the input parameters and the lack of ability to cover unforeseen events, the model represents a best-case scenario with 100% operational efficiency.

The uncertainties associated with the result increase for operations of longer duration. This is due to the effect of several mechanism, e.g., human fatigue caused by prolonged working h, fatigue due to continuums repetitive operations (e.g., operator of FRC winches will have conducted several hundred hoists during a relatively short time frame), stretching of maintenance intervals for essential equipment, additional resources being introduced to the operation and variable metocean conditions.

The model assumes twin hoisting (hoisting 2 survivors simultaneously). It is experienced that when the helicopter approaches its full carrying capacity, it is preferred to conduct single hoist operations due to the challenge of the stowage of the survivors inside the helicopter.

If the survivors are in a physical state that requires single hoisting, e.g., being on a stretcher (e.g., due to serious injuries or hypothermia), the efficiency of the helicopter operation is reduced by more than 50%, further increasing the TTR substantially. Stowage of survivors on stretchers inside the helicopter is also highly time consuming. It is of very high importance that the survivors are in a physical state that enables an efficient hoist and stowage.

The efficiency of a SAR operation is highly dependent on numerous unknown variables. Based on experience from SAR-helicopter operators [11], the efficiency in a hoisting operation is reduced when rolling motion is encountered on the vessel/survival crafts the survivors are to be hoisted from. The rolling motion is related to a variety of parameters like vessel size, vessel heading, vessel metacentric height, sea state and wave periods. This study assumes 100% efficiency in the rescue operation. Due to factors like bad weather, lack of/improper communication/logistical challenges etc., the operational efficiency can be reduced significantly. In a real scenario, this could result in a substantial increase in the TTR, and this study is to be regarded as a best case.

5. Discussion

5.1. Model Results—Scenario 1

In Scenario 1 it is evident that PTS1, freighting the survivors by helicopter to a temporary place of safety established onshore/vessel of opportunity, is efficient, especially when the number of survivors is relatively low (e.g., below about 500 persons). This will require establishment of a safe haven, in addition to a fuel depo near the scene of the accident. The time utilized for the operation is greatly affected by the distance from the survival crafts to the temporary place of safety and fuel depo (Figure 4).

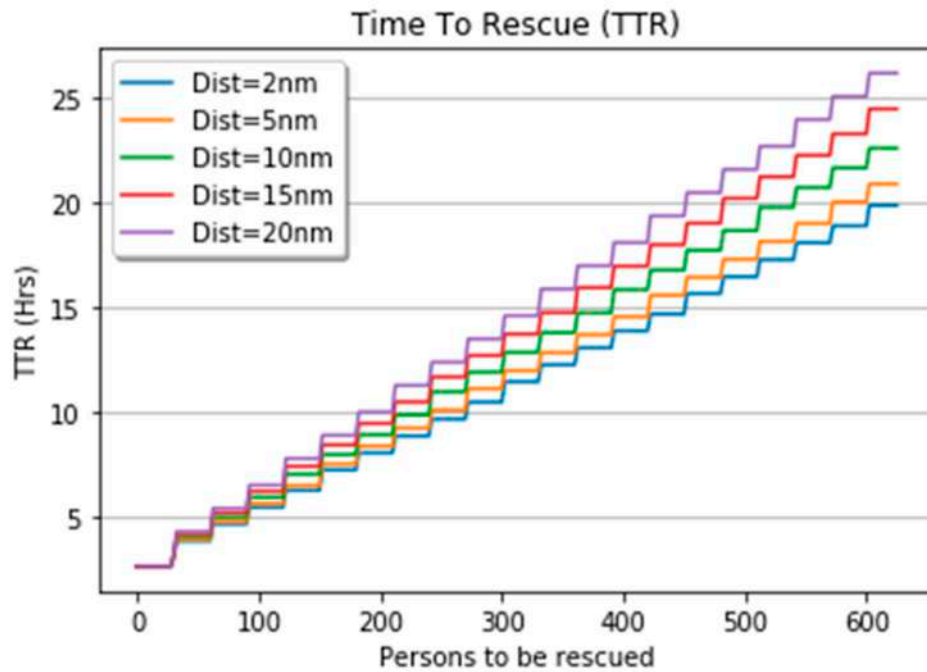


Figure 4. Time to rescue for different distances from scene of the incident to safe haven.

Increasing the distance from the incident to the temporary place of safety from 2 nautical miles to 20 nautical miles will result in an increased flying time per round trip for the helicopter. Based on Figure 4 it is evident that the increase in distance (from 2 nautical miles to 20 nautical miles) will reduce the efficiency of the operation by about 20%. However, the potential waiting time associated with multiple helicopter operations taking place in a limited airspace simultaneously will reduce the efficiency for short distances.

A more robust and realistic approach would be to focus on PTS3, as utilizing this approach, the helicopter will have access to required helicopter support systems at each drop off of survivors at the SAR-vessel. Utilization of this methodology was seen in the Maxim Gorkiy incident [6].

This is especially true when the number of survivors is approaching 600 or above, as the efficiency of PTS1 and PTS3 converges around this point.

Introducing a marine asset to the operation will also contribute to increasing redundancy and handling the scattering effect caused by the survival crafts.

Shipping survivors directly back to the helicopter hub will not be a feasible option unless the number of survivors is relatively low, involving only a few helicopter flights. This will also reduce the need for establishment of an onshore safety haven. An example of this was seen during the evacuation of the crew of the fishing vessel Northguider [11].

5.2. Model Results—Scenario 2

In Scenario 2 it is evident that PTS3 and PTS5 provide the lowest TTR. These paths to survival enable a simultaneous operation of 2 FRCs and 2 helicopters.

The lowest evacuation time observed is PTS5 where all the survivors are located onshore. In a real scenario, it would be advisable to establish a safe haven at this location (if possible), and at a later stage evacuate them in a controlled manner.

It is worth noting that even at these distances, very close to onshore infrastructure, PTS1 came out about average. This option does not take into account that FRC and smaller local vessels of opportunity could be utilized for evacuating personnel onto the shore. Few SAR-vessels have the capacity to handle 3000 survivors, and additional accommodation resources must be brought into the scene of the accident, either as other vessels or by establishing an onshore safe haven.

Based on the findings above it is evident that an onshore temporary place of safety would be an asset also for incidents that took place in close vicinity of onshore infrastructure.

5.3. Model Results—Scenario 3

In Scenario 3, marine resources are essential for the operation and they reduce the TTR by more than 50% compared to only utilizing helicopters. It is also clear that the time utilized by the marine resource to reach the scene of the accident only represents a small portion of the total time required for the rescue operation.

An operation that is to have a duration of several days will need to supply its own support functions. This includes additional personnel, FRC fuel, helicopter fuel, technical personnel and food. Establishing the logistics required for an efficient operation will require substantial efforts and time. Parallel to the first responders rushing to the scene of the accident, a logistics support system should be initiated and mobilized.

5.4. Common Denominators for All Scenarios

It is evident that for all scenarios the TTR is expected to be in the range of days, not h.

It is further apparent that three different key factors highly influence the TTR; the number of persons to be rescued, the number of evacuation platforms available and the distance to be travelled by the individual evacuation platforms.

The number of persons to be rescued represents a major driver when determining the TTR.

When the resources are at the scene of the incident, the number of evacuation platforms, e.g., number of FRCs and helicopters available, is critical in determining the time to rescue. Each individual platform provides rescue capacities as long as they can operate in parallel. The cumulative capacity of the evacuation platforms highly affects the total speed of the evacuation, which further defines the total time required for the rescue operation. Utilizing a substantial number of evacuation platforms in parallel will, however, demand a high capacity reception facility to handle the high and steady influx of survivors.

The distance travelled by the evacuation platforms is determined by the distance from the survival crafts to the temporary place of safety established onshore/vessel of opportunity/SAR-vessel. As this distance has to be travelled twice (back and forth) when picking up the survivors it will highly influence the TTR. It is of uttermost importance that the SAR-vessel maneuvers close to the survival crafts and that the temporary place of safety is established in close vicinity of the scene of the incident. The location of the helicopter fuel depots also plays a significant role when assessing the efficiency of the helicopters.

When evacuating a vessel in distress, involving an extensive number of rescue platforms will reduce the TTR up to a certain point. Beyond that, it will only increase the robustness of the operation. It is also important to consider the capacity of the reception facilities. The capacity of the reception facilities and the capacity of the evacuation has to be harmonized for an efficient operation. During the

Viking Sky incident, the onshore casualty reception facility was manned with about 100 volunteers from the Red Cross in addition to professional health workers, providing first aid and psychological support [12].

During the Viking Sky incident 397 persons were evacuated in about 16 h, giving an average time of 2.4 min per person. Five helicopters were involved in the operation, and the helicopters were refueled at the same time as they were dropping off the survivors. However, only one helicopter was able to conduct hoisting operations at the vessel at any time due to issues caused by turbulence, [12–14]. The indications of reduced efficiency during utilization of several helicopters together is also addressed in the guidelines defined by [15]. They state that an efficiency of 50% is to be expected for the second helicopter arriving at the scene of the accident.

It is evident that the distance from the nearest helicopter base/SAR-vessel influences the TTR. In scenario 3 the lowest TTR was about 40 h utilizing a combination of helicopters, FRCs and a SAR-vessel. Out of this time the SAR-vessel utilizes about 13 h and the helicopters utilizes about 1.6 h to get to the scene of the incident. This represents respectively about 30% and 2.5% of the total TTR. From a cost/benefit perspective, the recommended focus should be on increasing the rate of survivor evacuation by increasing the number of evacuation platforms not only focusing on reducing the response time.

In PTS 5 and PTS6 the survivors were able to reach shore by their own means. If the location is suitable, it would most likely be advisable to establish a temporary place of safety at this location instead of moving the survivors.

During the Maxim Gorkiy incident about 325 people were rescued in about 3.5 h [6]. This means an average of 0.65 minute per person. This achievement was achieved utilizing multiple helicopters landing and refueling onboard KV Senja, in addition to survivors directly climbing/being onto the aft deck of the SAR-vessel. The large discrepancy between the evacuation speed (time utilized per person) in the Maxim Gorkiy scenario compared with the evacuation time in the Viking Sky or Northguider scenario is mainly due to survivors evacuating directly from the survival crafts onto the aft deck of KV Senja from the life boats by walking/climbing. This reduced the need for FRC/hoisting operations which are time consuming.

To be able to conduct this operation on calm seas was a necessity. Despite the extraordinary good conditions, there were incidents where helicopters almost slide off the helideck and lifeboats obtained considerable damage under the stern/side of KV Senja, due to the rolling motion of the vessel.

Conduction of part of the operation was beyond normal regulatory directives but a chosen option due to the limited time available.

This incident proves the importance of multiple evacuation platforms being utilized simultaneously. It also indicates the increase in speed when having a system that enables the survivors to “walk” off the evacuation platform instead of being hoisted/lifted.

5.5. Robustness of the Operation

The model is based on 100% functionality of all technical equipment. Malfunction and technical breakdowns are to be expected for an operation that is to have a duration of several days. Due to lack of infrastructure, reduced availability of critical spare parts and technical competence, the operation can be significantly delayed when comparing to a real SAR operation; according to the results from the application of the model.

To reduce the likelihood of the above-mentioned mechanism, it is important to evaluate different aspects of the robustness of the operations, Table 3.

PTS6 assumes that the survivors have been able to reach a protected location onshore. With the exception of PTS6, it is clear that none of the PTS's are clearly favorable. It is however clear that mobilizing many assets to the scene of the accident is of high importance to increase the robustness of the operation.

Table 3. Robustness of the different paths to survival.

Survival Path	Robustness Weather	Robustness Technical	Robustness Human Element
PTS1	High	Low	Medium
PTS2	High	Low	Low
PTS3	Medium	Medium	Medium
PTS4	Low	High	High
PTS5	High	Medium	High
PTS6	High	High	High

The weather limitations associated with FRC operations will also affect the robustness of the operation. According to JRCC Bodø, personnel transfer by FRC is not advisable in seas above 1 m unless the FRC operators have special training and the survivors are fit [6]. For most of the offshore sector in the North Sea, the wave height limitations for a specially trained crew is defined to be a significant wave height of 4.5 m [16].

If the survivors seek a sheltered location or the shore, the probability of efficient FRC operations would significantly increase.

The effect of having a SAR-vessel at the scene of the accident increases both the robustness from a technical and a human element perspective. The vessel would provide valuable assets like helicopter logistic support, food, water, medical facilities and improved abilities for communication.

5.6. Human Resources Required in an Efficient SAR Operation

When dimensioning a SAR-system it is important to consider the human resources involved in the operation. For an operation that is to be conducted on a continuous basis for several days it is important to follow standard operation procedures to prevent development of fatigue and reduce the likelihood of failures.

Below (Table 4) is an example of the human resources involved in transportation and reception of survivors from survival crafts. This does not take into account the resources needed for staffing of SAR-vessel operations, first aid treatment or accommodation of the survivors.

Table 4. Human resources required for a multiday SAR operation.

Operation	Minimum Number of Persons Conducting Operational Tasks	Minimum Number of Persons Allocated to the Operation on a Continuous Basis (3 Shifts)
FRC operation		
FRC crew	3	9
Crane operators	2	6
Reception facilities (only registration)	2	6
Total FRC operation	7	21
Helicopter operation		
Pilots	2	6
Winch operator	1	3
Mechanic	1	3
Vessel HKO + 2 NAVKIS	3	9
FDO (Flight Deck Officer)	1	3
FDA (Flight Deck Assistant)	1	3

Table 4. Cont.

Operation	Minimum Number of Persons Conducting Operational Tasks	Minimum Number of Persons Allocated to the Operation on a Continuous Basis (3 Shifts)
FDM (Flight Deck Crew)	4	12
Mechanic preparing heli-fuel	1	3
Reception facilities (only registration, no medical treatment)	2	6
Total Helicopter operation	16	48
Total all transportation operations		69

The table indicates what would ideally be required for a multiday SAR operation. The figure does only take into account the evacuation processes and does not address the personnel required for, e.g., casualty treatment or organizing logistics. Much of the above-mentioned personnel would not be available as the first responders rush to the scene of the accident. Mobilization and transportation of additional required personnel to the scene of the incident should be initiated in the early phases of the operation.

It is also worth considering mobilization of the human resources required for the survivor reception facilities, including the staffing of safe havens. In the Viking Sky incident, there were about 100 persons involved in the reception and premedical treatment of the survivors [12].

6. Conclusions

Despite the uncertainty associated with the model, there are several learning points identified. Increasing the number of evacuation platforms greatly affects the TTR. Utilization of FRCs and helicopters simultaneously proved to be the beneficial for all three scenarios. However, this requires access to helicopter support functions (e.g., ability to refuel) and the reception facilities to be dimensioned to handle a large influx of survivors.

For incidents taking place in remote areas (far from infrastructure and SAR-vessels), the time required for the SAR-vessel to arrive at site affects the rate of rescue. The following generalization can be made for the most efficient path to survival:

- Less than 40 survivors—PTS2, utilizing helicopters, freighting the survivors directly back to the helicopter base.
- 50 to about 600 survivors—PTS1, utilizing helicopters, establishing a temporary place of safety onshore while waiting for arrival of SAR-vessels as long as helicopter fuel is available in the vicinity.
- More than about 600 survivors—PTS3, utilizing a combination of all evacuation platforms available.

In all cases the survivors would benefit from seeking sheltered waters/the shore to increase the efficiency of the rescue operation.

It is also evident that access to helicopter fuel/support facilities is essential for prolonged operations involving helicopters. All paths to survival, except PTS2, require this in the vicinity of the scene of the incident. The issue of access to helicopter support facilities was also essential for the successful outcome of the Maxim-Gorkiy incident [6]. Shore-based depots located in vicinity of the scene of the accident, available before any SAR-vessels arrive, utilized in combination with SAR-vessels with helicopter facilities is regarded as the most beneficial approach.

7. Recommendations

The general learning points can be divided into two different categories: vessel operator recommendations and SAR operator recommendations.

7.1. Vessel Operator Recommendations

From the perspective of a vessel operator, the following issues are to be considered:

- For vessels containing more than a couple of hundred persons, the time to rescue is expected to be days not h for most areas of the Arctic/Antarctic.
- The number of persons onboard is a key parameter when estimating TTR. As a result, it is to be expected a longer TTR for a large passenger vessel than for a smaller vessel.
- The availability of SAR-resources is critical when determining TTR, and it is to be recognized that prolonged helicopter operations are not a viable option for a large part of the Arctic/Antarctic due to lack of support infrastructure, e.g., helicopter fuel.
- Rescue by marine resources will require relatively calm waters (wave height below 1 meter is recommended by JRCC Bodø) [7].
- The survivors should try to avoid spreading over a large geographical area (reduce the scattering effect) and seek sheltered waters or preferably evacuate to onshore. This will increase the probability for efficient evacuation operations, reduce the probability for conducting helicopter hoisting operations and reduce the TTR and increase the probability of survival
- Having a companion vessel (twin vessel operation) can increase safety. This will require special training and purposely built equipment to enable efficient ship to ship transfer of personnel. This is only a viable option in calm waters.
- Installation of helicopter support facilities onboard passenger vessels/vessel of convenience can substantially increase both the efficiency and the duration of helicopter operations.

7.2. SAR Operator Recommendations

From the perspective of a SAR operator, the following issues are to be considered:

- Dispatching a combination of purposely built and trained marine SAR-resources to the scene of the accident to provide a safe haven, helicopter support facilities and enabling of FRC operations are essential to reduce the TTR and increase the robustness of the operation.
- Mobilization of additional resources (including personnel) is critical for logistics and support of an extended operation that is to last for several days.
- Maximize of the number of evacuation platforms available at the scene of the incident will in most cases reduce the TTR.
- The reception facilities must be dimensioned for the capacities provided by the cumulative capacity provided by the evacuation platforms.
- For many scenarios involving a substantial number of passengers, an onshore temporary place of safety is a critical asset. Equipment and personnel should be readily available at the helicopter base and pre-established helicopter fuel depots should be available in the geographical area of interest.
- Contingency plans addressing mobilization and transportation of additional essential SAR-personnel to the scene of the accident should be prepared as an efficient operation of an extended duration will most likely involve more than 100 SAR personnel at the scene of the accident.
- It is important to consider the safety, food and water required to support the SAR-resources brought to the scene of the accident.
- Helicopter fuel depots—the depots should be located at short distances from each other to reduce the time utilized for transportation. The depots should enable helicopter operations for a duration equivalent to the time required for SAR-vessel to reach the area.

8. Concluding Remarks

In the risk assessment required by the IMO Polar Code, a majority of the vessel operators aim for the minimum time to rescue requirement of “minimum 5 days” [1].

Being rescued within the timeframe defined will require an enormous functional SAR-system in place, in addition to favorable metocean conditions. This is especially valid for larger vessels carrying more than a couple of hundred people. Within the IMO Polar Code area, the SAR-resources are sparse and far apart. When conducting the risk assessment as defined in the “Polar Water Operation Manual”, it is important to consider the elements described in this manual to ensure the time defined as “time to rescue” is valid for the area of operation.

It is also of importance that the governmental agencies responsible for the SAR facilities are actively communicating the availability and functionality of the SAR system within geographical areas. This information is essential input for the marine industry to enable defining a realistic time to rescue.

9. Epilog

Deficiencies in a vessels SOLAS equipment [9] will cause incompliance with the governing rules and regulations. Such a vessel would be detained and prohibited from leaving port as the functionality of the safety equipment would be regarded as not adequate to provide the functionality required for survival in the event of an incident involving the vessel.

Bad weather will also reduce the functionality of the safety equipment. A relatively high significant wave height will prohibit launching of the lifeboats/life rafts and evacuation of the vessel in distress would not be possible.

A vessel with compliant SOLAS equipment would not be restricted from leaving port, despite a valid weather forecast defining conditions where the functionality of the safety equipment is severely reduced. In this event, the vessel operators purposely put the vessel in a position where they should know that the safety is compromised.

This paradox imposed on the marine industry is relatively recent. In previous times the vessels traveled slowly, and the weather predictions were unreliable or unavailable. In more recent times the accuracy and availability of weather forecasts has improved significantly, and most vessels can avoid bad weather, if prioritized.

For vessels operating on the high seas, avoidance of bad weather is at times difficult. However, most cruise/passenger vessels operate in coastal waters for a larger part of the time. Avoidance of situations where the functionality of the safety equipment is significantly reduced is perfectly possible with today’s technology. This will require prioritizing safety and a willingness to bear the cost associated with the implications of the mitigation measures.

Slogans like “Never compromise on safety” are frequently observed in the marine industry. However, as the industry accepts the risks associated with lack of functionality of safety equipment associated with bad weather, safety is compromised every day, in all parts of the world. Operating with risk acceptance criteria that compromise on safety is not necessarily a bad thing—a human life has a price. It is, however, important that this fact is accepted and communicated to relevant parties, including the passenger who puts his/her life in the hands of the vessel operator.

It should be noted that the paper is based on the results of a series of search and rescue exercises conducted in the waters north of Spitzbergen, Norway from 2016 to 2018, [17–20].

Author Contributions: Conceptualization, K.E.S. and A.K.; Investigation, K.E.S., J.E.J., S.H. and G.J.; Methodology, A.J.; Project administration, E.B. and G.J.; Resources, E.B. and G.J.; Supervision, O.T.G.; Writing—original draft, K.E.S.; Writing—review and editing, O.T.G. All authors have read and agreed to the published version of the manuscript.

Funding: This research received no external funding.

Conflicts of Interest: The authors declare no conflict of interest.

References

1. Visit Svalbard/MIMIR. Destinasjon Svalbard mot 2025. 2015. Available online: <https://www.visitsvalbard.com/dbimgs/Masterplan%20Destinasjon%20Svalbard%20mot%202025.pdf> (accessed on 22 November 2020). (In Norwegian)
2. International Maritime Organization, Shipping in Polar Waters. 2019. Available online: <https://www.imo.org/en/mediacentre/hottopics/polar/pages/default.aspx> (accessed on 22 November 2020).
3. Norsk Polar Institutt. (not dated). Cruise Handbook. Available online: <http://cruise-handbook.npolar.no/en/kongsfjorden/fjortende-julibukta.html> (accessed on 22 November 2020).
4. International Maritime Organization. *IMO COMSAR 10*; International Maritime Organization: London, UK, 2006.
5. Ridder, H.-G. *The Theory Contribution of Case Study Research Designs, Business Research*; Springer: Heidelberg, Germany, 2017; ISSN 2198-2627. Available online: <http://dx.doi.org/10.1080/1088937X.2019.1597394> (accessed on 22 November 2020).
6. Hovden, S.T. *Redningsdåden*; Commentum Forlag AS: Sandnes, Norway, 2012. (In Norwegian)
7. Prestøy, R. Joint Rescue Coordination Center, Bodø, Norway. Rescue Coordinator, Interviewed by Solberg, K.E., 3 May 2019.
8. Olsen, E. Police Chief Inspector, Svalbard, Interviewed by Solberg, K.E., 24 June 2019.
9. Johansen, G. University of Tromsø/KV Svalbard. Former Second in Command, Interviewed by Solberg, K.E., 3 May 2019.
10. International Maritime Organization. *SOLAS—International Convention for the Safety of Life at Sea*; International Maritime Organization: London, UK, 2004. Available online: http://library.arcticportal.org/1696/1/SOLAS_consolidated_edition2004.pdf (accessed on 22 November 2020).
11. Hagen, S. Lufttransport AS, Longyearbyen. SAR Chief Pilot, Interviewed by Solberg, K.E., 2 May 2019.
12. Verdens Gang. Cruiseskipet Viking Sky Med Motorstans—Dramatisk Evakuering. 2019. Available online: <https://www.vg.no/nyheter/innenriks/i/1nOlqB/cruiseskipet-viking-sky-med-motorstans-dramatisk-evakuering> (accessed on 22 November 2020).
13. NRK. Viking Sky Fekk Trøbbel—Dette Har Skjedde. 2019. Available online: https://www.nrk.no/mr/viking-sky-fekk-trobbel_-dette-har-skjedde-1.14487961 (accessed on 22 November 2020).
14. NRK. Cruiseskip i Trøbbel Utanfor Møre og Romsdal. 2019. Available online: <https://www.nrk.no/mr/cruiseskip-i-trobbel-utanfor-more-og-romsdal-1.14487336> (accessed on 22 November 2020).
15. Norsk Olje og Gass. *Anbefalte Retningslinjer for Etablering av Områdeberedskap, Rev 3*; Norsk Olje og Gass: Stavanger, Norway, 2015.
16. Vinnem, J.E. *Retningslinjer for Områdeberedskap—Underlagsrapport, Forutsetninger og Faglige Vurderinger*; Norsk Olje og Gass: Bryne, Norway, 2012.
17. Solberg, K.E.; Gudmestad, O.T.; Kvamme, B.O. *SARex Spitzbergen: Search and Rescue Exercise Conducted off North Spitzbergen: Exercise Report*; University of Stavanger: Stavanger, Norway, 2016. Available online: <https://uis.brage.unit.no/uis-xmlui/handle/11250/2414815> (accessed on 22 November 2020).
18. Solberg, K.E.; Gudmestad, O.T.; Skjærseth, E. *SARex2: Surviving a Maritime Incident in Cold Climate Conditions*; University of Stavanger: Stavanger, Norway, 2017. Available online: <https://uis.brage.unit.no/uis-xmlui/handle/11250/2468805> (accessed on 22 November 2020).
19. Solberg, K.E.; Gudmestad, O.T. *SARex3: Evacuation to Shore, Survival and Rescue*; University of Stavanger: Stavanger, Norway, 2018. Available online: <https://uis.brage.unit.no/uis-xmlui/handle/11250/2578301> (accessed on 22 November 2020).
20. Solberg, K.E.; Gudmestad, O.T. Findings from Two Arctic Search and Rescue Exercises North of Spitzbergen. *Polar Geogr.* **2019**, *42*, 160–175. [CrossRef]

Publisher’s Note: MDPI stays neutral with regard to jurisdictional claims in published maps and institutional affiliations.



© 2020 by the authors. Licensee MDPI, Basel, Switzerland. This article is an open access article distributed under the terms and conditions of the Creative Commons Attribution (CC BY) license (<http://creativecommons.org/licenses/by/4.0/>).

ABOUT UMT FACULTY

SDI

Selective Dissemination of Information (SDI) service is a current-awareness service offered by the PSNZ for UMT Faculty Members. The contents selection criteria include current publications (last 5 years), highly cited and most viewed/downloaded documents. The contents with pdf full text from subscribed databases are organized and compiled according to a monthly theme which is determined based on the topics of specified interest.

For more information or further assistance, kindly contact us at 09-6684185/4298 or email to psnz@umt.edu.my/sh_akmal@umt.edu.my

Thank you.

**Perpustakaan Sultanah Nur Zahirah
Universiti Malaysia Terengganu
21030 Kuala Nerus, Terengganu.**

Tel. : 09-6684185 (Main Counter)

Fax : 09-6684179

Email : psnz@umt.edu.my